Åbo Akademi University

Daniel Valtakari

The Role of Metal Ions in Selective and Sustainable Processes

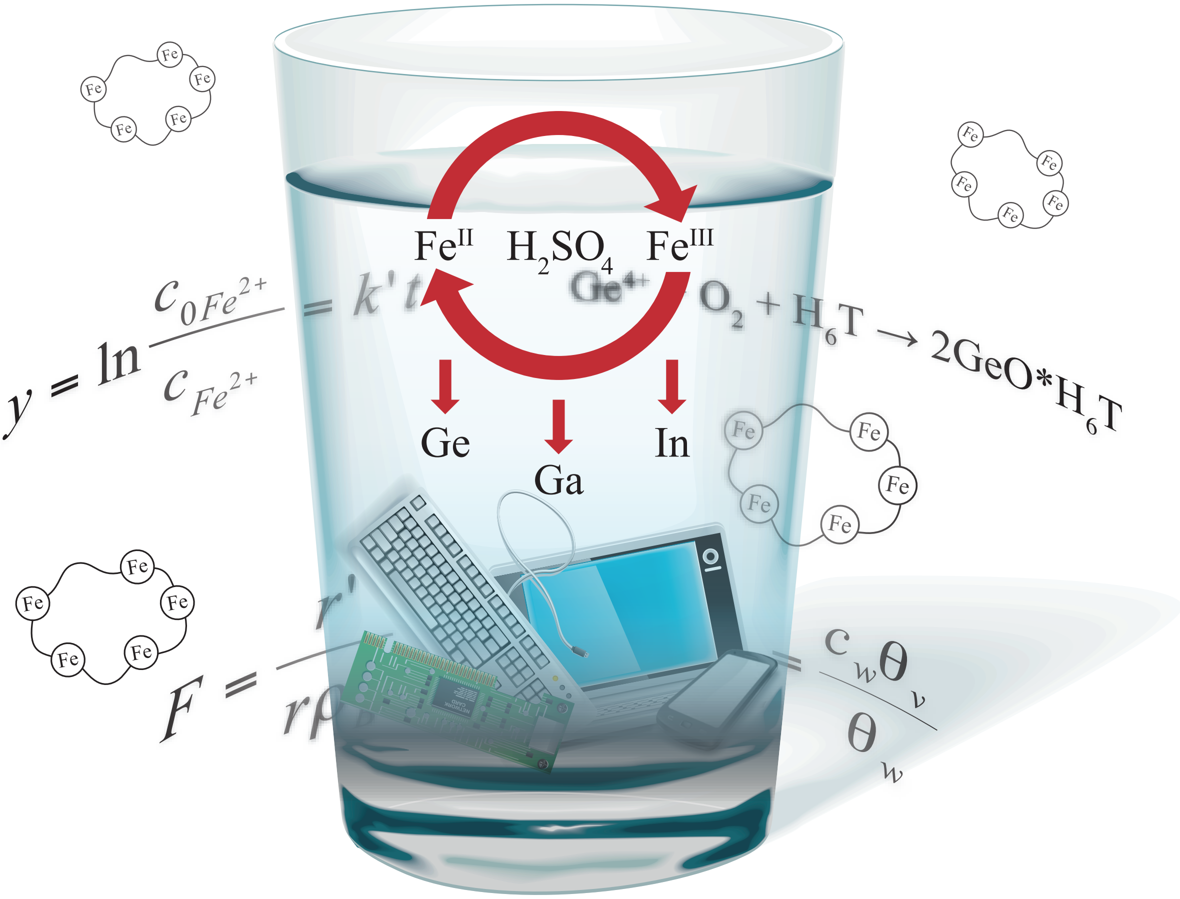

Daniel Valtakari
Born 1966 in Pomorie, Bulgaria

Lic. Sc. (Tech.), 2011
Åbo Akademi University, Turku/Åbo, Finland

M.Sc. Chem. Eng., 1997
Åbo Akademi University, Turku/Åbo, Finland

Cover art

László Restyánszki
H-1142 Budapest, Ungvár u. 22/A.
Phone: +36-20-9368-581
E-mail: rl-design@hdsnet.hu

The Role of Metal Ions in Selective and Sustainable Processes

Doctoral thesis

Daniel Valtakari

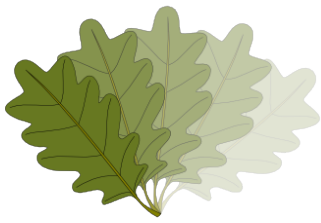

Johan Gadolin
Process Chemistry Centre

Laboratory of Industrial Chemistry and Reaction Engineering
Faculty of Science and Engineering / Chemical Engineering
Åbo Akademi University

Turku/Åbo 2015

Supervised by

Professor Tapio Salmi
Åbo Akademi University

Reviewers

Professor Juha Tanskanen
University of Oulu

Docent Pekka Ihalainen
General Manager
Ympäristöasiantuntijoiden keskusliitto YKL ry

Opponent

Professor Ilkka Turunen
Lappeenranta University of Technology

ISBN 978-952-12-3270-1

Painosalama Oy – Turku, Finland, 2015

Preface

The presented work was carried out as part of two separate projects: a project to produce ferrosulphate flocculants for municipal water purification purposes and a project researching an improved hydrometallurgical zinc production process. The first one was carried out at the Laboratory of Industrial Chemistry and Reaction Engineering in cooperation with the companies Kemira (Finland) and Kemwater (Sweden) and the second was carried out at the Laboratory of Industrial Chemistry and Reaction Engineering and Laboratory of Analytical Chemistry in cooperation with Outokumpu Research Oy, Outokumpu Research Oy and TEKES (Technology Development Centre).

Professor Tapio Salmi supervised the first part of the research work and Professor Tapio Salmi and Emeritus Professor Lars-Eric Lindfors at the Laboratory of Industrial Chemistry and Reaction Engineering supervised the second part of the research work.

At the Laboratory of Analytical Chemistry MSc. (Chem.) Stig-Göran Huldén participated in the research and supervised by Professor Ari Ivaska and Docent Leo Harju.

I thank laboratory manager PhD Kari Eränen and PhD Johan Wärnå for their help in constructing the experimental equipment and laboratory manager MSc. Paul Ek, Maarit Hammert and MSc. (Chem. Eng.) Cecilia Still for valuable analysis work. Professor Tapio Salmi and PhD Johan Wärnå have also contributed to the simulations and model calculations presented in the work. I wish to thank PhD Mats Rönnholm for valuable discussions and advice during the period of work.

I also wish to thank my co-workers MSc. Stig-Göran Huldén and PhD Sigmund Fugleberg for the cooperation during the research and Professor Ari Ivaska for the valuable help I received. MSc. Krister Steinby and Professor Matti Hotokka are acknowledged for the valuable work in RAMAN-spectroscopic measurements.

A special thank is given to Lars Gillberg, Kemwater, and Docent Päivi Mäki-Arvela, Laboratory of Industrial Chemistry, for their very special support.

I thank my parents Roussanka and Pertti and my brother Dimitar (Mitko) for just being there.

I wish to express my gratitude to my supervisor Professor Tapio Salmi for the support and advice during all the research work and cooperation since many years.

Finally, I need and wish to thank my wife Petya for all the support and help that I received, not only for this work, but also throughout our married life.

Isabelle and Sebastien, thank you for making every moment count.

Daniel Valtakari
Turku, 2015

Abstract

Daniel Valtakari

The role of metal ions in selective and sustainable processes

Doctoral thesis, Laboratory of Industrial Chemistry and Reaction Engineering, Johan Gadolin Process Chemistry Centre (PCC), Faculty of Science and Engineering, Åbo Akademi University, 2015.

Keywords: ferric sulphate, ferrous sulphate, sulphuric acid, active carbon, noble metals, oxidation, reduction, kinetic modelling, water purification, iron, indium, gallium, germanium, zinc, tannic acid, tannin, catalyst, hydrometallurgy, precipitation, recycling.

Sustainability and recycling are core values in today's industrial operations. New materials, products and processes need to be designed in such a way as to consume fewer of the diminishing resources we have available and to put as little strain on the environment as possible. An integral part of this is cleaning and recycling. New processes are to be designed to improve the efficiency in this aspect.

Wastewater, including municipal wastewaters, is treated in several steps including chemical and mechanical cleaning of waters. Well-cleaned water can be recycled and reused. Clean water for everyone is one of the greatest challenges we are facing today.

Ferric sulphate, made by oxidation from ferrous sulphate, is used in water purification. The oxidation of ferrous sulphate, $FeSO_4$, to ferric sulphate in acidic aqueous solutions of H_2SO_4 over finely dispersed active carbon particles was studied in a vigorously stirred batch reactor. Molecular oxygen was used as the oxidation agent and several catalysts were screened: active carbon, active carbon impregnated with Pt, Rh, Pd and Ru. Both active carbon and noble metal–active carbon catalysts enhanced the oxidation rate considerably. The order of the noble metals according to the effect was: Pt >> Rh > Pd, Ru. By the use of catalysts, the production capacities of existing oxidation units can be considerably increased. Good coagulants have a high charge on a long polymer chain effectively capturing dirty particles of the opposite charge. Analysis of the reaction product indicated that it is possible to obtain polymeric iron-based products with good coagulation properties.

Systematic kinetic experiments were carried out at the temperature and pressure ranges of 60-100°C and 4-10 bar, respectively. The results revealed that both non-catalytic and catalytic oxidation of Fe^{2+} to Fe^{3+} take place simultaneously. The experimental data were fitted to rate equations, which were based on a plausible reaction mechanism: adsorption of dissolved oxygen on active carbon, electron transfer from Fe^{2+} ions to adsorbed oxygen and formation of surface hydroxyls. A comparison of the Fe^{2+} concentrations predicted by the kinetic model with the experimentally observed concentrations indicated that the mechanistic rate equations were able to describe the intrinsic oxidation kinetics of Fe^{2+} over active carbon and active carbon-noble metal catalysts.

Engineering aspects were closely considered and effort was directed to utilizing existing equipment in the production of the new coagulant. Ferrous sulphate can be catalytically oxidized to produce a novel long-chained polymeric iron-based flocculent in an easy and affordable way in existing facilities. The results can be used for modelling the reactors and for scale-up.

Ferric iron (Fe^{3+}) was successfully applied for the dissolution of sphalerite. Sphalerite contains indium, gallium and germanium, among others, and the application can promote their recovery. The understanding of the reduction process of ferric to ferrous iron can be used to develop further the understanding of the dissolution mechanisms and oxidation of ferrous sulphate.

Indium, gallium and germanium face an ever-increasing demand in the electronics industry, among others. The supply is, however, very limited. The fact that most part of the material is obtained through secondary production means that real production quota depends on the primary material production. This also sets the pricing. The primary production material is in most cases zinc and aluminium. Recycling of scrap material and the utilization of industrial waste, containing indium, gallium and geranium, is a necessity without real options.

As a part of this study plausible methods for the recovery of indium, gallium and germanium have been studied. The results were encouraging and provided information about the precipitation of these valuables from highly acidic solutions.

Indium and gallium were separated from acidic sulphuric acid solutions by precipitation with basic sulphates such as alunite or they were precipitated as basic sulphates of their own as galliunite and indiunite. Germanium may precipitate as a basic sulphate of a mixed composition. The precipitation is rapid and the selectivity is good. When the solutions contain both indium and gallium then the results show that gallium should be separated before indium to achieve a better selectivity.

Germanium was separated from highly acidic sulphuric acid solutions containing other metals as well by precipitating with tannic acid. This is a highly selective method. According to the study other commonly found metals in the solution do not affect germanium precipitation.

The reduction of ferric iron to ferrous, the precipitation of indium, gallium and germanium, and the dissolution of the raw materials are strongly depending on temperature and pH. The temperature and pH effect were studied and which contributed to the understanding and design of the different process steps. Increased temperature and reduced pH improve the reduction rate.

Finally, the gained understanding in the studied areas can be employed to develop better industrial processes not only on a large scale but also increasingly on a smaller scale. The small amounts of indium, gallium and germanium may favour smaller and more locally bound recovery.

Referat

Daniel Valtakari

Metalljonernas roll i utvalda selektiva och hållbara processer

Doktorsavhandling, Laboratoriet för Teknisk kemi och reaktionsteknik, Processkemiska Centret Johan Gadolin, Fakulteten för Naturvetenskaper och Teknik, Åbo Akademi, 2015.

Nyckelord: ferrisulfat, ferrosulfat, svavelsyra, aktivt kol, ädelmetaller, oxidering, reducering, kinetisk modellering, vattenrening, järn, indium, gallium, germanium, zink, tanninsyra, katalysator, hydrometallurgi, utfällning, återvinning.

Hållbarhet och återvinning är centrala värden för dagens industriella verksamhet. Nya material, produkter och processer måste planeras på ett sådant sätt att de konsumerar mindre av de minskande tillgängliga resurserna och att de belastar miljön så litet som möjligt. En inbyggd del av detta är rengöring och återvinning. Nya processer bör planeras på ett sådant sätt att de förbättrar effektiviteten i detta hänseende.

Avfallsvatten, inklusive kommunala avloppsvatten, behandlas typiskt i flera steg, som omfattar kemisk och mekanisk rengöring av vatten. Väl rengjort vatten kan återvinnas och återanvändas. Rent vatten för alla är en av de största utmaningarna vi står inför i dag.

Ferrisulfat, som tillverkas genom oxidation av ferrosulfat, används inom vattenrening. Oxidationen av ferrosulfat, $FeSO_4$, till ferrisulfat i sura vattenhaltiga lösningar av H_2SO_4 över fint dispergerade partiklar av aktivt kol studerades i en tryckreaktor under kraftig omrörning. Molekylärt syre användes som oxidationsmedel och flera katalysatorer undersöktes: aktivt kol och aktivt kol impregnerat med Pt, Rh, Pd och Ru. Både aktivt kol och ädelmetall-aktivt kol katalysatorer ökade oxidationshastigheten avsevärt. Ordningen på ädelmetallerna enligt effektiviteten var: Pt >> Rh> Pd, Ru. Genom användning av katalysatorer kan tillverkningskapaciteten för befintliga oxidationsenheter heter ökas avsevärt. Goda koaguleringsmedel har en hög laddning på en lång polymerkedja som effektivt fångar smutspartiklarna av motsatt laddning. Analys av reaktionsprodukten indikerade att det är möjligt att erhålla polymera järnbaserade produkter med goda koagulationsegenskaper.

Systematiska kinetiska experiment utfördes inom ett temperatur- och tryckintervall på 60-100°C respektive 4-10 bar. Resultaten visade att både katalytisk och icke-katalytisk oxidation av Fe^{2+} till Fe^{3+} sker samtidigt. De experimentella data infördes i matematiska hastighetsuttryck, som baserade sig på en möjlig reaktionsmekanism: adsorption av upplöst syre på aktivt kol, elektronöverföring från Fe^{2+} joner till adsorberat syre och av hydrolys på ytan. En jämförelse av Fe^{2+}-koncentrationen förutspådd av den kinetiska modellen med de experimentellt observerade koncentrationerna indikerade att de kinetiska ekvationerna kunde förutspå den väsentliga oxidationskinetiken för Fe^{2+} över katalysatorer med aktivt kol och aktivt kol med ädelmetaller.

Tekniska aspekter beaktades noga och möda lades ned på att kunna utnyttja existerande utrustning i produktionen av den nya koagulanten. Ferrosulfat kan katalytiskt oxideras för att producera en ny långkedjad järnbaserad polymer på ett enkelt och förmånligt sätt i existerande anläggningar. Resultaten kan utnyttjas för reaktormodellering och uppskalning.

Trevärt järn (Fe^{3+}) utnyttjades framgångsrikt vid upplösningen av zinkblände (sphalerit), som innehåller bl.a. indium, gallium och germanium. Metoden kan främja återvinningen. Genom att förstå reduktionsprocessen av trevärt järn till tvåvärt järn kan man vidare utveckla förståelsen av upplösnings- och oxideringsmekanismen för ferrosulfat.

Indium, gallium och germanium står inför en hela tiden växande efterfrågan inom bl.a. elektronikindustrin. Utbudet är, tyvärr, begränsat. Faktumet att största delen av produktionen består av sekundär produktion betyder att den verkliga produktionen beror på den primära produktionen. Detta påverkar även prissättningen. Den primära produktionen ger i de flesta fall zink och aluminium. Återvinningen av skrot och utnyttjandet av industriavfall som innehåller indium, gallium och germanium är ett måste utan verkliga alternativ.

Som en del av denna studie undersöktes möjliga metoder för återvinningen av indium, gallium och germanium. Resultaten var uppmuntrande och gav information om utfällningen av dessa värdefulla metaller ur kraftigt sura lösningar.

Indium och gallium separerades ur sura svavelsyralösningar via utfällning med basiska sulfater såsom alunit eller så utfälldes de som sina egna basiska sulfater såsom galliunit och indiunit. Germanium kan utfällas i form av basisk sulfat av blandad sammansättning. Utfällningen är rask och selektiviteten är god. Då lösningen innehöll både indium och gallium så visade resultaten att gallium bör separeras före indium för att uppnå en bättre selektivitet.

Germanium separerades också från starkt sura svavelsyralösningar innehållande andra metaller genom utfällning med tanninsyra. Det här är en högselektiv metod. Enligt undersökningen påverkar inte andra vanligt förekommande metaller germaniumutfällningen.

Reduktionen av trevärt järn till tvåvärt järn, utfällningen av indium, gallium och germanium samt upplösningen av råmaterialen är kraftigt beroende av temperatur och pH. Temperatur- och pH-effekten studerades vilket bidrog till att förstå och planera de olika processtegen. Ökad temperatur och minskat pH förbättrade reduktionen.

Slutligen, den erhållna kunskapen inom de utforskade områdena kan utnyttjas för att utveckla bättre industriella processer inte bara i stor skala utan även allt mer i mindre skala. De små mängderna av indium, gallium och germanium kan gynna återvinningen i mindre och mera lokal skala.

Publications (and personal contribution)

1.	Markus, H., Fugleberg, S., Valtakari, D., Salmi, T., Murzin, D. Yu., Lahtinen, M., 2004a, Kinetic modelling of a solid–liquid reaction: reduction of ferric iron to ferrous iron with zinc sulphide. Chemical Engineering Science, Volume 59, Issue 4, p 919–930. **Major contribution:** Experimental work.
2.	Markus, H., Fugleberg, S., Valtakari, D., Salmi, T., Murzin, D. Yu., Lahtinen, M., 2004b, Reduction of ferric to ferrous with sphalerite concentrate, kinetic modelling. Hydrometallurgy, Volume 73, Issues 3–4, p 269–282. **Major contribution:** Experimental work.
3.	Rönnholm, M. R., Wärnå, J., Valtakari, D., Salmi T., Laine, E., 2001, Kinetics and mass transfer effects in the oxidation of ferrous sulfate over doped active carbon catalysts, Catalysis Today 66, p 447-452. **Major contribution:** Experimental work, editing the article.
4.	Valtakari, D., 1999, Catalytic Preparation of Ferric sulphate, Licentiate Thesis. Åbo Akademi University, Laboratory of Industrial Chemistry and Reaction Engineering, Turku. **Major contribution:** Experimental work, writing the thesis.
5.	Valtakari, D., Rönnholm, M. R., Wärnå, J., Salmi, T., Laine, E., Luoma, M., (2001, submitted for publication, unpublished), The intrinsic kinetics of ferrous sulphate oxidation on active carbon. **Major contribution:** Experimental work, writing the article.

Other publications and conference presentations

Salmi, T., Tirronen, E., Lehtonen, J., Paatero, E., Valtakari, D., 2003, Modeling of Complex Organic Solid-Liquid Reaction Systems in Stirred Tanks, Ind. Eng. Chem. Res. 2003, 42, 2516-2524.

Salmi, T., Tirronen, E., Lehtonen, J., Paatero, E., Valtakari, D., 2003, Modelling of Complex Organic Solid-Liquid Reaction Systems in Stirred Tanks, Industrial & Engineering Chemistry Research, Vol. 42, Nr. 12, Pages 2516-2524

Salmi, T., Valtakari, D., Paatero, E., Holmbom, B., Sjöholm, R., 1993, Kinetic study of the carboxyalkylation of cellulose, Institutionen för teknisk kemi, Kemisk-Tekniska Fakulteten vid Åbo Akademi Åbo Akademi publications

Salmi, T., Valtakari, D., Paatero, E., Holmbom, B., Sjöholm, R., 1994, Kinetic Study of the Carboxymetylation of Cellulose, Industrial & Engineering Chemistry Research, Vol. 33: Issue 6: Pages 1454-1459, June 1994

Valtakari, D., Rönnholm, M. R., Wärnå, J., Salmi, T., Laine, E., Luoma, M., (1999), The intrinsic kinetics of ferrous sulphate oxidation on active carbon, Europacat – IV, 1999

Rönnholm, M. R., Wärnå, J., Valtakari, D., Salmi T., Laine, E., 2000, Kinetics and mass transfer effects in the oxidation of ferrous sulfate over doped active carbon catalysts, Third International Congress “Catalysis in Multiphase Reactors” CAMURE 3, Naples 29-31 May 2000

List of Appendices

Societal background

The purpose of the thesis is to discuss the need for environmentally friendly and sustainable methods based on the oxidation and reduction of iron in H_2SO_4 solutions.

A new water purification agent, a flocculent, for primarily municipal waste waters was invented and produced by oxidation of ferrous sulphate in aqueous solution of H_2SO_4 to long chained polymeric ferric sulphate along with a new production method developed for the purpose. This goal had previously not been achieved despite numerous research efforts in the field. In order to obtain the desired product, a new catalytic production method was needed. The new agent is non-toxic and environmentally friendly in its use and more efficient compared to aluminium-based flocculants. It also flocculates more efficiently and sediment more rapidly compared to earlier iron based flocculants and references, Figure 1. The iron-based agent is also less expensive than the competing aluminium-based one. The developed kinetic model for the oxidation reaction including catalysts can be used for further simulations and reactor design.

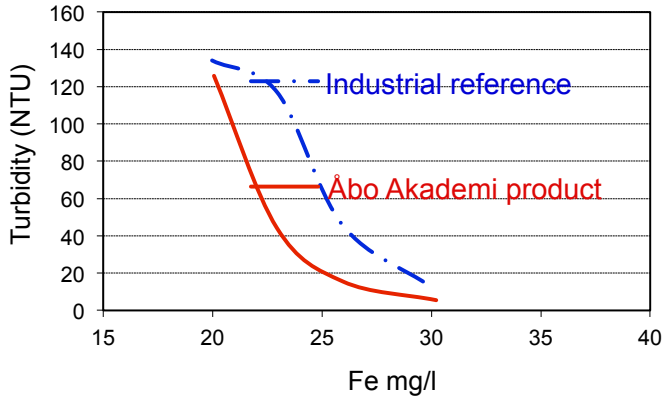

Figure 1. A product from Åbo Akademi compared to an industrial reference, Kemira PIX-115.

Precipitation of indium, gallium and germanium was studied along with the reduction of ferric iron to ferrous iron in acidic H_2SO_4 solutions containing zinc sulphide or minerals containing zinc sulphide. The worldwide supply of these valuable metals, 0., is limited while the demand is increasing on a long perspective. It is therefore necessary to apply new production methods and explore sources, which are currently not interesting for various reasons. Indium, gallium and germanium are considered minor metals and are mainly produced as by-products in primary metals production, mainly zinc and aluminium (Alfantazi, 2003, Brown, 1998a,b; Kramer, 1998a,b).

Indium, gallium and germanium precipitation from highly acidic sulphuric acid solutions promote the development of sustainable recovery methods and advanced recirculation alternatives. Currently a great deal of these valuable metals are recovered as secondary products during primary production meaning that their supply and pricing depends on the primary production of mainly zinc and aluminium. Insufficient secondary recovery and recirculation is not yet efficient enough to affect this way of prising.

The studies were carried out as a part of industrial cooperation and a special focus was on the products and methods.

Estimated global availability of indium (In), gallium (Ga) and germanium (Ge) and production and price in 2002 and 2011, (Tolcin, 2012a,b; Brown, 2002a,b; Guberman, 2012a,b; Jaskula, 2012a,b; Jaskula, 2013; Kramer, 2002a,b; Jorgenson, 2002a,b, Licht et al., 2015; www.strategic-metal.typepad.com, 2015; Global and China Germanium Industry Report, 2013-2016; Polinares Consortium, 2012; Gibson, 2011).

Table 1. Estimated availability, production and price for indium, gallium and germanium. * Reserve estimation for indium is poor and will probably change and increase. Estimation vary between (metric tons) ~12 000 (Licht, 2015) to ~50 000 (Mikolajczak, 2009).

Metal	Estimated availability, Metric tons	Production 2001, Metric tons	Production 2011, Metric tons	Price 2001, €/gram	Price 2011, €/gram
Indium	11 875*	340	640	0.10	0.60
Gallium	>1 million*	203	474	0.53	0.57
Germanium	8 600	68	118	0.74	1.20

Contents

Introduction

Different processes and studies, seemingly independent from each other, at some point offer synergy effects and lead to new applications and ways of working. Sulphuric acid is the basis for many processes. It can be used for the production of water purification agents, for dissolution processes and for primary or secondary recovery and recirculation of valuable metals. The common factor in this work is sustainability and the responsibility for the environment we are living in.

1.1 Ferrous to ferric iron oxidation in this study

(Part 1)

Dating way back in time man has sought clean water. Clean water is needed in ever increasing amounts. This is partly because there is a rising number of people and partly because our way of life demands growing amounts of water per person.

Before modern water purification techniques were developed filtering and sedimentation was used to clean water, mainly from suspended solids. To speed up sedimentation dirt particles were flocculated. Originally natural coagulants were used (Prodanović et al., 2013; Birima et al., 2013) made from, for example, different kind of seeds. Later growing water consumption increased the demand for efficient industrially produced water purification agents. In large parts of the world, especially tropical countries, natural agents are still used (Birima et al., 2013).

The study and development of natural coagulants is still going on (Prodanović et al., 2013; Birima et al., 2013) and natural coagulants can be used along with other techniques in modern processes. Natural coagulants are part of the nutrients circulation in nature and their use seldom causes harm.

The requirements on clean water and water purification processes are increasing globally. At the same time a significant number of people live without enough affordable clean water although the right to clean water and sanitation is today considered to be a human right (UN, 2010).

Today's municipal water purification includes a wide array of technical options. The process optimation includes numerous parameters such as temperature, pH and type of natural waters in the area as well as health and safety issues. The chemicals that are used and the sludge that is produced by the purification process must not be hazardous for humans or any other kind of living organisms (plants, animals, etc.) (WHO, 1998; Abdullahi, 2011; Prodanović et al., 2013; Birima et al., 2013).

A typical process step in water purification is the coagulation and flocculation of suspended solids in the water. This is achieved by adding coagulants and, when necessary, flocculants. Al- and Fe-based coagulants are widely used. The coagulants have mostly a positive overall charge and will form neutral flocks with the usually negatively charged dirt-particles. Iron-based coagulants are considered safer and a large number of the literature concerned with the safety of coagulants in water purification deals with aluminium-based coagulants and purification and post-purification processes (sludge disposal etc.). Aluminium has no known function in living cells

(Prodanović et al., 2013) and is associated with Alzheimer's disease (Birima et al., 2013) and investigations regarding health effects are pending.

Iron-based coagulation agents include ferrous and/or ferric iron. Ferric iron based coagulants are produced by oxidising ferrous iron in highly acidic sulphuric acid solutions.

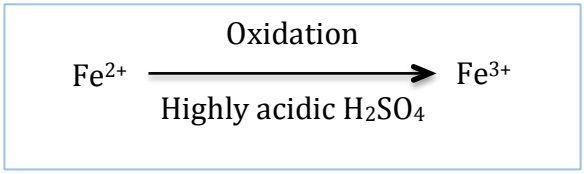

1.2 Ferric to ferrous iron reduction with zinc sulphide and sphalerite (Part 2)

Zinc and aluminium are two common metals in everyday use today. In historical times there was no available technology to produce them and the history of everyday aluminium and zinc use is therefore rather short. Nowadays the common production techniques for zinc include different hydrometallurgical processes (Lotens et al., 1987; Ekinci et al., 1998; Crundwell, 1987).

Hydrometallurgical zinc production processes involve leaching the zinc ore with highly acidic sulphuric acid solutions. The other way around zinc sulphide and sphalerite (zinc ore) can be used to reduce ferric iron to ferrous iron. Highly acidic sulphuric acid solutions are also used in oxidation-reduction processes containing ferrous and ferric iron. In addition to the reduction these processes include dissolution of solid particles. The understanding and modelling of these reactions contributes to the improvement of leaching and precipitation processes.

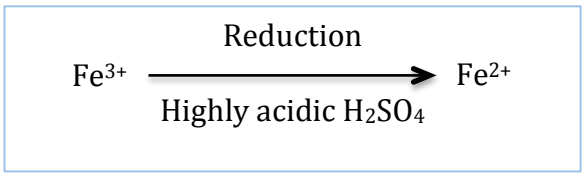

1.3 Indium, gallium and germanium recovery from acidic solutions (Part 3)

A typical industrial production process for new indium, gallium and germanium is a process where aluminium and zinc are the primary products and indium, gallium and germanium are secondary products (Alfantazi, 2003; Wurtz, 1880). This means that global availability of fresh indium, gallium and germanium is depending on the aluminium and zinc market demand. Indium, gallium and germanium are produced in very limited amounts and therefore any recyclable and recoverable material is valuable.

A great challenge for the indium, gallium and germanium production is the production process since the valuable metals are difficult to separate especially from zinc, iron and aluminium. A good yield may in some cases require complicated extraction processes and impact the efficiency and profitability of the process of primary products. Another challenge is the scrap material that is not recovered and recycled.

From the annual global production of indium, gallium and germanium about a quarter is lost after first use for different reasons, like non-profitable recovery. In many cases the reason is that the valuable metals exist in so small amounts in the appliances that it is not worth recovering and recycling them with today's processes. In the future we need, however, to improve the recycling (Licht et al., 2015). Recycling must be considered as a large process were the optimisation of the whole recycling process is more important than optimisation of individual partial process steps (Murzin, 2015). There are recycling systems in Europe, like the European Recycling Platform, http://erp-recycling.org/, but too often the result is that the materials end up in third world countries in landfills instead of being recycled. Africa has become (Azuka, 2009) the e-waste dumping ground for Europe, which can frequently be seen on international news media.

One step forward in the recycling is to make the processes simpler and applicable at local level. Waste should not be transported long distances for the reason that it cannot be treated properly. Parts that have no value should be disposed of at local facilities and valuable metals should be enriched and transported for further treatment at specialised facilities. Unnecessary transport should be avoided. Each of these steps is increasing sustainability.

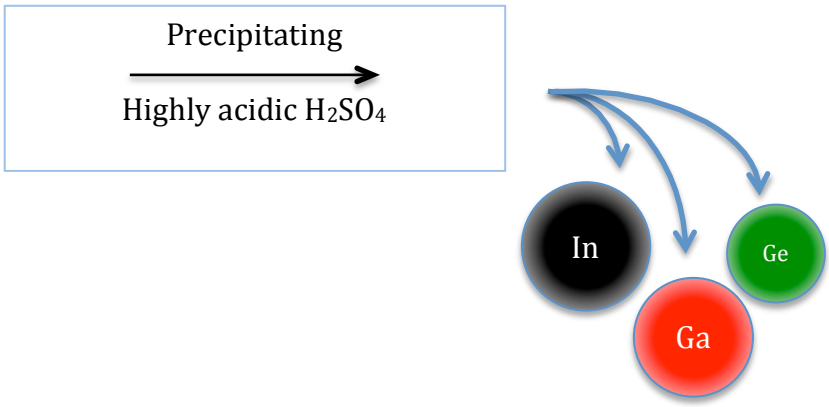

1.4 The main objectives of this thesis

The objectives of this work are to:

- Present a method to produce polymeric long-chained iron-based ferric sulphates for water purification purposes. To achieve this, suitable catalysts, a kinetic model of the oxidation of Fe^{2+} to Fe^{3+} and necessary reaction parameters will be introduced.
- Improve the understanding of the reactions between liquids and solids when reducing dissolved Fe^{3+} to Fe^{2+} in highly acidic solutions with zinc sulphide and sphalerite and the impact of the H_2SO_4-solvent on the process.
- Promote the understanding of indium, gallium and germanium precipitation from highly acidic sulphuric acid solutions that will contribute to sustainable production processes and new recovery and recirculation alternatives.

1.5 Part 1: Oxidation of Fe^{2+} to Fe^{3+}

Experimental and analytical section

The oxidation of the ferrous iron into ferric iron was carried out in a laboratory-scale pressurised autoclave (Parr 300 ml) equipped with an automatic data acquisition system that enabled continuous recording of the reactor pressure and temperature.

In order to perform successful oxidations on a laboratory scale, it was necessary to investigate the following:

- properties of materials needed in the oxidation,
- characterisation of the initial materials used,
- catalysts and catalyst properties,
- preparing the solution,
- oxidation of ferrous sulphate.

1.5.1 Properties and characterisation of the initial materials

Ferrous sulphate was selected according to industrial needs. The ferrous sulphate used was of technical quality and similar to that used in industrial processes. The sulphuric acid and the water used when dissolving the ferrous sulphate were both of high laboratory quality.

The ratios of the materials used defined the $[H_2SO_4]$-$[FeSO_4]$ and the [OH]-[Fe] ratios. These factors affected the product quality that the oxidation would give and the stability of the obtained products.

The $FeSO_4 \cdot 7H_2O$ content of the ferrous sulphate was calculated each time based on the titrimetric results from the analysis taken before the oxidation procedure. The initial amount of ferrous sulphate added to the mixture was fixed. The amounts of sulphuric acid and de-ionized water varied depending on the desired product and the [OH]-[Fe] and $[H_2SO_4]$-$[FeSO_4]$ ratios. In the production of Fe^{3+}-sulphates it is generally considered that $[H_2SO_4]$-$[FeSO_4]$ ratios between 0.30 and 0.50 enables the oxidation to give polymeric species, the optimum being found at the [OH]-[Fe] value 0.30.

1.5.2 Catalysts and catalyst properties

The active carbon catalysts used in this work were mainly based on the active carbon CPGlF / Fe60820A by Kemira. The particle size was analysed using Malvern 2601C and the average size of the carbon particles in the fraction was calculated from the particle-size distribution curves. The catalysts were characterised with nitrogen adsorption using Sorptomatic 1900, Carlo Erba Instruments.

Oxidation experiments were carried out with and without catalysts:

- oxidation without catalysts,
- oxidation with plain active carbons large particle size, app. 1-5 mm,
- oxidation with plain active carbon small particle size, < 45 μm, on average 14 μm,
- oxidation with active carbon support and a noble metal, small particle size, on average 18 μm,
- oxidation with fibrous catalyst supports,
- oxidation with noble metal coated mixer blades.

The purpose was to determine the non-catalytic and catalytic oxidation kinetics in order to optimise oxidation conditions.

1.5.3 Oxidation of ferrous sulphate

The dissolved Fe^{2+}-sulphate was oxidised in a pressurised semi-batch reactor with continuous oxygen input. The oxidation kinetics of $FeSO_4$-H_2SO_4 was studied at the temperature and pressure domains of 60–100°C and 0-10 bar, respectively. The initial concentration of $FeSO_4$ and H_2SO_4 were typically 2.4–2.6 M and 1.3 M, respectively.

After the initial Fe^{2+}-concentration was measured, the catalyst was added to the still warm solution. The reactor was closed and the stirring was switched on and gradually increased in order to disperse all of the catalyst with the $FeSO_4$-solution.

A vacuum was induced into the reactor so that no oxidation occurred while the temperature was elevated. The stirring was switched off during the vacuum procedure and then switched on again. The oxidation reaction at the desired temperature began when the oxygen entered the reactor. It was done in one of two alternative ways

1. constant oxygen in, but no flow-through, or
2. constant oxygen in and a flow-through.

Oxygen adsorption is efficient and the oxidation continues in an effective way, particularly when using the second option.

The solutions were oxidized for 2 hours and were then allowed to stay at room temperature for 48 hours. The measured noble metal content in the liquid phase also includes noble metal particles that have been mechanically removed from the active carbon surface by the vigorous stirring during the oxidation stage.

1.5.4 Analysis of Fe^{2+}

The concentration of Fe^{2+} in the acidic solution was determined by redox titration with a 0.100 M Ce-sulphate-solution. The inflexion point of the titration was recorded with a potentiograph equipped with Pt Titrode (zero...80°C) and Pt 1000 /B/2 (-50...+80°C) electrodes. The titration equipment that was used was Metrohm 736 GP Titrino, 728 Stirrer and Canon BJC-4200 printer.

Volumes of Ce-sulphate less than 2 ml after titration are not recommended due to difficulties in dosing accuracy. The first titration should be repeated, but later on that is not possible if short sample intervals are used. With active catalysts, the sample is further oxidised while waiting to be titrated. A sample of oxidised solution was analysed in 8 to 10 minutes. Samples should be taken only prior to titration.

1.5.5 Product characterisation

1.5.5.1 Ferron test for product characterisation

The existence of polyferric iron was investigated using a ferron-test, which is based on the measurement of the decomposition of Fe^{x}-compounds (x = +2, +3) in a ferron-solution (8-hydroxy-7-iodoquinoline-5-sulfonic acid at pH 4.3). The decomposition was observed at 600 nm with a Varian Series 634 spectrophotometer and the information was collected through a PICO ADC-16 to a data acquisition unit.

The reaction of mono- and polynuclear iron with ferron can be expressed as irreversible reactions as described below:

$$Fe_m + \text{ferron} \xrightarrow{k_m} \text{Fe-ferron} \qquad \text{Equation 1}$$

$$Fe_p + \text{ferron} \xrightarrow{k_p} \text{Fe-ferron} \qquad \text{Equation 2}$$

Fe_m = mononuclear Fe species Fe_p = polynuclear Fe species
k_m = mononuclear rate coefficient k_p = polynuclear rate coefficient

Fe-ferron denotes a common product and the exact stoichiometries of the reactions are ignored. Degradation of Fe_p to Fe_m may be a prerequisite for the formation of Fe-ferron from polynuclear species, but this rate-limiting step is included in k_p and the reaction is described accurately. Provided the quantity of ferron clearly exceeds that of Fe, the reaction rate will only be dependent on the amount of Fe.

1.5.5.2 Coagulation and flocculation tests for the product characterisation

The water purification effects of the obtained products were investigated using coagulation and flocculation tests. For water purification, if the same amount of coagulant of similar character is added, the better result is generally found with the coagulant with a higher overall charge. A product with better performance is assumed to have a higher overall charge and is considered more polymerised. Where all Fe^{2+} has been oxidised to Fe^{3+}, all iron is also polymerised.

The basic idea of coagulation and flocculation is that since most dirt-particles and pollutants have a negative charge, a molecule with a positive charge attaches to the surface of the dirt-particles and pollutants and a flock will be formed.

1.5.5.2.1 General water purification principle

Water purification includes the removal of dirt particles from wastewater. Especially small particles tend to float around and are unwilling to sediment in a reasonable time. For this purpose chemicals are added to coagulate with the dirt particles and subsequently form flocks. These flocks sediment rapidly enough for the process purposes.

Chemicals that are used generally include Al- or Fe-based hydroxides or sulphates or a mix of these. The choice of coagulants depends on for what purpose the purified water will be used and of the water purification process itself.

Before entering into the coagulation and flocculation steps the water must be screened, a step where particles large enough to be filtered are removed, and the pH must be adjusted according to the requirements of the following process steps. The coagulation and flocculation steps are enhanced if the water is to some extent alkaline. Acidic water can be adjusted to proper alkalinity by addition of hydroxides, lime or similar products. Too alkaline water can be treated with different acids, such as sulphuric acid or hydrochloric acid. Proper pH is important also, together with other factors, to limit the solubility of possible hazardous metals that can dissolve in the water after the purification process. Aluminium in water has been evaluated as a possible hazard (WHO, 1998).

1.5.5.2.2 Coagulation

Coagulation in water purification is a process where finely dispersed dirt particles are destabilised by a chemical that is added to the water. The destabilisation will cause the dirt particles to lump together forming larger flocks (WHO, 1996a).

The principle of coagulation is that when a salt with an overall positive charge is added to the water it will adsorb on the surface of the dirt particles that usually have a negative charge leading to a neutralisation of the charge of the formed new agglomerated particle (Engelhardt, 2010). Coagulation can be achieved both with natural coagulants as well as with synthetically produced ones (Prodanović et al., 2013).

The coagulation step consists of a quick and vigorous step where the coagulant chemical is added to the water. The time frame for the reaction step is no more than a fraction of a second to a few seconds. The mixing does not add value after the first seconds and a prolonged high energy mixing can instead lead to poor flocculation results in the next process step.

1.5.5.2.3 Flocculation

Flocculation is the process step following the coagulation step where the flocks are formed and then sedimented in the next step, in sedimentation basins or in clarifiers (WHO, 1996a).

Contrary to the coagulation process step the flocculation requires gentle handling. The mixing is slow with low energy input. The aim of the mixing is to make as many particles collide as possible without braking them, thus forming large flocks. The retention time should be around 30-45 minutes. For this research the water purification plants in Turku, Finland, and Helsingborg, Sweden, were studied.

After the flocculation the clear water moves forward to the next steps and the sedimented flocks are removed.

1.5.5.2.4 Sedimentation

The sedimentation step following the flocculation is basically a step with basins where the water is slowly moving through a number of basins and running over the edge of the basins. The flocks sediment at the bottom of the basins and are later removed as sludge.

Clarifiers can replace the sedimentation step. In the clarifiers the water moves through a system of upwards broadening pipes. The water speed is reduced when the water moves upwards and the flocks then sediment (WHO, 1996a). The clarifiers may also be used together with the sedimentation step for added efficiency.

1.5.5.2.5 Water purification – testing the results

The water purification process is monitored through different tests. The most relevant in this study are the turbidity test and the Jar test. Both are used to determine the removal of solid particles (TSS = total suspended solids) from the treated water.

Turbidity can be measured separately or directly as part of the process. The jar test requires sample testing in the laboratory to especially find the proper dosage of the coagulant that is added to the process.

1.5.5.2.5.1 Turbidity

Solid particles in the water reduce the water clarity. This reduction effect is called turbidity. The turbidity of the treated water can be used to control the water purification process and define on its part the end process quality. Reducing the number of particles in the water, i.e. by coagulation and flocculation, reduces turbidity. Turbidity is measured by measuring the amount of light that is scattered by the solid particles in the water (Oram, 2015; WHO, 1996b).

Turbidity can be measured for example by nephelometric turbidity units (NTU) or Jackson turbidity units (JTU), both methods being roughly equal (WHO, 1996b). As an example, drinking water should have a turbidity of less than 5 NTU/JTU (TU = turbid-

ity unit). Turbidity can also be measured according to the ISO 7027 standard (ISO, 1999/2010).

1.5.5.2.5.2 Jar test

The purpose of the jar test is to simulate the water treatment coagulation and flocculation steps in the water purification plant (Satterfield, 2005). Mixing speeds match both the coagulation step, with vigorous high energy mixing, and the flocculation step, with a gentle low energy mixing to allow flocks to form. The jar test results are used for process optimisation (Zainal-Abideen, 2012).

The jar test will give results about the flocculation rate and the particle type, size and volume of the flocks as well as the number of flocks that are obtained. The jar test will also allow for turbidity measurements at given dosages and process parameters.

The jar test is typically carried out in six glass containers of 1 litre with paddle stirrers. A test scheme is designed and the coagulants are added to the different containers following this scheme. Different amounts of coagulants are added to the different containers. The stirring is in the beginning vigorous and later gentle. The lowest dosage is usually lower than the actual one in the process and in a corresponding way the highest dosage is higher than the one used in the process. The exact amount of coagulants, the time and speeds for rapid and gentle mixing is noted and at the end the turbidity of the water in the different containers is measured. Additional parameters such as pH, temperature, additives and flow rate impact of the process are noted and calculated (Christophersen, 2015).

In this study the jar tests were mainly carried out at Kemira Kemwater facilities in Helsingborg, Sweden. Later Kemira carried out the analyses of the produced ferric sulphates without returning further results. The results were compared to Kemira's PIX products that were use as a standard in the project. At Åbo Akademi the focus was on the development of the oxidation process for the ferric sulphate production. The jar tests carried out by Åbo Akademi, both at Åbo Akademi and Kemira Kemwater in Helsingborg included the use of only one container per experiment (compare to Satterfield, 2005).

1.5.5.3 RAMAN-spectroscopy for the product characterisation

RAMAN-spectroscopy was used in the analysis of the raw material, the initial solutions and the final products. The RAMAN-spectrometer used was a BRUKER IFS (Bruker IFS Users manual). The laser was a Nd-YAG type laser: A pulsating laser, which was adjustable from 0 to 350 mW cw with a wavelength of 1.064 μm. At this wavelength no fluorescence appeared from impurities in the sample. The sensitivity of the detectors is also very high at this NIR (near infra red) wavelength.

The type of the RAMAN instrument used was FTRaman (Fourier transform) with a thickness of 1.0 cm, including the mirror. The data acquisition unit was based on digitalisation of the detector signal and the software used included several analytical functions such as inverse Fourier-transformation, Kramers-Kronig-analysis and supports RAMAN analysis.

1.5.6 Catalyst and end product characterisation results

The active carbon catalysts used in the present work were mainly based on the active carbon product CPGlF / Fe60820A obtained from Kemira. The fine ground carbon powder was prepared as part of the work in the Laboratory of Industrial Chemistry at Åbo Akademi. Only the fraction with a particle diameter below 45 μm was accepted with an average size of the carbon particles of 13.6 μm based on calculations done from the size distribution curves.

The active surface area was determined by physisorption, BET specific area, and it was 835 m^2/g for the studied catalysts. The specific pore volumes were 0.73 cm^3/g (**Appendix I, Physisorption**).

The dispersion of noble metals on active carbon support was determined by hydrogen adsorption. The adsorption isotherms were obtained at 25°C (for Pt and Rh) and 90°C (for Pd) and pressure $0.1\text{-}10^{-4}$ bar. The amount of reversible adsorbed gases was determined using the back-sorption method. Extrapolation of the adsorption isotherms to zero pressure was used for the determination of irreversibly adsorbed gases. Prior to hydrogen chemisorption, the catalysts were reduced at 300°C for 2 hours, followed by evacuation at 300°C and 10^{-6} bar for one hour. The purpose of the chemisorption was to determine the dispersion of the noble metal over the active carbon, and thus to form a model for the calculations of the respective values of r_x (x = noble metal) and so to separate the different catalytic effects from the non-catalytic oxidation effect (**Appendix I, Chemisorption**).

1.5.7 Ferron test on end products

The ferron test can be utilized for both quantitative and qualitative analysis. The purpose of quantitative and semi-quantitative ferron analysis is to measure the exact changes in the amounts of polymeric species of polyferric sulphate produced. The quantitative analysis is based on the difference between the base line and the curve. The difference between the two lines mentioned shows the amount of the polymeric product obtained.

The results from the ferron tests performed on the samples produced in this work were not reliable. The solutions did not show any activity when small sample quantities were used, and larger amounts of the sample precipitated. When analysed a pattern in the behaviour of the samples was found and this behaviour was used for qualitative comparison between different samples. The analytical response is stronger when the sample size is large enough. This will lead to the precipitation of the sample that has reacted with ferron.

The narrow area of operation where sufficient sample can be added into the test so that a curve will be seen but no precipitate will be obtained can then be avoided. The sample sizes used were also not dependent on a single factor, the sample in question alone, but several independent samples could be analysed with a proper dosage and the results could be compared. Since quantitative ferron analysis was not required, this method was more informative.

1.5.8 Coagulation and flocculation tests on end products

The products prepared at the Laboratory of Industrial Chemistry were compared to the Kemira products PIX-115 and PIX-322 in a standard synthetic wastewater solution. According to the tests significantly less of the Åbo Akademi coagulant is needed in wastewater cleaning compared to the PIX-standards (Valtakari, 1999). Savings of up to 15% in coagulant amounts are possible when using the formula developed at Åbo Akademi during this study.

1.5.9 RAMAN-spectroscopy on end products

The purpose of the RAMAN-spectroscopic investigations was to determine the existence of new polymeric ferrisulphate species. The product solution contained water that was also visible in RAMAN spectroscopy.

Several solutions with varying components included in the final product solution were tested and then matched against the product solution. Solutions produced with stoichiometric ratios that would not permit polymeric ferric sulphates were also analysed.

In the range of 1200 to 2200 $\Delta\rho/cm^{-1}$ the favourable product gives a response double to that of the unfavourable product. This range was interpreted to show additional OH-groups. These additional OH-groups are situated in the structure of what has now become a polymeric ferric species. In the more typical case where stoichiometric conditions are unfavourable to the formation of polymeric species the response in the RAMAN spectrum shows OH-groups in the water.

Results section

1.5.10 Kinetic experiments

A reaction mechanism for the oxidation of ferrous sulphate over active carbon was proposed by Valtakari et al. (2001), Valtakari (1999) and Rönnholm et al. (1999a). Oxidation was presumed to proceed on the active carbon surface, where the oxygen is dissociatively adsorbed. Fe^{2+} ions donate an electron to the adsorbed oxygen, which reacts with a hydronium ion forming a surface hydroxyl and releasing water. Two surface hydroxyls form water, leaving an oxygen-covered and a vacant site on the catalyst surface. The mechanism is summarised as follows (Valtakari, 1999):

Reaction step			Stoichiometric number (v')					
I	O_2	+	2*	⇌	2O*	+		¼
II	Fe^{2+}	+	O*	⇌	Fe^{3+}	+	O^{*-}	1
III	O^{*-}	+	H_3O^+	⇌	OH*	+	H_2O	1
IIIb	O^{*-}	+	H_2SO_4	⇌	OH*	+	HSO_4^-	1
IIIc	O^{*-}	+	HSO_4^-	⇌	OH*	+	SO_4^{2-}	1
IV	OH*	+	OH*	⇌	H_2O*	+	O*	½
V			H_2O*	⇌	H_2O	+	*	½
	Fe^{2+}	+	¼ O_2 + H_3O^+	⇌	Fe^{3+}	+	$^3/_2$ H_2O	

Equation 3

H_2SO_4 is a strong acid with a high degree of dissociation and the formation of surface hydroxyls is solely attributed to the hydronium ion in the above mechanism, leaving steps IIIb and IIIc out of the equation.

Steps I and II are considered to contribute to the overall oxidation rate. Further, it has been assumed that only step II is a rate-determining step (rds). Steps I, III, IV and V are expected to be rapid so the quasi-equilibrium hypothesis can be applied and the overall oxidation velocity is then given by (Valtakari, 1999; Valtakari et al., 2001)

$$r = r_2 = k_2 c_{Fe^{2+}} \theta_O - k_{-2} c_{Fe^{3+}} \theta_{O^-}$$

Equation 4

The coverages of the corresponding species are denoted by θ_o and θ_{o^-}. The application of the quasi-equilibrium approximation to steps I and III-V implies that

$$K_1 = \frac{\theta_O^2}{c_O \theta_v^2}$$

Equation 5

$$K_3 = \frac{\theta_{OH} c_w}{\theta_{O^-} c_{w^+}}$$

Equation 6

$$K_4 = \frac{\theta_w \theta_O}{\theta_{OH}^2}$$

Equation 7

$$K_5 = \frac{c_w \theta_v}{\theta_w}$$

Equation 8

where the subscripts – o, v, w and w+ – refer to oxygen, vacant sites, water (H_2O) and hydronium ions (H_3O^+), respectively. The surface coverage can be solved as a function of the fraction of vacant sites (θ_v) from Equations (5)-(8).

The expressions for θ_{O+} and θ_{O-} are inserted in the rate Equation (4) and the equilibrium constant for the overall reaction is thus given by

$$K_c = K_1^{1/4} K_2 K_3 K_4^{1/2} K_5^{1/2}$$

Equation 9

The rate equation becomes

$$r = k_2 K_1^{1/2} c_O^{1/4} c_{W^+}^{-1} (c_{Fe^{2+}} c_O^{1/4} c_{W^+} - \frac{c_{Fe^{3+}} c_W^{3/2}}{K_c}) \theta_v$$

Equation 10

The vacant sites fraction is solved from the site balance ($\theta_O + \theta_W + \theta_{OH} + \theta_{O-} + \theta_v = 1$). The expressions of the coverages, obtained from Equations (5)-(8), are inserted in the site balance and θ_v is solved as

$$\theta_v = \frac{1}{K_1^{1/2} c_O^{1/2} + K_5^{-1} c_W + K_1^{1/4} K_3^{-1} K_4^{-1/2} K_5^{-1/2} c_O^{1/4} c_W^{3/2} c_{W^+}^{-1} (K_3 c_W^{-1} c_{W^+} + 1) + 1}$$

Equation 11

The simplifying notations

$$K_0 = K_1,\ K_w = K_5^{-1},\ K' = K_1^{1/4} K_3^{-1} K_4^{-1/2} K_5^{-1/2},\ K'' = K_1^{1/4} K_4^{-1/2} K_5^{-1/2}$$

are introduced and the fraction of vacant sites becomes

$$\theta_v = \frac{1}{K_O^{1/2} c_O^{1/2} + K_W c_W + (K' c_W c_W^{-1} + K'') c_O^{1/4} c_W^{1/2} + 1}$$

Equation 12

The product $k_2K_1^{1/2}$ is now written as a constant $k' = k_2K_1^{1/2}$ and θ_v is inserted in Equation (10) giving the rate equation

$$r = \frac{k' c_O^{1/4} c_{w^+}^{-1} (c_{Fe^{2+}} c_O^{1/4} c_{w^+} - \frac{c_{Fe^{3+}} c_w^{3/2}}{K_C})}{K_O^{1/2} c_O^{1/2} + K_W c_W + (K' c_W c_{W^+}^{-1} + K'') c_O^{1/4} c_W^{1/2} + 1}$$

Equation 13

1.5.11 Non-catalytic reaction mechanism and rate equation

The non-catalytic gas-liquid reaction rate and mechanism as well as the liquid-phase process between Fe^{2+}-ions and dissolved oxygen are described by Valtakari (1999), Valtakari et al. (2001) and Rönnholm et al., (1999a).

The non-catalytic reaction mechanism is expected to advance with the formation of an intermediate complex between dissolved oxygen and Fe-ions and the cleavage of the O-O-bond of the complex. When two Fe^{2+} ions are added to dissolved oxygen it will lead to the formation of a peroxide-type complex that is quickly decomposed. The rate-determining step is expected to be the successive addition of Fe^{2+} ions to oxygen and is summarised as

$Fe^{2+} + O_2 \rightarrow Fe\text{-}O\text{-}O^{2+}$ (I)
$Fe^{2+} + Fe\text{-}O\text{-}O^{2+} \rightarrow Fe\text{-}O\text{-}O\text{-}Fe^{4+}$ (II)

Then remaining steps are combined to a quasi-equilibrium

$2\ Fe^{2+} + 4\ H_3O^+ + Fe\text{-}O\text{-}O\text{-}Fe^{4+} \rightleftharpoons 4Fe^{3+} + 6\ H_2O$ (III)

The rate expression for the non-catalytic process is thus obtained by applying the steady-state hypothesis to steps I and II ($r_1 = r_2$) and the quasi-equilibrium hypothesis to step III

$$r' = \frac{k_{nc2} K_{nc1} c^2_{Fe} c_O}{1 + k_{nc2} \frac{K_{nc1}}{k_{nc1}} c_{Fe}} (1 - f)$$

Equation 14

f is the factor for reverse reaction rate for the process and since the reaction equilibrium is strongly shifted to the products, f was approximated to be zero. (**Appendix I**)

1.5.12 Simplified rate equations

The general rate model for catalytic oxidation, Equation (13), contains several adjustable parameters. In order to reduce the number of adjustable parameters, the original model has to be simplified. If some of the surface intermediates can be assumed to be more plentiful than others and the concentrations of the surface hydroxyls and water can be considered negligible compared to those of O* and O*- ($K_W \approx 0$ and $K'' \approx 0$) then simplified rate equation (13) becomes

$$r = \frac{k' c_O^{1/4} (c_{Fe^{2+}} c_O^{1/4} c_{w^+} - \frac{c_{Fe^{3+}} c_w^{3/2}}{K_C})}{(K_O^{1/2} c_O^{1/2} + 1) c_{W^+} + K' c_O^{1/4} c_W^{3/2}}$$

Equation 15

If on the other hand oxygen and water are the dominating surface compounds then the simplified rate equation becomes

$$r = \frac{(\frac{k'' c_O^{1/4}}{c_{w^+}})(c_{Fe^{2+}} c_O^{1/4} c_{w^+} - \frac{c_{Fe^{3+}} c_w^{3/2}}{K_C})}{K_O'' c_O^{1/2} + 1} \approx k'' c_O^{1/2} c_{Fe^{2+}}$$

Equation 16

The rate equation (13) can be simplified even more, as the concentration of water can be assumed to be constant because of its high concentration, i.e. $K_W c_W \approx K'_W$. Equation (16) is now written as

$$r = \frac{(\frac{k'' c_O^{1/4}}{c_{w^+}})(c_{Fe^{2+}} c_O^{1/4} c_{w^+} - \frac{c_{Fe^{3+}} c_w^{3/2}}{K_C})}{K_O'' c_O^{1/2} + 1} \approx k'' c_O^{1/2} c_{Fe^{2+}}$$

Equation 17

where $k'' = k'/(K_W c_W)$ and $K_0'' = K_0^{1/2}/(K_W c_W)$

Fe^{2+} can be completely oxidized to Fe^{3+} in the presence of the catalyst. The rate equation can in that case be simplified with the irreversible case ($K_c \rightarrow \infty$), where the backward reaction terms are ignored. Factor k'' consists of a pre-exponential factor and an exponential term -E/RT.

1.5.13 Gas-liquid equilibrium

The concentration of dissolved oxygen appears in the rate equations, which was estimated from the oxygen solubility data in water, as described by the temperature-dependent correlation (Fogg et al., 1991)

$$\ln(\frac{atm}{H_O}) = A + \frac{B}{T} + C \ln T$$

Equation 18

where H_0 is Henry's constant and the coefficients A, B and C are listed in Table 2.

Table 2. Henry's coefficients for oxygen solubility in water (Fogg et al., 1991).

A	B	C	Temperature interval / K
-171.2542	8391.24	23.24323	273 - 333
-139.4850	6889.60	18.554	273 - 617

For a mixture of electrolytes, Weisenberger et al., (1996), have proposed the following relation:

$$\lg(\frac{c_{g,O}}{c_g}) = \sum_i (h_i + h_g)c_i$$

Equation 19

where h_i is an ion-specific parameter. Weisenberger and Schumpe (1996) extended the model of Schumpe (1993) to the temperature range of 273–353 K by assuming h_g, the gas-specific constant, to be a linear function of temperature:

$$h_g = h_{g,0} + h_T\,(T - 298.15\ K)$$

Equation 20

The numerical values used in this work are listed in Table 3.

Table 3. Gas solubility parameters in the temperature range 273 – 353 K (Weisenberger et al., 1996).

Parameters	h_i
$h_{G,O_2}/(m^3 kmol^{-1})$	0.0 -0.000334 (T/K-298.15)
$h_{H^+}/(m^3 kmol^{-1})$	0
$h_{Fe^{2+}}/(dm^3 kmol^{-1})$	0.1523
$h_{Fe^{3+}}/(dm^3 kmol^{-1})$	0.1161
$h_{SO_4^{2-}}/(dm^3 kmol^{-1})$	0.117

The mole fraction of oxygen at the gas-liquid interface is calculated from Henry's law,

$$x^*_{O_2} = \frac{p_{O_2}}{H}$$

Equation 21

The liquid phase concentration c_{O2}^* in the interface is calculated from $c^*_0 = x^*_{02}c_L$, c_L being the total concentration of the liquid.

In order to get a reliable value of the partial pressure of oxygen (p_{O2}) and as the solvent has a significant vapour pressure at the highest experimental pressures; the measured total pressure (P) has to be corrected with the vapour pressure of the H_2O-H_2SO_4-$FeSO_4$ solution, Equation (22).

$$p_{O_2} = P - \delta P_{H_2O}^{vp}$$

Equation 22

where P_{H2O}^{vp} represents the vapour pressure of water and δ is a correction factor depending on the solvent composition. The vapour pressure of water was calculated from a modified Antoine equation given by Reid et al., (1988)

$$\ln\left(\frac{P^{vp}}{Pc}\right) = \frac{(VP\ A)\,x + (VP\ B)\,x^{1.5} + (VP\ C)\,x^{3} + (VP\ D)\,x^{6}}{1 - x}$$

Equation 23

$$where \quad x = 1 - \frac{T}{Tc}$$

The parameters (VP A, VP B, VP C, VP D, Pc and Tc) are listed in Table 4.

Table 4. Physical parameters for vapour pressure calculations, (Reid et al., 1988).

VP A	-7.76451
VP B	1.45838
VP C	-2.77580
VP D	-1.23303
Tc[a]	647.14 K
Pc[a]	22.06 MPa
b_1	-0.2542
b_2	3.91
[a)] Lide, 1994	

The correction factor (δ) correlates to the proportion (weight) of sulphuric acid (w_{H2SO4}) in the solution. Based on data, published by Sippola (1992), an empirical correlation was generated

$$\delta = 1 + b_1 w_{H_2SO_4} + b_2 w_{H_2SO_4}^2$$

Equation 24

The values of the coefficients b_1 and b_2 are listed in Table 4.

According to calculations the vapour pressure of the solvent H_2SO_4 is usually in the range of 0.1 bar at 55°C and 0.6 bar at 100°C and going up to 9 bar at 200°C. The solvent vapour pressure has thus to be included in the model. This applies especially for the lowest experimental pressures and highest experimental temperatures.

The gas-phase mass transfer resistance of oxygen was considered to be insignificant, and the surface pressure p_{O2}^* was set to equal the bulk phase pressure of oxygen, p_{O2}. Since the oxygen concentration was high in the gas phase, the surface concentration of oxygen could be calculated from

$$c_O = c_O^* = \frac{p_{O_2} c_L}{H}$$

Equation 25

The liquid phase was assumed to be saturated with respect to oxygen, and the liquid-side mass transfer resistance of oxygen was taken to be negligible due to the vigorous stirring in the reactor.

1.5.14 Liquid-phase mass balances

The experiments were carried out within the regime of kinetic control, and as such, the mass balances for the liquid-phase components in the vigorously stirred batch reactor become very simple. For Fe^{2+} and Fe^{3+} ions the equation can be written as

$$\frac{dn_i}{dt} = r_i m_{cat} + r_i' V_L$$

Equation 26

where r_i and r'_i are the component generation rates originated from the catalytic and non-catalytic processes, respectively (Valtakari, 1999; Valtakari et al., 2001). Other symbols are explained in the Notation. In addition, the liquid volume can be assumed to be constant during the reaction (except for the withdrawal of the samples); thus the differentiation of dn_i/dt gives $V_L\ dc_i/dt$. The catalyst bulk density is defined as $\rho_B = m_{cat}/V_L$. The final form of the mass balance now becomes

$$\frac{dc_i}{dt} = \rho_B r_i + r_i'$$

Equation 27

For oxygen, no separate mass balance is needed since the solution was assumed to be saturated with respect to oxygen; the calculated saturation concentration c_0^* was inserted in to the rate equation. The effect of the film reaction at the gas-liquid interface was confirmed to be negligible by the estimation of the Hatta-number of the pseudo-first order reaction at the beginning of the experiment. The Hatta-number turned out to be very small (0.074) which implies that the enhancement factor is close to 1 (Valtakari, 1999; Rönnholm et al. 1999b; Valtakari et al., 2001).

The stoichiometry relates the generation rates to the reaction rates

$$r_i = v_i r$$

Equation 28

$$r_i' = v_i r'$$

Equation 29

1.5.15 Computational procedures

The reactor model, i.e. the system of ordinary differential equations (ODEs) was solved numerically during the course of parameter estimation. Software (ODESSA, Hindmarsh, 1983) was used in the numerical solution. The kinetic parameters were estimated by minimising the sum of residual squares (Q),

$$Q = \sum_{j} \left(w_{j,Fe^{2+},\exp} - w_{j,Fe^{2+},calc} \right)^2$$

Equation 30

where w_{exp} and w_{calc} denote the experimental and the calculated (Equation 30) weight fractions of Fe^{2+} ions respectively. A hybrid simplex-Levenberg-Marquardt algorithm (Marquardt, 1963) was used in the numerical minimisation. The model solution and parameter estimation were carried out within the framework of the software package Modest (Haario, 1994) designed for simulation, estimation and experimental planning.

1.5.16 Kinetic results over active carbon

The kinetics of the active carbon catalysed oxidation was studied by performing a series of tests at temperatures 60°, 80° and 100°C and pressures 4, 7 and 10 bar. The carbon used in the tests was of fine quality and the average particle size was 14 μm. Diffusion resistance was not considered a limiting factor. The oxidation rate is more depending on temperature than on pressure as is shown in Figure 2. The amount of fine ground active carbon catalyst used was 4.8 %-wt. The catalytic enhancement of the oxidation is most prominent at the beginning of the oxidation. Later the interaction between catalyst particles and Fe^{2+}-ions diminishes due to the changes in the Fe^{2+}-concentrations.

Pure active carbon can be used successfully in the production of ferric sulphates. The larger amount of catalyst needed compared to the first experiment and catalysts lost is compensated for by the more attractive price of active carbon.

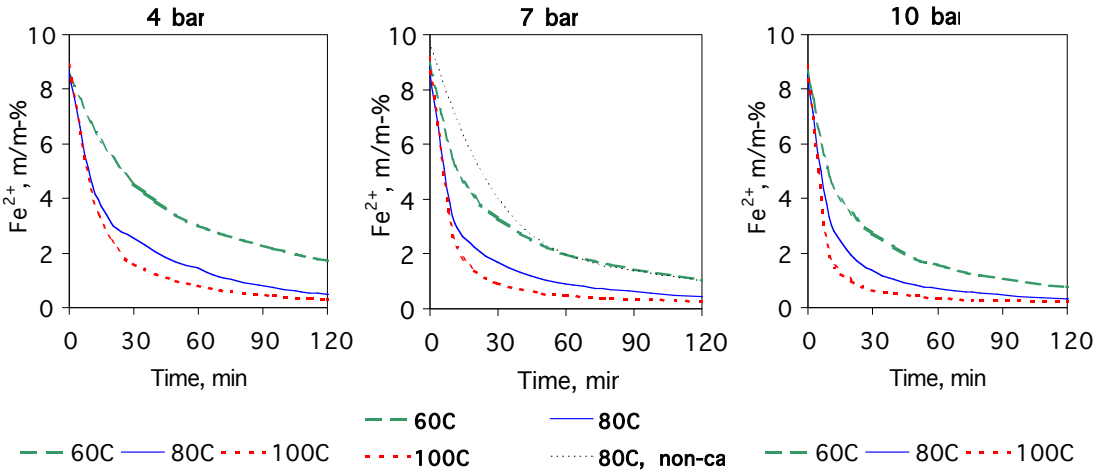

Figure 2. Oxidation kinetics from experiments on fine ground active carbon as a catalyst.

1.5.17 Kinetic results over combined active carbon–noble metal catalysts

To improve the oxidation kinetics further the use of noble metals on active carbon support was investigated. The improvement of the oxidation kinetics was significant. The strongest catalytic effect still appears in the beginning of the oxidation, but due to the more powerful catalyst, oxidation continues longer. In addition, the ferrous sulphate can now undergo serious oxidation at lower temperatures. This may be of benefit both in the production of polymeric ferric species, and in improved cost efficiency in further applications.

The noble metals that were used were Pt, Rh, Pd and Ru. All noble metals were on the active carbon support, the average particle size being 18 μm, and with 1 %-wt of noble metal content. The amount of catalyst used in the oxidation was 1.2 %-wt (Pt, Rh), 6 %-wt (Ru) and 3 %-wt (Pd).

The highest oxidation rate for Fe^{2+} was achieved with Pt on an active carbon support, as presented in Figure 3. The Pd-catalyst was on a granulated active carbon support, which may have affected the diffusion of the solution. The comparison of the noble metal catalysts leads to the following conclusion: Pt >> Rh > Pd > Ru.

The solubility of Pt and Ru in the ferrous sulphate solution was also studied by ICPM-analysis. For Pt, the dissolved amount, 0.17 %-wt, was negligible. For Ru the dissolved amount was 3.75 %-wt.

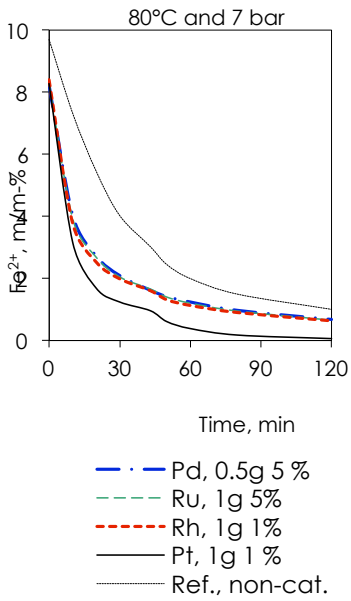

Figure 3. The effect of noble metals on the active carbon support (experimental results).

Since the particle size and the total amount of catalyst, noble metal + active carbon, were the same for both Pt and Ru, the conclusion is that Pt on an active carbon support is more suitable for the hostile environment of the ferric sulphate solution than Ru, in addition to the better catalytic capacity.

Generally, the most suitable noble metal is Pt. It is efficient at low temperatures, Figure 4. The polymeric ferric species were produced using Pt as a noble metal on the active carbon support.

A complete oxidation series was carried out for both Pt and Rh in the same way as for the fine ground active carbon. The temperatures used were 60°, 80° and 100°C and pressures 4, 7, 10 bar, Figures 4.-6. The conclusion is the same as with plain active carbon: temperature is more important than pressure for the oxidation as seen in Figure 4.

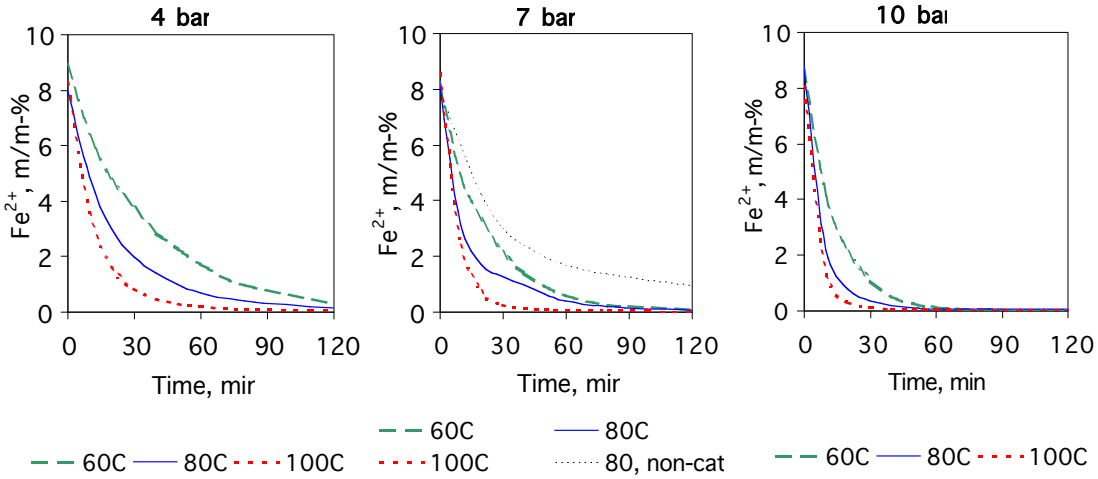

Figure 4. Platinum as the noble metal on an active carbon support. Experimental kinetic curves at different temperatures and different pressures.

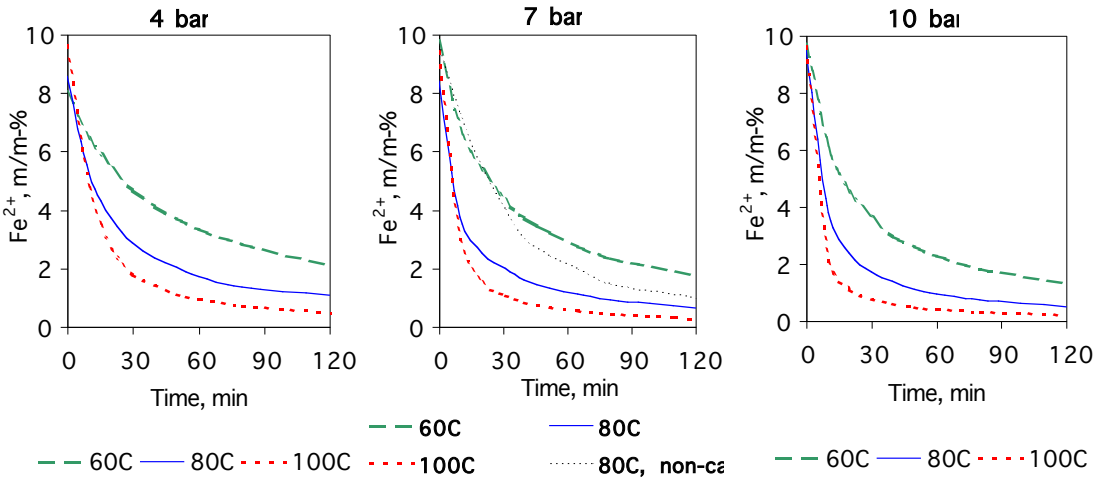

Figure 5. Rhodium as the noble metal on an active carbon support. Experimental kinetic curves at different temperatures and different pressures.

The most important catalysts are presented in Figure 6. The pure active carbon, Pt and Rh on active carbon support are compared to the non-catalytic oxidation.

The effect of different concentrations of catalyst on the oxidation of ferrous sulphate is shown in Figure 7. The mass of the catalyst and the oxidation time have been multiplied and the product of the values indicates the effect of the combination used. As can be seen from the figure, the values differ slightly from the mean value. This could be considered as part of the fluctuation during the experimental procedure. Taking the low levels of Fe^{2+} remaining at the end of the oxidation into account and the impact of a small analytic error on the final results, the conclusion is that oxidation with different amounts of catalysts follows a predictable behaviour and corresponds to the expected values.

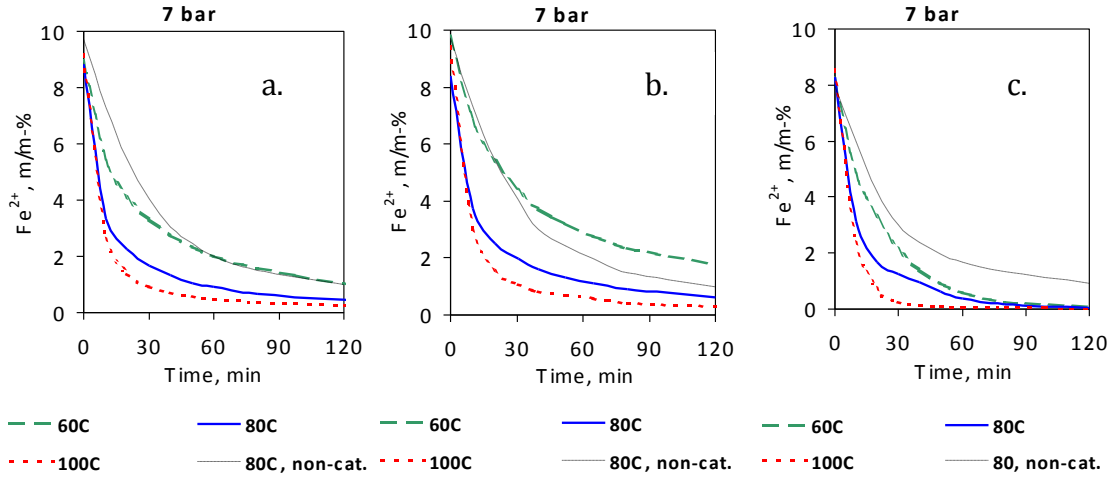

Figure 6. Oxidations with different catalysts at different temperatures and at 7 bar pressure: a. active carbon (fine ground), b. Rh 1% on an active carbon support and c. Pt 1% on an active carbon support, experimental values.

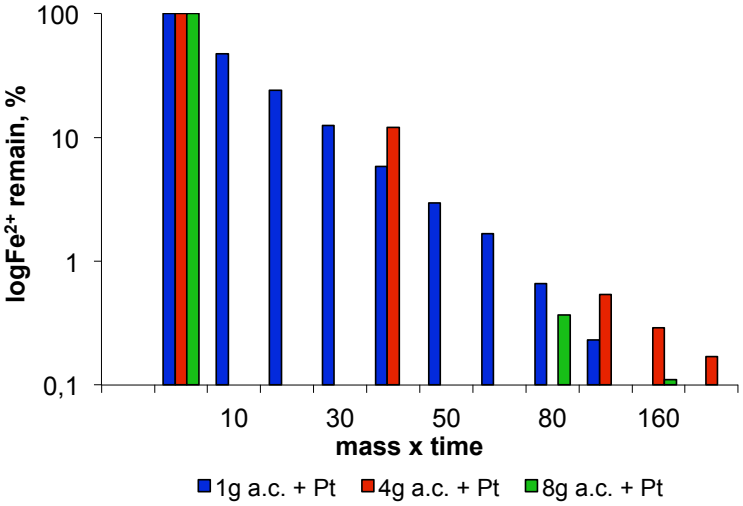

Figure 7. The effect of different catalyst concentrations on the oxidation of ferrous sulphate, experimental values.

The different types of oxidation (non-catalytic, catalytic with active carbon and catalytic with active carbon and a noble metal) under different conditions, Figure 8. , are compared in Table 5. The purpose was to estimate the time needed for Fe^{2+}-conversions of 90% and 99%. The estimation is based on simulations performed using the model and calculations presented earlier in this work.

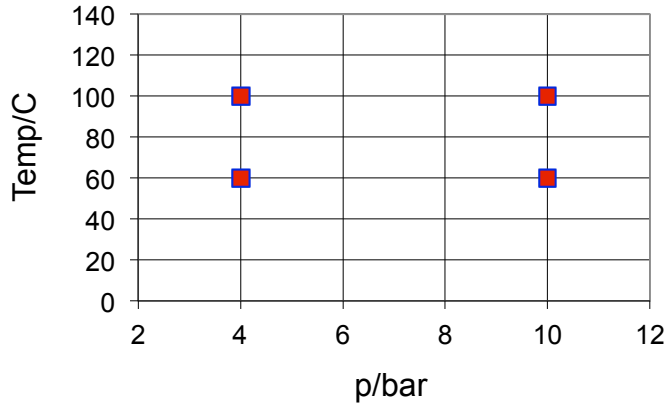

Figure 8. Experimental conditions for the compared non-catalytic, catalytic with active carbon and catalytic with active carbon and a noble metal experiments.

Table 5. The time (min) needed for the $Fe^{2+} \rightarrow Fe^{3+}$ -conversions of 90% and 99%. Amount of catalyst ≈ 27 g/l.

Oxidation	**4 bar**	**10 bar**	**4 bar**	**10 bar**	**4 bar**	**10 bar**	**4 bar**	**10 bar**
	60°C	**60°C**	**100°C**	**100°C**	**60°C**	**60°C**	**100°C**	**100°C**
	$Fe^{2+} \rightarrow Fe^{3+}$-Conversion 90%				*$Fe^{2+} \rightarrow Fe^{3+}$-Conversion 99%*			
Non-catal.	600	300	200	60	4700	1900	1400	470
Act.carbon	400	200	200	50	1200	700	400	170
Act.carb.+Pt	22	14	11	7	43	27	20	12

1.5.18 Modelling results

Typical kinetic results show, that the oxidation rate increases with increased temperature and oxygen pressure, temperature being more significant (Valtakari, 1999). The mechanistic rate equations (14) and (17) suggest that the reaction order might be between 1 and 2 for Fe^{2+}. In spite of the fact that saturation concentration of oxygen varies slightly during the course of the reaction because of the composition change in the liquid phase (Rönnholm et al., 1999a), it was assumed, as a first approximation, that the oxygen concentration is fairly constant in the liquid phase. Consequently, the experimental data can be checked using simple test plots for first and second order kinetics in batch reactors. For first and second order kinetics, the following time dependencies of the concentrations imply

$$y = \ln \frac{c_{0Fe^{2+}}}{c_{Fe^{2+}}} = k' t \qquad (1^{st} \text{ order})$$

Equation 31

$$y = \frac{c_{0Fe^{2+}}}{c_{Fe^{2+}}} - 1 = k' c_{0Fe^{2+}} t \qquad (2^{nd} \text{ order})$$

Equation 32

where c_{0Fe2+} is the initial concentration of Fe^{2+}. The ordinates (y) plotted versus the reaction time are displayed for some typical experiments in Figure 9. As the figure reveals, the overall reaction order with respect to Fe^{2+} is much closer to 2 than 1, which confirms the strong role of the non-catalytic oxidation in the overall process: the non-catalytic oxidation follows second order kinetics very closely Figure 9.

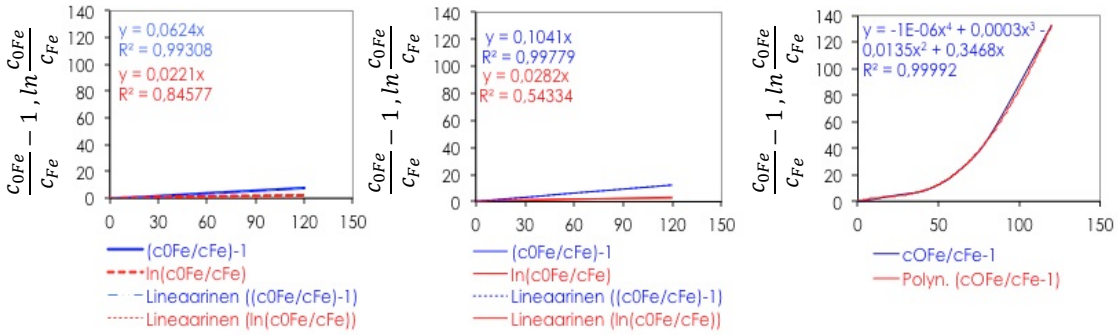

Figure 9. First (in red) and second (in blue) order plots for a non-catalytic and two catalytic oxidations of ferrosulphate. The R^2-values for second order plots exceed 0.99 and is for the first order plots considerably less indicating that the reactions are closer to second order than first order. Non-catalytic run (left), catalytic run with Rh on an active carbon support (middle), catalytic run with Pt on an active carbon support (right, trend line in red). T = 80°C and p = 7 bar, experimental results.

After this preliminary screening, the rate parameters were determined by non-linear regression analysis, and the results, which indicate that the catalytic processes have the apparent activation energy 32 kJ/mol, are summarised in Table 6.

Table 6. Kinetic parameters for the oxidation of Fe^{2+} over active carbon, estimated with non-linear regression

Total sum of squares (corrected for mean)			201.7	
Residual sum of squares			4.729	
Std. error of estimate			0.1953	
Explained (%): 97.66				
	Estimated Parameters	Estimated Std Error	Est. Relative Std Error (%)	Parameter/ Std. Error
k_0''	$0.507 *10^{-2}$	$0.117 *10^{-3}$	2.3	43.5
E/R	$0.393 *10^{4}$	$0.174 *10^{3}$	4.4	22.6

The correlation matrix of the parameters:

1.000

0.311 1.000

$$k'' = k_0'' e^{\frac{-E_a}{R}\left(\frac{1}{T}-\frac{1}{T_{ref}}\right)} \quad , k_0'' = \frac{l^{\frac{3}{2}}}{mol^{\frac{1}{2}} g min}$$

Examples of the fit of the model to experimental data are shown in Figures 1. and 2. in Appendix I. A comparison between the experimental and predicted concentrations of Fe^{2+} reveals that the proposed kinetic model is able to reproduce the experimental data with a satisfactory accuracy; the deviation between experimental and calculated concentrations always remained below 5%. The contour plots and the parameter estimation statistics (Tables 6. and 7.) show that the parameters are well identified: the relative standard error of the parameters is less than 5%.

Finally, the contributions of the non-catalytic and catalytic reaction rates under the experimental conditions were compared by calculating the ratio (F); defined as

$$F = \frac{r'}{r\rho_B}$$

Equation 33

where r' and r are obtained from Equations (14) and (17), respectively. The ratio was calculated within the range c_{Fe} = 0 … 2.2 mol/l (p_O = 4 bar 60°C and 10 bar 100°C), which corresponds the progress of a typical oxidation experiment. Ratio F is displayed in Figure 11. The figure shows that the non-catalytic contribution is most prominent at the beginning of the reaction and at high oxygen pressures. This is as expected on the basis of the rate equation (Equations (14-17): the reaction order with respect to oxygen is higher for the non-catalytic process, which verifies that the non-catalytic process is favoured by high oxygen pressure.

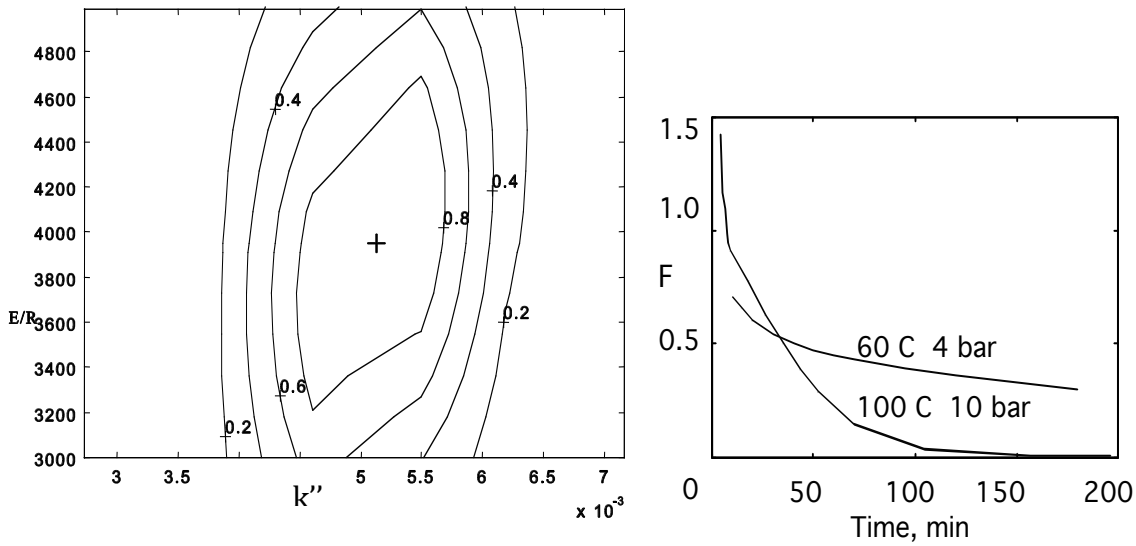

Figure 10. Contour plot for the activation energy and rate constant in catalytic oxidation of the ferrosulphate based on experimental results. (left)

Figure 11. The reaction rate ratio versus time for non-catalytic and catalytic oxidation of ferrous sulphate under different experimental conditions. The non-catalytic contribution is most prominent at the beginning of the reaction and at high oxygen pressures. (right)

1.5.19 The noble metal effect

After determination of the non-catalytic and catalytic effects of active carbon in ferrous sulphate oxidation, the results obtained were compared to the experimental data. Further, the experimental data from oxidations with noble metal on active carbon supports were fitted into the models and tested. This finally lead to the conclusion that the noble metal effect on the active carbon support in the oxidation of ferrous sulphate can be explained by and Equations 17, 34 and 35.

$$r = r_{\text{non-catalytic}} + r_{\text{catalytic, active carbon}} + r_{\text{catalytic, noble metal}}$$

Equation 34

$$r_{cat.,noblemetal} = \frac{(\frac{k''' c_O^{1/4}}{c_{w^+}})(c_{Fe^{2+}} c_O^{1/4} c_{w^+} - \frac{c_{Fe^{3+}} c_w^{3/2}}{K_C})}{K_O''' c_O'^{1/2} + 1}$$

Equation 35

Rate parameters were determined by non-linear regression analysis, and the results are summarized in Table 7.

Table 7. Kinetic parameters for the oxidation of Fe^{2+} over active carbon + noble metal, estimated with non-linear regression

Total sum of squares (corrected for means)	$0.1505 * 10^3$
Residual sum of squares	6.196
Std. error of estimate	0.2800

Explained (%): 95.88

	Estimated Parameters	Estimated Std Error	Est. Relative Std Error (%)	Parameter/ Std. Error
K_0''''	0.187	$0.592 * 10^{-2}$	3.2	31.6
E/R	$0.205 * 10^4$	$0.229 * 10^3$	11.2	9.0

The correlation matrix of the parameters:

1.000
0.496 1.000

$$k'' = k_0''^{\frac{-E_a}{R}(\frac{1}{T}-\frac{1}{T_{ref}})} \quad , k_0'' = \frac{l^{\frac{3}{2}}}{mol^{\frac{1}{2}} gmin}$$

1.6 Part 2: Ferric to ferrous iron reduction with zinc sulphide and sphalerite

Experimental and analytical section

1.6.1 Reduction of Fe^{3+} to Fe^{2+}

The study of the Fe^{3+} reduction to Fe^{2+} with ZnS and sphalerite (an ore containing ZnS) solid-liquid reaction that takes place in a highly acidic liquid environment was carried out on a laboratory scale, Table 8.

The experiments were carried out in a 1 000 ml isothermal batch reactor with 750 ml of solution. An eight-blade pitch-blade turbine rotor at 420 rpm was used for stirring. In order to study mass transfer effects the stirring speed was varied. The reactor had a heating jacket using silicone oil for the heat transfer and it was provided with baffles for more efficient mixing, with an oil lock for added temperature stability and a reflux condenser to minimise evaporation. The liquids were preheated to reaction temperature and added to the reactor.

The reaction was performed under atmospheric pressure for 2 hours (ZnS experiments) and 4 hours (sphalerite experiments) with some exceptions in both cases and under a constant nitrogen (99.999%, AGA) flow to exclude effects from oxygen in the air.

During the experiments temperature and redox potential was continuously monitored with a Metrohm platinum electrode using an Ag/AgCl reference electrode in a 3 mol/l KCl solution.

The liquid-solid molar ratio was kept constant during the experiments and the ratio was set at

$$\text{ratio}_{\text{ZnS-Fe}^{3+}} = 0.5\text{-}2.0{:}1$$
$$\text{ratio}_{\text{sphalerite-Fe}^{3+}} = 0.5\text{-}2.1{:}1$$

The Fe^{3+} concentration was varied between at 0.1-0.4 mol/l during the experiments.

The stoichiometric ratio of reducing agent, sulphide sulphur, is 0.5:1 and super stoichiometric ratio is 2.1:1 in the sphalerite experiments. In the ZnS experiments the stoichiometric ratio of reducing agent, zinc sulphide, is 1:1 and super stoichiometric ratio is 2.0:1.

The sulphuric acid concentration in the experiments was between 0.20-1.02 mol/l. The sulphuric acid concentration had a very strong effect on the reduction rate when ZnS was used but no effect when sphalerite was used.

The temperature was varied between 75°-95°C to investigate the temperature effect on the reduction rate. Samples of 5 ml were withdrawn at constant intervals for further analysis. The solid-liquid ratio was not affected as the withdrawn samples contained equivalent amounts of solid and liquid compared to the experimental solution.

Table 8. Properties and proportions of the main chemicals in the solutions.

	Sphalerite*	**ZnS****
H_2SO_4, purity/supplier	95-96% / J.T.Baker	95-96% / J.T.Baker
Ferric iron sulphate $Fe_2(SO_4)_3 \bullet 5H_2O$	97% / Aldrich	97% / Aldrich
T	75°-95°C	75°-95°C
$C_{Fe^{3+},\ initial}$	0.1-03 mol/l	0.2-0.4 mol/l
$R_{reducing\ agent:Fe^{3+}}$	0.5-2.1:1	0.5-2.0:1
c_{H2SO4}	0.2-1.02 mol/l	0.41-1.02 mol/l
Ore	*Red Dog –sphalerite containing concentrate available as sulphur sulphide 26.9%	** ZnS purity 97%, supplied by Riedel-de Haën

The sulphide amount for the sphalerite experiments was determined by analysing the leach residue that was taken from an experiment with stoichiometric ratio of reducing agent. As the sulphur in pyrite was not available for the reduction reaction it was not considered and the final sulphur sulphide amount was estimated to 26.9 wt-%. It was concluded that this was all available for the reduction reaction.

Table 9. The amount of elements in the solution with sphalerite.

Element in solution	**Amount in solution**
Zinc	54.0 wt-%
Sulphur	29.2 wt-%
Iron	5.1 wt-%
Lead	3.2 wt-%
Cadmium	0.32 wt-%
Silicon	1.5 wt-%
Copper	0.15 wt-%
Other metals	< 0.1 wt-%

The solid particle samples with unreacted and reacted ZnS and sphalerite particles were analysed with SEM-EDS and Malvern 2601C to find out particle size and particle size distribution. Samples containing solid particles and liquid were injected into test tubes. The solid material was washed repeatedly after it had settled and the liquids had been removed. The washed material was carefully homogenised with a spatula and then analysed with the SEM-EDS.

Particle size analysis for particles in solution was carried out with Malvern 2601C Particle Sizer. These results would also contain information about particle size distribution. The particle size measured with the Malvern is based on either the volume for a sphere with the same volume as the particle or the area where the diameter for the particle is calculated to be the same as for a sphere with the same surface area.

SIA analysis (Sequential Injection Analysis) was used to determine the concentrations of ferric ions in the solutions (Ruzicka et al., 1990). SIA was used with the reagent Tiron, 1,2-dihydroxy-3,5-benzenedisolphonic acid disodium salt dissolved in 0.005 mol/l sulphuric acid, with the concentration 0.05 mol/l. The SIA works with piston pumps that first suck the samples and then the reagents and after that injects them into the photoreactor detector chamber. In the detector chamber the sample and reagent are mixed creating a product that is then measured. Prior to every analysis the system is flushed clean. The results are recorded automatically and a chart with the calculated height, area and width of the resulting peak is compared to the ratio of the obtained product and can be plotted.

Results section

1.6.2 Dissolution of solid particles

The liquid media in the experiments is based on an acidic sulphuric acid solution. This, together with the reactions occurring in the liquid phase, brings to the dissolution of the solid particles. Dissolution of solid particles is a complex reaction where the dissolution rate depends on several different factors, such as mass and charge transfers and chemical reactions (Momade et al., 1999). The dissolution is affected also by the solution properties and structural properties of the particles to be dissolved. Another factor that can retard the dissolution rate is the formation of solid sulphur particles (Lochmann et al., 1995), Equation (36). Neither during the zinc sulphide or sphalerite reactions did a product layer form and slow down the reaction (Momade et al., 1999). This was confirmed by later analysis carried out as part of the study.

The delicate balance in pH, concentrations of the different agents and temperature will finally determine the dissolution degree and rates as well as conversions.

1.6.3 Reduction with zinc sulphide and sphalerite

The experiments confirmed that both zinc sulphide and sphalerite can be used for the reduction of ferric iron, Figures 12. and 13. The actual mechanism when ferric iron is reduced with zinc sulphide could be debated (Markus et al. 2004a). It is, however, known that a simultaneous leaching of the sphalerite will take place.

Different initial zinc sulphide to ferric iron molar ratios were used in the experiments. Also the sulphuric acid concentration, Figures 16. and 17., temperature, Figures 14. and 15., and pH were varied, Table 8. Increased ratio of reduction agent to ferric iron increased the reduction rate, Figures 22. and 23.

The reduction of ferric to ferrous iron by zinc sulphide can be explained by the overall reaction stoichiometry

$$Fe_2(SO_4)_{3\,(aq.)} + ZnS_{\,(s)} \rightarrow 2FeSO_{4\,(aq.)} + ZnSO_{4\,(aq.)} + S_{\,(S)}$$

Equation 36

When zinc sulphide or zinc sulphide concentrate (sphalerite) is dissolved in the process two alternative paths exist

$$ZnS_{\,(S)} + H_2SO_4 \rightarrow ZnSO_4 + H_2S_{\,(aq.)}$$

Equation 37

$$Fe_2(SO_4)_3 + H_2S_{\,(aq.)} \rightarrow 2FeSO_4 + H_2SO_4 + S_{\,(S)}$$

Equation 38

It is possible that both reactions take place at the same time, but that is difficult to establish.

The reaction between ferric ions (Fe^{3+}) and solid ZnS was later studied (Salmi et al., 2010) confirming that elemental sulphur (Crundwell, 1987; Lotens et al., 1987; Lochmann et al., 1995, Palencia Perez et al., 1991), Equation 36, is formed through an intermediate reaction step and immediately removed from the surface. The shrinking particle model (Palencia Perez et al., 1991) could thus be applied and Salmi et al., 2010 (Crundwell, 1987), then wrote the reaction mechanism as

$$\begin{aligned} ZnS_{(s)} + Fe^{3+} &\rightleftharpoons I_1 && \text{(I)} \\ I_1 + Fe^{3+} &\rightleftharpoons I_2 && \text{(II)} \\ I_2 &\rightleftharpoons S_{(s)} + 2Fe^{2+} + Zn^{2+} && \text{(III)} \\ \hline ZnS_{(s)} + 2Fe^{3+} &\rightleftharpoons S_{(s)} + 2Fe^{2+} + Zn^{2+} \end{aligned}$$

Equation 39

A general model, with one term representing the reaction path where sulphuric acid participates in the reaction, Equations (37) and (38), and an other term represents the reaction between ferric iron and zinc sulphide, Equation (36), leads to the expression (Markus et al., 2004b, **Appendix II**)

$$r = k_1 \exp\left(-\frac{E_{a1}}{R}\left(\frac{1}{T}-\frac{1}{T_{mean}}\right)\right)\left(\frac{c_S}{c_{0S}}\right)^{p_1} c_{H_2SO_4}^{p_2} c_{Fe^{3+}}^{p_3} + k_2 \exp\left(-\frac{E_{a2}}{R}\left(\frac{1}{T}-\frac{1}{T_{mean}}\right)\right)\left(\frac{c_S}{c_{0S}}\right)^{p_4} c_{Fe^{3+}}^{p_5}$$

Equation 40

When sulphuric acid participation can be neglected and the reduction rate is proportional to the amount of reduction agent, as is the case with sphalerite as reduction agent, the reduction rate expression can be simplified (Markus et al. 2004b)

$$r = k \exp\left(-\frac{E_a}{R}\left(\frac{1}{T}-\frac{1}{T_{mean}}\right)\right)\left(\frac{c_S}{c_{0S}}\right) c_{Fe^{3+}}^{1.1}$$

Equation 41

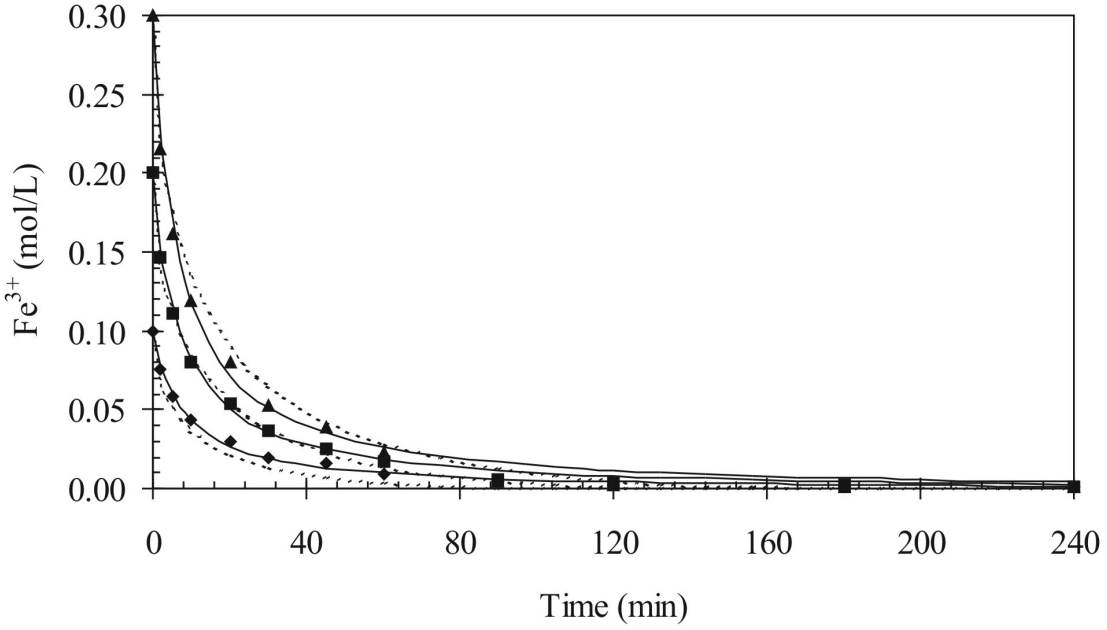

Figure 12. A higher concentration of ferric iron enhances the reduction rate. Examples of influence of initial concentration of ferric iron: ◆ = 0.1 mol/L, ■ = 0.2 mol/L, and ▲ = 0.3 mol/L. Conditions: reduction agent-to-ferric iron molar ratio, 1.1:1; sulphuric acid concentration, 0.41 mol/L; temperature, 95°C. Solid lines and dashed lines depict the fit of the models that explain the reaction kinetics. Solid lines = fit of model F1, dashed lines = fit of model D4. Sphalerite experiments. (Markus et al., 2004b).

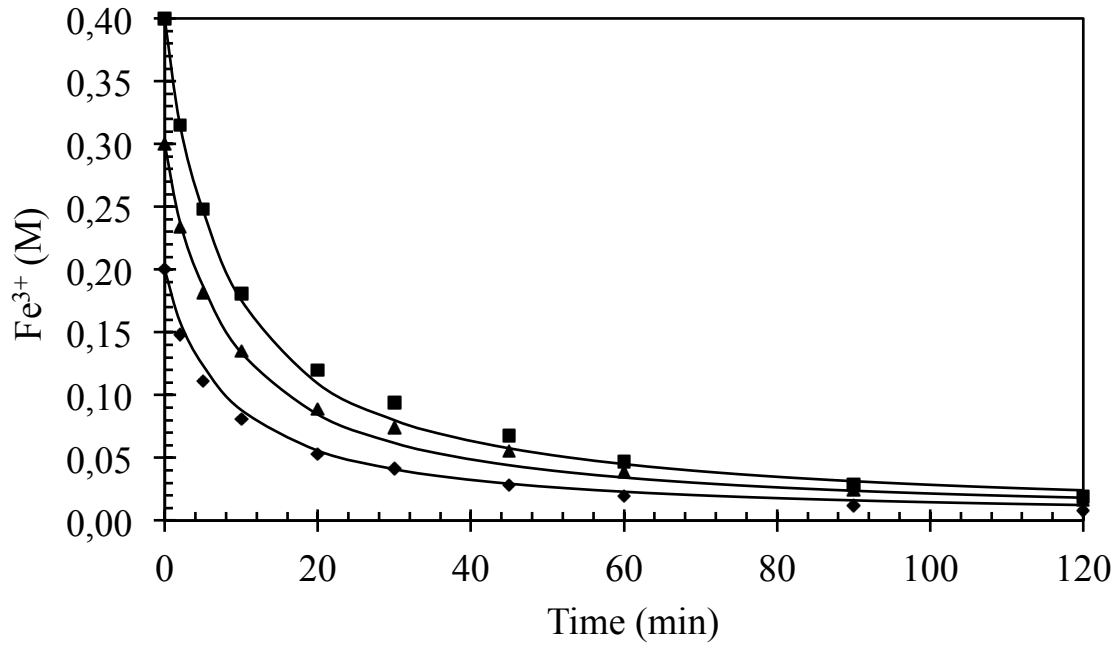

Figure 13. A higher concentration of ferric iron enhances the reduction rate. Examples of influence of initial concentration of ferric iron: ◆ = 0.2 M, ▲ = 0.3 M, and ■ = 0.4 M. Conditions: zinc sulphide-to-ferric iron molar ratio, 1:1; sulphuric acid concentration, 0.41 mol/l; temperature, 85°C. Zinc sulphide experiments. (Markus et al., 2004a).

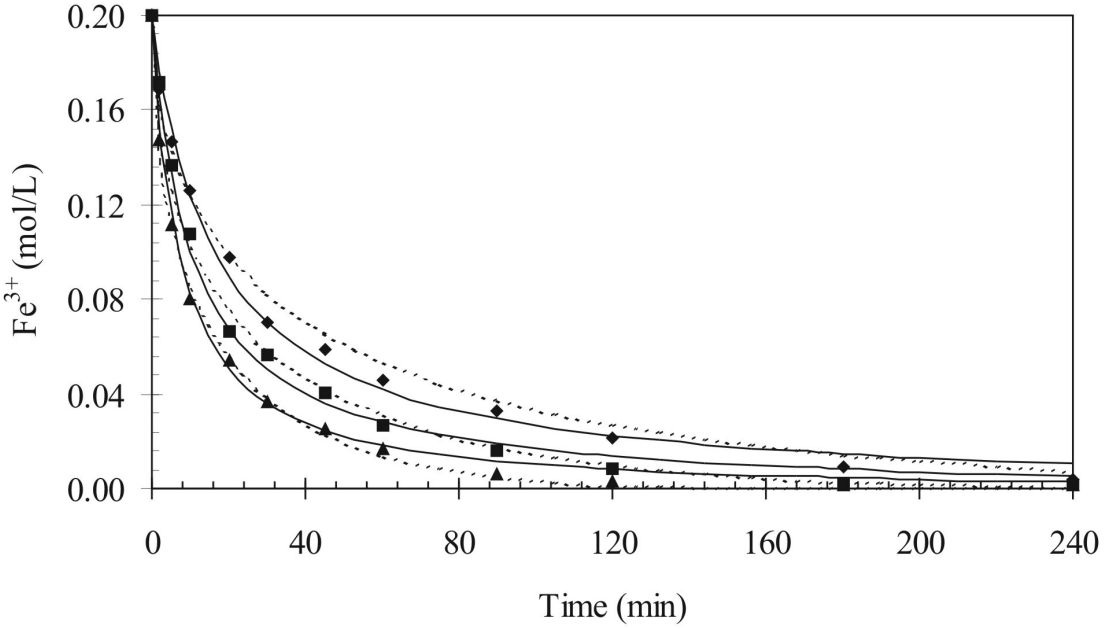

Figure 14. An increased temperature has a significant improving impact on the reaction rate. Examples of influence of temperature: ◆ = 75°C, ■ = 85°C, and ▲ = 95°C. Conditions: reduction agent-to-ferric iron molar ratio, 1.1:1; initial concentration of ferric iron, 0.2 mol/L; sulphuric acid concentration, 0.41 mol/L. Solid lines = fit of model F1, dashed lines = fit of model D4. Solid lines and dashed lines depict the fit of the models that explain the reaction kinetics. Sphalerite experiments. (Markus et al., 2004b).

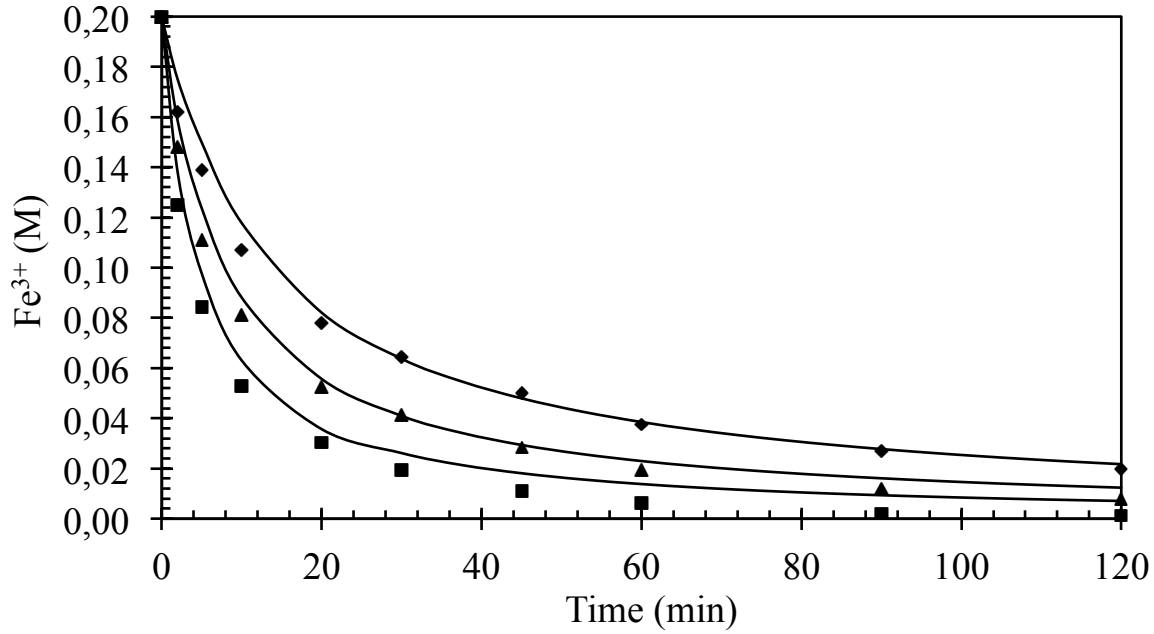

Figure 15. An increased temperature has a significant improving impact on the reaction rate. Examples of influence of temperature: ◆ = 75°C, ▲ = 85°C, and ■ = 95°C. Conditions: zinc sulphide-to-ferric iron molar ratio, 1:1; initial concentration of ferric iron, 0.2 M; sulphuric acid concentration, 0.41 mol/l. Zinc sulphide experiments. (Markus et al., 2004a).

The reduction reaction is strongly depending on the temperature as depicted in Figures 14. and 15. and the reaction rate increases with increased temperature (Ekinci et al., 1998).

1.6.4 The sulphuric acid effect

Sphalerite is a zinc sulphide containing ore that will in some cases bring to entirely different behaviour as expected when comparing to those were pure zinc sulphide (ZnS) is used.

In the experiments where pure zinc sulphide was used it became apparent that the sulphuric acid increased the reaction rate, Figure 16. Results would later reveal that this effect is proportional to the concentration of sulphuric acid indicating that the sulphuric acid acts as an intermediate stage in a reaction that takes place in the liquid phase.

In corresponding experiments with sphalerite the sulphuric acid had nearly no effect on the reaction rate, Figure 17.

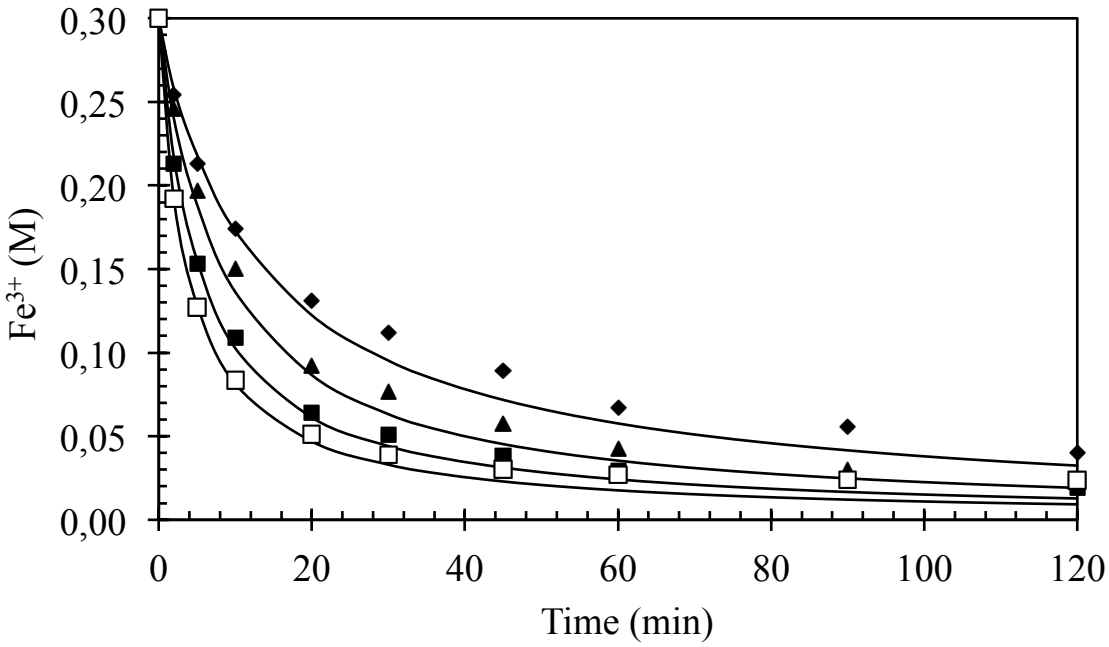

Figure 16. An increased sulphuric acid concentration increased the reaction rate when pure zinc sulphide is used. Examples of influence of sulphuric acid concentration: ◆ = 0.41 mol/l, ▲ = 0.61 mol/l, ■ = 0.82 mol/l, and □ = 1.02 mol/l. Conditions: zinc sulphide-to-ferric iron molar ratio, 1:1; initial concentration of ferric iron, 0.3 M; temperature, 75°C. Zinc sulphide experiments. (Markus et al., 2004a).

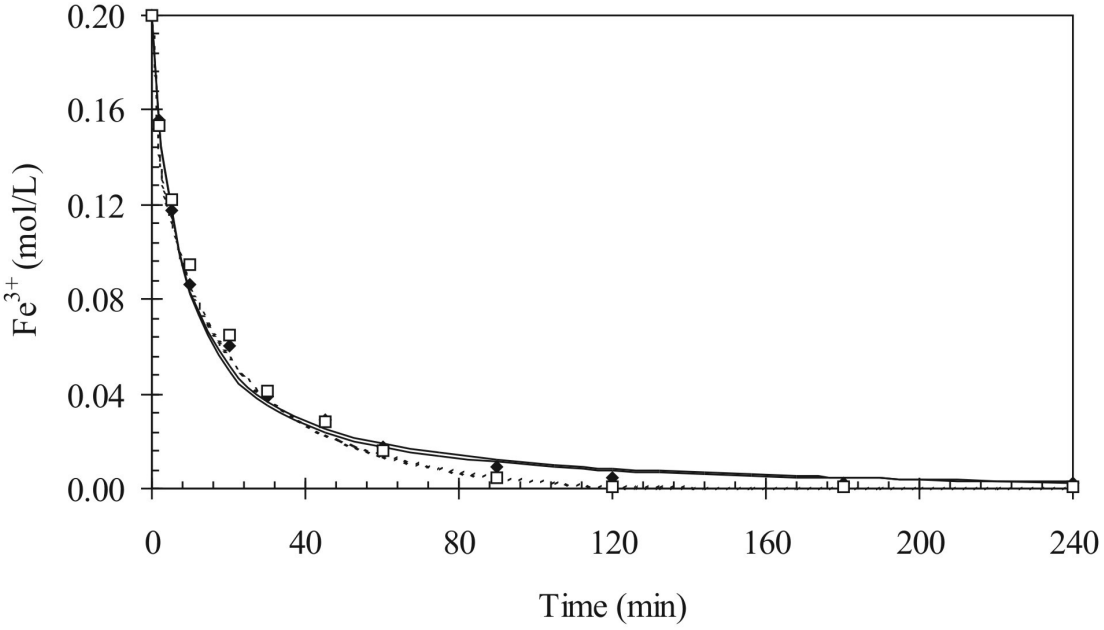

Figure 17. An increased sulphuric acid concentration added no significant increase to the reaction rate when sphalerite is used. Examples of influence of sulphuric acid concentration: ◆ = 0.20 mol/L and □ = 1.02 mol/L. Conditions: reduction agent-to-ferric iron molar ratio, 1.1:1; initial concentration of ferric iron, 0.2 mol/L; temperature, 95°C. Solid lines and dashed lines depict the fit of the models that explain the reaction kinetics. Solid lines = fit of model F1, dashed lines = fit of model D4. Sphalerite experiments. (Markus et al., 2004b).

1.6.5 Analysis of particles and reducing agent and solvent effects

Simultaneously with the dissolution of zinc particles new particles emerge. The SEM-EDS and Malvern results indicated that elemental sulphur particles were formed (Crundwell, 1987; Lotens et al., 1987; Lochmann et al., 1995, Palencia Perez et al., 1991) and that they are larger than the zinc sulphide particles that were consumed. According to this no sulphur layer (product layer) was formed on the zinc sulphide particles (Momade et al., 1999). The SEM-EDS analysis showed remains of zinc, sulphur, iron and lead (sphalerite experiments), Figure 18.

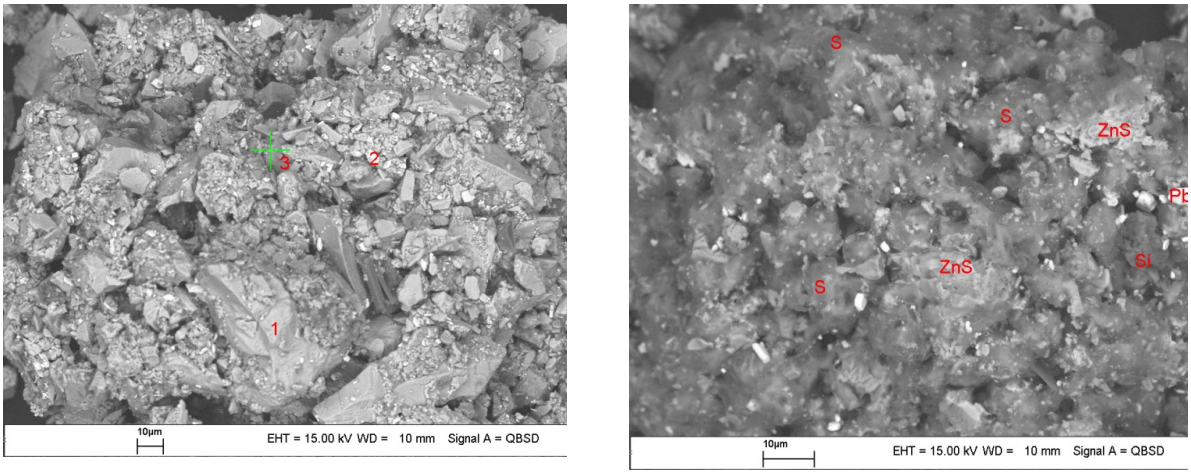

Figure 18. Elemental sulphur particles were formed during the dissolution process with sphalerite. No (sulphur) product layer was formed. SEM-EDS microgram of sphalerite concentrate. (left picture) unleached material (× 500), point analysis by EDS: (1) 50.83 atom-% sulphur, 47.09 atom-% zinc, and 2.08 atom-% iron, (2) lead and sulphur, and (3) 57.21 atom-% sulphur, 12.75 atom-% zinc, and 30.04 atom-% iron. (right picture) leach residue in 4 h (× 1000), points of zinc sulphide, sulphur, lead and sulphur, as well as silicon are marked in the picture. Conditions: reduction agent-to-ferric iron molar ratio, 1.1:1; initial concentration of ferric iron, 0.2 mol/L; sulphuric acid concentration, 0.41 mol/L; temperature, 95°C. Sphalerite experiments. (Markus et al., 2004b).

Zinc sulphide was dissolved and at the same time sulphur particles were formed (Lochmann et al., 1995; Lotens et al., 1987), Figure 19. The formed sulphur particles together with the unreacted zinc sulphide would give two separate peaks in the particle size distribution. The particle size distribution with laser diffraction technique revealed unreacted material with a multi-size distribution. As a result from the experiments with ZnS as a reducing agent it was concluded that sulphur forms larger particles than zinc sulphide. In both cases (ZnS and sphalerite) the experiments showed that the particle size distribution became bimodal pointing to the conclusion that sulphur forms separate particles and not a product layer, Figures 20. and 21. To confirm this in the sphalerite case further experiments would be needed to study sphalerite particles with unimodal particle size distribution.

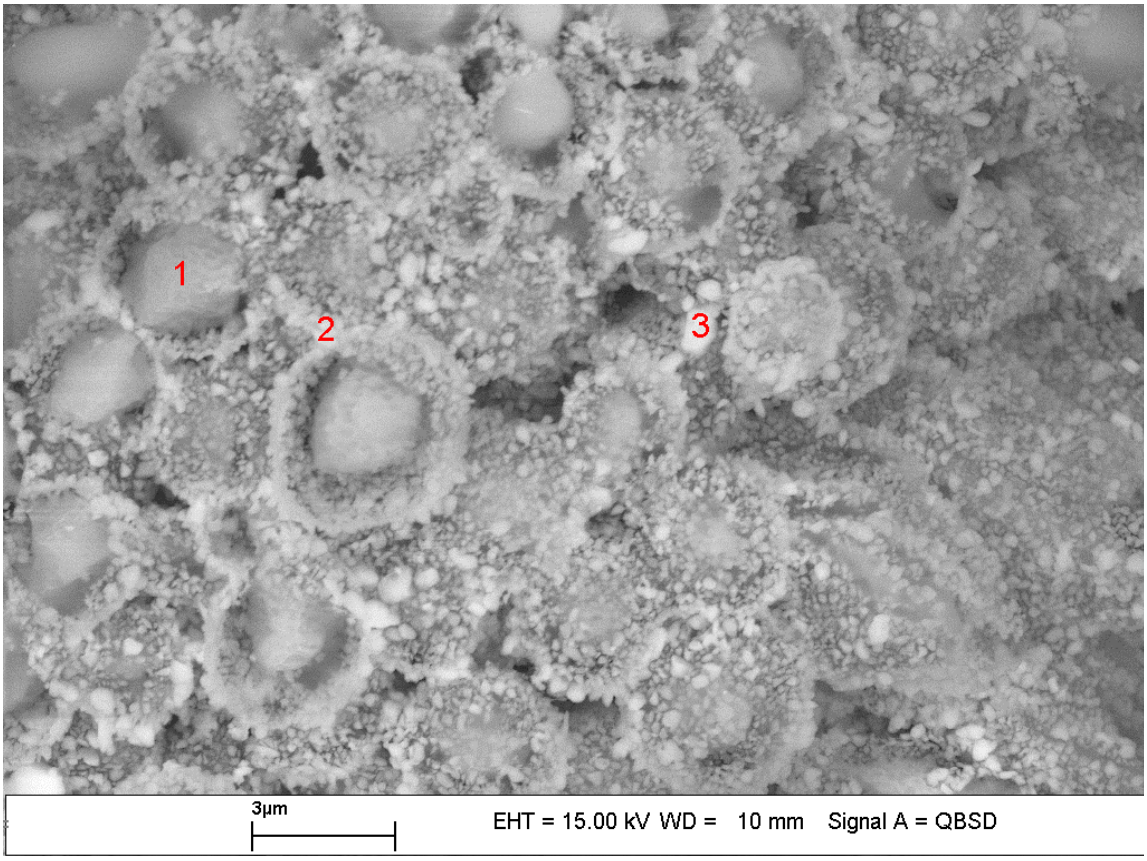

Figure 19. Elemental sulphur particles were formed during the dissolution process with zinc sulphide. No (sulphur) product layer was formed. SEM-EDS micrograph of final leach residue in 2 h (× 5000). Darker areas consist of more sulphur, lighter areas of more zinc. Result from point analysis performed by EDS: (1) 96.61% sulphur, 3.36% zinc, (2) 75.39% sulphur, 24.61% zinc, and (3) 69.96% sulphur and 30.05% zinc. Conditions: zinc sulphide-to-ferric iron molar ratio, 1:1; initial concentration of ferric iron, 0.4 M; sulphuric acid concentration, 0.41 mol/l; temperature, 95°C. Zinc sulphide experiments. (Markus et al., 2004a).

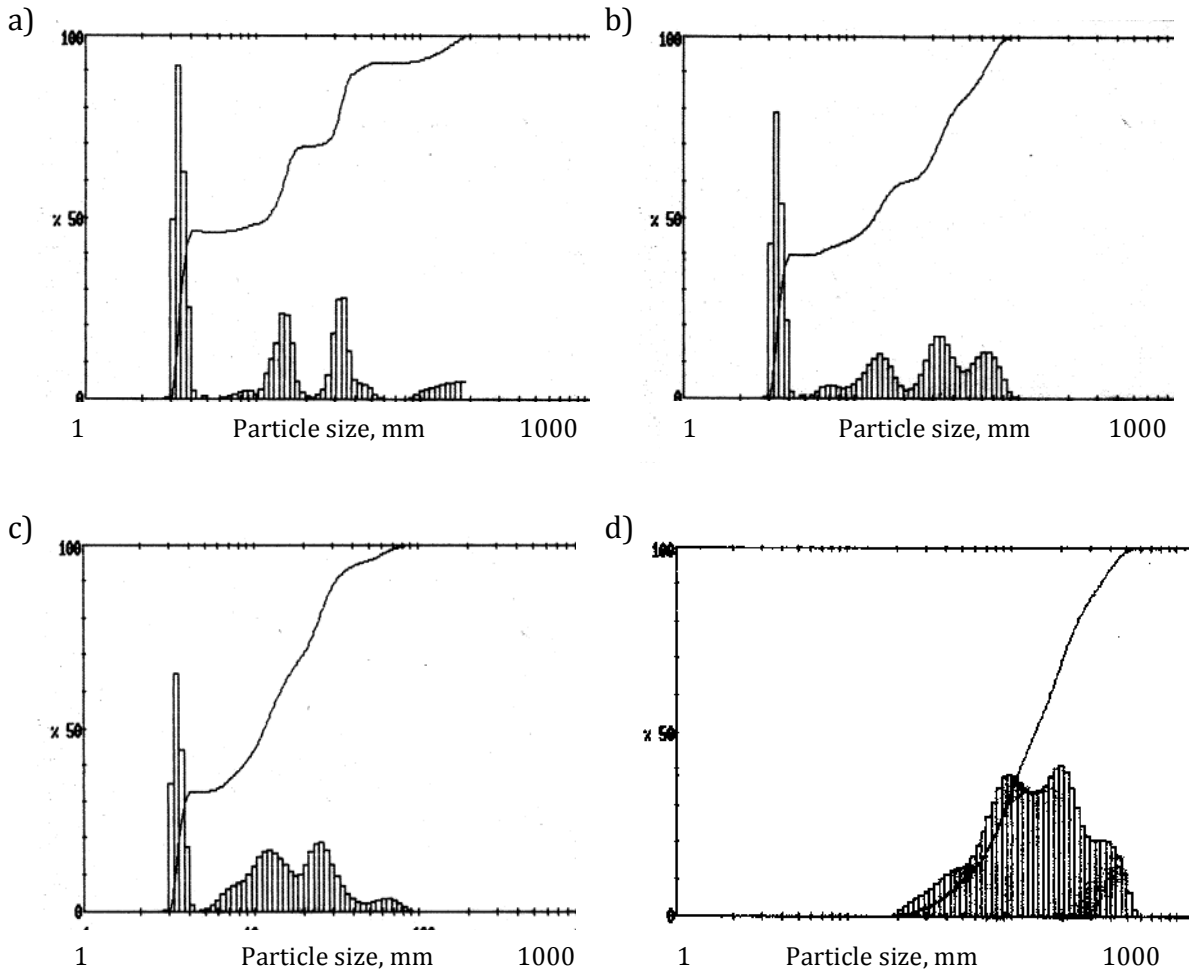

Figure 20. Examples of particle size distribution in the sphalerite experiments determined by laser diffraction technique. (a) unreacted sphalerite concentrate dispersed in water (100 mm objective), (b) leached in 7 minutes (100 mm objective), (c) leached in 35 minutes (100 mm objective), and (d) leach residue in 4 h (63 mm objective). Conditions: reduction agent-to-ferric iron molar ratio, 1.1:1; initial concentration of ferric iron, 0.2 mol/L; sulphuric acid concentration, 0.41 mol/L; temperature, 85°C. Sphalerite experiments, (Markus et al., 2004b).

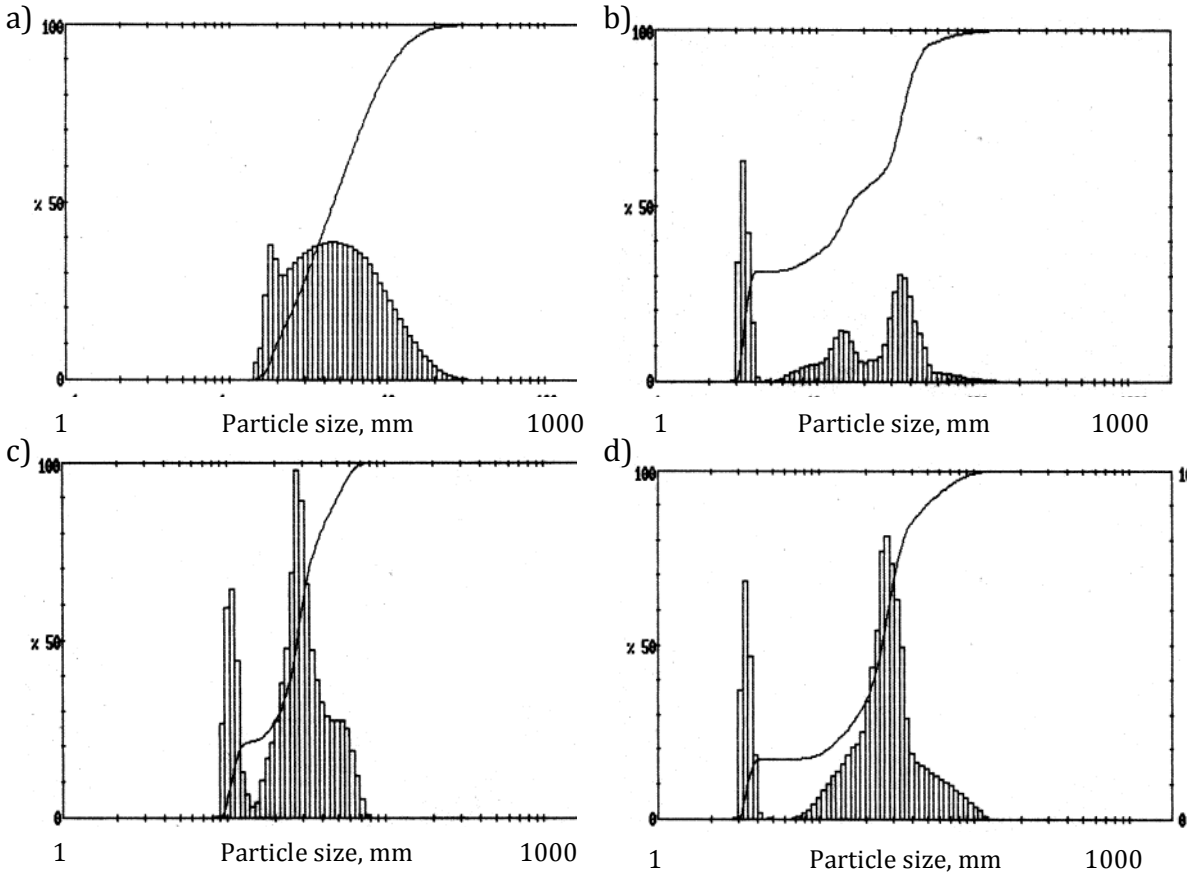

Figure 21. Examples of particle size distribution in the zinc sulphide experiments determined by laser diffraction technique. (a) unreacted ZnS dispersed in water (63 mm objective), (b) leached in 7 minutes (100 mm objective), (c) leached in 35 minutes (300 mm objective), and (d) leach residue in 2 h (100 mm objective). Conditions: zinc sulphide-to-ferric iron molar ratio, 1:1; initial concentration of ferric iron, 0.4 M; sulphuric acid concentration, 0.41 mol/l; temperature, 75°C. Zinc sulphide experiments. (Markus et al., 2004a).

1.6.6 Kinetics

The reactions carried out in the study are solid-liquid reactions and to determine the reaction kinetics the obtained results were compared to several existing models for solid-liquid reactions (Markus et al., 2004 (a, b)). The experimental data seemed to fit a model where the reaction rate is proportional to the concentration of the reduction agent and the ferric iron concentration (Palencia Perez et al., 1991), Figures 22. and 23. In addition to this, in the experiments with ZnS as a reducing agent, the sulphuric acid had a significant impact on the reaction rate. Sulphuric acid participated in the reaction and increased the reduction rate.

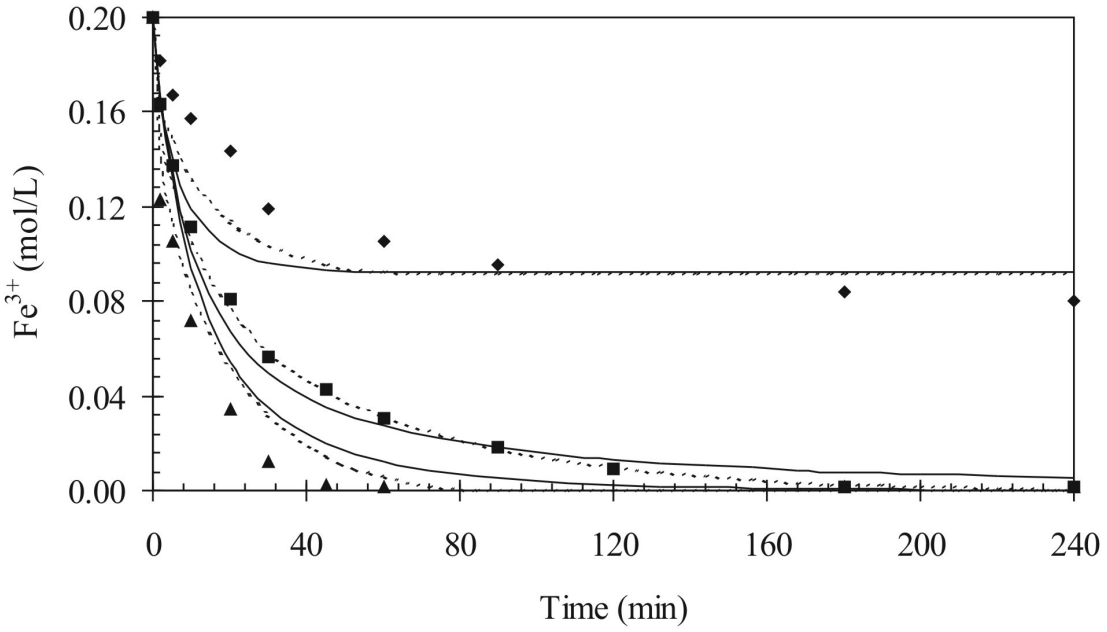

Figure 22. The reaction rate is proportional to the concentration of the reduction agent (sphalerite) and the ferric iron concentration. Examples of influence of reduction agent-to-ferric iron molar ratio: ◆ = 0.5:1, ■ = 1.1:1, and ▲ = 1.6:1. Conditions: initial concentration of ferric iron, 0.2 mol/L; sulphuric acid concentration, 1.02 mol/L; temperature, 85°C. Solid lines and dashed lines depict the fit of the models that explain the reaction kinetics. Solid lines = fit of model F1, dashed lines = fit of model D4. Sphalerite experiments. (Markus et al., 2004b).

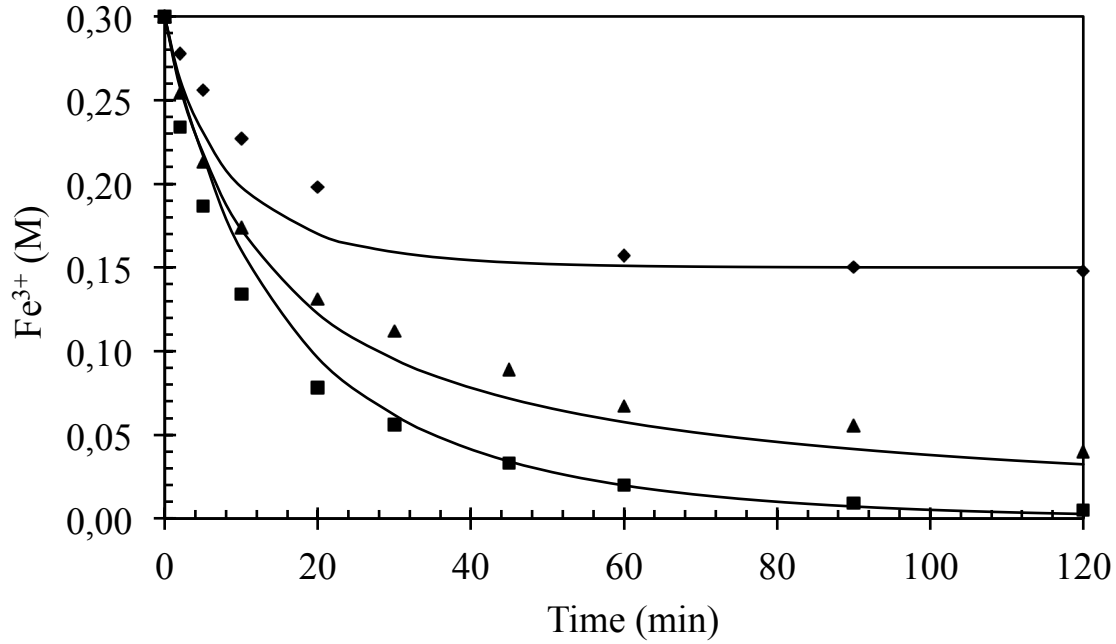

Figure 23. The reaction rate is proportional to the concentration of the reduction agent (zinc sulphide) and the ferric iron concentration. Examples of influence of zinc sulphide-to-ferric iron molar ratio: ◆ = 0.5:1, ▲ = 1:1, and ■ = 2:1. Conditions: initial concentration of ferric iron, 0.3 M; sulphuric acid concentration, 0.41 mol/l; temperature, 75°C. Zinc sulphide experiments. (Markus et al., 2004a).

1.6.7 Modelling

Markus et al. (2004a,b) generated in their work different models to explain the influence on the reduction rates by

- initial concentration of ferric ion
- temperature
- sulphuric acid concentration
- reduction agent-to- ferric iron molar ratio

ZnS (Markus et al., 2004a) and sphalerite (Markus et al., 2004b) were used as reduction agent and separate models were generated for them. Rate expressions were obtained when the experimental data was fitted to the models. The experimental results and the fit of the models are depicted in Figures 12.-17. and 22.-23.

Expressions of $g(\alpha)$ and $f(c_S)$ for the kinetic models with the ZnS experimental works are explained in Table 10. The function $g(\alpha)$ has not been used in the estimation but has been given for easier model identification.

Results from the modelling for the reduction rates for experiments with ZnS, Equations (42) and (43), are then presented in Table 11. and results for Equation (44) are presented in Table 12.

The rate expressions in Equations (42) and (43) (by Markus et al., 2004a) were used when the models were fitted to the experimental data from the ZnS experiments:

Equation 42 – was used for the models F1, F3/2, F2, R2–R4, and D10
Equation 43 – was used for the models D3–D5, and D8

$$r = k \exp\left(- \frac{E_a}{R} \left(\frac{1}{T} - \frac{1}{T_{mean}} \right) \right) \left(\frac{c_{ZnS}}{c_{0ZnS}} \right)^{p_1} c_{H_2SO_4}^{p_2} c_{Fe^{3+}}^{p_3}$$

Equation 42

$$r = k \exp\left(- \frac{E_a}{R} \left(\frac{1}{T} - \frac{1}{T_{mean}} \right) \right) \frac{\left(\frac{c_{ZnS}}{c_{0ZnS}} \right)^{p_1}}{1 - \left(\frac{c_{ZnS}}{c_{0ZnS}} \right)^{p_4}} c_{H_2SO_4}^{p_2} c_{Fe^{3+}}^{p_3}$$

Equation 43

$$r = k_1 \exp\left(- \frac{E_{a1}}{R} \left(\frac{1}{T} - \frac{1}{T_{mean}} \right) \right) \left(\frac{c_{ZnS}}{c_{0ZnS}} \right)^{p_1} c_{H_2SO_4}^{p_2} c_{Fe^{3+}}^{p_3} + k_2 \exp\left(- \frac{E_{a2}}{R} \left(\frac{1}{T} - \frac{1}{T_{mean}} \right) \right) \left(\frac{c_{ZnS}}{c_{0ZnS}} \right)^{p_4} c_{Fe^{3+}}^{p_5}$$

Equation 44

For practical purposes Markus et al. (2004a) used a simple model (F1) to describe the reaction kinetics when using ZnS as reduction agent. When the reduction is proportional to the ferric iron and reduction agent concentrations then a simpler rate expression can be used, Equation (45) and this is depicted in Figures 13., 15., 16., and 23.

$$r = k \exp\left(- \frac{E_a}{R} \left(\frac{1}{T} - \frac{1}{T_{mean}} \right) \right) \left(\frac{c_{ZnS}}{c_{Zn0S}} \right) c_{H2SO4}^{1.5} c_{Fe3+}$$

Equation 45

Expressions of $g(\alpha)$ and $f(c_S)$ for the kinetic models with the sphalerite works are explained in Table 14. The function $g(\alpha)$ has not been used in the estimation but has been given for easier model identification.

The rate expressions in Equations (46) and (47) were used when the models were fitted to the experimental data from the sphalerite experiments:

Equation 46 – was used for the models F1, F3/2, F2, R2–R4, and D10
Equation 47 – was used for the models D3–D5, and D8

$$r = k \exp\left(- \frac{E_a}{R} \left(\frac{1}{T} - \frac{1}{T_{mean}} \right) \right) \left(\frac{c_S}{c_{0S}} \right)^{p_1} c_{H_2SO_4}^{p_2} c_{Fe^{3+}}^{p_3}$$

Equation 46

by Markus et al. (2004b)

$$r = k \exp\left(- \frac{E_a}{R} \left(\frac{1}{T} - \frac{1}{T_{mean}} \right) \right) \frac{\left(\frac{c_S}{c_{0S}} \right)^{p_1}}{1 - \left(\frac{c_S}{c_{0S}} \right)^{p_4}} c_{H_2SO_4}^{p_2} c_{Fe^{3+}}^{p_3}$$

Equation 47

by Markus et al. (2004b)

Results from the modelling of the reduction rates for experiments with sphalerite, Equations (46) and (47), used in the work by Markus et al. (2004b), are presented in Table 14.

Table 10. Expressions of $g(\alpha)$ and $f(c_S)$ for the kinetic models used in the work with ZnS as reduction agent by Markus et al. (2004a)

Notation	$g(\alpha)$	$f(c_{ZnS})$	Type of model	p_1	p_4
F1	$-\ln(1-\alpha)$	c_{ZnS}/c_{0ZnS}	First order kinetics	1	–
F3/2	$(1-\alpha)^{-1/2} - 1$	$(c_{ZnS}/c_{0ZnS})^{3/2}$	Three-halves order kinetics	$^3/_2$	–
F2	$(1-\alpha)^{-1}$	$(c_{ZnS}/c_{0ZnS})^2$	Second order kinetics	2	–
R2	$1 - (1-\alpha)^{1/2}$	$(c_{ZnS}/c_{0ZnS})^{1/2}$	One-half order kinetics; two-dimensional advance of the reaction interface	$^1/_2$	–
R3	$1 - (1-\alpha)^{1/3}$	$(c_{ZnS}/c_{0ZnS})^{2/3}$	Two-thirds order kinetics; three-dimensional advance of the reaction interface	$^2/_3$	–
R4	$1 - (1-\alpha)^{2/3}$	$(c_{ZnS}/c_{0ZnS})^{1/3}$	One-thirds order kinetics; film diffusion	$^1/_3$	–
D3	$[1 - (1-\alpha)^{1/3}]^2$	$(c_{ZnS}/c_{0ZnS})^{2/3}/(1 - (c_{ZnS}/c_{0ZnS})^{1/3})$	Jander; three-dimensional	$^2/_3$	$^1/_3$
D4	$1 - 2\alpha/3 - (1-\alpha)^{2/3}$	$(c_{ZnS}/c_{0ZnS})^{1/3}/(1 - (c_{ZnS}/c_{0ZnS})^{1/3})$	Crank-Ginstling and Broun-shtein	$^1/_3$	$^1/_3$
D5	$[1/(1-\alpha)^{1/3} - 1]^2$	$(c_{ZnS}/c_{0ZnS})^{5/3}/(1 - (c_{ZnS}/c_{0ZnS})^{1/3})$	Zhuravlev, Lesokhin and Tempelman	$^5/_3$	$^1/_3$
D8	$[1 - (1-\alpha)^{1/2}]^2$	$(c_{ZnS}/c_{0ZnS})^{1/2}/(1 - (c_{ZnS}/c_{0ZnS})^{1/2})$	Jander; cylindrical diffusion	$^1/_2$	$^1/_2$
D10	$1/(1-\alpha)^{1/3} - 1$	$(c_{ZnS}/c_{0ZnS})^{4/3}$	Dickinson and Heal	$^4/_3$	–

Table 11. Results from the modelling for the experiments with ZnS as reduction agent for Equations (42) and (43) by Markus et al. (2004a).

Model	p_1 (fixed)	p_4 (fixed)	k	E_a (kJ/mol)	p_2 (H_2SO_4)	p_3 (Fe^{3+})	Residual SS Q	Ex-plained R^2 (%)
F1	1	–	0.19 ± 0.01 $l^{1.51}/(mol^{1.51}min)$	67.1 ± 2.6	1.48 ± 0.05	1.03 ± 0.05	0.0231	98.08
F3/2	$^3/_2$	–	0.16 ± 0.01 $l^{1.26}/(mol^{1.26}min)$	71.7 ± 2.1	1.53 ± 0.04	0.73 ± 0.03	0.0128	98.93
F2	2	–	0.13 ± 0.01 $l^{1.05}/(mol^{1.05}min)$	77.2 ± 2.6	1.60 ± 0.05	0.45 ± 0.04	0.0176	98.54
R2	$^1/_2$	–	0.26 ± 0.03 $l^{1.83}/(mol^{1.83}min)$	63.9 ± 3.7	1.46 ± 0.07	1.37 ± 0.07	0.0507	95.78
R3	$^2/_3$	–	0.23 ± 0.02 $l^{1.71}/(mol^{1.71}min)$	64.8 ± 3.3	1.46 ± 0.06	1.25 ± 0.06	0.0394	96.72
R4	$^1/_3$	–	0.29 ± 0.03 $l^{1.93}/(mol^{1.93}min)$	63.0 ± 4.0	1.45 ± 0.08	1.48 ± 0.04	0.0640	94.67
D3	$^2/_3$	$^1/_3$	0.01 ± 0.00 $l^{1.18}/(mol^{1.18}min)$	81.5 ± 3.2	1.70 ± 0.06	0.48 ± 0.05	0.0257	97.86
D4	$^1/_3$	$^1/_3$	0.01 ± 0.05 $l^{1.29}/(mol^{1.29}min)$	76.9 ± 2.7	1.63 ± 0.05	0.66 ± 0.02	0.0206	98.29
D5	$^5/_3$	$^1/_3$	0.01 ± 0.15 $l^{0.93}/(mol^{0.93}min)$	96.7 ± 6.5	1.93 ± 0.12	0.00 ± 0.01	0.0720	94.00
D8	$^1/_2$	$^1/_2$	0.01 ± 0.03 $l^{1.26}/(mol^{1.26}min)$	78.0 ± 2.8	1.65 ± 0.05	0.61 ± 0.05	0.0212	98.23
D10	$^4/_3$	–	0.17 ± 0.01 $l^{1.35}/(mol^{1.35}min)$	70.0 ± 2.1	1.52 ± 0.04	0.83 ± 0.04	0.0145	98.80

Table 12. Results from the modelling for the experiments with ZnS as reduction agent for Equation (44) by Markus et al. (2004a).

	not fixed	$p_1 = 1$	$p_1, p_4 = 1$	$p_1 = 2/3$	$p_4 = 2/3$	$p_1 = 1$, $p_4 = 2/3$
k_1	0.16 ± 0.01 $l^{1.58}$/($mol^{1.58}$min)	0.17 ± 0.01 $l^{1.77}$/($mol^{1.77}$min)	0.23 ± 0.05 $l^{2.23}$/($mol^{2.23}$min)	0.20 ± 0.02 $l^{2.13}$/($mol^{2.13}$min)	0.17 ± 0.02 $l^{1.34}$/($mol^{1.34}$min)	0.19 ± 0.02 $l^{1.49}$/($mol^{1.49}$min)
E_{a1} (kJ/mol)	81.4 ± 2.8	81.8 ± 2.9	85.7 ± 10.2	84.1 ± 3.4	68.4 ± 3.3	66.8 ± 3.8
p_1	1.22 ± 0.08	1	1	2/3	1.72 ± 0.05	1
p_2	1.75 ± 0.05	1.80 ± 0.04	2.08 ± 0.33	1.95 ± 0.06	1.62 ± 0.06	1.46 ± 0.09
p_3	0.83 ± 0.06	0.97 ± 0.06	1.15 ± 0.17	1.18 ± 0.04	0.72 ± 0.05	1.03 ± 0.08
k_2	0.01 ± 0.004 $mol^{0.96}$/($l^{0.96}$min)	0.01 ± 0.002 $mol^{0.99}$/($l^{0.99}$min)	0.02 ± 0.01 $mol^{0.16}$/($l^{0.16}$min)	0.03 ± 0.003 $mol^{0.90}$/($l^{0.90}$min)	5e-4 ± 6e-4 $mol^{0.79}$/($l^{0.79}$min)	8e-8 ± 8e-4 $mol^{0.95}$/($l^{0.95}$min)
E_{a2} (kJ/mol)	13.8 ± 27.2	20.3 ± 18.9	33.6 ± 29.6	40.6 ± 12.5	113.7 ± 32.2	33.9 ± 2.1e3
p_4	6.56 ± 1.26	6.16 ± 0.59	1	4.74 ± 0.32	2/3	2/3
p_5	0.04 ± 0.24	0.01 ± 0.10	0.84 ± 0.21	0.10 ± 0.13	0.21 ± 0.38	0.05 ± 1.8e3
R^2 (%)	99.30	99.25	98.14	99.07	99.07	98.08

Table 13. Expressions of $g(\alpha)$ and $f(c_S)$ for the kinetic models used in the work with sphalerite as reduction agent by Markus et al. (2004b).

Notation	$g(\alpha)$	$f(c_S)$	Type of model	p_1	p_4
F1	$-\ln(1-\alpha)$	c_S/c_{0S}	First order kinetics	1	–
F3/2	$(1-\alpha)^{-1/2} - 1$	$(c_S/c_{0S})^{3/2}$	Three-halves order kinetics	$^3/_2$	–
F2	$(1-\alpha)^{-1}$	$(c_S/c_{0S})^2$	Second order kinetics	2	–
R2	$1 - (1-\alpha)^{1/2}$	$(c_S/c_{0S})^{1/2}$	One-half order kinetics; two-dimensional advance of the reaction interface	$^1/_2$	–
R3	$1 - (1-\alpha)^{1/3}$	$(c_S/c_{0S})^{2/3}$	Two-thirds order kinetics; three-dimensional advance of the reaction interface	$^2/_3$	–
R4	$1 - (1-\alpha)^{2/3}$	$(c_S/c_{0S})^{1/3}$	One-thirds order kinetics; film diffusion	$^1/_3$	–
D3	$[1 - (1-\alpha)^{1/3}]^2$	$(c_S/c_{0S})^{2/3}/(1 - (c_S/c_{0S})^{1/3})$	Jander; three-dimensional	$^2/_3$	$^1/_3$
D4	$1 - 2\alpha/3 - (1-\alpha)^{2/3}$	$(c_S/c_{0S})^{1/3}/(1 - (c_S/c_{0S})^{1/3})$	Crank-Ginstling and Brounshtein, mass transfer across a non-porous product layer	$^1/_3$	$^1/_3$
D5	$[1/(1-\alpha)^{1/3} - 1]^2$	$(c_S/c_{0S})^{5/3}/(1 - (c_S/c_{0S})^{1/3})$	Zhuravlev, Lesokhin and Tempelman, diffusion, concentration of penetrating species varies with α	$^5/_3$	$^1/_3$
D8	$[1 - (1-\alpha)^{1/2}]^2$	$(c_S/c_{0S})^{1/2}/(1 - (c_S/c_{0S})^{1/2})$	Jander; cylindrical diffusion	$^1/_2$	$^1/_2$
D10	$1/(1-\alpha)^{1/3} - 1$	$(c_S/c_{0S})^{4/3}$	Dickinson and Heal, transfer across the contracting area	$^4/_3$	–

Table 14. Results from the modelling for the experiments with sphalerite as reduction agent by Markus et al. (2004b).

Model	p_1 (fixed)	p_4 (fixed)	k	E_a *(kJ/mol)*	p_2 (H_2SO_4)	p_3 (Fe^{3+})	Residual SS Q	Explained R^2 (%)
F1	1	–	0.07 ± 0.01 $l^{0.15}/(mol^{0.1}min)$	47.4 ± 4.4	0.04 ± 0.05	1.11 ± 0.09	0.0312	95.06
F3/2	$^3/_2$	–	0.05 ± 0.01 $mol^{0.16}/(l^{0.16}min)$	54.3 ± 4.1	0.05 ± 0.05	0.79 ± 0.08	0.0262	95.85
F2	2	–	0.03 ± 0.00 $mol^{0.47}/(l^{0.47}min)$	61.7 ± 4.2	0.06 ± 0.05	0.47 ± 0.08	0.0259	95.91
R2	$^1/_2$	–	0.11 ± 0.02 $l^{0.47}/(mol^{0.47}min)$	40.7 ± 5.0	0.03 ± 0.06	1.44 ± 0.10	0.0408	93.54
R3	$^2/_3$	–	0.10 ± 0.01 $l^{0.36}/(mol^{0.36}min)$	42.8 ± 4.6	0.03 ± 0.06	1.33 ± 0.06	0.0371	94.13
R4	$^1/_3$	–	0.13 ± 0.02 $l^{0.58}/(mol^{0.58}min)$	38.8 ± 4.9	0.03 ± 0.06	1.55 ± 0.07	0.0449	92.89
D3	$^2/_3$	$^1/_3$	0.002 ± 0.02 $mol^{0.61}/(l^{0.61}min)$	64.3 ± 3.5	0.01 ± 0.04	0.38 ± 0.06	0.0179	97.16
D4	$^1/_3$	$^1/_3$	0.002 ± 0.01 $mol^{0.41}/(l^{0.41}min)$	59.4 ± 3.3	0.01 ± 0.04	0.58 ± 0.06	0.0169	97.33
D5	$^5/_3$	$^1/_3$	0.001 ± 0.02 $mol^{0.99}/(l^{0.99}min)$	78.7 ± 5.5	0.01 ± 0.07	0.00 ± 0.10	0.0343	94.57
D8	$^1/_2$	$^1/_2$	0.003 ± 0.01 $mol^{0.47}/(l^{0.47}min)$	60.9 ± 3.3	0.01 ± 0.04	0.52 ± 0.06	0.0169	97.32
D10	$^4/_3$	–	0.05 ± 0.01 $mol^{0.06}/(l^{0.06}min)$	52.0 ± 4.2	0.05 ± 0.05	0.89 ± 0.08	0.0274	95.67

1.7 Part 3: Precipitation of indium, gallium and germanium

Indium, gallium and germanium precipitation was studied using industrial raw materials from Outokumpu zinc factory[1] in Kokkola, Finland. The environment and parameters for the experiments was kept as close to the industrial process as possible. A precondition for the experiments was that a new process step would affect the existing zinc recovery process as little as possible. Still, the study and the results can be applied to other processes as well.

Native NL2-solution (Neutral Leach 2 –solution) from an actual process was used. For reference also synthetic solutions were prepared and studied under the same circumstances as the native process liquors. Outokumpu zinc factory in Kokkola provided the NL2-solutions and the reference solutions were prepared using ultra-purified ELGA water.

Experimental and analytical section

1.7.1 Precipitation of indium, gallium and germanium

1.7.1.1 Background for the experiments

The experiments were carried out either in native NL2-solution or in pure aqueous solution, depending on the intentions. An experiment carried out in NL2-solution simulated production conditions both physically and chemically. An experiment in aqueous solutions would give a reference for the physical and chemical behaviour of the NL2-solution tests or it would be used for synthesis of pure basic sulphate material as a reference for the databases and the basic sulphates obtained in the NL2-solution tests.

1.7.1.2 Experimental setup

The experiments were carried out at 95°C under continuous stirring. During the experiment parameters such as time, pH, conductivity and temperature were monitored and recorded.

The centre of the experiments were three Torrey Pines heater and stirrer plates, models HS 30 (2 pieces), and HS 10-2 (1 piece) with Torrey Pines HS 30-600 (glass) and HS 30-603 (steel) thermo elements.

The pH and the conductivity of the solution were recorded with the simultaneous use of a Radiometer Meterlab PHM 210 pH-meter with a pHC2401-8 electrode and a Radiometer Meterlab CDM 210 conductometer with temperature correction during the data acquisition and the data was collected with a computer.

[1] At the time of the project the zinc factory was part of Outokumpu and was later sold to Boliden.

1.7.1.3 Chemicals used in the precipitation experiments

The target metals investigated are in such small concentrations in the native NL2-solution that it was necessary to spike the solutions with predetermined amounts of the target metals needed. For this purpose gallium sulphate, indium sulphate and germanium hydroxide of analytical purity were used, Table 15.

When synthetic solutions were used, i.e. solutions based on ultra purified ELGA water, it was necessary also to add other vital chemicals that are present in the native NL2-solution. Thus, also aluminium hydroxide, ferrous- and ferric sulphate were added when required. Also these were of analytical grade.

Table 15. Chemicals used in the basic sulphates and tannic acid experiments.

Compounds used	**Formula**	**Source**
NL2-solution	Mixture	Kokkola Zink Oy
ELGA-water	Purified water	ELGA-purifier, ÅA lab.
Tannic acid	$C_{76}H_{52}O_{46}$	Not Available
Gallium sulphate	$Ga_2(SO_4)_3*18H_2O$	ALFA
Indium sulphate	$In_2(SO_4)_3*6H_2O$	ALFA
Germanium hydroxide	GeO_2	ALFA
Aluminium sulphate	$Al_2(SO_4)_3*18H_2O$	KEBO lab Oy
Ferrous sulphate	FeO_4S*7H_2O	ALDRICH
Ferric sulphate	$Fe_2(SO_4)_3*5H_2O$	ALDRICH
Sulphuric acid	H_2SO_4	J. T. Baker Chemicals NV
Nitric acid	HNO_3	J. T. Baker Chemicals NV
Sodium hydroxide	NaOH	J. T. Baker Chemicals NV
Potassium hydroxide	KOH	J. T. Baker Chemicals NV
Magnesium hydroxide	$Mg(OH)_2$	J. T. Baker Chemicals NV
Ammonia	NH_4	Not Available

In the cases when the pH of the solution needed to be adjusted the proper acids and bases were used. The acids used were sulphuric acid and nitric acid. Nitric acid was mainly used for keeping the liquid samples precipitation free prior to analysis with the DCP. The bases used were sodium hydroxide, potassium hydroxide and magnesium hydroxide, all analytical purity grades.

1.7.1.4 Experimental procedure

1.7.1.4.1 Precipitation experiments as or with basic sulphates

The experiments had to reveal suitable operating conditions for a precipitation based on basic sulphates formation. During the experiments parameters such as sampling time, solution temperature and pH were recorded.

The experiments were carried out at different volumes depending on the sampling need. If no or few intermediate samples were required, then the experiments were carried out in closed 50 ml reactors preventing any evaporation. Up to five reactors could be used at the same time and the external conditions were the same for all. A heating and stirring system was designed specially for the experiments with the 50 ml reactors, Figure 24.

Figure 24. A mini-reactor system/water-bath on a Torrey Pines HS30-2 mixer plate. The plate includes electronically controlled mixer and heater. Each reactor tube (50 ml) contains a small magnet propelled by a larger magnet in the bath, placed in a cut decanter glass in the middle of the vessel.

In the case of basic sulphates synthesis or kinetic experiments larger reactors for volumes up to 1 000 ml were used to allow for more product or repeated sampling.

To be able to closer simulate the production conditions the NL2-solution or ELGA-water used in the experiments was preheated to the reaction temperatures before any mixing was allowed with the other reagents. Thus all experiments could be considered as started at target temperature, usually 90°C. The mixing of the reagents was done quickly and so the experiment had begun.

The experiments were run between 6–72 hours. A possible loss in the solution by evaporation was accounted for by correcting the volumes.

1.7.1.4.2 Precipitation experiments with tannic acid

The tannic acid experiments have been carried out with the simultaneous use of a conductometer (Radiometer, Meterlab CDM 210) and pH-meter (Radiometer, Meterlab PHM 210) with temperature correction during the data acquisition, Figure 25. The data was collected with a computer. The experiments were run between 0.5–72 hours. A possible loss in the solution by evaporation was accounted for.

Figure 25. Equipment for conductometric, pH and redox and measurements.

To avoid interference between the units, an optical connector was placed between the pH-meter and the computer. The sampling intervals could easily be adjusted to the needs of the individual experiments. The recorded data has after the experimental runs been transferred to EXCEL for further analysis of the data.

1.7.1.5 Closing the experiments

After the experimental runs were over a final sample was taken of both liquid and solid phases. In some cases, when there was enough material, some of the suspension would be left aside and analysed later to study the ageing effect. Also any available precipitate was saved for further experiments (stability tests etc.) and analysis (composition etc.).

1.7.2 Analysing the precipitation of indium, gallium and germanium

1.7.2.1 Sample preparation

When large experimental volumes, >50 ml, or continuous sampling were used the samples were withdrawn from the reactor with a syringe equipped with a suction filter to avoid basic sulphate crystals uptake. The sample volume was between 3–5 ml depending on the dilution needs. Before dilution 0.05 ml nitric acid (HNO_3) was added to avoid further precipitation and a change in the target metal levels in the sample solution.

When small experimental volumes, 50 ml, were used without intermediate sampling then one sample was withdrawn according to the above description and another one was prepared by centrifugation of the rest of the sample when still hot, >80°C. In this sample the clear liquid phase was separated from the precipitate and nitric acid was added as above. The precipitate was washed three times with sufficient amounts of water.

1.7.2.2 DCP-AES

The analysis of the target metals was carried out by analysing the liquid phase with Direct Current Plasma Emission Spectroscopy (DCP–AES). The target metal content of the liquid phase gave a direct indication of the success of the precipitation in each case, (Sara et al., 1981).

The accuracy of the used method and instrument are considered good and it met the accuracy requirements posed on it. An instrument with simultaneous multi element detection capacity would have been preferred by the team, but was economically out of range in this particular project. However, all samples could be analysed, and in cases of doubt, the samples were re-analysed after a thorough calibration of the instrument. Strange and non-fitting results were discarded only after repeating the experiment in question since the possibility that new reactions might take place and that formed compounds might transform into other ones had to be accounted for.

During the DCP–AES analysis the instrument was calibrated both prior to the analysis and during the analysis. In some cases a clear instrumental drift would be detected and the instrument had to be calibrated again and the samples had to be reanalysed.

The analysed concentrations varied from 5 mg/l to 3 000 mg/l (as undiluted). The accurate working range of the instrument varies between 3 mg/l to 100 mg/l (Ga) or 3 mg/l to 1 000 mg/l (In), depending on the analysed metal in question. Dilutions were made according to that.

1.7.2.3 Titration Fe(III)-EDTA

During the project Fe contents had to be measured frequently. This was done spectrophotometrically without indicators allowing for a fast and precise analysis with a minimum of effort. The method is developed at the Laboratory of Analytical Chemistry and is one of the basic methods students are required to learn. The method is especially suitable not only for our work since samples need no particular pretreatment but occasional dilution. L. Harju and S-G. Huldén describe the method in detail (Harju et al., 1980(a,b)) and it allows also for spectrophotometric titration of some other metal ions, depending on pH range and wavelength.

The Fe(III)–EDTA titration without an indicator is based on the formation of a stable 1:1 Fe(III)–EDTA chelate spectroscopically detectable at λ = 370 – 450 nm. Fe(II) reacting with EDTA will not be detected in the used wavelength and pH range, (Harju et al., 1980a). The titration proceeds through a 2:1 Fe(III)–EDTA chelate (Fe = 2, EDTA = 1). The titration is illustrated in Figure 26. with lines for the 2:1 titration (L1), 1:1 titration (L2) and achieved equivalence (Eq.).

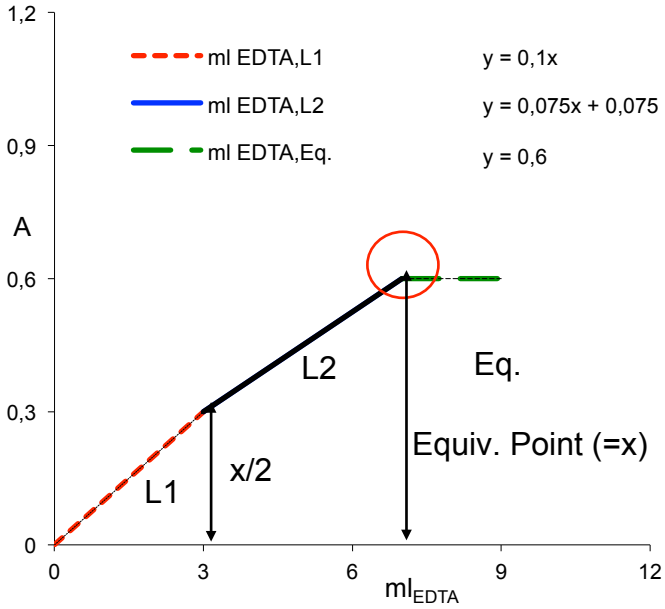

Figure 26. Spectroscopic titration of Fe(III) with EDTA without an indicator: λ = 370–450 nm and pH = 0–6, illustrated with a schematic graph. The equivalence volume of titrated EDTA is found where the lines for L2 and Eq. cross (encircled).

The equivalence volume of the EDTA used may be read from the graph at the crossing point of the lines L2 and Eq. in Figure 26. It may also be calculated from the equations of the lines obtained by linear regression. In an equal manner, the crossing point of the lines L1 and L2 indicate the halfway consumption of the reaction. The starting point of the titration is the same as the starting point of line L1.

During the oxidation some of the Fe(II) may start to oxidize to Fe(III), which in turn will react with the added EDTA. This will then induce an error in the titration and the initial Fe(III)-contents will appear higher than they are. Thus the titration should be carried out rather swiftly.

Although there are several metal ions that react with EDTA (In, Fe(II), Al, Ca, Mg, Na, K) none of them will interfere with the spectroscopical titration of Fe(III). Spectroscopical titration is successful if pH is kept between 0 and 6 and if a wavelength between 370 and 450 nm is used, as the conditional stability constants of some metal-EDTA complexes as functions of pH in Figure 27. indicates.

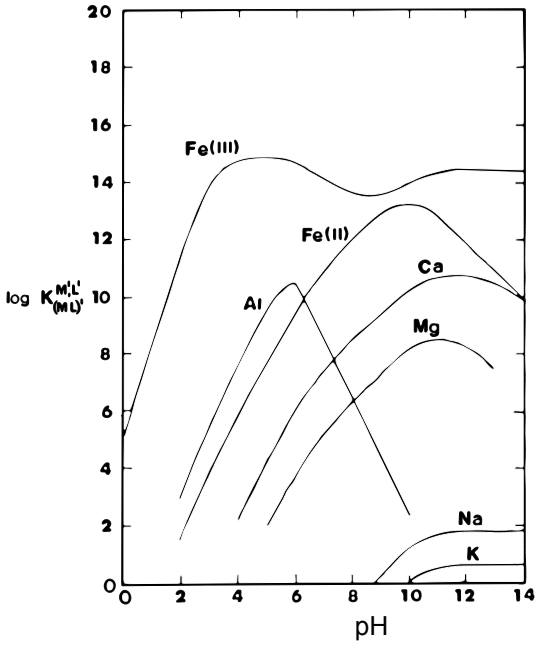

Figure 27. Conditional stability constants of some metal EDTA-complexes as functions of pH, (Harju et al., 1980a).

The analysis of the experimental Fe-solutions was done with Metrohm Spectrophotometer, Figure 28. , with a dip-in light electrode and a range from 400 nm to 700 nm. The addition of EDTA was done through a Titrino 751 GPD titrimeter monitored by a Toshiba Satellite 4080 portable computer with a TiNET titration program. Depending on estimated Fe(III) concentrations the samples were analysed as such or as diluted. The titration was almost completely automatical and only the equivalence volume of EDTA had to be calculated to corresponding Fe(III) values.

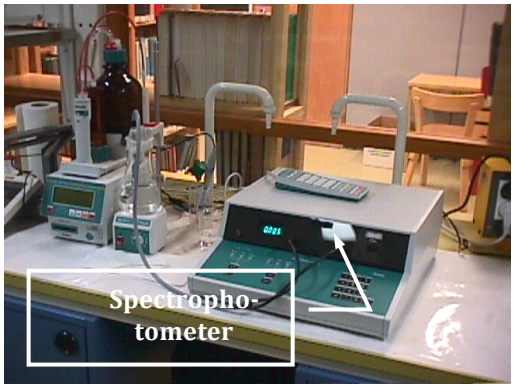

Figure 28. Metrohm Spectrophotometer with a Titrino 751 GPD titrimeter (front right), dip in light-electrode (400-700 nm) and Stirrer 728 (back left).

The pH was kept low in the diluted samples by using pre-acidified water with a pH < 1.6 to dilute the samples. This corresponded to the average pH of our samples. The TiNET program was run on fixed sampling intervals. A 0.05–0.1 M EDTA solution prepared from titrisols was mainly used. The equipment was tested and calibrated with synthetic and spiked process Fe(III)- and {Fe(III) - Fe(II)}-solutions.

The application of the Spectrophotometric titration of Fe^{3+} with EDTA -procedure in the laboratory is easy and quick. The following procedure has been used:

1. A sample is taken. The volume is noted in ml.
2. The sample is diluted with acidic water, pH ~ 1.5 or with a buffer solution of pH ~1.5.
3. The diluted sample volume is noted an indicated as V_0.
4. The sample is placed in the photometer.
5. The sample is titrated with EDTA.

The data is graphically processed to find the equivalence point. The result, ml EDTA consumed, is converted to amount Fe^{3+} (g/l) in the sample solution.

An example is depicted in Figures 29. and 30. (not from the actual test series), an actual test run is depicted in Figures 31. and 32. and the parameters for this test are given in Table 16.

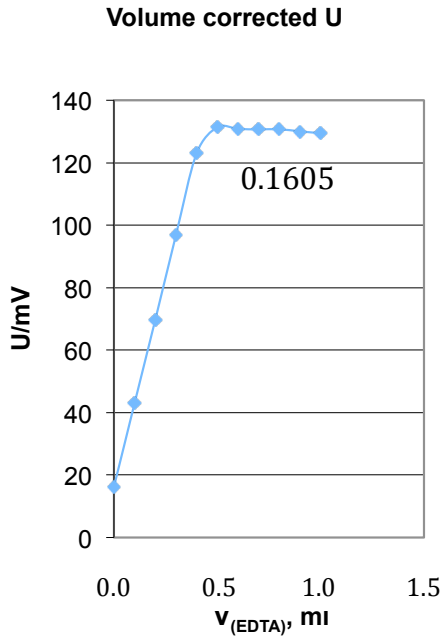

Figure 29. Volume corrected Fe(III)–EDTA titration.

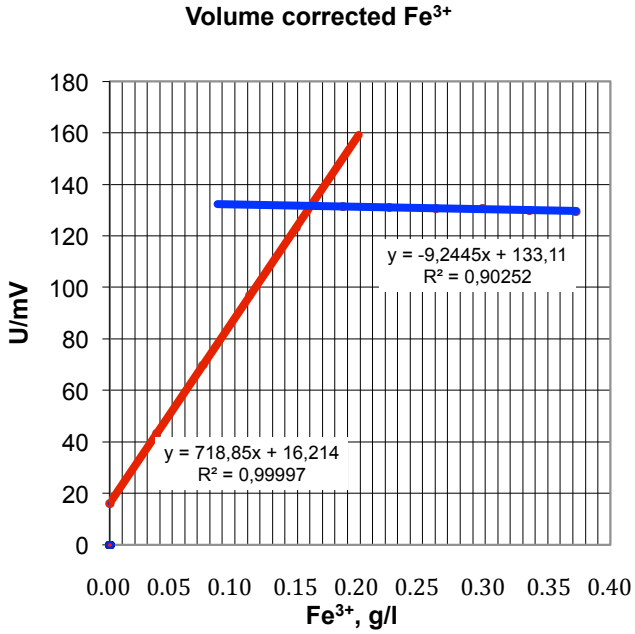

Figure 30. Fe(III)–EDTA volume corrected titration on the x-axis with EDTA values converted to giving directly Fe^{3+} concentration g/l.

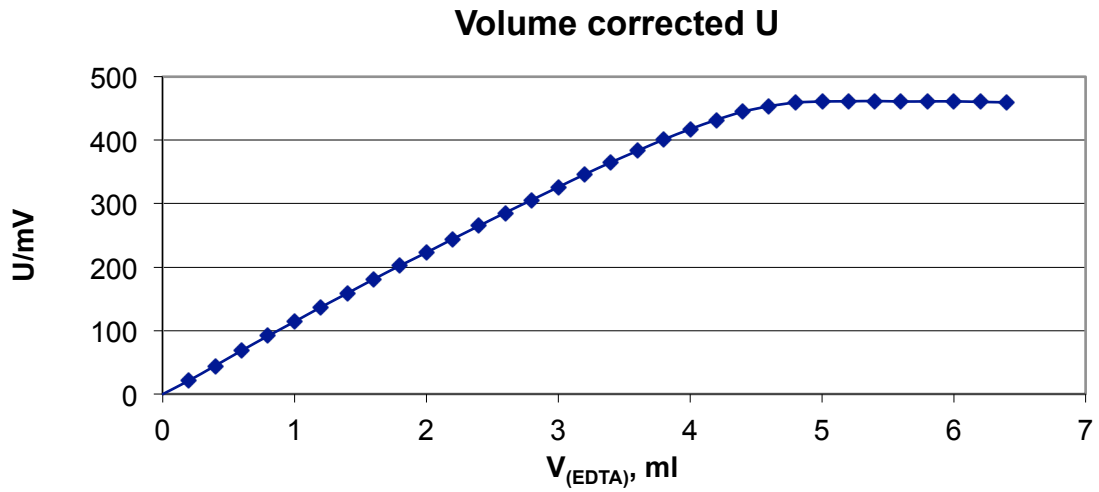

Figure 31. Photometric titration of Fe(III) and Fe(II) with EDTA. Volume corrected U is shown in the figure. Parameters are given in Table 16.

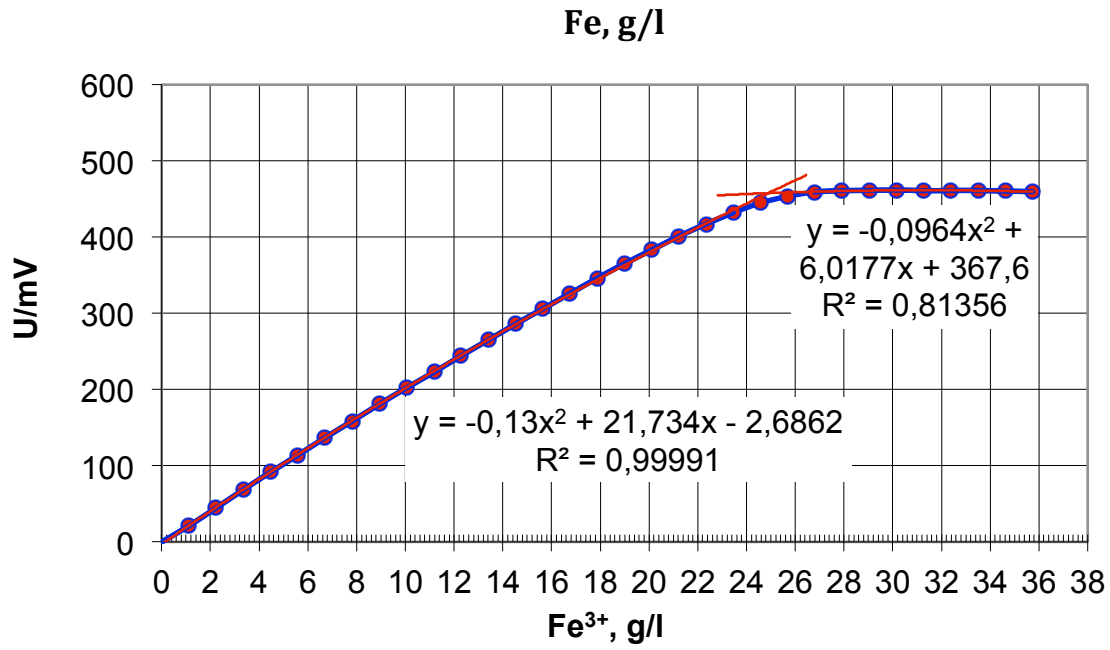

Figure 32. Photometric titration of Fe(III) and Fe(II) with EDTA. Volume corrected U shown in the upper figure. Parameters are given in Table 16.

Table 16. Photometric titration of Fe(III) and Fe(II) with EDTA

Determination of Fe(II) and Fe(III)		
Test run ID:	00022402	
Conc $_{(EDTA)}$:	0.05	M
Added H_2O_2:	1	ml
$V_{(sample)}$:	0.5	ml
$V_{(initial)}$:	28	ml
Conc Fe:	24.3	g/l

1.7.3 Sulphuric acid effect

Sulphuric acid as a solvent is an essential factor. The different methods that have been studied and are presented in this study have all been carried out in highly acidic sulphuric acid solutions. To some extent the sulphuric acid can participate in the overall reaction.

The sulphuric acid effect depends also on the type of process and chemicals that are used. If a solution contains or is treated with ZnS or sphalerite that can make a difference also on the sulphuric acid participation in the process.

1.7.4 pH effect

The formation and precipitation kinetics of basic sulphates are highly pH-dependent and pH below 3.7 favours the precipitation reactions. Experimental conditions were as close to the real zinc process production conditions as possible at pH below 3.7 and temperature at 85°-90°C.

The pH range for successful precipitation is rather narrow and critical. Going outside the effective pH range may mean that In, Ga and Ge precipitation will be limited or cease and different precipitation will start to form.

The pH must be well optimised also when In and Ga recovery is performed in other processes than in zinc production.

1.7.5 Precipitation agent effect

The different precipitation were studied in under similar and conditions typical for an industrial zinc recovery process. The objective was to find out how basic sulphates – processes and precipitation by tannic acid can be used for the recovery of In, Ga and Ge.

1.7.5.1 Basic sulphates and precipitation

The precipitation and separation of In and Ga from zinc production process liquors using basic sulphates is a selective recovery method that minimally alters the conditions in the main process. The aim has been to recover In and Ga from the process solutions either by directly precipitating them as basic sulphates or by co-precipitation with the basic aluminium sulphate *alunite*. The focus has been on In and Ga basic sulphates and precipitation, both in native process liquors and synthetic water based solutions. The effects of interfering metal ions in the process solution have been studied as well as simultaneous In and Ga basic sulphates formation.

The presented study has a focus on In and Ga basic sulphates and precipitation, both in native process liquors and synthetic water based solutions. The effects of interfering metal ions in the process solution have been studied as well as simultaneous In and Ga basic sulphates formation. Optimal precipitation conditions have also been

studied and the precipitation is most successful at pH 1.5–3.7, depending on the kind of basic sulphate.

Basic sulphates are crystalline and rather beautiful with their symmetric forms. They are based on, for example, Al, In, Ga or Fe and formed in H_2SO_4-solutions. The formation is rapid at elevated temperatures above 70°C. Chemically the basic sulphates may be described as

$MX_3(SO_4)_2(OH)_{6(s)}$

Where X = Al^{3+}, Ga^{3+}, In^{3+}, M = K^+, Na^+, NH_4^+, H_3O^+.

The basic sulphates are formed according to the formula:

$$3X_2(SO_4)_{3(aq)} + M_2SO_{4(aq)} + 12H_2O \rightarrow 2MAl_3(SO_4)_2(OH)_{6(s)} + 6H_2SO_{4(l)}$$

Equation 48

Where X = Al_3^+, Ga_3^+, In_3^+, M = K^+, Na^+, NH_4^+, H_3O^+.

Basic sulphates relevant for the work are given in Table 17.

Table 17. Basic sulphates of Al, Ga, In and Fe.

Basic sulphate	**Formula**
Alunite	$MAl_3(SO_4)_2(OH)_6$
Galliunite	$MGa_3(SO_4)_2(OH)_6$
Indiunite	$MIn_3(SO_4)_2(OH)_6$
Jarosite	$MFe_3(SO_4)_2(OH)_6$

Basic sulphates are soluble in sulphuric acid or in liquors with high sulphuric acid content but not soluble in water. The solubility is also strongly affected by pH and temperature.

The basic sulphates have a nice regular crystalline structure and the X-atoms vary from species to species. In some cases, for example Al and Ga, the atoms are to some extent interchangeable, (Dutrizac et al., 2000), depending on the size of the ions, Figure 33. This behaviour can be used in co-precipitation of similar elements.

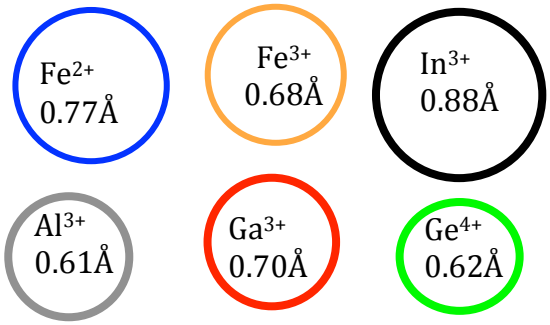

Figure 33. Ion radius for In, Ga, Ge, Al and Fe ions (1 Å = 10^{-10} m), (Lang, 2014).

According to the study at the given process environment a temperature above 70°C is required for basic sulphates to be formed. For precipitation and co-precipitation of In and Ga a suitable pH is required and is around 1.5–3.7 depending of the kind of basic sulphate in question. Co-precipitation of In and Ga with alunite is most successful at pH 1.5–2.5 and precipitation of In and Ga as basic sulphates is most successful at pH between 2.7–3.6. The obtained precipitates are washable and do not dissolve in water.

The experiments showed that Ga precipitate is not only formed faster, more than twice as rapidly as In (**Appendix III**, Figure 28), but also sediments quicker than corresponding In precipitate. In both cases the samples were treated in the same manner and the centrifuge was used at the same rpm. A clear explanation for the different precipitation and sedimentation rates was not found. A plausible explanation may be the different particle size of the precipitate where the In precipitate may have a smaller particle size and thus be forming a colloidal solution.

The study did not give a clear answer on whether to precipitate In and Ga directly as a basic sulphate or to co-precipitate with a basic sulphate that may have been prepared in advance or in situ.

X-ray diffraction (XRD) -results from Outokumpu/Pori showed that Ga precipitates as basic Ga-sulphates while In precipitates could not be identified but seem to be a mixture of different In compounds.

1.7.5.2 Alunite – a basic aluminium sulphate

Alunite is a crystal, Figure 34. , consisting of oxygen (54.08%), sulphur (15.48%), hydrogen (1.46%) and aluminium (19.54%) and has a molecular weight of 414.21 g. Alunite properties are given in Table 18.

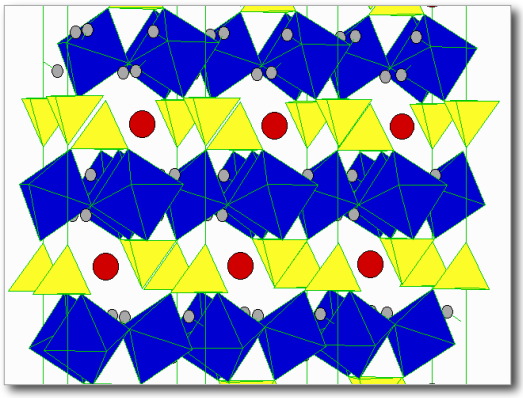

Figure 34. An image of the crystal structure of alunite (K, Na, NH_4)$Al_3(SO_4)_2(OH)_6$. It has Al in octahedral coordination (blue) and sulphur in tetrahedral coordination (yellow) and potassium in irregular 12-fold coordination (red), (http://www.a-m.de/englisch/-lexikon/mineral/sulfate/alunit.htm , © 2000 Büro für angewandte Mineralogie · Dr. Stephan Rudolph · D-47918 Tönisvorst).

The chemical formula for the basic aluminium sulphate alunite is $MAl_3(SO_4)_2(OH)_6$, and is formed according to:

$$3Al_2(SO_4)_{3(aq)} + M_2SO_{4(aq)} + 12H_2O \rightarrow 2MAl_3(SO_4)_2(OH)_{6(s)} + 6H_2SO_{4(l)}$$

Equation 49

M = K^+, Na^+, NH_4^+, H_3O^+.

Table 18. Alunite properties, (http://www.a-m.de/englisch/lexikon/mineral/-sulfate/alunit.htm, © 2000 Büro für angewandte Mineralogie · Dr. Stephan Rudolph · D-47918 Tönisvorst.).

Alunite	
Chemistry	$KAl_3[(OH)_6\|(SO_4)_2]$
Hardness	3.5 - 4
Lustre	vitreous, pearly
Colour	white, grey, yellowish grey, reddish grey or yellowish white
Density [g/cm³]	2.6 - 2.9
Crystal	habit trigonal
Cleavage, fracture	[0001] good
Other characteristics and occurrences	Rock-forming mineral, formed by alteration of feldspar-rich rocks
Molecular weight [g/mol]	414.21
Oxygen	54.08 %
Sulphur	15.48 %
Hydrogen	1.46 %
Aluminium	19.54 %

In the study alunite is added to the liquor or produced in situ for the purpose of precipitating Ga in a selective manner. Al and Ga have an ion radius close to each other and this is considered to be a contributing factor. The particle size effect was, however, not studied separately and was not part of the work.

Alunite can also be used to precipitate In but the precipitation is not as efficient and as complete as for Ga. It was also interesting to find out that Ge was not precipitated with alunite. In the cases were Ge did precipitate it was as co-precipitation and highly pH dependent.

Galliunite is the most stable of the studied jarosite type compounds and precipitates well. The formation of galliunite is slow but can be boosted with ferric iron.

It is possible that Al will also form a mixed type basic sulphate together with In and Ga that will be, according to Scott (1990) and Stofferegen et al. (1990):

$2Na(M_3(SO_4)_2(OH)_6)$

$M = Al^{3+}, In^{3+}, Ga^{3+}$

Ge was not precipitated with alunite.

1.7.5.3 Galliunite – a basic gallium sulphate

The chemical formula for the basic gallium sulphate galliunite is $MGa_3(SO_4)_2(OH)_6$, and is formed as shown in:

$$3Ga_2(SO_4)_{3(aq)} + M_2SO_{4(aq)} + 12H_2O \rightarrow 2MGa_3(SO_4)_2(OH)_{6(s)} + 6H_2SO_{4(l)}$$

Equation 50

$M = K^+, Na^+, NH_4^+, H_3O^+$.

Galliunite can be precipitated either as a basic sulphate, galliunite, or by a co-precipitation with alunite. In both cases up to a complete removal of Ga can be obtained. The process is strongly dependent on temperature (above 70°C) and pH (1.5 – 3.7 depending on precipitation method). In case of co-precipitation it has to be separately evaluated if the basic sulphate is produced in situ or in advance and then added to the process. The study did not give a clear answer to this question.

The removed Ga precipitate is non-soluble in water and washable. The method is also rather selective. If the target solution contains In as well, then In will precipitate to some extent and this has to be accounted for.

1.7.5.4 Indiunite – a basic indium sulphate

The chemical formula for the basic indium sulphate indiunite is $MIn_3(SO_4)_2(OH)_6$, and is formed as shown:

$$3In_2(SO_4)_{3(aq)} + M_2SO_{4(aq)} + 12H_2O \rightarrow 2MIn_3(SO_4)_2(OH)_{6(s)} + 6H_2SO_{4(l)}$$

Equation 51

$M = K^+, Na^+, NH_4^+, H_3O^+$.

In precipitation from the standard process liquor was studied. It can be precipitated and sedimented but slightly less efficiently than Ga. If, in case of precipitation as a

basic sulphate, the solution contains Ga then In recovery will fall behind that of Ga and both will suffer if the aim is to have a selective precipitation. If both can be precipitated at the same time or the used solutions do not contain Ga then In can be separated by precipitation as a basic sulphate. When using co-precipitation with alunite then In will not precipitate and Ga can be removed rather selectively.

1.7.5.5 Jarosite – a basic iron sulphate

Jarosite is a well-known basic sulphate of iron used in the waste treatment of hydrometallurgical Zn plants. It has a very low solubility and is used to remove accumulated iron and other undesired elements from the process. Jarosite is very efficient in removing In and Ga as well, (Dutrizac et al., 2000). Removing In and Ga from jarosite is difficult. This may be due to the very similar chemistry between Fe, In and Ga. Thus recovering In and Ga from jarosite in an economically feasible way is a challenge.

Jarosite is formed according to:

$$3Fe_2(SO_4)_{3(aq)} + M_2SO_{4(aq)} + 12H_2O \rightarrow 2MFe_3(SO_4)_2(OH)_{6(s)} + 6H_2SO_{4(l)}$$

Equation 52

$M = K^+, Na^+, NH_4^+, H_3O^+$.

Germanium is not forming a jarosite precipitate. It may, however, be co-precipitated together with other precipitates.

1.7.5.6 Tannic acid

Tannin, usually containing up to 50-80% of tannic acid (Kul et al., 2008), is widely used in different metal recovery processes and tannin and tannic acid as recovery agents are continuously studied, (Nakamura et al., 1998, (a, b); Liang et al., 2008 (a, b); Kul et al., 2008). The tannic acid properties are presented in Table 19.

Tannic acid readily reacts with the Ge in the solution, Equation 53, Table 20, Figure 35. , (Kul et al., 2008). In the studied process environment the reaction is selective. Precipitating and separating Ge from zinc production process liquors using tannic acid minimally affects the conditions in the main process. Although the zinc production process liquors are here used as a reference, the method may be applied also to other solutions of similar consistency.

$$Ge^{4+} + O_2 + H_6T \rightarrow 2GeO*H_6T$$

Equation 53

H_6T = tannic acid

Table 19. Properties of tannic acid, (Wolfram|Alpha Knowledgebase, 2015).

Tannic acid	
Formula*	$C_{76}H_{52}O_{46}$
Molecular weight*, g/mol	1701.23
Melting point*	210°C (slight decomposition)
Solubility in water**	Soluble
Solubility in alcohol**	Very soluble
Source*: Wolfram|Alpha Knowledgebase, 2015	
Source**: experimentally tested during the study	

Table 20. Tannic acid reactions with different ions in a synthetic water solution. The ions have been added to the solution in corresponding order. KCl was added to precipitate the reacted Ge-tannic acid. The volume used was 25 ml.

Element	**Concentration, mg/ml**	**Colour**	**Type**	**Solubility**
$Al^{(III)}$	1000	Clear		Ok
$Ga^{(III)}$	1000	Clear		Ok
$In^{(III)}$	1000	Clear		Ok
$Pb^{(II)}$	1000	Clear		Ok
$Cu^{(II)}$	1000	Clear		Ok
$Zn^{(II)}$	1000	Clear		Ok
$Co^{(II)}$	1000	Clear		Ok
$Ni^{(II)}$	1000	Clear		Ok
$Bi^{(III)}$	1000	Clear		Ok
$Ag^{(I)}$	1000	Clear		Ok
$Fe^{(II)}$	1000	Blue	Disapp.	Ok
$Fe^{(III)}$	1000	Blue	Disapp.	Ok
$Ti^{(IV)}$	1000	Yellow	Stable	Ok
$Sn^{(IV)}$	1000	Clear		Ok
$Si^{(IV)}$	1000	Clear		Ok
$Ce^{(IV)}$	1000	Clear		Ok
$Ge^{(IV)}$	*1000*	*Brownish*	*Stable*	*Precipitates*
KCl*	Saturated	Clear		

Of the tested ions only Ge precipitated when KCl was added to help precipitate the reacted Ge-tannic acid. The results are in line with studies on behaviour of tannins in germanium recovery by tannin processes, Figure 35. , (Liang, 2008b).

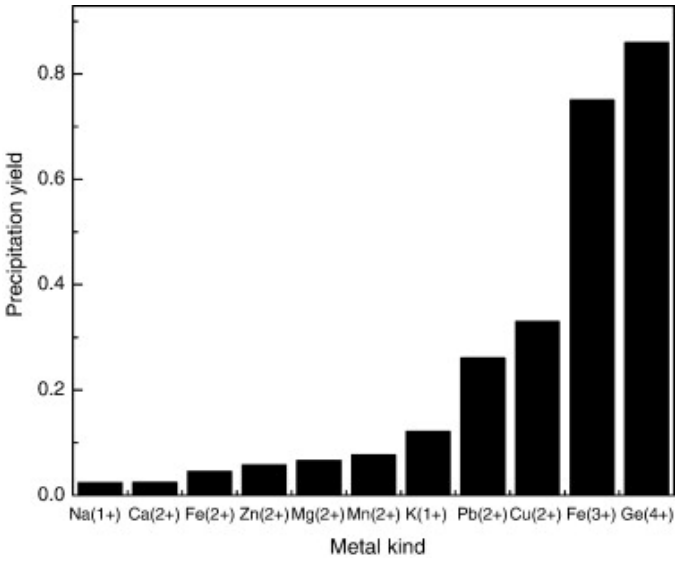

Figure 35. Binding ability of metal in single-metal solution and by tannin process. Complexation condition: stirring rate, 10 rps; complexation temperature, 373 K; complexation duration, 500 s (Liang, 2008b).

1.7.6 Concluding remarks

The experiments clearly show that tannic acid can successfully be used to precipitate germanium from highly acidic H_2SO_4-solutions. Furthermore, tannic acid can successfully be used to precipitate Ge in a selective manner in the studied environment. The precipitation is rapid and almost all germanium has been precipitated within 40 minutes. Ge precipitation is rapid enough to take place before In and Ga have had the time to form compounds that are able to precipitate.

A part of gallium (about 40%) was co-precipitated during germanium precipitation from native process solutions. Aluminium and iron did not affect the precipitation reaction or outcome, Table 20.

The selectivity of the process (step) is high and is not disturbed by other elements in the studied solutions (**Appendix IV**). Thus the tannic acid – Ge precipitation can be used as a selective process step for precipitating Ge. The results of the experiments are not completely in line with some other results mentioned in the literature (Liang et al., 2008 (a, b); Zhou et al., 2013) that find the use of tannic acid less attractive. The experiments were, however, well prepared and carried out carefully and repeated to confirm the outcome.

Conclusions and future perspectives

1.8 Oxidation of Fe^{2+} to Fe^{3+} with catalysts

The oxidation kinetics of ferrous sulphate to ferric sulphate was studied for both catalysed and non-catalysed reactions. The aim was to produce and verify the existence of polymeric ferric sulphate species and determine the favourable conditions for polymerization.

A kinetic model was developed based on ionic and molecular mechanisms. The fit of the model was thoroughly studied and the model was found to describe the experimental data very well. The developed kinetic model can be used in reactor simulations and reactor design.

The catalytic effects in the oxidation of ferrous sulphate to ferric sulphate were studied using active carbon and noble metals on active carbon supports. Active carbon and noble metals considerably enhanced the reaction rates. The outstanding effect of platinum as a noble metal on active carbon support on the oxidation rates should be noted. Consequently, the capacity of existing reactors can be multiplied by the use of catalysts similar those screened in the current work.

Polymeric ferric sulphates were produced. The existence of the polymeric species was verified both analytically and by comparison with available high-class reference materials. The obtained product was considerably better than the references and showed good ageing stability without any additives.

Polymeric ferric sulphates can be produced in existing facilities without changes in existing technical equipment. The ratios of the chemicals used should be recalculated, probably leading to lower chemical costs in production. Customers can be offered an improved product that is usable over a wider pH range.

1.9 Reduction of Fe^{3+} to Fe^{2+} with zinc sulphide and sphalerite

The reduction of ferric iron to ferrous iron with zinc sulphide and sphalerite as the reducing agent was studied in an isothermal, stirred batch reactor. The aim was to gain further understanding of the reactions and rates when Fe^{3+} was reduced to Fe^{2+} with ZnS and sphalerite.

For ferric iron, in acidic sulphuric acid solutions, the reduction rate increased when the ferric iron concentration and the reducing agent amount in proportion to the ferric iron amount were increased.

The sulphuric acid concentration had a strong enhancing effect on the reduction rate when ZnS was used but it did not affect the reduction rate when sphalerite was used. In the ZnS case the effect is proportional to the H_2SO_4 concentration in the power of 1.5. The experimental results for the ZnS alternative indicate that the reaction is carried out in the liquid phase with an intermediate step where H_2SO_4 participates in the reaction. The sphalerite experiments indicate that the reaction rate depends on the amount of reducing agent in the first order.

The reaction rate is strongly dependent on the temperature and the rate increases with increased temperature. This applies to both the reducing agents, zinc sulphide and sphalerite.

A product layer was not formed to decrease the reaction rate in neither the case with ZnS nor with sphalerite. The study showed that separate sulphur particles were formed instead.

1.10 Precipitation of In, Ga and Ge

Indium, gallium and germanium were precipitated in a selective way. The experiments indicate that further research should be carried out especially in the area of recirculation and recovery from other than currently used main sources.

These valuable metals are at the moment treated as secondary products in the primary recovery of zinc and aluminium. This reflects both their availability and their market price. Recovery from secondary sources and recirculation would shift the supply and price towards markets expectations and actual demand.

Indium and gallium can be selectively precipitated with basic sulphates, such as alunite, or as basic sulphates themselves, such as indiunite and galliunite.

The study did not give a clear answer on whether to precipitate directly as a basic sulphate or to co-precipitate with a basic sulphate that may be prepared in advance or in situ.

In case of precipitation as a basic sulphate, the solution contains Ga then In recovery will fall behind that of Ga and both will suffer if the aim is to have a selective precipitation. If both can be precipitated at the same time or the used solutions do not contain Ga then In can be separated by precipitation as a basic sulphate. When using co-precipitation with alunite then In will not precipitate and Ga can be removed rather selectively.

Germanium was precipitated very selectively with tannic acid. While tannic acid use has its challenges in traditional hydrometallurgical processes there is use for it in the alternative processes in the future.

Further studies should be carried out where the studied methods would be applied on new material sources. These sources can be waste from primary metal production or recycled material and scrapped products.

Sustainable and ecologically friendly production of In, Ga and Ge can be achieved by promoting the use of materials and sources regarded as waste by other players. The understanding of the selective precipitation and recovery processes studied in the present work is a step in this direction.

Notations

1.11 List of symbols (Part 1)

A gas-liquid mass transfer area
A, B, C parameters for Henry's constant
a gas-liquid mass transfer area-to-liquid volume
a_1, a_2 rate parameters for non-catalytic oxidation
b_n parameters for estimating solvent vapour pressure correction
c concentration
F ratio between non-catalytic and catalytic reaction rate
f factor for the reverse reaction rate

$$f = \frac{c_{Fe^{3+}}^4 c_w^4}{K_c c_{Fe}^4 c_0 c_v^4}$$

H_0 Henry's constant
h salting out coefficient
K equilibrium constant
K', K'' lumped equilibrium constants
k rate constant
k', k'' lumped rate constants
k_L mass transfer coefficient in liquid phase
m mass
N molar flux
n amount of substance
p partial pressure
Pc critical pressure
r reaction rate
r_i generation rate of compound i
R^2 correlation coefficient
t time
T absolute temperature
Tc critical temperature
V volume
VP n parameter in vapour pressure equation
w weight fraction
x mole fraction
z valence
δ vapour pressure correction
v stoichiometric coefficient
v' stoichiometric number
ρ_B catalyst bulk density
θ surface coverage

1.12 List of symbols (Part 2)

c concentration
E_a activation energy
f rate function
g integrated rate function
k rate constant at reference temperature (T_{mean})
$k´$ rate constant
$k´´$ modified rate constant
M molar mass
m mass
p_1, p_2, p_3, p_4, p_5 rate exponents
Q sum of residual squares
R gas constant
R^2 degree of explanation
r rate
T temperature
t time
V_L liquid volume

Greek letters
α conversion
ν stoichiometric coefficient

1.13 Subscripts and superscripts

B bulk, in bulk density (ρ_B)
c concentration based quantity
cat catalyst
g, G gas
i component index
j reaction index
L liquid phase
nc non-catalytic
T thermodynamic quantity
v vacant site
+ anion
- cation
* interfacial quantity

1.14 Abbreviations

Sulphuric acid
0 total (of sulphate)
O oxygen (O_2 or surface oxygen O*)
O^- charged oxygen ion (O^{*-})
OH surface hydroxyl (OH*)
SO_4 sulphate ion (SO_4^-)
W water (H_2O)
W+ hydronium ion (H_3O^+)
* surface site
NL2 Neutral Leach 2 (process solution from a certain part of the hydrometallurgical zinc process)
ELGA Ultra purified water (Elga LLC, Veolia Water Solutions & Technologies)
DCP-AES Direct Current Plasma Emission Spectroscopy
EDTA Ethylenediaminetetraacetic acid (for the spectrophotometric Fe-EDTA – titration)

References

Abdullahi, M. E., Musa, L., 2011, Recovery of coagulants from water works sludge: A review, Pelagia Research Library, Advances in Applied Science Research, 2011, 2 (6):410-417

Alfantazi, A.M., Moskalyk, R.R., 2003, Processing of indium: a review, Minerals Engineering 16 (2003) 687–694

Azuka, A. I., 2009, The Influx of Used Electronics into Africa: A Perilous Trend, 5/1 Law, Environment and Development Journal (2009), p. 90, available at http://www.lead-journal.org/content/09090.pdf

Birima, A. H., Hammad, H. A., Desa, M. N. M., Muda, Z. C., 2013 Extraction of natural coagulant from peanut seeds for treatment of turbid water, 4th International Conference on Energy and Environment 2013 (ICEE 2013), IOP Publishing, OP Conf. Series: Earth and Environmental Science 16 (2013) 012065 doi:10.1088/1755-1315/16/1/012065

Brown, R. D., 1998a, Germanium, U.S. Geological Survey Publications

Brown, R. D., 1998b, Indium, U.S. Geological Survey Publications

Brown, R. D., 2002a, Germanium, U.S. Geological Survey Publications

Brown, R. D., 2002b, Indium, U.S. Geological Survey Publications

BRUKER OPTIK GmbH, 1998, Bruker IFS Users manual.

Christophersen, D., 2015, Jar Testing Procedures, Veolia Water Solutions

Crundwell, F.K., 1987. Kinetics and mechanism of the oxidative dissolution of a zinc sulphide concentrate in ferric sulphate solutions. Hydrometallurgy 19, 227–242

Dutrizac, J. E., Chen, T. T., 2000, The Behaviour of Gallium During Jarosite Precipitation, Canadian Mineralogist, Vol. 39, Issue 1, pp. 1-14

Ekinci, Z., Colak, S., Cakici, A., Sarac, H., 1998. Leaching kinetics of sphalerite with pyrite in chlorine saturated water. Minerals Engineering 11 (3), 279–283

Engelhardt, T. L., April 2010, Coagulation, Flocculation and Clarification of Drinking Water, Drinking Water, Hach Company, Guide

Fogg, P. G. T., Gerrard, W., 1991, Solubility of Gases in Liquids, Wiley, Chichester

Gibson, C., Hayes, T., October 2011, Indium and gallium overview, Edison investment research

Global and China Germanium Industry Report, 2013-2016, PR Newswire Association LLC., A UBM plc company

Guberman, D. E., 2012a, Germanium, U.S. Geological Survey Publications

Guberman, D. E., 2012b, Germanium, U.S. Geological surveys minerals yearbook — 2012 U.S. Geological Survey Publications

Haario, H., 1994, Modest User's Guide, ProfMath Oy, Helsinki (1994)

Harju, L., Huldén, S-G., 1980a, Determination of Total Iron in Standard Rocks by Spectrophotometric Titration with EDTA, Talanta, Vol. 27, 811-814

Harju, L., Huldén, S-G., 1980b, Standardization of EDTA by Spectrophotometric Titration, with Metallic Copper as Standard, Talanta, Vol. 27, 815-817

Hindmarsh, A., ODEPACK, 1983, A systemized collection of ODE solvers. Scientific Computing (edited by Stepleman J. S. et al.,), pp. 55-64. IMACS North-Holland, Amsterdam

ISO 7027:1999 (2010 update) - Water quality -- Determination of turbidity

Jaskula, B. W., 2012a, Gallium, U.S. Geological Survey Publications

Jaskula, B. W., 2012b, Gallium, U.S. Geological surveys minerals yearbook — 2012 U.S. Geological Survey Publications

Jaskula, B. W., 2013, Gallium, USGS 2011 Minerals Yearbook, U.S. Department of the Interior February, U.S. Geological Survey

Jorgenson, J. D., 2002a, Germanium, U.S. Geological surveys minerals yearbook — 2002 U.S. Geological Survey Publications

Jorgenson, J. D., 2002b, Indium, U.S. Geological surveys minerals yearbook — 2002 U.S. Geological Survey Publications

Kramer, D. A., 1998, Gallium, U.S. Geological Survey Publications

Kramer, D. A., 2002a, Gallium, U.S. Geological Survey Publications

Kramer, D. A., 2002b, Gallium, U.S. Geological surveys minerals yearbook — 2002 U.S. Geological Survey Publications

Kul, M., Topkaya, Y., June 2008, Recovery of germanium and other valuable metals from zinc plant residues, Hydrometallurgy, Volume 92, Issue 3-4, Pages 87–94

Lang, H., Fall 2014, Geology 284: Mineralogy, West Virginia University, Dept. of Geology & Geography

Liang, D., Wang, J. and Wang, Y., November 2008a, Germanium recovery by co-precipitation of germanium and iron in conventional zinc metallurgy, The Journal of The Southern African Institute of Mining and Metallurgy, VOLUME 108, 715-718

Liang, D., Wang, J., Wang, F., Jibo Jiang, August 2008b, Behavior of tannins in germanium recovery by tannin process, Hydrometallurgy, Volume 93, Issue 3-4, Pages 140–142

Licht, C., Peiro´, L. T., Villalba, G., 2015, Global Substance Flow Analysis of Gallium, Germanium, and Indium, Journal of Industrial Ecology

Lide, D. R., 1994, CRC Handbook of Chemistry and Physics, 75th edition, 6-56

Lochmann, J., Pedlík, M., 1995. Kinetic anomalies of dissolution of sphalerite in ferric sulfate solution. Hydrometallurgy 37, 89–96

Lotens, J.P., Wesker, E., 1987. The behaviour of sulphur in the oxidative leaching of sulphidic minerals. Hydrometallurgy 18, 39–54

Markus, H., Fugleberg, S., Valtakari, D., Salmi, T., Murzin, D. Yu., Lahtinen, M., 2004a, Kinetic modelling of a solid–liquid reaction: reduction of ferric iron to ferrous iron with zinc sulphide, Chemical Engineering Science, Volume 59, Issue 4, 919–930

Markus, H., Fugleberg, S., Valtakari, D., Salmi, T., Murzin, D. Yu., Lahtinen, M., 2004b, Reduction of ferric to ferrous with sphalerite concentrate, kinetic modelling, Hydrometallurgy, Volume 73, Issues 3–4, 269–282

Marquardt, D. W., 1963, An algorithm for least squares estimation on nonlinear parameters, SIAM J. 11, 431-441

Mikolajczak, C., 2009, Availability of indium and gallium, Indium Corporation

Momade, F.W.Y., Momade, Zs.G., 1999. A study of the kinetics of reductive leaching of manganese oxide ore in aqueous methanol– sulphuric acid medium. Hydrometallurgy 54, 25–39

Murzin, D. Yu., 2015, Chemical Reaction Technology, Walter de Gruyter GmbH, Berlin/Boston

Nakamura, Y., Shirato, W., Nakamura, Y., 1998b New Liquid Waste Control with Tannin Adsorbent, Proceedings of the 11th Pacific Basin Nuclear Conference

Nakamura, Y., Shirato, W., Yamakawa, H., Tominaga, Y., Nakamura Y., 1998a, Liquid Waste Treatment System with Insoluble Tannin, 62th Annual Meeting of The Society of Chemical Engineers

Oram, B., 2015, Stream Water Quality - Importance of Total Suspended Solids / Turbidity, Turbidity and Total Suspended Solids Surfacewater Monitoring, Water Research Center

Palencia Perez, I., Dutrizac, J.E., 1991. The effect of the iron content of sphalerite on its rate of dissolution in ferric sulphate and ferric chloride media. Hydrometallurgy 26, 211–232

Polinares Consortium, 2012, Fact Sheet: Indium, POLINARES working paper n. 39

Prodanović, J., Šćiban, M., Antov, M., 2013, Improvement of wastewater treatment by use of natural coagulants, Journal of Economic Development, Environment and People Volume 2, Issue 2

Reid R. C., Prausnitz, J. Poling, M., B. E., 1988, The Properties of Gases and Liquids, McGraw Hill, New York

Ruzicka, J., Marshall, G.D., 1990. Sequential injection: a new concept for chemical sensors, process analysis and laboratory assays. Analytica chimica acta 237, 329–343

Rönnholm, M. R., Wärnå, J., Salmi, T., Turunen, I., Luoma, M., 1999a, Oxidation Kinetics of Ferrous Sulphate over Active Carbon, Industrial & Engineering Chemistry Research, 7, 38

Rönnholm, M. R., Wärnå, J., Salmi, T., Turunen, I., Luoma, M., 1999b, Kinetics of oxidation of ferrosulphate with molecular oxygen, Chem. Eng. Sci., 54

Salmi, T., Grenman, H., Bernas, H., Wärnå, J., Murzin, D. Yu., August 2010, Mechanistic modelling of kinetics and mass transfer for a solid-liquid system: Leaching zinc with ferric iron, Chemical Engineering Science, Volume 65, Issue 15, Pages 4460-4471

Sara, R., Huldén, S-G, Harju, L., 1981, Kaariplasmaemissio (DCP) analyysitekniikkana, Kemia-Kemi, n:o 12, page 774-778

Satterfield, Z. P. E., 2005, Jar Testing, Tech Brief

Schumpe, A., 1993, The Estimation of Gas Solubilities in Salt Solutions, Chem. Eng. Sci., 48, 153

Scott, K. M., 1990, Origin of alunite- and jarosite-group minerals in the Mt. Leyshon epithermal gold deposit, northeast Queensland, Australia, American Mineralogist, Volume 75, pages 1176-1181

Sippola, H., 1992, Rautasulfaatin liukoisuuden mallitus rikkihappo-vesisysteemissä, Licentiate thesis, Teknillinen korkeakoulu, Espoo

Stofferegen, R. E., Cygan, G. L., 1990, An experimental study of Na-K exchange between alunite and aqueous sulfate solutions, American Mineralogist, Volume 75, pages 209-220

Tolcin, A. C., 2012a, Indium, U.S. Geological Survey Publications

Tolcin, A. C., 2012b, Indium, U.S. Geological surveys minerals yearbook — 2012 U.S. Geological Survey Publications

UN, 2010, The human right to water and sanitation, Resolution 64/292, United Nations

Valtakari, D., 1999, Catalytic Preparation of Ferric sulphate, Licentiate Thesis. Åbo Akademi University, Laboratory of Industrial Chemistry and Reaction Engineering, Turku

Valtakari, D., Rönnholm, M. R., Wärnå, J., Salmi, T., Laine, E., Luoma, M., (2001, submitted for publication), The intrinsic kinetics of ferrous sulphate oxidation on active carbon

Weisenberger, S., Schumpe, A., 1996, Estimation of Gas Solubilities in Salt Solutions at Temperatures from 273 K to 363 K, AIChE Journal, Vol 42, Nr 1, 298

WHO, 1996a, Coagulation, flocculation and clarification, Fact Sheet 2.13, Fact Sheets on Environmental Sanitation

WHO, 1996b, Turbidity measurement, Fact Sheet 2.33, Fact Sheets on Environmental Sanitation

WHO, 1998, Aluminium in Drinking-water, WHO/SDE/WSH/03.04/53

Wolfram|Alpha Knowledgebase, 2015

Wolfram|Alpha Knowledgebase, 2015, United States Geological Survey, World Mineral Data, Global and China Germanium Industry Report 2012-2015, 2015 Wolfram Alpha LLC_A Wolfram Research Company

Wurtz, C. A., 1880, Elements of Modern Chemistry. Reprint. London: Forgotten Books, 2013. 336

www.a-m.de/englisch/lexikon/mineral/sulfate/alunit-kris1.htm, © 2000 Büro für angewandte Mineralogie · Dr. Stephan Rudolph · D-47918 Tönisvorst.

www.a-m.de/englisch/lexikon/mineral/sulfate/alunit.htm, © 2000 Büro für angewandte Mineralogie · Dr. Stephan Rudolph · D-47918 Tönisvorst.

www.strategic-metal.typepad.com, 2015

Zainal-Abideen, M., Aris, A., Yusof, F., Abdul-Majid, Z., Selamat, A., Omar, S. I., 2012, Optimizing the coagulation process in a drinking water treatment plant – comparison between traditional and statistical experimental design jar tests, Water Science & Technology, IWA Publishing 2012

Zhou, Z., Chu, G., Gan, H., Yang, T., Chen, L., 2013, Ge and Cu recovery from precipitating vitriol supernatant in zinc plant

I

I Oxidation of Fe^{2+} to Fe^{3+} by catalytic preparation of ferric sulphate

I.1. About water purification in general

According to the UN resolution 64/292 the right to clean water and sanitation has been recognised as a human right (UN, 2010). At the same time demand for water in general and clean water in particular is increasing while water supplies are diminish for different reasons.

Municipal wastewater is treated with the purpose of recirculating the water or to clean it before releasing it back to the nature. The cleaning processes typically consist of several steps including chemical and mechanical treatment at water purification plants.

Water purification includes the removal of dirt particles from wastewater. For this purpose chemicals are added to coagulate with the dirt particles (coagulation) and subsequently form flocks (flocculation). The formed flocks sediment and are removed from the process as a sludge.

Typical coagulants that are used today include aluminium- and iron based polymers and mixtures of these. The choice of coagulant depends on multiple factors, including type of water, pH, end use of water and disposal options for the accumulated sludge. Aluminium-based coagulants are associated with possible risks to humans and plant life if they remain in the water or leak from the sludge (Prodanović et al., 2013; Abdullahi et al., 2010; WHO, 1998).

Coagulants react with dirt particles and form flocks. If necessary, also flocculants are added. The formed flocks are removed and the obtained sludge is disposed of in a safe manner. The coagulants can be recovered to increase overall efficiency and to reduce sludge amounts (Abdullahi et al., 2010).

Iron based coagulants are attractive for several reasons, as for example

- the purity of the treated water is high,
- heavy-metal content is low,
- biological decomposition products are efficiently reduced,
- biological decomposition products can be reduced at low pH,
- ferric sulphate can be used for sludge conditioning,
- pH level can be well controlled,
- sludge production is low and can be well controlled,
- good cost efficiency,
- flocks are rapidly formed,
- ferric sulphate does not have colouring effects like ferrous sulphate. In municipal water treatment all iron-based compounds

I.2. Introduction to the study

Ferric sulphate, $Fe_2(SO_4)_3$, is used in water purification. Oxidation of ferrous sulphate, $FeSO_4$, to ferric sulphate in acidic aqueous solutions of H_2SO_4 over finely dispersed active carbon particles was studied in a vigorously stirred batch reactor. Molecular oxygen was used as the oxidation agent and several catalysts were screened: active carbon, active carbon impregnated with Pt, Rh, Pd and Ru. Both active carbon and noble metal-active carbon catalysts enhanced the oxidation rate considerably. The order of the noble metals according to the effect was: Pt >> Rh > Pd, Ru. By the use of catalysts the production capacities of existing oxidation units can be increased. Analysis of the reaction product indicated that it is possible to obtain polymeric products with good coagulation properties.

Systematic kinetic experiments were carried out at the temperature and pressure ranges of 60-100°C and 4-10 bar, respectively. The results revealed that both non-catalytic and catalytic oxidation of Fe^{2+} take place simultaneously. The experimental data were fitted to rate equations, which were based on a plausible reaction mechanism: adsorption of dissolved oxygen on active carbon, electron transfer from Fe^{2+} ions to adsorbed oxygen and formation of surface hydroxyls. A comparison of the Fe^{2+} concentrations predicted by the kinetic model with the experimentally observed concentrations indicated that the mechanistic rate equations were able to describe the intrinsic oxidation kinetics of Fe^{2+} over active carbon and active carbon-noble metal catalysts.

I.3. The use of ferrosulphate – examples

I.3.1. Major areas of ferrosulphate use

Ferrous and ferric sulphates have several applications in the everyday life. Some of the major application areas of ferrous sulphate are:

- as a raw material for chemicals in waste water and freshwater treatment,
- as an additive in cement and concrete production and
- as a raw material for video- and audiocassette coatings.

Ferrous sulphate is added to cement and concrete in the grinding process. Cement raw material, especially in Finland, contains chromium. The task of ferrous sulphate task is to inhibit chromium from causing allergic symptoms in people.

The magnetic surface of less expensive video- and audiocassettes is made from an iron layer. The cassettes are usually referred to as ferro-cassettes.

The main area of interest and the point of focus of this work is the use of Fe^{3+}-sulphate in water purification. The raw material for the various ferric sulphate (Fe^{3+}) is ferrous sulphate (Fe^{2+}).

I.3.2. Other areas of ferrous sulphate use

Ferrous sulphates are used, for instance,

- as an additive in agricultural fertilisers and
- as an additive in animal forage and feed

The purpose of using ferrous sulphate as an additive in fertilisers is its ability to hinder moss from growing, as the pH in the soil falls to a level unsuitable for moss. Ferrous sulphate in very small amounts in animal forage and feed improves the iron values in animal blood.

I.3.3. Fe^{3+}-sulphate in water purification

Fe^{3+}-sulphate can be used in water purification as a pure iron-product or mixed with Al-compounds. Fe^{3+}-sulphate alone can be used in monomer or polymer forms. The more common form is the monomer, which can be obtained from Fe^{2+}-sulphate by oxidation without any special treatment. Optimisation of the oxidation process resulting in a high output of Fe^{3+}-sulphate not contaminated with Fe^{2+}-sulphate, however, requires a more sophisticated process.

The production of polymerised Fe^{3+}-sulphate is complicated and several parameters affect the process. This is particularly important, if the process requires heterogeneous catalysts. An effective catalyst for the oxidation of Fe^{2+}-sulphate to Fe^{3+}-sulphate is active carbon. The process is friendly to the environment and no NO_x-compounds are left in the product or are emitted into the air. This is the case with competing oxidation processes, which use nitrogen in some form (HNO_3, NO_2, $NaNO_2$ etc.).

Fe^{3+}-sulphate mixed with Al-compounds is widely used in water purification. The purpose is to benefit from the different flocculation properties that Fe- and Al-compounds have. Fe-compounds function at a slightly higher pH range than Al-compounds (Handbook on Water Treatment, 1990).

I.3.3.1. Why Fe^{3+}-sulphate is used in water purification

Iron-based water purification chemicals can be produced for the treatment of drinking water, wastewater and sewage. There are several reasons for using iron-based water purification chemicals including

- after treatment with this kind of chemicals, the purity is high and the heavy-metal content is low,
- ferric sulphate can be used for sludge conditioning,
- iron products are efficient in eliminating hydrogen sulphide and thus reducing odour,
- iron products are efficient in reducing biological decomposition products at low pH.

Iron-based coagulants can be used as primary and secondary coagulants. They can be used in direct, simultaneous and post-precipitation. Flocculation capabilities are good and flocks are rapidly formed. The formed flocks are large and heavy and they sedi-

ment well. The pH of the treated water and sludge production can be well controlled. The usable pH is higher than with Al-based coagulants. Sludge production is low and the amount of organic matter is efficiently reduced. In municipal water treatment, all iron-based compounds are Fe^{3+}-based because of the colouring effects that Fe^{2+}-based compounds have. The cost efficiency of iron-based coagulants can be considered to be good.

I.3.4. General background for the oxidation of Fe^{2+}

The oxidation of ferrous sulphate to ferric sulphate take place in acidic aqueous solutions,

$$4Fe^{2+} + O_2 + 4H_3O^+ \rightarrow 4Fe^{3+} + 6H_2O$$

The oxidation process takes place spontaneously in liquid the phase, if dissolved oxygen or air is present (non-catalytic oxidation).

The kinetics of non-catalytic oxidation of ferro-ions has been screened by several investigators in the past (Mathews et al., 1972) and later on by (Valtakari, 1999; Rönnholm et al., 1999 (a, b); Valtakari et al., 2001). A summary of rate equations previously proposed for the non-catalytic and catalytic oxidation is given in Table 1.

Non-catalytic oxidation is feasible, but an elevated oxygen pressure is necessary to obtain high conversions, which guarantee the absence of ferrous ions in the product solution. The progress of a non-catalytic oxidation experiment is depicted in Figures 1. and 2.

As can be seen from Figures 1. and 2., it is necessary to use oxygen pressures 4–10 bar to achieve a 97-99 % conversion of Fe^{2+} within a reasonable reaction time (< 4 h) (Valtakari, 1999; Valtakari et al., 2001). It is known (Derka 1993, 1994; Geng 1993) that the oxidation velocity can be considerably enhanced using the appropriate catalysts, which enable the use of lower oxygen pressures and shorter residence times in the industrial units. For instance, HNO_3, H_2O_2 and $NaNO_2$ are mentioned as potential catalytic species in the oxidation of Fe^{2+} to Fe^{3+} (Kuznetsova et al., 1995). The area is dominated by patent literature (Derka 1993, 1994, Geng 1993), while original articles considering the catalytic oxidation of Fe^{2+} are very scarce (Naito, 1979). In particularly, kinetic investigations are missing.

In the industrial production of Fe^{3+}, the knowledge of oxidation kinetics is of crucial importance: kinetic models can be used in design, scale-up and retrofitting of production units. The catalytic oxidation kinetics of ferrosulphate over commercially sized (1.0–3.0 mm) active carbon has been previously studied (Rönnholm et al., 1998, 1999a; Valtakari, 1999; Valtakari et al. 2001). Typical kinetic curves recorded in the presence of active carbon are displayed in Figures 1. and 2. Mathematical modelling and calculations revealed that the non-catalytic and catalytic oxidation processes take place simultaneously. Estimation of the effectiveness factors – e.g. numerical simulation of the concentration profiles inside the catalyst particle indicated, that the catalytic oxidation process over the commercial-size active carbon particles is retarded by the intraparticular diffusion resistance (Rönnholm et al., 1998). In order to achieve

the ultimate oxidation velocity over active carbon, it is necessary to work with catalyst particles in μm-scale. The endeavour of the current study is to experimentally determine the intrinsic kinetics of ferrosulphate oxidation over active carbon-based catalysts, to develop kinetic models for oxidation and to characterise the oxidation product.

Table 1. Rate equations for the oxidation of Fe^{2+} in H_2SO_4 by molecular oxygen.

$r = kc_{Fe^{2+}} p_{O_2}$	25 – 40°C (George, 1954)	non-catalytic
$r = \sum_{j=1}^{2} k_j e^{-Ej/RT} c_{Fe^{2+}} p_{O_2}$	140 – 180°C (Huffman et al. (1956)	non-catalytic
$r = kc^2_{Fe^{2+}} c^{0.5}_{CuSO_4} p_{O_2}$	100 – 130°C (McKay et al., 1958)	catalytic, (with $CuSO_4$ as heterogeneous catalyst)
$r = kc^2_{Fe^{2+}} c_{O_2}$	100 – 200°C (Cornelius et al., 1958)	non-catalytic
$r = kc^2_{Fe^{2+}} c^{1.04}_{O_2} c^{-0.35}_{H^+}$	20 – 50°C (Keenan, 1969)	
$r = kc^2_{Fe^{2+}} c_{O_2} c^{-0.25}_{H^+}$	30 – 80°C (Mathews & et al., 1972)	non-catalytic
$r = \frac{k' K_{O_2} K^2_{Fe(II)} W P_{O_2} \left[Fe^{2+}\right]^2}{\left(1 + K_{O_2} P_{O_2} + K_{Fe(II)}\left[Fe^{3+}\right] + K_{H^+}\left[H^+\right] + K_{Fe(III)}\left[Fe^{3+}\right]\right)^3}$	40°C (Naito, 1979) over active carbon catalyst	

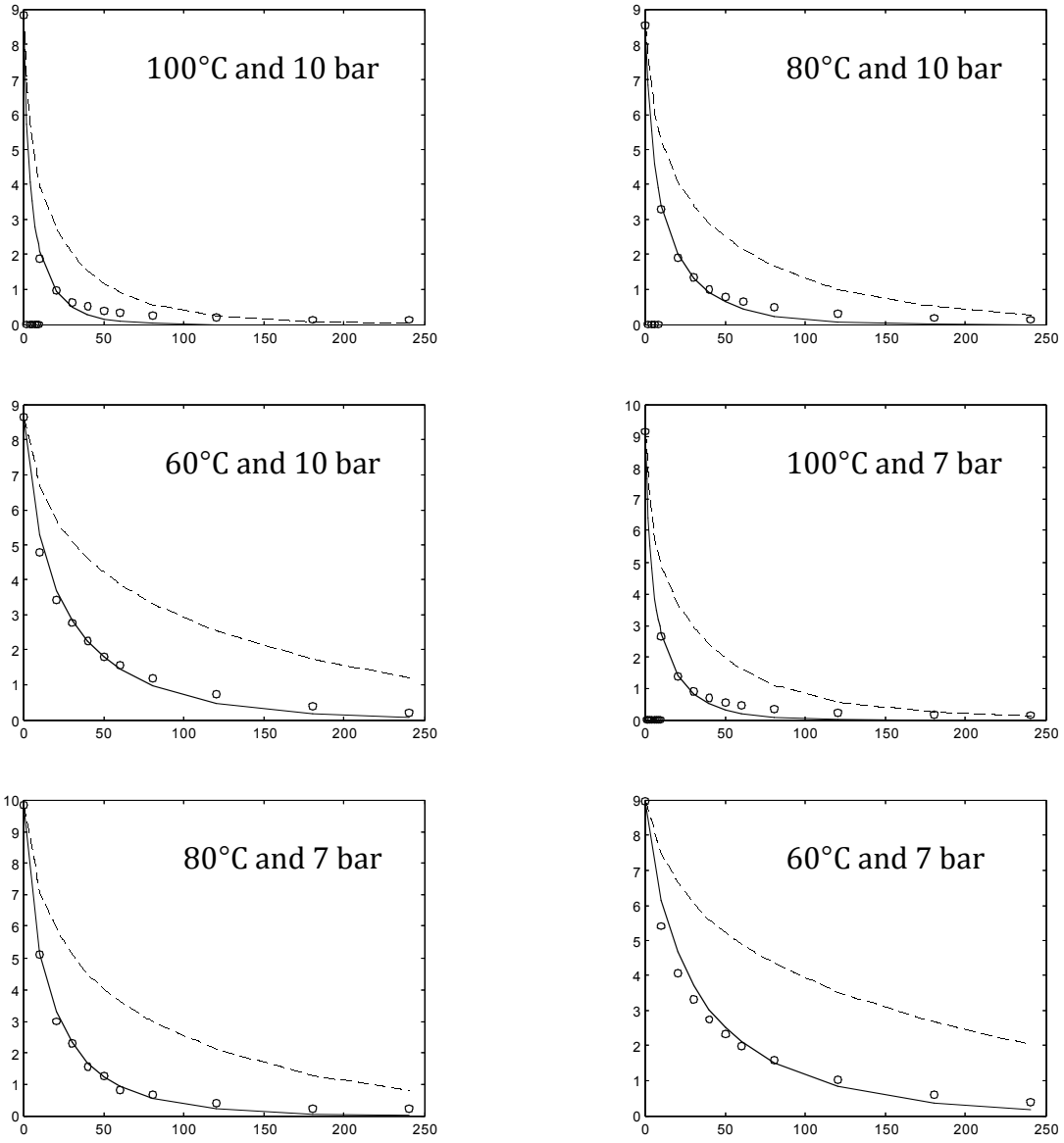

Figure 1. Oxidation of ferrosulphate over active carbon and without a catalyst. Fit of the model to experimental data (Fe^{2+} w/% versus time (min)); dotted lines: non-catalytic oxidation, continuous lines: combined catalytic and non-catalytic oxidation. Y-axis = pressure in bar, x-axis = time in minutes.

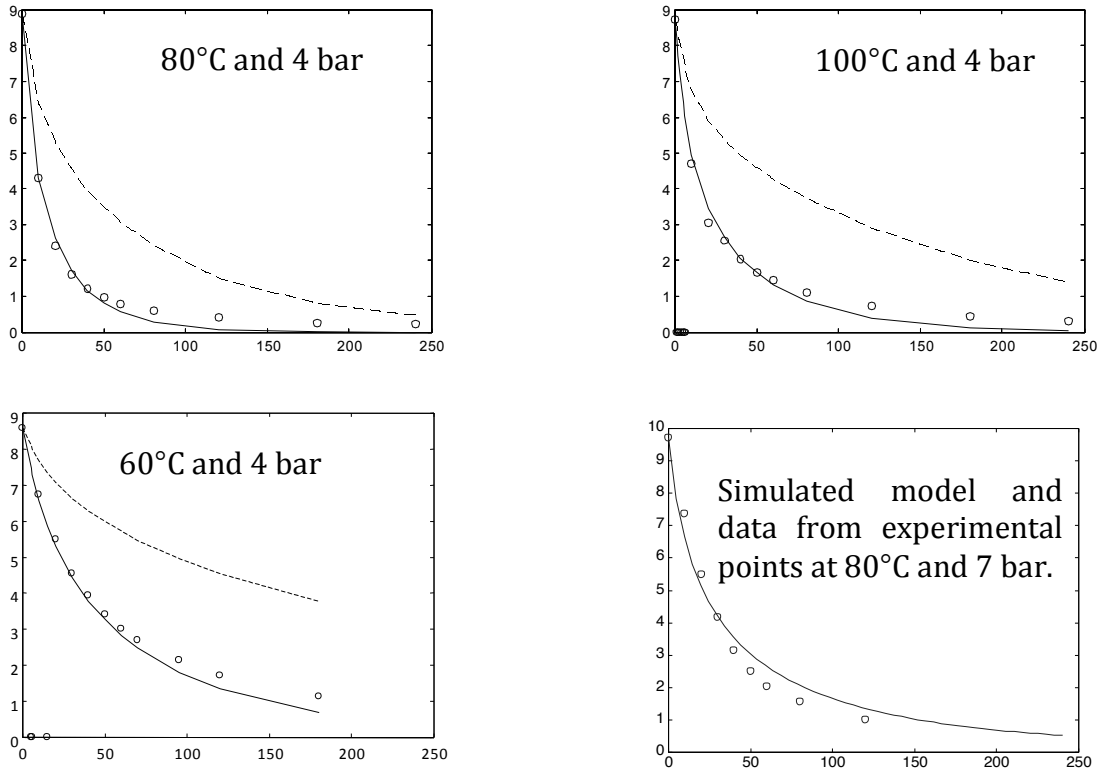

Figure 2.Oxidation of ferrosulphate over active carbon and without a catalyst. Fit of the model to experimental data (Fe^{2+} wt-% versus time (min)); dotted lines: non-catalytic oxidation, continuous lines: combined catalytic and non-catalytic oxidation. The last figure shows a comparison of the model with independent experimental data, which were not used in parameter estimation. Y-axis = pressure in bar, x-axis = time in minutes.

I.3.5. The aim of the work

I.3.5.1. Investigating different catalysts for the oxidation of Fe^{2+}

In this work, the main catalysts under investigation have been active carbon or active carbon supported noble metals. The purpose has been to screen the possibilities to use active carbon in the oxidation of Fe^{2+}. To date, active carbon catalysts have been considered too slow for oxidation of this kind. The oxidations have instead been performed in the absence of active carbon catalysts, or with other catalysing agents both in the presence and in the absence of active carbon. The most significant agents contain nitrogen in some form, for example HNO_3 and NO_x, or sodium, for example $NaClO_3$ and $NaNO_2$. Some good oxidizing agents, such as $CuSO_4$, H_2O_2 and KCl, are avoided because they are poisonous, expensive or otherwise unsuitable.

Some other methods were also tried in this work, including noble metal plated stirrer blades, other than noble metals on active carbon supports and fibrous catalysts as noble metal supports. Because this was not the main focus of interest, limited effort could be put into those investigations and the results were not encouraging. There exists, however, a potential in oxidative technologies that could be studied in the future.

I.3.5.2. Determination of the oxidation kinetics

As mentioned above, in the industrial production of Fe^{3+}, knowledge of the oxidation kinetics is of crucial importance: kinetic models can be used in the design, scale-up and retrofitting of production units. In this work, oxidation kinetics was studied for the catalytic and the non-catalytic oxidation reactions. The influence of the catalyst and the noble metals on the oxidation kinetics was studied, as well as the effect of pressure, temperature and catalyst dosage and raw materials (ferrous sulphate, sulphuric acid, etc.).

The oxidation could in the end be performed at such a rate that time was not a limiting factor for the process on a laboratory scale.

Experimental and analytical section

I.3.6. Product characterisation

One of the tasks of the work was to characterise the products, which were produced. Monomeric compounds are the first and easiest option. In water purification, polymeric Fe^{3+}-compounds are desirable due to the better purifying abilities of molecules with a higher positive charge. To produce polymeric Fe^{3+}-compounds is delicate work and the results are strongly dependent on the circumstances.

After the products were obtained, they were characterised, including titrimetric analysis as well as spectrophotometric and Raman tests. FTIR has been used in previous studies to prove the existence of polymeric iron.

I.3.7. Experimental equipment

The oxidation experiments were carried out in a laboratory scale autoclave (Parr 300 ml) equipped with an automatic data acquisition system that enabled continuous recording of the reactor pressure and temperature. The reactor system is displayed in Figures 3. and 4.

I.3.8. Oxidation of Fe^{2+}-sulphate

In order to perform successful oxidations on a laboratory scale, it was necessary to investigate the following

a) properties of materials needed in the oxidation,
b) measurement of the initial materials used,
c) catalysts and catalyst properties,
d) preparing the solution,
e) oxidation of ferrous sulphate.

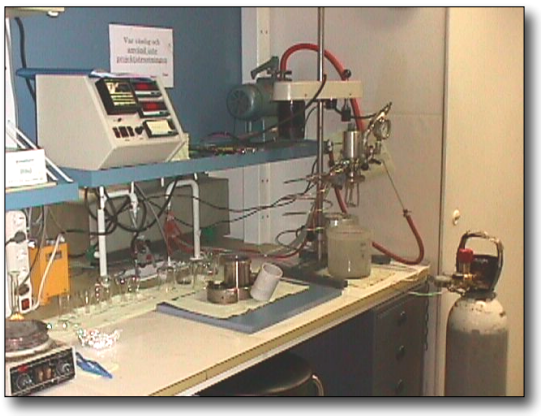

Figure 3. The experimental equipment for the oxidation of ferrosulphate.

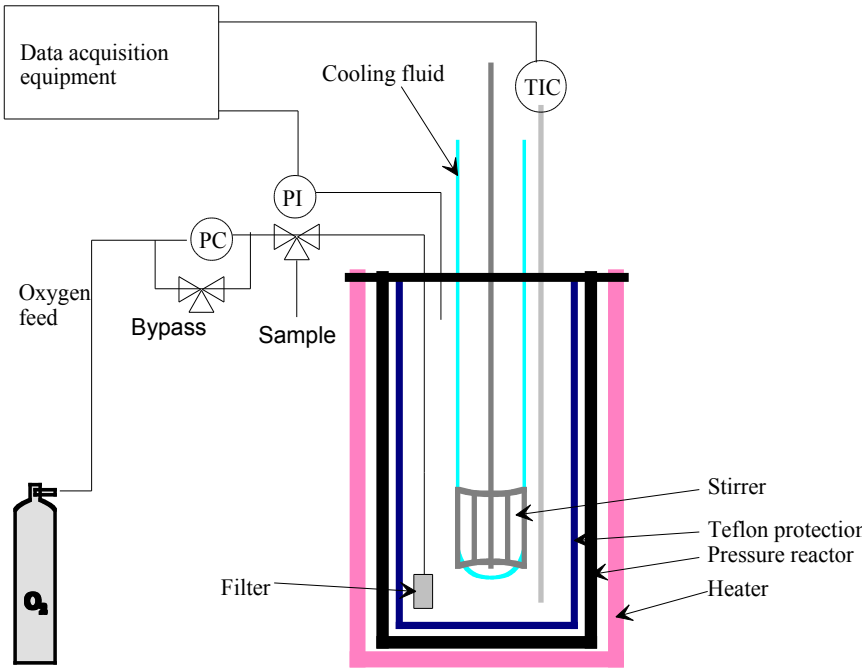

Figure 4. The experimental equipment; a schematic representation.

I.3.9. Properties of materials needed in the oxidation

The ferrous sulphate needed was selected according to industrial needs. Thus, the ferrous sulphate used was of technical quality and similar to that used in industrial processes. However, the sulphuric acid and the water used when dissolving the ferrous sulphate, were both of high laboratory quality, as seen in Table 2.

Table 2. Materials used in the oxidation of ferrous sulphate.

Material	**Quality**	**Purity**	**Source**
Ferrous sulphate	Industrial	~ 75 %	Kemira Pigments, Pori, Finland
Sulphuric acid	Pro analysis	> 98 %	Fisher Scientific, Leicester., UK
De-ionized water	Ultra pure	18.2 Ω	Elga Maxima purifier

I.3.10. Measurement of the initial materials

The ratios of the materials used defined the $[H_2SO_4]$-$[FeSO_4]$ and the [OH]-[Fe] ratios. These factors affected the products that the oxidation would give and the stability of the obtained products.

The $FeSO_4 \cdot 7H_2O$ content of the ferrous sulphate was calculated each time based on the titrimetric results from the analysis taken before the oxidation procedure. The initial amount of ferrous sulphate added to the mixture was fixed. The amounts of sulphuric acid and de-ionized water were varied, depending on the desired product and the [OH]-[Fe] and $[H_2SO_4]$-$[FeSO_4]$ ratios. In the production of Fe^{3+}-sulphates, it is generally considered that $[H_2SO_4]$-$[FeSO_4]$ ratios between 0.30 and 0.50 enables the oxidation to give polymeric species, the optimum being found at the [OH]-[Fe] value 0.30. The relationship between the values is explained by the formula

$$Fe^{3+}(OH)_n^{1-}(SO_4)_{3-n/2}^{2-}$$

Equation 1

and Table 3.

Table 3. Values of $[SO_4]$-[Fe], $[H_2SO_4]$-$[FeSO_4]$ and [OH]-[Fe] for 100 g of ferrous sulphate.

m_{H2SO4}	$[H_2SO_4]$-$[FeSO_4]$	$[SO_4]$-[Fe]	[OH]-[Fe]	m_{tot}
0.00	0.00	1.00	1.00	100.00
1.76	0.05	1.05	0.90	101.76
3.53	0.10	1.10	0.80	103.53
5.29	0.15	1.15	0.70	105.29
7.06	0.20	1.20	0.60	107.06
8.82	0.25	1.25	0.50	108.82
10.58	0.30	1.30	0.40	110.58
12.35	0.35	1.35	0.30	112.35
14.11	0.40	1.40	0.20	114.11
15.87	0.45	1.45	0.10	115.87
17.64	0.50	1.50		117.64

I.3.11. Catalysts and catalyst properties

I.3.11.1. Particle size distribution

The active carbons used in this work were mainly based on the active carbon CPGlF / Fe60820A by Kemira. The analysis was carried out using Malvern 2601C and the average size of the carbon particles in the fraction was calculated from the particle-size distribution curves.

I.3.11.2. Chemisorption

The catalysts were characterised with nitrogen adsorption using Sorptomatic 1900, Carlo Erba Instruments.

Oxidation studies were carried out with and without catalysts and they consisted of four groups:

1. oxidation without catalysts,
2. oxidation with plain active carbons, large particle size, app. 1-5 mm,
3. oxidation with plain active carbon, small particle size, < 45 μm, on average 14 μm,
4. oxidation with active carbon support and a noble metal, small particle size, on average 18 μm.

The purpose was to determine the non-catalytic and catalytic oxidation kinetics in order to optimise oxidation conditions. The active carbon catalysts were of commercial quality. The catalysts used and their physical properties are presented in Tables 4. and 5.

Table 4. Catalysts used in the oxidation of ferrous sulphate (complete test series).

Catalyst	Treatment	Size	Name	Code	Source
Active carbon	cat. active	~1 mm	Centaur	Fe51031B	Kemira
Active carbon	NaOH-treat.	3-5 mm	IVP	Fe 51012A	Kemira
Active carbon	acid treat.	~2 mm	CPGIF	Fe60820A	Kemira
Active carbon	acid treat.	~14 μm	CPGIF	Fe60820A	Kemira
Active carbon	1 % Pt	18 μm			Alfa
Active carbon	1 % Rh	18 μm			Alfa

Table 5. Catalysts tried in the oxidation of ferrous sulphate (only the suitability tested).

Catalyst	Treatment	Size	Code	Source
Active carbon	1 wt-% Pd	18 μm		Alfa
Active carbon	5 wt-% Pt	18 μm	5R18	Alfa
Active carbon	5 wt-% Ru	18 μm		Fluka
Smoptech I	1.8 wt-% Pt	fibres		Smoptech
Smoptech II	5 wt-% Pt	fibres		Smoptech
Mixer blades	Rh-plated	[1]8 cm^2		ÅA

[1] The influence of the surface porosity on the area were not calculated because the tests did not continue.

I.3.12. Oxidation

I.3.12.1. Oxidation without catalysts

The oxidations carried out without catalysts were used as references for the catalytic oxidation series.

I.3.12.2. Oxidation with plain active carbons, large particle size

The initial catalytic tests were carried out using common large-sized active carbons, the particle size being between 1 mm and 5 mm. Four different qualities of active carbon catalysts were screened, as shown in Table 4.

I.3.12.3. Oxidation with plain active carbon, small particle size

The active carbon studies were continued using small particles, the particle size being under 45 μm and the average particle size being 13.6 μm. The active carbons used here were mainly based on the active carbon CPGlF / Fe60820A by Kemira.

I.3.12.4. Oxidation with active carbon support and a noble metal, small particle size

Oxidation experiments with noble metal on active carbon support were carried out directly with carbon particles of small size. In this way, phenomena such as diffusion resistance were absent and the work could focus on the enhancement of the catalytic effect provided by the noble metal. Several noble metals are of principal interest, but not all of them are suitable for the environment where the oxidation takes place. Platinum and rhodium were chosen for further testing, platinum being chemically resistant and rhodium as a reference.

I.3.12.5. Oxidation with fibrous catalyst supports

Fibrous catalysts (Smoptech) were tried because of the easy use and recovery of the catalyst, but the oxidation results were too modest. Using this kind of catalysts would benefit the technical performance of the oxidation work, but the catalysts need to be tuned to the kind of solution and oxidation process currently used.

I.3.12.6. Oxidation with noble metal coated mixer blades

The use of noble metal-coated mixer blades was also tried. Although not very large in area, the noble metal plated mixer comes in touch with a large volume of the solution.

The ratio

$$R = \frac{V_{FeSO_4-solution}}{A_{Mixerblades} \cdot t_{Contacttime}}$$

Equation 2

is dependent on the rotation speed of the mixer-blades and in this particular case technical limitations did not permit further investigations. Future tests with adequate equipment might be an option.

I.3.13. Preparation of the solution

To dissolve the $FeSO_4$-powder successfully the following steps are essential:

1. the $FeSO_4$-powder is measured into the reactor vessel,
2. water is added until the $FeSO_4$-powder is covered,
3. all of the H_2SO_4 is added,
4. the rest of the water is added,
5. the reactor vessel is heated and kept at 58°C under constant stirring.

Because $FeSO_4$-powder is moist and the moisture in the powder varies locally in the container, it is not practical to aim at the same starting level measured by the solutions Fe^{2+}-contents. Too much time and effort will be lost.

In the experiments referred to in this work, the absolute amount of the $FeSO_4$-powder measured was kept constant. Thus, the initial concentration of Fe^{2+} varied. Before starting the oxidation, the solution was titrated and the Fe^{2+}-level determined. Excess water from the $FeSO_4$-powder was added to the total amount of water in further calculations.

If the water added before the addition of H_2SO_4 is insufficient, the $FeSO_4$-powder will not dissolve completely and the oxidation will be incomplete. This mistake cannot be rectified afterwards. The addition of H_2SO_4 results in an exothermic reaction and the evaporated water is of importance. The measurements and calculations referred to in this work have all been done by weight and not by volume. Too much water at the beginning slows the dissolving of the $FeSO_4$-powder in the solution.

When all components except the catalyst were inside, the reactor vessel was covered and heated to 58°C, this being an optimum for the solubility at atmospheric pressure. Minor changes in the Fe^{2+}-levels are not of importance, since they are measured before starting the oxidation. However, evaporation of water is significant, because it will change the concentration levels of the products thus affecting the reactions and calculations.

A pre-prepared initial solution of good quality, i.e. with plenty of Fe^{2+} and little Fe^{3+}, is clear and lemon-coloured. A low-quality $FeSO_4$-powder results in a brownish or brown solution. All completely dissolved solutions are clear, irrespective of colour.

I.3.14. Oxidation of ferrous sulphate

The dissolved Fe^{2+}-sulphate was oxidised in a pressurised semi-batch reactor with continuous oxygen input. The oxidation kinetics of $FeSO_4$-H_2SO_4 was studied at the temperature and pressure domains of 60–100°C and 0-10 bar, respectively. The ini-

tial concentration of $FeSO_4$ and H_2SO_4 were typically 2.4–2.6 M and 1.3 M, respectively.

The steps in the oxidation procedure are as follows,

1. the catalyst is added to the $FeSO_4$-solution,
2. the reactor is closed,
3. the catalyst is mixed into the $FeSO_4$-solution,
4. a vacuum is induced into the reactor,
5. the temperature is elevated to the desired level,
6. oxygen is let in under vigorous stirring.

After the initial Fe^{2+}-concentration was measured, the catalyst was added to the still warm solution.

The reactor was closed and the stirring was switched on and gradually increased in order to mix all of the catalyst with the $FeSO_4$-solution. If this step was omitted, then the vacuum inducement sucked out some of the catalyst. If the stirring is too violent at the beginning, then the catalyst stains the upper parts of the reactor and does not participate in the oxidation.

A vacuum was induced into the reactor so that no oxidation occurred while the temperature was elevated. The stirring was switched off during the vacuum procedure and then switched on again.

The oxidation reaction at the desired temperature began when the oxygen entered the reactor. It was done in one of two alternative ways:

1. constant oxygen in, but no flow-through, or
2. constant oxygen in and a flow-through.

In the first option the oxygen-flow is constantly on, but as much gas is accepted as the pressure drop from the reaction required. Part of the consumed oxygen is in this case replaced by gases other than oxygen (H_2O and impurities from the oxygen bottle) and the relative partial pressure of oxygen drops.

In the second option, the oxygen-flow is still constant but in this case all of the gas not used by the reaction will eventually be replaced by fresh gas. The oxygen level will be kept at the desired constant level. Further, this option helps to add a continuous strong oxygen-flow directly into the $FeSO_4$-solution from the bottom in the reactor model used in this work.

In the second option, the vigorous stirring helps to beat the oxygen into the solution, and the oxidation results are significantly better than when using the first option. In both cases, the stirring has to be vigorous enough to suck the end of the vortex down to the mixer-blades. The mixer-blades should be partly emerged in liquid for any oxidation to happen at all, as illustrated by Figure 5. A sinter at the end of the oxygen inlet adds to the oxidation effect by producing smaller bubbles and giving a larger contact area between liquid-phase and gas-phase.

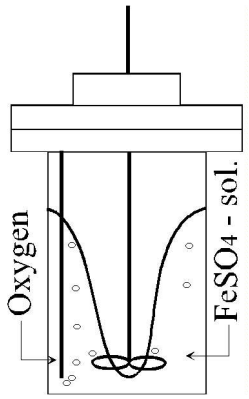

Figure 5. The reactor under vigorous stirring conditions.

Oxygen adsorption is good and the oxidation continues in an effective way, particularly when using the second option.

I.3.15. Titrimetric analysis of Fe^{2+}

The concentration of Fe^{2+} in the acidic solution was determined by redox titration with a 0.100 M Ce-sulphate-solution. The inflexion point of the titration was recorded with a potentiograph equipped with Pt Titrode (zero...80°C) and Pt 1000 /B/2 (-50...+80°C) electrodes. The titration equipment, Metrohm 736 GP Titrino, 728 Stirrer and Canon BJC-4200, is shown in Figure 6.

Figure 6. Metrohm titrimeter equipment and a Canon data-output unit.

The following titration procedure was used:

1. a sample was withdrawn,
2. it was added to a H_2SO_4-solution,
3. the solution was titrated with Ce-sulphate.

The sample used at the beginning was 0.3–0.5 g. A larger sample would have consumed Ce-sulphate and taken longer time. During the oxidation process the sample size was increased in order to obtain more reliable information. Volumes of Ce-sulphate less than 2 ml after titration are not recommended due to difficulties in dosing accuracy. For the same reason, the pipes of the titration equipment should be flushed with Ce-sulphate solution before titration commences. The first titration should be repeated, but later on that is not possible if short sample intervals are used. With strong catalysts, the sample is further oxidised while waiting to be titrated. A

sample of oxidised solution was analysed in 8 to 10 minutes. Samples should be taken only prior to titration.

I.3.16. Product characterisation

I.3.16.1. Ferron test

The existence of polyferric iron was investigated using a ferron-test, which is based on the measurement of the decomposition of Fe^{x}-compounds (x = +2, +3) in a ferron-solution (8-hydroxy-7-iodoquinoline-5-sulfonic acid, Fig. 8) at pH 4.3. The decomposition was observed at 600 nm with a Varian Series 634 spectrophotometer and the information was collected through a PICO ADC-16 to a Mikro Mikko 4TT M 336 data acquisition unit shown in Figure 7.

The ferron test can be used for both quantitative and qualitative analysis.

The reaction of mono- and polynuclear Fe with ferron can be expressed as irreversible reactions as described below.

$$Fe_m + \text{ferron} \xrightarrow{k_m} \text{Fe-ferron}$$

Equation 3

$$Fe_p + \text{ferron} \xrightarrow{k_p} \text{Fe-ferron}$$

Equation 4

Fe_m = mononuclear Fe species Fe_p = polynuclear Fe species
k_m = mononuclear rate coefficient k_p = polynuclear rate coefficient

Fe-ferron denotes a common product and the exact stoichiometries of the reactions are ignored. Degradation of Fe_p to Fe_m may be a prerequisite for the formation of Fe-ferron from polynuclear species, but this rate-limiting step is included in k_p and the reaction is described accurately. Provided the quantity of ferron clearly exceeds that of Fe, the reaction rate will only be dependent on the amount of Fe.

Figure 7. Spectrophotometer for ferron tests.

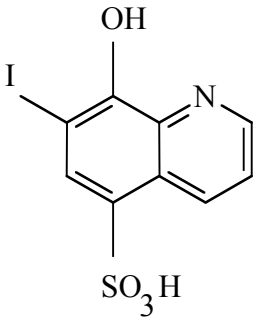

Figure 8. The structural formula of ferron.

The ferron solution was prepared in advance and the sample (0…20 μl) was added to the ferron solution (20 ml). The mixture was vigorously shaken for one minute, after which it was poured into the cuvette that had been flushed with the same mixture. The cuvette was inserted into the spectrophotometer as quickly as possible since the reaction already proceeded. The starting point was dependent on how rapidly the procedure was completed but it was never completely accurate.

I.3.16.2. Coagulation and flocculation tests

I.3.16.2.1. Coagulation

Coagulation in water purification is a process where finely dispersed dirt particles are destabilised by a chemical that is added to the water. The destabilisation will cause the dirt particles to lump together forming larger flocks (WHO, 1996a).

The principle of coagulation is that when a salt with an overall positive charge is added to the water it will adsorb on the surface of the dirt particles that usually have a negative charge, Figure 9, leading to a neutralisation of the charge of the formed new agglomerated particle, Figure 10, (Engelhardt, 2010). Coagulation can be achieved both with natural coagulants as well as with synthetically produced ones (Prodanović et al., 2013).

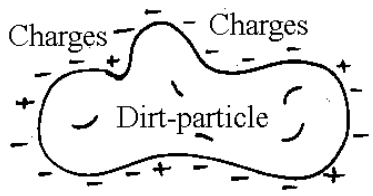

Figure 9. A dirt-particle. Schematic presentation of the surface charges on a dirt-particle.

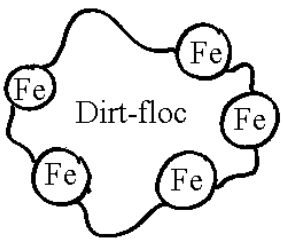

Figure 10. The coagulant-flocculent produces a flock by attaching to the surface of the dirt-particles.

The coagulation step consists of a quick and vigorous step where the coagulant chemical is added to the water. The time frame for the reaction step is no more than a fraction of a second to a few seconds. The mixing does not add value after the first seconds and a prolonged high energy mixing can instead lead to poor flocculation results in the next process step.

I.3.16.2.2. Flocculation

Flocculation is the process step following the coagulation step where the flocks are formed and then sedimented in the next step, in sedimentation basins or in clarifiers (WHO, 1996a).

Contrary to the coagulation process step the flocculation requires gentle handling. The mixing is slow with low energy input. The aim of the mixing is to make as many particles collide as possible without braking them, thus forming large flocks. The retention time should be around 30-45 minutes. For this research the water purification plants in Turku, Finland, and Helsingborg, Sweden, were studied.

After the flocculation the clear water moves forward to the next steps and the sedimented flocks are removed.

I.3.16.2.3. Sedimentation

The sedimentation step following the flocculation is basically a step with basins where the water is slowly moving through a number of basins and running over the edge of the basins. The flocks sediment at the bottom of the basins and are later removed as sludge.

Clarifiers can replace the sedimentation step. In the clarifiers the water moves through a system of upwards broadening pipes. The water speed is reduced when the water moves upwards and the flocks then sediment (WHO, 1996a). The clarifiers may also be used together with the sedimentation step for added efficiency.

I.3.16.2.4. Water purification – testing the results

The water purification process is monitored through different tests. The most relevant in this study are the turbidity test and the Jar test. Both are used to determine the removal of solid particles (TSS = total suspended solids) from the treated water.

Turbidity can be measured separately or directly as part of the process. The jar test requires sample testing in the laboratory to especially find the proper dosage of the coagulant that is added to the process.

I.3.16.2.5. Turbidity

Solid particles in the water reduce the water clarity. This reduction effect is called turbidity. The turbidity of the treated water can be used to control the water purification process and define on its part the end process quality. Reducing the number of particles in the water, i.e. by coagulation and flocculation, reduces turbidity. Turbidity is measured by measuring the amount of light that is scattered by the solid particles in the water (Oram, 2015; WHO, 1996b).

Turbidity can be measured for example by nephelometric turbidity units (NTU) or Jackson turbidity units (JTU), both methods being roughly equal (WHO, 1996b). As an example, drinking water should have a turbidity of less than 5 NTU/JTU (TU = turbidity unit). Turbidity can also be measured according to the ISO 7027 standard (ISO, 1999/2010).

I.3.16.2.6. Jar test

The purpose of the jar test is to simulate the water treatment coagulation and flocculation steps in the water purification plant (Satterfield, 2005). Mixing speeds match both the coagulation step, with vigorous high energy mixing, and the flocculation step, with a gentle low energy mixing to allow flocks to form. The jar test results are used for process optimisation (Zainal-Abideen, 2012).

The jar test will give results about the flocculation rate and the particle type, size and volume of the flocks as well as the number of flocks that are obtained. The jar test will also allow for turbidity measurements at given dosages and process parameters.

The jar test is typically carried out in six glass containers of 1 litre with paddle stirrers. A test scheme is designed and the coagulants are added to the different containers following this scheme. Different amounts of coagulants are added to the different containers. The stirring is in the beginning vigorous and later gentle. The lowest dosage is usually lower than the actual one in the process and in a corresponding way the highest dosage is higher than the one used in the process. The exact amount of coagulants, the time and speeds for rapid and gentle mixing is noted and at the end the turbidity of the water in the different containers is measured. Additional parameters such as pH, temperature, additives and flow rate impact of the process are noted and calculated (Christophersen, 2015).

In this study the jar tests were mainly carried out at Kemira Kemwater facilities in Helsingborg, Sweden. Later Kemira carried out the analyses of the produced ferric sulphates without returning further results. The results were compared to Kemira's PIX products that were use as a standard in the project. At Åbo Akademi the focus was on the development of the oxidation process for the ferric sulphate production. The jar tests carried out by Åbo Akademi, both at Åbo Akademi and Kemira Kemwater in Helsingborg included the use of only one container per experiment (compare to Satterfield, 2005).

The flocculation tests were performed at Kemira Chemicals, Oulu Research Centre. The products made at the Laboratory of Industrial Chemistry, Åbo Akademi, were compared to Kemira products PIX-115 and PIX-322 in standard synthetic wastewater solutions.

I.3.16.3. RAMAN-spectroscopy

RAMAN-spectroscopy was used in the analysis of the raw material, the initial solutions and the final products. The RAMAN-spectrometer used was a BRUKER IFS 66 (Burker Optik GmbH, 1998) (including the interferometer necessary for RAMAN) with the RAMAN supplement FRA 106. The laser was of the Nd-YAG type laser: A pulsating laser, which was adjustable between 0–350 mW with a wavelength of 1.064

nm. At this wavelength no fluorescence appeared from impurities in the sample. The sensitivity of the detectors is also very high at this NIR (near infra red) wavelength.

The type of the RAMAN instrument used was FTRaman (Fourier transform) with a thickness of 1.0 cm, including the mirror. The data acquisition unit was based on digitalisation of the detector signal with a high-speed A/D card and 19 bit dynamics. The data acquisition was carried out with a "fast acquisition processor (AQP)", placed on a card inside a personal computer. The operative system was OS/2, which enabled multitasking without disturbing the data acquisition process. The software used was called OPUS/IR-2 and included several analytical functions such as inverse Fourier-transformation, Kramers-Kronig-analysis and supports RAMAN analysis.

Results section

I.4. Results from catalyst characterisation

I.4.1. Surface studies

I.4.1.1. Particle size distribution

The active carbon catalysts used in the present work were mainly based on the active carbon product CPGlF / Fe60820A obtained by Kemira. The fine ground carbon powder was prepared as part of the work in the Laboratory of Industrial Chemistry at Åbo Akademi. Only the fraction with a particle diameter below 45 μm was accepted. The analysis was carried out using Malvern 2601C showed that the average size of the carbon particles in the fraction was 13.6 μm based on calculations done from the size distribution curves, Figure 11.

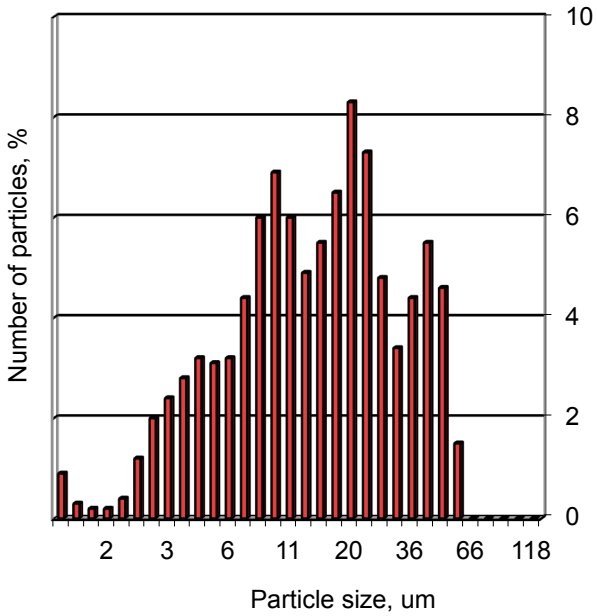

Figure 11. Particle size distribution of active carbon.

I.4.1.2. Physisorption

The BET specific surface area and the specific pore volume of the catalysts were determined by nitrogen adsorption using a Sorptomatic 1900, Carlo Erba Instruments. The BET specific area and the specific pore volumes of the catalysts were 835 m^2/g and 0.73 cm^3/g respectively.

The physical properties of the fine active carbon catalysts are shown in Table 6.

Table 6. The physical properties of the fine active carbon catalysts.

Catalyst	**Size µm**	**Name**	**Code**	**Source**	**BET m^2/g**	**Spec.pore vol. cm^3/g**
A.c. acid treat.	14	CPGlF	Fe60820A	Kemira	835	0.73
A.c. + 1% Pt	18			Alfa		
A.c. + 1% Rh	18			Alfa		

I.4.2. Chemisorption

The dispersion of noble metals on active carbon support was determined by nitrogen adsorption using a Sorptomatic 1900, Carlo Erba Instruments.

The adsorption isotherms were obtained at 298 Kelvin (for Pt and Rh) and 363 Kelvin (for Pd) and pressure 0,1–10^{-4} bar. The amount of reversible adsorbed gases was determined using the back-sorption method. Extrapolation of the adsorption isotherms to zero pressure was used for the determination of irreversibly adsorbed gases. Prior to hydrogen chemisorption, the catalysts were reduced at 573 Kelvin for 2 hours, followed by evacuation at 573 Kelvin and 10^{-6} bar for one hour.

The results of the chemisorption of noble metal catalysts on active carbon support are shown in Table 7.

Table 7. The results of the chemisorption of noble metal catalysts on active carbon support.

Catalyst	**Size µm**	**Me-disp. %**	**Particle d_m / nm**	**Source**
A.c.+1wt-% Pt	18	65.7	15.5	Alfa
A.c.+1%wt-Rh	18	63.4	17.1	Alfa
A.c.+1% wt-Pd	18	70.7	16.0	Alfa

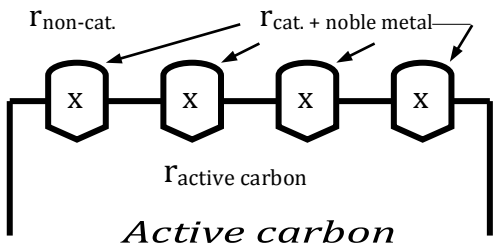

Figure 12. Sources for different r_x, x = noble metal.

The purpose of the chemisorption was to determine the dispersion of the noble metal over the active carbon, and thus to form a model for the calculations of the respective values of r_x (x = noble metal) and so to separate the different catalytic effects from the non-catalytic oxidation effect. The sources for the different r_x are shown in Figure 12.

I.4.3. Ferron test

I.4.3.1. Quantitative ferron analysis

The purpose of quantitative and semi-quantitative ferron analysis is to measure the exact changes in the amounts of polymeric species of polyferric sulphate produced as illustrated in Figure 13.

According to different sources, this method has been applied successfully on Al^{3+}- or Al^{3+}/Fe^{3+}-compounds but also for a number of other metals, such as Sn^{2+}, Cu^{2+}, Mo^{6+}, Cr^{6+}, Ni^{2+}.

The quantitative analysis is based on the difference between the base line and the curve. The difference between the two lines mentioned shows the amount of the polymeric product obtained, Figure 13.

I.4.3.2. Qualitative ferron analysis

The results from the ferron tests performed on the samples produced in this work were not reliable. The solutions did not show any activity when small sample quantities were used, and larger amounts of the sample precipitated.

When analysed a pattern in the behaviour of the samples was found and this behaviour was used for qualitative comparison between different samples, Figure 14. Some of the samples precipitated because of the larger sample volume, even though the sample size was the same between samples studied at the same time.

The analytical response is stronger when the sample size is large enough. This will lead to the precipitation of the sample that has reacted with ferron. The difference between the formation speed of a Fe-ferron chelate and the precipitation speed of the formed chelate is displayed in the form of a curve as illustrated in Figure 14.

The narrow area of operation where a sufficiently big sample can be added into the test so that a curve will be seen but no precipitation will occur can then be avoided.

The sample sizes used were also not dependent on a single factor, the sample in question alone, but several independent samples could be analysed with a proper dosage and the results could be compared. Because quantitative ferron analysis was not required, this method was more informative.

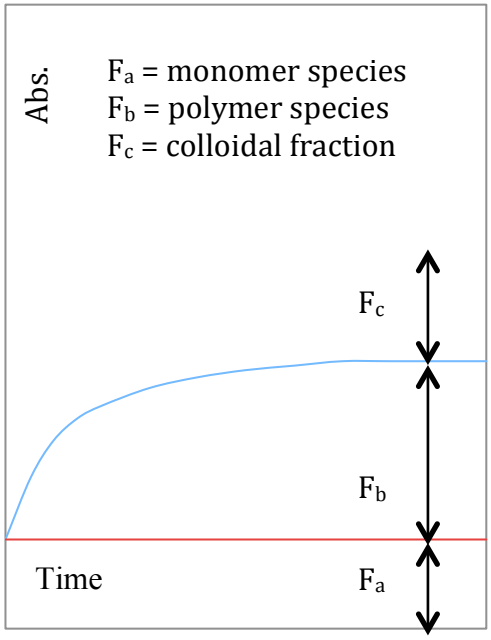

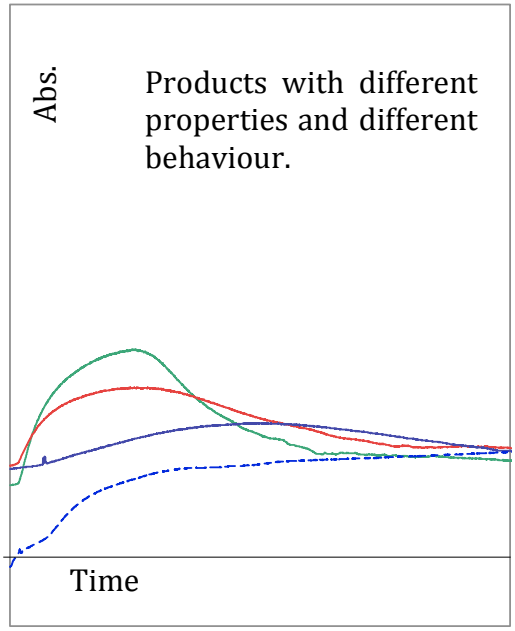

Figure 13. Quantitative analysis using the ferron test (left figure).
Figure 14. Qualitative ferron analysis (right figure).

I.4.4. Flocculation tests

The products prepared at the Laboratory of Industrial Chemistry were compared to the Kemira products PIX-115 and PIX-322 in a standard synthetic wastewater solution, as shown in Figure 15., (Valtakari, 1999). The figure clearly shows that significantly less of the Åbo Akademi flocculent is needed in wastewater cleaning. Savings of up to 15% in flocculent amounts are possible when using the formula developed at Åbo Akademi.

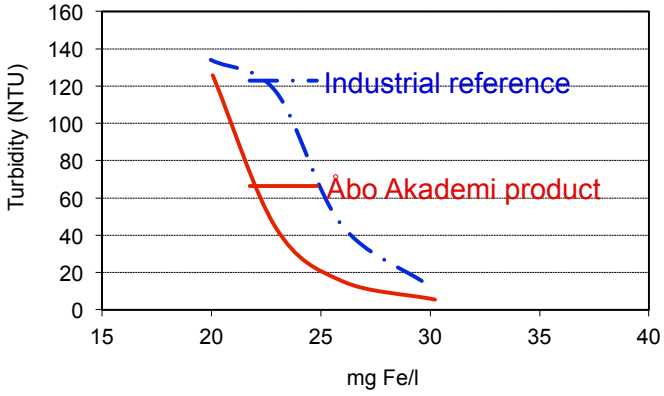

Figure 15. One product from Åbo Akademi compared to an industrial reference.

I.4.5. RAMAN spectroscopy

The purpose of the RAMAN spectroscopic investigations was to determine the existence of new polymeric ferrosulphate species. The product solution contained water that was also visible in RAMAN spectroscopy, although the problem was not as big as with FTIR.

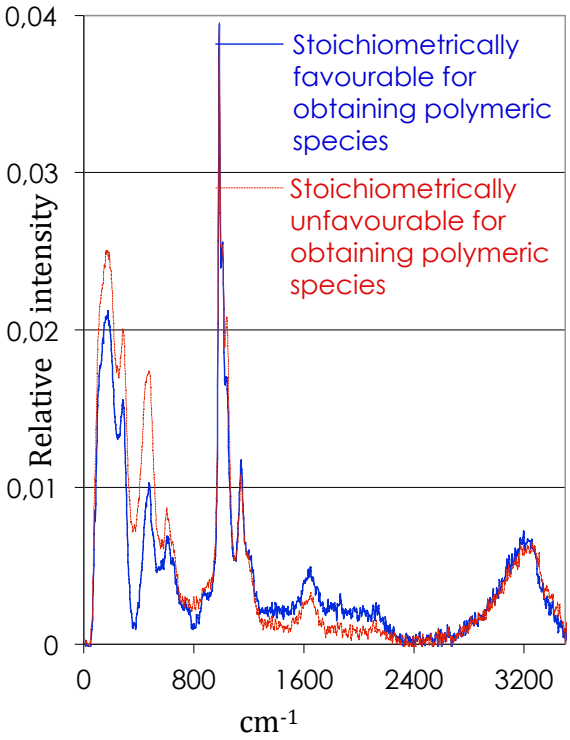

Figure 16. Raman-spectra for stoichiometrically different product solutions; one is in favour of polymeric species and one is not.

Several solutions with varying components included in the final product solution were tested and then matched against the product solution. Solutions produced with stoichiometric ratios that would not permit polymeric ferric sulphates were also analysed, Figure 16. A RAMAN spectrum with solutions that are stoichiometrically both favourable and unfavourable in regard to polymeric ferrosulphate species is shown in Figure 16. In the range of 1200 to 2200 $\Delta\rho/cm^{-1}$ the favourable product gives a response double to that of the unfavourable product. This range was interpreted to show additional OH-groups. These additional OH-groups are situated in the structure of what has now become a polymeric ferric species. In the more typical case where stoichiometric conditions are unfavourable to the formation of polymeric species, the response in the RAMAN spectrum shows OH-groups in the water.

I.4.6. Kinetic results

I.4.6.1. Methods

I.4.6.1.1. Catalytic reaction mechanism and rate equations

A reaction mechanism for the oxidation of ferrous sulphate over active carbon was proposed by our group (Rönnholm et al., 1999a). The fundamentals of the reaction mechanism are shortly reviewed here.

Oxidation was presumed to proceed on the active carbon surface, where the oxygen is dissociatively adsorbed. Fe^{2+} ions donate an electron to the adsorbed oxygen, which reacts with a hydronium ion forming a surface hydroxyl and releasing water. Two surface hydroxyls form water, leaving an oxygen-covered and a vacant site on the catalyst surface. The mechanism is summarised in Equation 5 as follows:

Reaction step	Stoichiometric number (v')							
I	O_2	+	2*	⇌	2O*	+		¼
II	Fe^{2+}	+	O*	⇌	Fe^{3+}	+	O*-	1
III	O*-	+	H_3O^+	⇌	OH*	+	H_2O	1
IIIb	O*-	+	H_2SO_4	⇌	OH*	+	HSO_4^-	1
IIIc	O*-	+	HSO_4^-	⇌	OH*	+	SO_4^{2-}	1
IV	OH*	+	OH*	⇌	H_2O*	+	O*	½
V			H_2O*	⇌	H_2O	+	*	½
	Fe^{2+}	+	¼ O_2 + H_3O^+	⇌	Fe^{3+}	+	$^3/_2$ H_2O	

Equation 5

H_2SO_4 is a strong acid with a high degree of dissociation and the formation of surface hydroxyls is solely attributed to the hydronium ion in the above mechanism, leaving steps IIIb and IIIc out of the equation.

Steps I and II are considered to contribute to the overall oxidation rate. Further, it has been assumed that only step II is a rate-determining step (rds). Steps I, III, IV and V are expected to be rapid so the quasi-equilibrium hypothesis can be applied and the overall oxidation velocity is then given by (Valtakari, 1999; Valtakari et al., 2001)

$$r = r_2 = k_2 c_{Fe^{2+}} \theta_0 - k_{-2} c_{Fe^{3+}} \theta_{0-}$$

Equation 6

The coverages of the corresponding species are denoted by θ_o and θ_{o-}. The application of the quasi-equilibrium approximation to steps I and III-V implies that

$$K_1 = \frac{\theta_O^2}{c_O \theta_v^2}$$

Equation 7

$$K_3 = \frac{\theta_{OH} c_w}{\theta_{O^-} c_{w^+}}$$

Equation 8

$$K_4 = \frac{\theta_w \theta_O}{\theta_{OH}^2}$$

Equation 9

$$K_5 = \frac{c_w \theta_v}{\theta_w}$$

Equation 10

where the subscripts – o, v, w and w+ – refer to oxygen, vacant sites, water (H_2O) and hydronium ions (H_3O^+), respectively. The surface coverage can be solved as a function of the fraction of vacant sites (θ_v) from Equations (7)-(10).

The expressions for θ_{O+} and θ_{O-} are inserted in the rate Equation (6) and the equilibrium constant for the overall reaction is thus given by

$$K_c = K_1^{1/4} K_2 K_3 K_4^{1/2} K_5^{1/2}$$

Equation 11

the rate equation becomes

$$r = k_2 K_1^{1/2} c_0^{1/4} c_{W^+}^{-1} (c_{Fe^{2+}} c_0^{1/4} c_{W^+} - \frac{c_{Fe^{3+}} c_W^{3/2}}{K_c}) \theta_v$$

Equation 12

The vacant sites fraction is solved from the site balance ($\theta_O + \theta_W + \theta_{OH} + \theta_{O-} + \theta_v = 1$). The expressions of the coverages, obtained from Equations (7)-(10), are inserted in the site balance and θ_v is solved as

$$\theta_v = \frac{1}{K_1^{1/2} c_0^{1/2} + K_5^{-1} c_W + K_1^{1/4} K_3^{-1} K_4^{-1/2} K_5^{-1/2} c_0^{1/4} c_W^{3/2} c_{W^+}^{-1} (K_3 c_W^{-1} c_{W^+} + 1) + 1}$$

Equation 13

The simplifying notations

$$K_0 = K_1, \quad K_w = K_5^{-1}, \quad K' = K_1^{1/4} K_3^{-1} K_4^{-1/2} K_5^{-1/2}, \quad K'' = K_1^{1/4} K_4^{-1/2} K_5^{-1/2}.$$

are introduced and the fraction of vacant sites becomes

$$\theta_v = \frac{1}{K_0^{1/2} c_0^{1/2} + K_W c_W + (K' c_W c_W^{-1} + K'') c_0^{1/4} c_W^{1/2} + 1}$$

Equation 14

The product $k_2K_1^{1/2}$ is now written as a constant $k' = k_2 K_1^{1/2}$ and θ_v is inserted in Equation (12) giving the rate equation

$$r = \frac{k' c_O^{1/4} c_{w^+}^{-1} (c_{Fe^{2+}} c_O^{1/4} c_{w^+} - \frac{c_{Fe^{3+}} c_w^{3/2}}{K_C})}{K_O^{1/2} c_O^{1/2} + K_W c_W + (K' c_W c_{W^+}^{-1} + K'') c_O^{1/4} c_W^{1/2} + 1}$$

Equation 15

I.4.6.2. Non-catalytic reaction mechanism and rate equation

The non-catalytic gas-liquid reaction rate and mechanism as well as the liquid-phase process between Fe^{2+}-ions and dissolved oxygen are described by Valtakari (1999), Valtakari et al. (2001) and Rönnholm et al. (1999a).

The non-catalytic reaction mechanism is expected to advance with the formation of an intermediate complex between dissolved oxygen and Fe-ions and the cleavage of the O-O-bond of the complex. When two Fe^{2+} ions are added to dissolved oxygen it will lead to the formation of a peroxide-type complex that is quickly decomposed. The rate-determining step is expected to be the successive addition of Fe^{2+} ions to oxygen and is summarised as

$$Fe^{2+} + O_2 \rightarrow Fe\text{-}O\text{-}O^{2+} \quad (I)$$
$$Fe^{2+} + Fe\text{-}O\text{-}O^{2+} \rightarrow Fe\text{-}O\text{-}O\text{-}Fe^{4+} \quad (II)$$

Then remaining steps are combined to a quasi-equilibrium:

$$2\ Fe^{2+} + 4\ H_3O^+ + Fe\text{-}O\text{-}O\text{-}Fe^{4+} \rightleftharpoons 4Fe^{3+} + 6\ H_2O \quad (III)$$

The rate expression for the non-catalytic process is thus obtained by applying the steady-state hypothesis to steps I and II ($r_1 = r_2$) and the quasi-equilibrium hypothesis to step III

$$r' = \frac{k_{nc2} K_{nc1} c^2_{Fe} c_O}{1 + k_{nc2} \frac{K_{nc1}}{k_{nc1}} c_{Fe}} (1 - f)$$

Equation 16

f is the factor for reverse reaction rate for the process and since the reaction equilibrium is strongly shifted to the products, f was approximated to be zero. Experimental results are displayed in Figure 1. and Figure 2. and the kinetic parameters are listed in Table 8.

Table 8. Results from fitting the parameters for the non-catalytic reaction (Equation. 2), (Valtakari, 1999; Rönnholm et al. 1999b, Valtakari et al., 2001).

a_2	10.411	$M^{-2}\ min^{-1}$
a_1	0.5812	M / min
E / R	5123 K	$T_{ref} = 80^{\circ}C$

I.4.6.3. Simplified rate equations

The general rate model for catalytic oxidation, Equation (15), contains several adjustable parameters. In order to reduce the number of adjustable parameters, the original model has to be simplified. If some of the surface intermediates can be assumed to be more plentiful than others and the concentrations of the surface hydroxyls and water can be considered negligible compared to those of O* and O*- ($K_W \approx 0$ and $K'' \approx 0$) then simplified rate equation (15) becomes

$$r = \frac{k' c_O^{1/4} (c_{Fe^{2+}} c_O^{1/4} c_{w^+} - \frac{c_{Fe^{3+}} c_w^{3/2}}{K_C})}{(K_O^{1/2} c_O^{1/2} + 1) c_{W^+} + K' c_O^{1/4} c_W^{3/2}}$$

Equation 17

If on the other hand oxygen and water are the dominating surface compounds then the simplified rate equation becomes

$$r = \frac{(\frac{k'' c_O^{1/4}}{c_{w^+}})(c_{Fe^{2+}} c_O^{1/4} c_{w^+} - \frac{c_{Fe^{3+}} c_w^{3/2}}{K_C})}{K_O'' c_O^{1/2} + 1} \approx k'' c_O^{1/2} c_{Fe^{2+}}$$

Equation 18

The rate equation (15) can be simplified even more, as the concentration of water can be assumed to be constant because of its high concentration, i.e. $K_W c_W \approx K'_W$. Equation (18) is now written as

$$r = \frac{(\frac{k'' c_O^{1/4}}{c_{w^+}})(c_{Fe^{2+}} c_O^{1/4} c_{w^+} - \frac{c_{Fe^{3+}} c_w^{3/2}}{K_C})}{K_O'' c_O^{1/2} + 1} \approx k'' c_O^{1/2} c_{Fe^{2+}}$$

Equation 19

where $k'' = k'/(K_W c_W)$ and $K_0'' = K_0^{1/2}/(K_W c_W)$

Fe^{2+} can be completely oxidized to Fe^{3+} in the presence of the catalyst (Valtakari, 1999; Valtakari et al., 2001). The rate equation can in that case be simplified with the irreversible case ($K_c \rightarrow \infty$), where the backward reaction terms are ignored. Factor k'' consists of a pre-exponential factor and an exponential term -E/RT.

I.4.6.4. Gas-liquid equilibrium

The concentration of dissolved oxygen appears in the rate equations, which was estimated from the oxygen solubility data in water, as described by the temperature-dependent correlation (Fogg et al., 1991)

$$\ln(\frac{atm}{H_O}) = A + \frac{B}{T} + C \ln T$$

Equation 20

where H_0 is Henry's constant and the coefficients A, B and C are listed in Table 9.

Table 9. Henry's coefficients for oxygen solubility in water (Fogg et al., 1991).

A	B	C	Temperature interval / Kelvin
-171.2542	8391.24	23.24323	273 - 333
-139.4850	6889.60	18.554	273 - 617

For a mixture of electrolytes, Weisenberger et al., (1996) have proposed the following relation:

$$\lg(\frac{c_{g,O}}{c_g}) = \sum_i (h_i + h_g)c_i$$

Equation 21

where h_i is an ion-specific parameter. Weisenberger and Schumpe (1996) extended the model of Schumpe (1993) to the temperature range of 273 – 353 Kelvin by assuming h_g, the gas-specific constant, to be a linear function of temperature:

$$h_g = h_{g,O} + h_T\,(T - 298.15\ K)$$

Equation 22

The numerical values used in this work are listed in Table 10.

Table 10. Gas solubility parameters in the temperature interval 273 – 353 K (Weisenberger et al., 1996).

Parameters	h_i
$h_{G,O_2}/(m^3 kmol^{-1})$	0.0 -0.000334 (T/K-298.15)
$h_{H^+}/(m^3 kmol^{-1})$	0
$h_{Fe^{2+}}/(dm^3 kmol^{-1})$	0.1523
$h_{Fe^{3+}}/(dm^3 kmol^{-1})$	0.1161
$h_{SO_4^{2-}}/(dm^3 kmol^{-1})$	0.117

The mole fraction of oxygen at the gas-liquid interface is calculated from Henry's law,

$$x^*_{O_2} = \frac{p_{O_2}}{H}$$

Equation 23

The liquid phase concentration c_{O2}^* in the interface is calculated from $c^*_0 = x^*_{02} c_L$, c_L being the total concentration of the liquid.

In order to get a reliable value of the partial pressure of oxygen (p_{O2}) and as the solvent has a significant vapour pressure at the highest experimental pressures; the measured total pressure (P) has to be corrected with the vapour pressure of the H_2O-H_2SO_4-$FeSO_4$ solution, Equation 24.

$$p_{O_2} = P - \delta P_{H_2O}^{vp}$$

Equation 24

where P_{H2O}^{vp} represents the vapour pressure of water and δ is a correction factor depending on the solvent composition. The vapour pressure of water was calculated from a modified Antoine equation given by Reid et al., (1988)

$$\ln\left(\frac{P^{vp}}{Pc}\right) = \frac{(VP\ A)\,x + (VP\ B)\,x^{1.5} + (VP\ C)\,x^3 + (VP\ D)\,x^6}{1 - x}$$

Equation 25

$$where \quad x = 1 - \frac{T}{Tc}$$

The parameters (VP A, VP B, VP C, VP D, Pc and Tc) are listed in Table 11.

Table 11. Physical parameters for vapour pressure calculations, Reid et al., (1988)

VP A	-7.76451
VP B	1.45838
VP C	-2.77580
VP D	-1.23303
Tc	647.14 K (= 374°C)*
Pc	22.06 MPa*
b_1	-0.2542
b_2	3.91
*Lide, 1994	

The correction factor (δ) correlates to the proportion (weight) of sulphuric acid (w_{H2SO4}) in the solution. Based on data, published by Sippola (1992), an empirical correlation was generated

$$\delta = 1 + b_1 w_{H_2SO_4} + b_2 w_{H_2SO_4}^2$$

Equation 26

The values of the coefficients b_1 and b_2 are listed in Table 11.

According to calculations the vapour pressure of the solvent H_2SO_4 is usually in the range of 0.1 bar at 55°C and 0.6 bar at 100°C and going up to 9 bar at 200°C. The sol-

vent vapour pressure has thus to be included in the model. This applies especially for the lowest experimental pressures and highest experimental temperatures.

The gas-phase mass transfer resistance of oxygen was considered to be insignificant, and the surface pressure p_{O2}^* was set to equal the bulk phase pressure of oxygen, p_{O2}. Since the oxygen concentration was high in the gas phase, the surface concentration of oxygen could be calculated from

$$c_O = c_O^* = \frac{p_{O_2} c_L}{H}$$

Equation 27

The liquid phase was assumed to be saturated with respect to oxygen, and the liquid-side mass transfer resistance of oxygen was taken to be negligible due to the vigorous stirring in the reactor.

I.4.6.5. Liquid-phase mass balances

The experiments were carried out within the regime of kinetic control, and as such, the mass balances for the liquid-phase components in the vigorously stirred batch reactor become very simple. For Fe^{2+} and Fe^{3+} ions the equation can be written as

$$\frac{dn_i}{dt} = r_i m_{cat} + r_i' V_L$$

Equation 28

where r_i and r'_i are the component generation rates originated from the catalytic and non-catalytic processes, respectively (Valtakari, 1999; Valtakari et al., 2001). Other symbols are explained in the Notation. In addition, the liquid volume can be assumed to be constant during the reaction (except for the withdrawal of the samples); thus the differentiation of dn_i/dt gives $V_L\, dc_i/dt$. The catalyst bulk density is defined as $\rho_B = m_{cat}/V_L$. The final form of the mass balance now becomes

$$\frac{dc_i}{dt} = \rho_B r_i + r_i'$$

Equation 29

For oxygen, no separate mass balance is needed since the solution was assumed to be saturated with respect to oxygen; the calculated saturation concentration c_0^* was inserted in to the rate equation. The effect of the film reaction at the gas-liquid interface was confirmed to be negligible by the estimation of the Hatta-number of the pseudo-first order reaction at the beginning of the experiment. The Hatta-number turned out to be very small (0.074) which implies that the enhancement factor is close to 1 (Valtakari, 1999; Rönnholm et al. 1999b; Valtakari et al., 2001).

The stoichiometry relates the generation rates to the reaction rates:

$$r_i = v_i r$$

Equation 30

$$r_i' = v_i r'$$

Equation 31

I.4.6.6. Computational procedures

The reactor model, i.e. the system of ordinary differential equations (ODEs) was solved numerically during the course of parameter estimation. Software (ODESSA, Hindmarsh, 1983) was used in the numerical solution. The kinetic parameters were estimated by minimising the sum of residual squares (Q),

$$Q = \sum_j \left(w_{j,Fe^{2+},\exp} - w_{j,Fe^{2+},calc} \right)^2$$

Equation 32

where w_{exp} and w_{calc} denote the experimental and the calculated (Equation 27) weight fractions of Fe^{2+} ions respectively. A hybrid simplex-Levenberg-Marquardt algorithm (Marquardt, 1963) was used in the numerical minimisation. The model solution and parameter estimation were carried out within the framework of the software package Modest (Haario, 1994) designed for simulation, estimation and experimental planning.

I.4.7. Kinetic results over active carbon

The kinetics of the active carbon catalysed oxidation was studied by performing a series of tests at temperatures 60°, 80° and 100°C and pressures 4, 7 and 10 bar. The carbon used in the tests was of fine quality and the average particle size was 14 μm. Diffusion resistance was not considered a limiting factor. The oxidation rate is more depending on temperature than on pressure as is shown in Figure 17. The amount of fine ground active carbon catalyst used was 4.8 %-wt. The catalytic enhancement of the oxidation is most prominent at the beginning of the oxidation. Later the interaction between catalyst particles and Fe^{2+}-ions diminishes due to the changes in the Fe^{2+}-concentrations.

Pure active carbon can be used successfully in the production of ferric sulphates. The larger amount of catalyst needed compared to the first experiment and catalysts lost is compensated for by the more attractive price of active carbon.

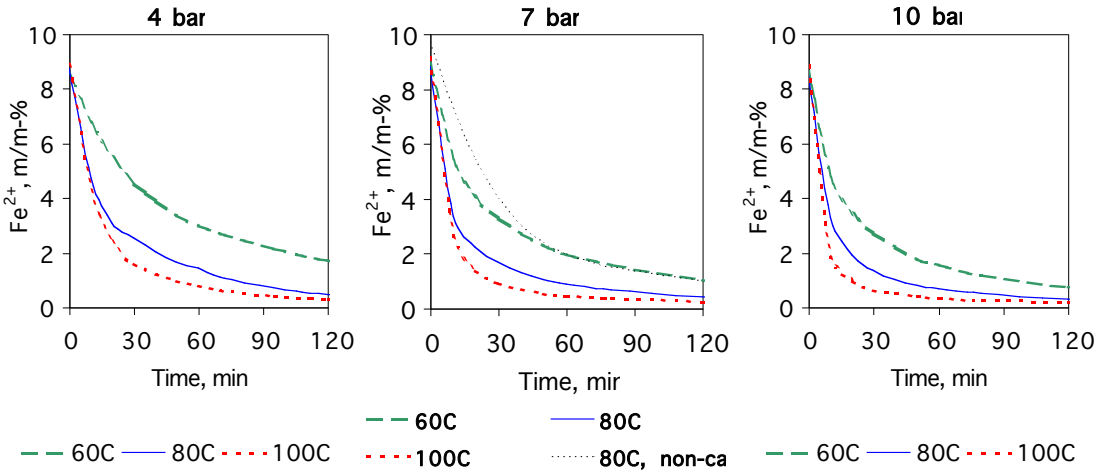

Figure 17. Oxidation kinetics from experiments on fine ground active carbon as a catalyst.

I.4.8. Kinetic results over combined active carbon - noble metal catalysts

To improve the oxidation kinetics further the use of noble metals on active carbon support was investigated. The improvement of the oxidation kinetics was significant. The strongest catalytic effect still appears in the beginning of the oxidation, but due to the more powerful catalyst, oxidation continues longer. In addition, the ferrous sulphate can now undergo serious oxidation at lower temperatures. This may be of benefit both in the production of polymeric ferric species, and in improved cost efficiency in further applications.

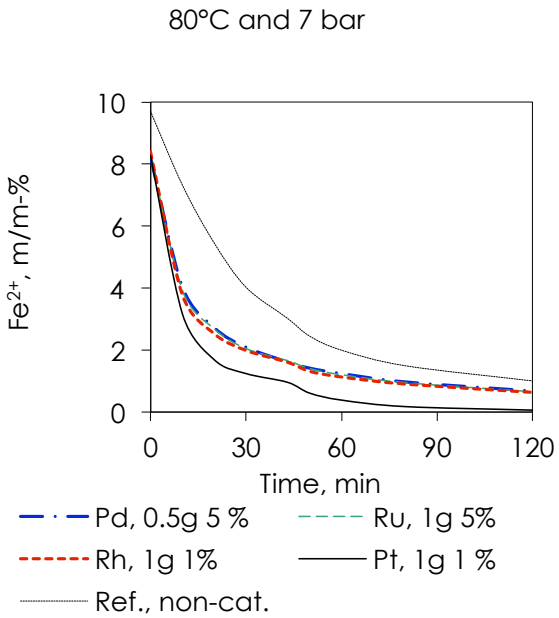

Figure 18. The effect of noble metals on the active carbon support (experimental results).

The noble metals that were used were Pt, Rh, Pd and Ru. All noble metals were on the active carbon support, the average particle size being 18 μm, and with 1 %-wt of no-

ble metal content. The amount of catalyst used in the oxidation was 1.2 %-wt (Pt, Rh), 6 %-wt (Ru) and 3 %-wt (Pd).

The highest oxidation rate for Fe^{2+} was achieved with Pt on an active carbon support, as presented in Figure 18. The Pd-catalyst was on a granulated active carbon support, which may have affected the diffusion of the solution. The comparison of the noble metal catalysts leads to the following conclusion: Pt >> Rh > Pd > Ru.

The solubility of Pt and Ru in the ferrous sulphate solution was also studied by ICPM-analysis. The solutions were oxidized for 2 hours and were then allowed to stay at room temperature for 48 hours. The measured noble metal content in the liquid phase also includes noble metal particles that might have been mechanically removed from the active carbon surface by the vigorous stirring during the oxidation stage. For Pt, the dissolved amount, 0.17 %-wt, was negligible. For Ru the dissolved amount was 3.75 %-wt. The particle size and the total amount of catalyst, noble metal + active carbon, were the same for both Pt and Ru, so the conclusion is that Pt on an active carbon support is more suitable for the hostile environment of the ferric sulphate solution than Ru, in addition to the better catalytic activity.

Based on the experimental results, the most suitable noble metal for this purpose is Pt. It is efficient at low temperatures and there is good oxidation, Figure 19. The polymeric ferric species were produced using Pt as a noble metal on the active carbon support.

A complete oxidation series was carried out for both Pt and Rh in the same way as for the fine ground active carbon. The temperatures used were 60, 80 and 100°C and pressures 4, 7, 10 bar, Figures 19. and 20. The conclusion is the same as with plain active carbon: temperature is more important than pressure for the oxidation as seen in Figure 21.

The most important catalysts are presented in Figure 21. The pure active carbon, Pt and Rh on active carbon support are compared to the non-catalytic oxidation.

The effect of different concentrations of catalyst on the oxidation of ferrous sulphate is shown in Figure 22. The mass of the catalyst and the oxidation time have been multiplied and the product of the values indicates the effect of the combination used. As can be seen from the figure, the values differ slightly from the mean value. This could be considered as part of the fluctuation during the experimental procedure. Taking the low levels of Fe^{2+} remaining at the end of the oxidation into account and the impact of a small analytic error on the final results, the conclusion is that oxidation with different amounts of catalysts follows a predictable behaviour and corresponds to the expected values.

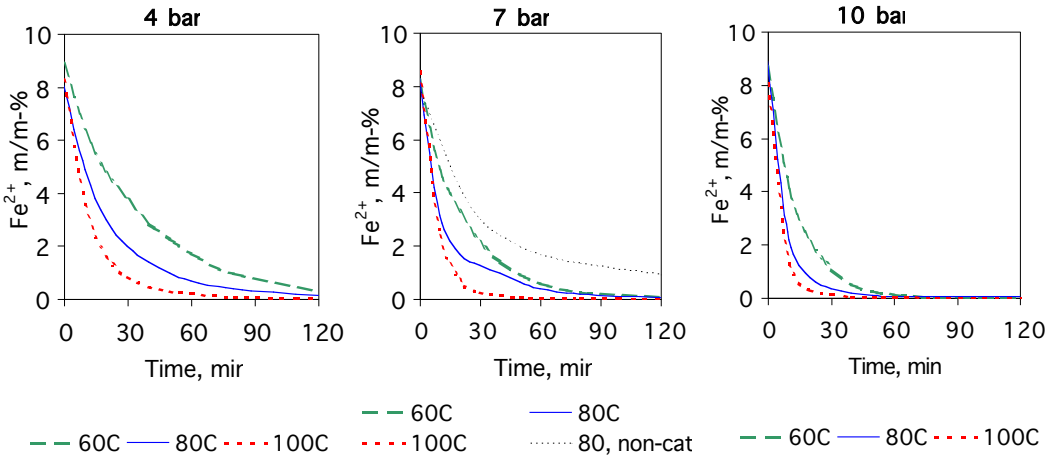

Figure 19.Platinum as the noble metal on an active carbon support. Experimental kinetic curves at different temperatures and different pressures.

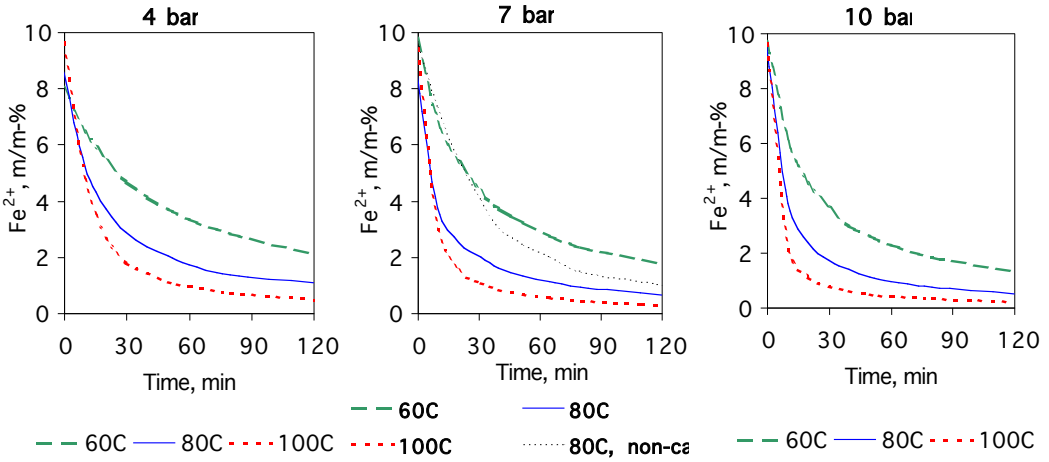

Figure 20.Rhodium as the noble metal on an active carbon support. Experimental kinetic curves at different temperatures and different pressures.

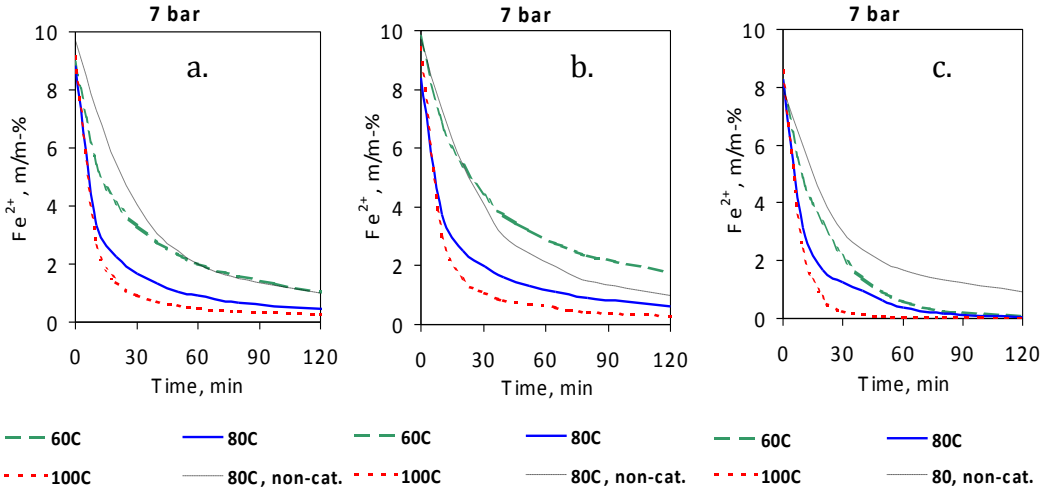

Figure 21. Oxidations with different catalysts at different temperatures and at 7 bar pressure: a. active carbon (fine ground), b. Rh 1% on an active carbon support and c. Pt 1% on an active carbon support, experimental values.

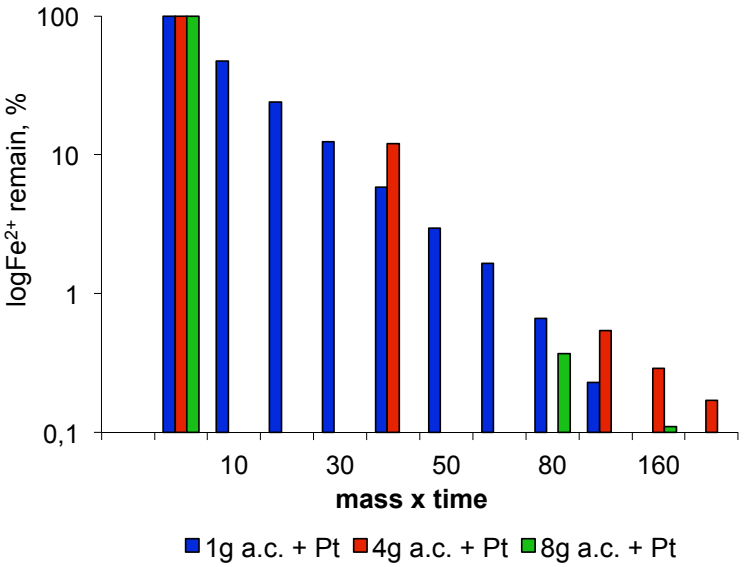

Figure 22. The effect of different catalyst concentrations on the oxidation of ferrous sulphate, experimental values.

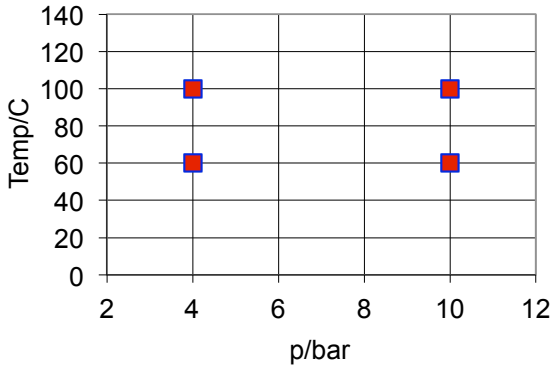

Figure 23. Experimental conditions for the compared non-catalytic, catalytic with active carbon and catalytic with active carbon and a noble metal experiments.

The different types of oxidation (non-catalytic, catalytic with active carbon and catalytic with active carbon and a noble metal) under different conditions, Figure 23., are compared in Table 12. The purpose was to estimate the time needed for Fe^{2+}-conversions of 90% and 99%. The estimation is based on simulations performed using the model and calculations presented earlier in this work.

Table 12. The time (min) needed for the Fe^{2+}-conversions of 90% and 99%. Amount of catalyst ≈ 27 g/l.

Oxidation	**4 bar**	**10 bar**	**4 bar**	**10 bar**	**4 bar**	**10 bar**	**4 bar**	**10 bar**
	60°C	**60°C**	**100°C**	**100°C**	**60°C**	**60°C**	**100°C**	**100°C**
	Conversion 90%				*Conversion 99%*			
Non-catal.	600	300	200	60	4700	1900	1400	470
Act.carbon	400	200	200	50	1200	700	400	170
Act.carb.+Pt	22	14	11	7	43	27	20	12

I.4.9. Modelling results

Typical kinetic results show, that the oxidation rate increases with increased temperature and oxygen pressure. The mechanistic rate equations (16) and (19) suggest that the reaction order might be between 1 and 2 for Fe^{2+}. In spite of the fact that saturation concentration of oxygen varies slightly during the course of the reaction because of the composition change in the liquid phase (Rönnholm et al., 1999a), it was assumed, as a first approximation, that the oxygen concentration is fairly constant in the liquid phase. Consequently, the experimental data can be checked using simple test plots for first and second order kinetics in batch reactors. For first and second order kinetics, the following time dependencies of the concentrations imply

$$y = \ln \frac{c_{0Fe^{2+}}}{c_{Fe^{2+}}} = k't \qquad \text{(1st order)}$$

Equation 33

$$y = \frac{c_{0Fe^{2+}}}{c_{Fe^{2+}}} - 1 = k' c_{0Fe^{2+}} t \qquad \text{(2nd order)}$$

Equation 34

where c_{0Fe2+} is the initial concentration of Fe^{2+}. The ordinates (y) plotted versus the reaction time are displayed for some typical experiments in Figure 24. As the figure reveals, the overall reaction order with respect to Fe^{2+} is much closer to 2 than 1, which confirms the strong role of the non-catalytic oxidation in the overall process: the non-catalytic oxidation follows second order kinetics very closely, Figure 24.

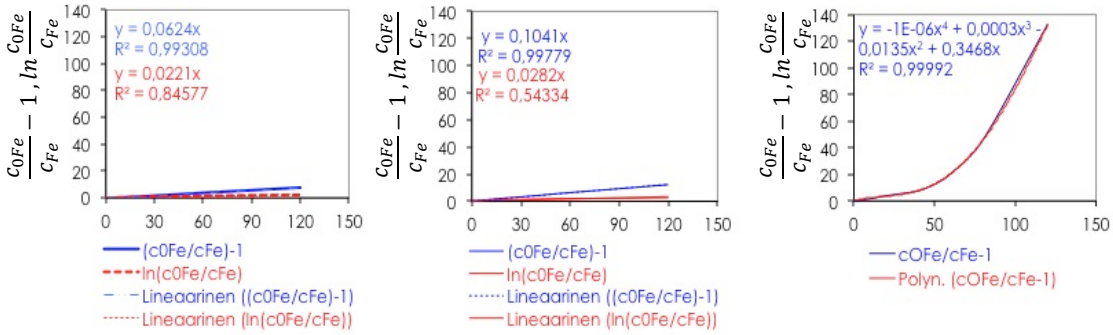

Figure 24. First (in red) and second (in blue) order plots for a non-catalytic and two catalytic oxidations of ferrosulphate. The R^2-values for second order plots exceed 0.99 and is for the first order plots considerably less indicating that the reactions are closer to second order than first order. Non-catalytic run (left), b. catalytic run with Rh on an active carbon support (middle), c. catalytic run with Pt on an active carbon support (right, tend line in red). T = 80°C and p = 7 bar.

After this preliminary screening, the rate parameters were determined by non-linear regression analysis, and the results, which indicate that the catalytic processes have the apparent activation energy 32 kJ/mol, are summarised in Table 13.

Table 13. Kinetic parameters for the oxidation of Fe^{2+} over active carbon

Total sum of squares (corrected for mean)	201.7			
Residual sum of squares	4.729			
Std. error of estimate	0.1953			
Explained (%): 97.66				
	Estimated Parameters	Estimated Est. Std Error	Relative Std Error (%)	Parameter/ Std. Error
k_0''	$0.507 *10^{-2}$	$0.117 *10^{-3}$	2.3	43.5
E/R	$0.393 *10^{+4}$	$0.174 *10^{+3}$	4.4	22.6

The correlation matrix of the parameters:

1.000
0.311 1.000

$$k'' = k_0''^{\frac{-E_a}{R}(\frac{1}{T}-\frac{1}{T_{ref}})} \quad , k_0'' = \frac{l^{\frac{3}{2}}}{mol^{\frac{1}{2}}gmin}$$

Examples of the fit of the model to experimental data are shown in Figures 1. and 2. A comparison between the experimental and predicted concentrations of Fe^{2+} reveals that the proposed kinetic model is able to reproduce the experimental data with a satisfactory accuracy; the deviation between experimental and calculated concentrations always remained below 5%. The contour plots (Figure 25.) and the parameter estimation statistics (Tables 13. and 14.) show that the parameters are well identified: the relative standard error of the parameters is less than 5%.

Finally, the contributions of the non-catalytic and catalytic reaction rates under the experimental conditions were compared by calculating the ratio (F); defined as

$$F = \frac{r'}{r\rho_B}$$

Equation 35

where r' and r are obtained from Equations 16. and 19., respectively. The ratio was calculated within the range c_{Fe} = 0 … 2.2 mol/l (p_O = 4 bar 60°C and 10 bar 100°C), which corresponds the progress of a typical oxidation experiment. Ratio F is displayed in Figure 26.

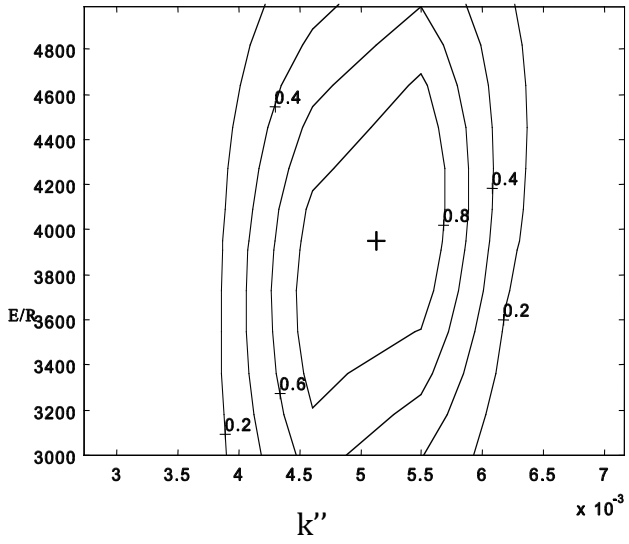

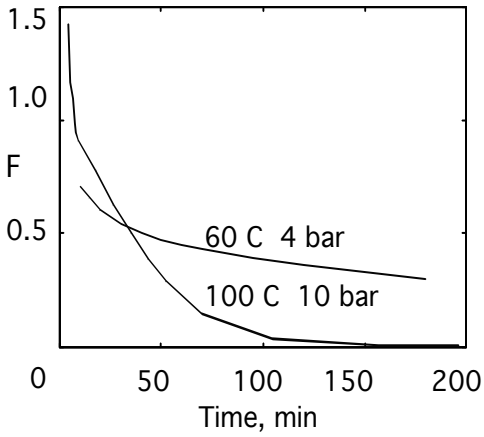

Figure 25. Contour plot for the activation energy and rate constant in catalytic oxidation of the ferrosulphate (left figure).

Figure 26. The reaction rate ratio versus time for non-catalytic and catalytic oxidation of ferrous sulphate under different experimental conditions. The non-catalytic contribution is most prominent at the beginning of the reaction and at high oxygen pressures. (right figure).

The figure shows that the non-catalytic contribution is most prominent at the beginning of the reaction and at high oxygen pressures. This is as expected on the basis of the rate equation (Equations 16-19.): the reaction order with respect to oxygen is higher for the non-catalytic process, which verifies that the non-catalytic process is favoured by a high oxygen pressure.

I.4.10. The noble metal effect

After determination of the non-catalytic and catalytic effects of active carbon in ferrous sulphate oxidation, the results obtained were compared to the experimental data. Further, the experimental data from oxidations with noble metal on active carbon supports were fitted into the models and tested. This finally lead to the conclusion that the noble metal effect on the active carbon support in the oxidation of ferrous sulphate can be explained by Equations 19. and 36-37.

$$r = r_{\text{non-catalytic}} + r_{\text{catalytic, active carbon}} + r_{\text{catalytic, noble metal}}$$

Equation 36

$$r_{cat.,noblemetal} = \frac{(\frac{k''' c_O^{1/4}}{c_{w^+}})(c_{Fe^{2+}} c_O^{1/4} c_{w^+} - \frac{c_{Fe^{3+}} c_w^{3/2}}{K_C})}{K_O''' c_O'^{1/2} + 1}$$

Equation 37

Rate parameters were determined by non-linear regression analysis, and the results are summarized in Table 14.

Table 14. Kinetic parameters for the oxidation of Fe^{2+} over active carbon + noble metal, estimated with non-linear regression

Total sum of squares (corrected for means)	$0.1505 *10^3$
Residual sum of squares	6.196
Std. error of estimate	0.2800

Explained (%): 95.88

	Estimated Parameters	Estimated Std Error	Est. Relative Std Error (%)	Parameter/ Std. Error
K_0''''	0.187	$0.592 *10^{-2}$	3.2	31.6
E/R	$0.205 *10^4$	$0.229 *10^3$	11.2	9.0

The correlation matrix of the parameters:

1.000
0.496 1.000

$$k'' = k_0''^{\frac{-E_a}{R}(\frac{1}{T}-\frac{1}{T_{ref}})} \quad , k_0'' = \frac{l^{\frac{3}{2}}}{mol^{\frac{1}{2}}gmin}$$

I.5. Conclusions and future perspectives

The oxidation kinetics was studied for ferrous sulphate to ferric sulphate both catalysed and non-catalysed reactions. The aim was to produce and verify the existence of polymeric ferric sulphate species and determine the favourable conditions for polymerization.

A kinetic model was developed based on ionic and molecular mechanisms. The fit of the model was thoroughly studied and the model was found to describe the experimental data very well. The developed kinetic model can be used in reactor simulations and reactor design.

The catalytic effects in the oxidation of ferrous sulphate to ferric sulphate were studied using active carbon and noble metals on active carbon supports. Active carbon and noble metals considerably enhance the reaction rates. The outstanding effect of Pt as a noble metal on active carbon support on the oxidation rates should be noted. Consequently, the capacity of existing reactors can be multiplied by the use of catalysts similar those screened in the current work.

Polymeric ferric sulphates were produced. The existence of the polymeric species was verified both analytically and by comparison with available high-class reference materials. The obtained product was considerably better than the references and showed good ageing stability without additives.

Polymeric ferric sulphates can be produced in existing facilities without changes in technical equipment. The ratios of the chemicals used should be recalculated, probably leading to lower chemical costs in production. Customers can in the future be offered an improved product that is usable over a wider pH range.

I.6. Some new development in the oxidation of ferrous iron to ferric iron for the purpose of municipal wastewater treatment

Original articles about catalytic oxidation of Fe^{2+} are scarce. Relevant articles are listed in the references and referred to in the study.

An important study (internship report by Margaux Lhuissier in 2013) in the catalytic and non-catalytic oxidation of Fe^{2+} into Fe^{3+} resulted in a simulated kinetic model (Lhuissier, 2013) of the oxidation in order to produce trivalent ions for the flocculation step in water treatment. The obtained results show that non-catalytic oxidation is not sufficient and thus a catalyst is needed. The work was carried out at the laboratory of Industrial Chemistry and Reaction Engineering at Åbo Akademi University and supervised by Professor Tapio Salmi and Professor Johan Wärnå.

The work of Margaux Lhuissier develops further the ideas and principles presented in the licentiate thesis by Valtakari and described in this study as well.

I.7. Appendices to Fe^2 oxidation to Fe^{3+}

I.7.1. Experiments and parameters

Table 15. Experiments and parameters.

RUN	m_{FeSO4}/g	m_{H2SO4}/g	ad m_{H2O}/g	$M_{catalyst}$/g type	T / ºC	C_{Fe2+}, start%	C_{Fe2+}, end%	p/bar
97111001	69.93	3.00	133.29	8.010	100	9.94	4.84	10
97111201	70.02	3.00	133.50	8.000	100	9.59	0.26	10
97111801	70.00	3.14	133.35	8.000	65	10.50	0.18	10
97112101	70.00	3.00	133.00	8.000	65	10.22	0.23	10
97112401	70.00	3.01	133.00	8.000	65	10.24	0.18	10
97112701	70.00	3.00	133.00	no	65	9.93	0.37	10
97112801	70.00	2.99	133.01	8.000	65	9.91	0.63	10
97120101	70.00	3.00	133.11	no	65	9.97	1.11	10
97120901	70.00	3.04	133.01	no	100	10.38	0.42	5
97121401	70.00	3.00	133.54	no	no react.	10.23	10.23	no press.
98011301	70.00	3.03	133.17	no	65	10.37	0.04	10
98012001	70.00	3.00	133.25	no	no react.	~10	~10	no press.
98012201	70.00	3.00	133.06	no	no react.	9.69	9.69	no press.
98012301	70.00	9.02	133.02	no	no react.	~10	~10	no press.
98013001	100.00	17.25	200.00	no	60	~8.7	0.09	~10
98020301	100.00	16.47	126.47	6 (HNO3)	60		0.02	10
98022501	100.00	17.25	200.00	2.000	60	8.76	0.91	10
98022601	100.00	17.25	200.00	2.000	60	~8.7	0.91	10
98030501	100.00	17.30	200.00	2.000	60	8.63	0.52	10
98030601	100.00	17.25	200.00	2.000	60	8.50	0.68	10
98030901	100.00	17.25	200.00	2.000	60	8.66	0.02	10
98031001	100.00	17.25	200.00	1.000	60	9.32	0.77	10
98031101	100.00	17.25	200.00	1.990	60	8.52	no	10
98031201	100.00	17.28	200.00	2.000	60	~ 8.7	0.31	10
98032601	100.00	17.25	200.00	1.000	60	8.68	0.01	10
98033001	100.00	17.29	200.00	no	60	7.90	0.82	10
98033101	100.00	17.24	200.00	no	60	8.65	0.88	10
98050501	105.00	19.21	200.00	4.000	no react.			10
98050502	105.00	19.21	200.00	4.00+1dr	60			10
98050601	105.00	19.03	200.00	4.000	60	8.67	0.22	10

98050701	105.00	19.12	200.63	4.000	100	8.84	0.12	10
98050801	105.00	19.10	200.23	4.000	60	8.58	0.78	4
98051101	105.00	19.12	200.07	4.000	100	8.91	0.24	4
98051301	105.00	19.13	200.13	4.000	80	8.74	0.31	4
98052501	105.00	19.09	200.03	4.000	80	8.54	0.13	10
98052601	105.00	19.12	200.20	4.000	60	8.97	0.39	7
98052801	105.00	19.14	200.80	4.000	100	9.16	0.15	7
98052901	105.00	19.09	200.22	4.000	80	8.84	0.19	7
98061501	10.50	19.15	200.00	4.0000	80	0.99	0.02	7
98061701	105.00	12.70	200.02	4.0000	80	8.45	0.25	7
98061702	10.50	1.26	200.00	not put in	no react.			
98062201	10.50	1.29	200.80	4.0000	80	0.87	0.07	7
98062301	105.00	16.54	200.38	4.0000	80	8.55	0.23	7
98062401	105.00	19.11	200.24	0.0	80	8.33	0.39	7
98062501	105.00	19.12	200.38	1.22 H3PO4	80	8.32	0.39	7
98062601	105.00	19.12	200.04	3.02 H2O2	80	8.42	0.41	7
98063001	105.00	12.70	200.88	10.0 HNO3	80	8.21	0.00	7
98070101	105.00	12.73	200.13	1.00 HNO3	80	8.35	0.63	7
98070201	105.00	16.00	130.00	16.0 HNO3	80	12.58	0.01	10
98070701	105.00	19.14	200.50	0.5 a.c.Pt 5%	80	8.23	0.68	7
98083101	105.00	19.10	200.24	Rh-blades	80	8.08	7.64	7
98090101	105.00	19.12	200.30	ox.flow-thr.	80	8.10	0.87	7
98090201	105.00	19.12	200.19	no	80	8.09	0.98	7
98090301	105.00	19.10	200.03	ox.flow-thr.	80	8.11	0.78	7
98090401	105.00	19.14	200.15	ox.flow-thr.	80	7.74	0.53	7
98090701	105.00	19.10	200.70	Act.C+Pt1%	80	8.29	0.06	7
98090801	105.00	19.10	200.21	Act.C+Rh1%	80	8.40	0.64	7
98090901	105.00	19.12	200.06	Act.C+Pt1%	60	8.25	0.07	7
98091001	105.00	19.10	200.46	Act.C+Pt1%	100	8.59	0.02	7
98091101	105.00	19.11	200.18	Act.C+Pt1%	100	8.09	0.02	10
98091401	105.00	19.11	200.02	no	80	8.34	0.89	7
98091501	105.00	19.09	200.30	Act.C+Ru5%	80	8.07	0.73	7
98091601	105.00	19.12	200.08	Smoptech	80	7.94	0.85	7
98091701	105.00	19.11	200.03	Act.C+Ru5%	80	8.29	0.66	7
98091801	105.00	19.11	200.90	Act.C+Pt1%	60	8.92	0.31	4
98092101	105.00	19.09	200.13	Smoptech	80	8.48	0.85	7
98092301	105.00	19.10	200.11	Act.C+Pt1%	80	8.04	0.13	4
98092401	105.00	19.09	200.07	Act.C+Pt1%	100	8.28	0.05	4
98092501	105.00	19.10	200.07	Act.C+Pt1%	60	8.68	0.02	10
98092801	105.00	19.11	200.14	Act.C+Pt1%	80	8.87	0.03	10
98092901	105.00	19.10	200.39	Act.C+Rh1%	60	8.06	2.13	4
98093001	105.00	19.10	200.42	Act.C+Rh1%	80	8.58	1.08	4

98110301	105.00	19.11	200.25	no	80	7.97	0.92	7
98110401	105.00	19.12	200.28	no	80	9.70	1.00	7
98110501	105.00	19.09	200.00	no	80	9.72	0.99	7
98113001	105.00	19.12	200.40	no	80	9.69	1.04	7
98120101	105.00	19.16	200.02	no	100	9.75	0.64	4
98120201	105.00	19.12	200.11	Act.C+Rh1%	100	9.64	0.48	4
98120301	105.00	19.10	200.32	Act.C+Rh1%	100	9.65	0.22	10
98120401	105.00	19.09	200.22	Act.C+Rh1%	80	9.50	0.49	10
98120701	105.00	19.10	200.14	Act.C+Rh1%	60	9.73	1.29	10
98122101	105.00	19.17	200.38	Act.C+Rh1%	100	9.44	0.29	7
99010501	105.00	19.11	200.40	Act.C+Rh1%	60	9.81	1.76	7
99011201	105.00	12.00	200.06	Act.C+Pt1%	60	9.81	0.02	10
99012801	105.00	12.49	200.23	Act.C+Pt1%	80	9.64	0.00	20

I.7.2. Computer codes for parameter estimation

The namelist file of the parameters used in a heterogeneous active carbon catalysed reaction simulation.

```
simulation

&project
 projectname = 'fersim'
/


&files
 nsets = 1

 resultfile = 'simdv1d.sim'
 ndumpp     = 400
/

Comments
 optimizer  = 'simflex' 'simlev' 'levmar' 'lmdiff'

&problem
 task  = 'sim'
 model = 'ode'
 odesolver = 'odessa'
/

&modelpar
nstates = 7
modelvar = 'vr     global  0
    mcat    global  4.0
    vl      global  0.0
    ncom    globali 5
    tempe   global  100
    w_h2so4 global 0.25
    trycket global  10
    volym   global  150.0d0

    modelhom  globali 2
    modelhet  globali 1
    mod_oxy_sol  globali 0
    do_pH       globali 0

    kla    global  1.0d10
    vg     global  0.00021
    rho    global  1333.0d0

    pm1    global  21.6
```

```
    pm2    global  36.8
    pm3    global  0.0d0
    pm4    global  4176
    pm5    global  0.0d0

    pm6    global  0.507d-2
    pm7    global  1.0d30
    pm8    global  0.0d0
    pm9    global  3930
    pm10   global  0.0d0
    pm11   global  1.0d0
    pm12   global  0.5d0

    time      odevar 0 990;
    s0(1:7)  initval  10.00d0; 1.290d0; 1.0d-6; 0.0d0; 51.7d0; 0; 0;'


/

&filepar
 nobs(1) = 100
 nydata(1) = 7

/

&print
 echo = 1
 echodata = 1
 optmonit = 1
 debug = 0
 stats = 1
 jacout = 1
/

&design
/

&simflex
 itmaxs = 20
/

&levmar
 reltollm=1.0d-10
 iterdflm=100
/


&newton
/
```

```
&odessa
 satol = 1.0d-6
 srtol = 1.0d-6
/

&euler
/
```

I.8. References

Abdullahi, M. E., Musa, L., 2011, Recovery of coagulants from water works sludge: A review, Pelagia Research Library, Advances in Applied Science Research, 2011, 2 (6):410-417

BRUKER OPTIK GmbH, 1998, Bruker IFS Users manual

Christophersen, D., 2015, Jar Testing Procedures, Veolia Water Solutions

Cornelius, R. J., Woodstock, J. T., 1958, Pressure leaching of manganese ore, part I: Kinetic spects, Proc. Aust. Inst. Min. Met., No. 185: 65-107

Derka, J. R., 1993, US005194241A

Derka, J. R., 1994, US005332565A

Engelhardt, T. L., April 2010, Coagulation, Flocculation and Clarification of Drinking Water, Drinking Water, Hach Company, Guide

Fogg, P. G. T., Gerrard, W., 1991, Solubility of Gases in Liquids, Wiley, Chichester

Geng, W., 1993, CN 1071895A

George, P., 1954, The oxidation of ferrous perchlorate by molecular oxygen, J. Chem. Soc., 4:4349-4359

Haario, H., 1994, Modest User's Guide, ProfMath Oy, Helsinki (1994)

Handbook on Water Treatment, 1990, Kemira Kemi AB, Helsingborg, Sweden

Hindmarsh, A., ODEPACK, 1983, A systemized collection of ODE solvers. Scientific Computing (edited by Stepleman J. S. et al.,), pp. 55-64. IMACS North-Holland, Amsterdam

Huffman, R. E., Davidson, N., 1956, Kinetics of ferrous iron-oxygen reaction in sulphuric acid, J. Am. Chem. Soc. 78:4836-4842

ISO 7027:1999 (2010 update) - Water quality -- Determination of turbidity

Keenan, E. A., 1969, Bacterial benefication of uranium materials, Ph. D. Thesis (unpublished), The University of New South Wales

Kuznetsova, N. I., Likholobov, V. A., Gurrath, M., Boehm, H. P., 1995, Promotion effect of carbon on the oxidation of ferrous ions by oxygen in the presence of sodium nitrite, Applied Catalysis A: General 128, 41-52

Lhuissier, M., 2013, Catalytic and Non-catalytic Kinetic Model simulation of the oxidation of FeII into FeIII as part of the step of Coagulation-Flocculation for Water Treat-

ment, Åbo Akademi University, Laboratory of Industrial Chemistry and Reaction Engineering, Internship Report

Lide, D. R., 1994, CRC Handbook of Chemistry and Physics, 75th edition, 6-56

Marquardt, D. W., 1963, An algorithm for least squares estimation on nonlinear parameters, SIAM J. 11, 431-441

Mathews, C. T., Robins, R. G., 1972, Oxidation of ferrous sulphate solutions by molecular oxygen, Proc. Aust. Inst. Min. Met., No 242

McKay, D. R., Halpern, J., 1958, A kinetic study of the oxidation of pyrite in aqueous suspensions, Trans. Met. Soc. A.I.M.E, 212:301-309

Naito, K., 1979, Oxidation of Iron(II) Ion in Sulfuric Acid Solution by Oxygen with Activated Carbon Catalyst, Nippon Kagaku Kaishi, 7, 848-54

Oram, B., 2015, Stream Water Quality - Importance of Total Suspended Solids / Turbidity, Turbidity and Total Suspended Solids Surfacewater Monitoring , Water Research Center

Prodanović, J., Šćiban, M., Antov, M., 2013, Improvement of wastewater treatment by use of natural coagulants**,** Journal of Economic Development, Environment and People Volume 2, Issue 2

Reid R. C., Prausnitz, J. Poling, M., B. E., 1988, The Properties of Gases and Liquids, McGraw Hill, New York

Rönnholm, M. R., Wärnå, J., Salmi, T., September 1998, Two and Three Phase Oxidation Kinetics of Ferrous Sulphate ISCRE 15, Newport Beach

Rönnholm, M. R., Wärnå, J., Salmi, T., Turunen, I., Luoma, M., 1999a, Oxidation Kinetics of Ferrous Sulphate over Active Carbon, Industrial & Engineering Chemistry Research, 7, 38

Rönnholm, M. R., Wärnå, J., Salmi, T., Turunen, I., Luoma, M., 1999b, Kinetics of oxidation of ferrosulphate with molecular oxygen, Chem. Eng. Sci., 54

Satterfield, Z. P. E., 2005, Jar Testing, Tech Brief

Schumpe, A., 1993, The Estimation of Gas Solubilities in Salt Solutions, Chem. Eng. Sci., 48, 153

Sippola, H., 1992, Rautasulfaatin liukoisuuden mallitus rikkihappo-vesisysteemissä, Licentiate thesis, Teknillinen korkeakoulu, Espoo

UN, 2010, The human right to water and sanitation, Resolution 64/292, United Nations

Valtakari, D., 1999, Catalytic Preparation of Ferric sulphate, Licentiate Thesis. Åbo Akademi University, Laboratory of Industrial Chemistry and Reaction Engineering, Turku

Valtakari, D., Rönnholm, M. R., Wärnå, J., Salmi, T., Laine, E., Luoma, M., (2001, submitted for publication), The intrinsic kinetics of ferrous sulphate oxidation on active carbon

Weisenberger, S., Schumpe, A., 1996, Estimation of Gas Solubilities in Salt Solutions at Temperatures from 273 K to 363 K, AIChE Journal, Vol 42, Nr 1, 298

WHO, 1996a, Coagulation, flocculation and clarification, Fact Sheet 2.13, Fact Sheets on Environmental Sanitation

WHO, 1996b, Turbidity measurement, Fact Sheet 2.33, Fact Sheets on Environmental Sanitation

WHO, 1998, Aluminium in Drinking-water, WHO/SDE/WSH/03.04/53

Zainal-Abideen, M., Aris, A., Yusof, F., Abdul-Majid, Z., Selamat, A., Omar, S. I., 2012, Optimizing the coagulation process in a drinking water treatment plant – comparison between traditional and statistical experimental design jar tests, Water Science & Technology, IWA Publishing 2012

II

II. Ferric to ferrous iron reduction with zinc sulphide and sphalerite

II.1. Background

Ferric iron reduction to ferrous iron was studied at the laboratory of Industrial Chemistry and Reaction Engineering at Åbo Akademi University. The studies had several objectives, among others to understand

- reaction kinetics of the reduction reaction,
- performance of the reduction agent ZnS and sphalerite,
- similarities and differences in the ZnS and sphalerite reactions,
- possible formation of particle layer that could affect the reduction rate,
- possible formation of particles that could affect the reduction reaction,
- influence of temperature, concentration and pH of the reaction solution,
- participation of sulphuric acid in the reduction reaction,
- modelling of the reaction kinetics.

Based on the studies two papers were published in 2004 by Markus et al.

The main relevance for this study is the effects of the sulphuric acid on the dissolution reaction and reactions in the liquid phase. The dissolution of the solid particles and effects of structural properties and possible formation of a product layer was also studied. Mass and charge transfers and chemical reactions also affect the dissolution as well as structural properties of the particles to be dissolved.

II.2. Summary

As no product layer was formed it became evident that the dissolution rate was slowed down by the formation of solid sulphur particles. The dissolution degree and conversions will also depend on the balance between pH, concentrations of the different agents and temperature.

The study confirmed that both zinc sulphide and sphalerite can be used for the reduction of ferric iron. If sphalerite is used then a simultaneous leaching of sphalerite will take place.

The sulphuric acid has a significant impact on the reactions rate when zinc sulphide is used and this effect is proportional to the concentration of sulphuric acid. This indicates that the sulphuric acid acts as an intermediate stage in the reaction in the liquid phase. In corresponding experiments with sphalerite no such effect was noted.

II.3. Kinetic modelling of a solid–liquid reaction: Reduction of ferric iron to ferrous iron with zinc sulphide

ELSEVIER

Chemical Engineering Science 59 (2004) 919–930

Chemical Engineering Science

www.elsevier.com/locate/ces

Kinetic modelling of a solid–liquid reaction: reduction of ferric iron to ferrous iron with zinc sulphide

Heidi Markus[a], Sigmund Fugleberg[a], Daniel Valtakari[a], Tapio Salmi[a], Dmitry Yu. Murzin[a,*], Marko Lahtinen[b]

[a] *Laboratory of Industrial Chemistry, Process Chemistry Group, Åbo Akademi University, Biskopsgatan 8, FIN-20500 Åbo/Turku, Finland*
[b] *Outokumpu Research Oy, P.O. Box 60, FIN-28101 Björneborg/Pori, Finland*

Received 6 May 2003; received in revised form 17 September 2003; accepted 24 October 2003

Abstract

Reduction of metal ions with solid compounds can be used as a model system to verify various models for reactions between liquids and reactive solids. The reduction of dissolved ferric iron (Fe^{3+}) to ferrous iron (Fe^{2+}) with solid zinc sulphide (ZnS) was investigated in an isothermal, completely back-mixed batch reactor. The influence of temperature, initial concentration of ferric iron, zinc sulphide-to-ferric iron molar ratio, and sulphuric acid concentration on the reduction kinetics was investigated. Analysis of unreacted and reacted ZnS was performed by SEM–EDS and laser diffraction techniques to study the changes of the solid particles with time and to verify whether a product layer was present. The results did not reveal formation of any product layer, thus excluding the shrinking core (product layer) model. The experimental data were compared with several models proposed for solid–liquid reactions, representing first and second order kinetics, reaction rates controlled by surface reactions on spherical and cylindrical particles, as well as diffusion through a stagnant film and product layer. From the estimation results, it was concluded that a very good description is obtained with a simple model, where the reaction rate is proportional to the concentration of reduction agent, zinc sulphide, and to the concentration of ferric iron. The sulphuric acid had a crucial influence on the reduction kinetics; the rate being proportional to the concentration of the sulphuric acid in the power of 1.5. This indicates that the reaction between zinc sulphide and ferric iron goes through a state where sulphuric acid participates as an intermediate, thus the reaction takes place in the liquid phase. The model parameters were estimated by regression analysis. The results demonstrated clearly, that model discrimination per se is not enough to reveal the true mechanism of solid–liquid reactions, but a detailed study of solid particles is needed.

Keywords: Kinetics; Leaching; Modelling; Particle; Solid–liquid reaction; Zinc sulphide

1. Introduction

Dissolution of solid particles is a typical industrially relevant process, for instance in hydrometallurgy, medicine, oceanography, crystallography, ceramics and desalination, as well as in a number of biological and environmental precipitation processes. Not only the structural properties of the solid particles influence significantly the progress of the reaction, but also the reaction media has a great impact. In general, dissolution kinetics depends on the concentrations of the fluid reactants, mass transfer effects, as well as the structural properties of particle ensembles expressed by particle distribution functions.

Oxidative dissolution of sphalerite concentrate (zinc sulphide ores) with ferric iron has been described by several authors (Kammel et al., 1987; Verbaan and Crundwell, 1986; Palencia Perez and Dutrizac, 1991; Crundwell, 1987; Cheng et al., 1994; Suni et al., 1989; Lochmann and Pedlík, 1995). As the zinc is leached, the ferric iron is reduced to ferrous iron by the sulphur in the zinc sulphide according to the following overall reaction stoichiometry:

$$Fe_2(SO_4)_3(aq) + ZnS(s) \rightarrow 2FeSO_4(aq) + ZnSO_4(aq) + S(s). \quad (1)$$

The solid–liquid reaction takes place in acidic environment and elemental sulphur is the solid product formed. In currently applied large-scale zinc dissolution processes, the produced ferrous iron is re-oxidized in order to continue the leaching. However, if the aim is to reduce the ferric iron,

* Corresponding author. Tel.: +358-2-215-4985; fax: +358-2-215-4479.
E-mail address: dmurzin@abo.fi (D.Y. Murzin).

0009-2509/$ - see front matter © 2003 Elsevier Ltd. All rights reserved.
doi:10.1016/j.ces.2003.10.022

the zinc sulphide concentrate can also be used as a reduction agent and is then leached simultaneously.

Kammel et al. (1987) leached sphalerite in sulphuric acid–ferric sulphate solution and investigated the effect of copper-ion-additions and the grinding of the materials. Stoichiometric addition of ferric iron sulphate was sufficient for the dissolution of zinc, while overstoichiometric amounts of ferric iron did not improve the extraction; the maximum amount of zinc leached was limited by its solubility in the sulphate solution. The results demonstrated that zinc extraction increased with higher iron contents in the sphalerite lattice. X-ray analysis of the sphalerite samples indicated that the lattice distance of the unit cell increased with increasing iron content. As copper ions were added into the solution, the extraction of sphalerite with low iron content increased, while the zinc extraction decreased due to copper addition when the iron content of sphalerite exceeded about 1%. Apparently copper formed a sulphide film, which affected the leaching. It was shown that short grinding times were sufficient to accelerate the zinc dissolution.

Verbaan and Crundwell (1986) leached a sphalerite concentrate (Gamsberg ore deposit, Northern Cape of South Africa) in an acidic ferric sulphate solution. The reaction was described by an electrochemical charge-transfer model, in which the mineral surface potential was approximated by the redox potential of the solution for the ferrous–ferric redox couple. The shrinking core model with chemical reaction control was used and the rate was proportional to the surface area. The activation energy was estimated to 79.4 kJ/mol at 25–85°C.

Palencia Perez and Dutrizac (1991) leached sphalerite samples (size range 75–104 μm) in both ferric iron sulphate–sulphuric acid and ferric iron chloride–hydrochloric acid solutions. The influence of solid solution iron content on the leaching rate was investigated, the rate increased linearly with increasing iron content. The linear relationship between the dissolution rate and the iron content of the sphalerite was suggested to indicate that the leaching was controlled by the charge transfer at the sphalerite surface. The activation energy decreased as the iron content of the sphalerite increased. In ferric sulphate media, the activation energy was about 70 kJ/mol for sphalerite with an iron content of 0.04 wt% and approximately 40 kJ/mol for sphalerite with an iron content of 12.5 wt%. The experimental data were described by the function of surface reaction controlled leaching,

$$k't = 1 - (1 - \alpha)^{1/3} \quad (2)$$

at 50–90°C and for zinc extractions over 85% (k' is the rate constant, t is time, and α is conversion). The dissolution kinetics was similar in both ferric sulphate and ferric chloride systems.

Crundwell (1987) leached sphalerite concentrate (Gamsberg deposit, size range 44–53 μm) in a solution of ferric iron and sulphuric acid. Surface reaction control was applied, the linear dependence (Eq. (2)) deviated at 30 min of leaching (at about 70% conversion) and became parabolic. The deviation was explained by product-layer diffusion, but no analysis of leached particles was performed. The activation energy was estimated to 46 kJ/mol. The kinetics was explained by an electrochemical mechanism, where the charge transfer from solid to oxidant was the rate-limiting step.

Cheng et al. (1994) leached zinc sulphide concentrate (Mount Isa Mines, Australia) in a solution of ferric sulphate, sulphuric acid and sodium chloride. The shrinking core model was used to describe the dissolution reaction, limited by electrochemical processes in the beginning of the leaching, but later on, surface reaction and pore diffusion. The experimental data followed Eq. (2) until the concentrate was leached about 60–70%, after which pore diffusion was stated to control the reaction. To confirm this, additional prolonged experiments were performed for three hours; one of them was stopped after one hour and the residue was separated from the solution, dried and washed with carbon disulphide solution after which the residue was returned to the original solution and leached until three hours. It was claimed that the leaching rate was higher for the washed material compared to the other material, suggesting sulphur formation controlling the rate. The activation energy was 49 kJ/mol at 60–90°C, indicating surface-reaction control. The apparent rate constant was plotted against the reciprocal of the average particle diameter, which showed a straight line with a small intercept (which was assumed to be within the experimental error) indicating the leaching was controlled by surface reaction. The effect of ferric iron concentration was investigated and the zinc leaching rate increased with increasing concentration, until a ferric iron concentration was 1.00 mol/l, which was even slower than 0.10 mol/l and almost the same as 0.03 mol/l. This result was unexpected.

Suni et al. (1989) leached sphalerite concentrates in acidic ferric chloride solution. A model was developed, in which the leaching rate was surface-limited and the multi-size distribution of the sphalerite particles was taken into consideration by integration over a number of particle size classes, instead of using an average rate constant. For the first concentrate leached (45–106 μm), a two, four and five evenly distributed size fractions, as well as a normal distribution of five particle sizes, were used. The model predicted the leaching rate slightly better than the model using an average rate constant. As the second concentrate was used (14.3–250 μm), the result deviated remarkably from the surface reaction model ($< 90\%$ extraction). When the rate constant versus the inverse particle radius was plotted, a linear relationship was obtained, but with a nonzero intercept. When the model was changed, taken into consideration the nonzero intercept, a good fit of the experimental results from approximately equal weights of five and 10 particle size fractions, as well as 15 particle size fractions with a bimodal distribution was obtained. The results indicated that the prediction was strongly dependent on the form of the rate constant–particle size relationship assumed, for example,

a poor result was obtained with the second concentrate, as the relationship between the rate constant and inverse particle radius was assumed to go through the origo, as well as when the average rate constant was used. The good fit with an average rate constant with the first concentrate was a result of a relatively small particle size range.

Lochmann and Pedlík (1995) leached sphalerite concentrates (Horní Benešov ore deposit, Czech Republic as well as Rosh Pinah and Black Mountain, South Africa) in acidic ferric sulphate solution. A product layer was limiting the extraction, and to reveal the character of product, the passivated concentrate was washed to dissolve either anglesite, jarosite or elemental sulphur. As the washed concentrate was re-leached, an improved extraction was noticed just in the case where elemental sulphur was removed. Thus it was concluded that a layer of elemental sulphur controlled the dissolution rate.

Rath et al. (1981) dissolved chemical grade zinc sulphide powder (Riedel, 100% < 75 μm) in an aqueous ferric chloride solution. For ferric chloride concentration of 0.2 mol/l, the ratio between zinc sulphide and ferric iron was approximately stoichiometric, but at higher ferric iron concentrations (up to 0.8 mol/l), an overstoichiometric amount of ferric iron was used. A logarithmic plot of the rate constant against the ferric chloride concentration gave the slope of 1.37. The deviation from unity was explained as a result of the high concentrations of the ferric iron. Because of this, ferric chloride might have formed complexes as well as hydrolysis products. Instead, a logarithmic plot of the initial rate at 5 and 10 min against the ferric iron concentrations was applied, giving the slopes 1.12 and 1.28, respectively. The activation energy was 90.0 ± 12.5 kJ/mol at 30–70°C. The dissolution was established to follow the shrinking core model with diffusion through the product layer, and this assumption was made due to the fact that the equation of Crank–Ginstling and Brounshtein was describing the experimental data well.

In general it can be concluded that a variety of models have been applied in the literature and there is no consensus on the mechanism of ferric ions reduction with zinc sulphide.

The dissolution kinetics of a solid compound depends on the processes taking place at the solid–liquid boundary; the processes are complex and involve both chemical reactions and mass transfer. The solid–liquid reaction can occur at the surface of the solid, in the film around the solid or in the liquid bulk phase. Different steps, such as mass transfer, chemical reaction, and charge transfer, can determine the dissolution rate (Crundwell, 1987; Crundwell and Verbaan, 1987; Momade and Momade, 1999). The classical models used for solid–fluid reactions are the shrinking particle and the shrinking core (product layer) models (Levenspiel, 1972). The shrinking core model has been suggested by many authors to be valid for leaching of sphalerite (Palencia Perez and Dutrizac, 1991; Lochmann and Pedlík, 1995; Cheng et al., 1994; Suni et al., 1989; Ekinci et al., 1998; Babu et al., 2002). However, the opinion of the rate-determining step differs, some authors state that rate is controlled by the chemical reaction, while others propose that the mass transfer through the product layer controls the rate. However, kinetic modelling alone cannot provide an unequivocal answer on the mechanism, therefore particle characterization methods should be employed, too.

In this work, the reduction of ferric iron to ferrous iron with pure zinc sulphide was experimentally investigated. In order to determine whether a product layer was present, the particles were analysed by SEM–EDS and laser diffraction techniques. Several kinetic models of solid–liquid reactions were fitted to the experimental data. The models represent first- and second-order dependence of the reduction agent, surface reaction on spherical and cylindrical particles, as well as diffusion through the liquid film and the product layer. To clarify the underlying mechanism of sphalerite leaching—which has been attempted by several authors—pure zinc sulphide provides an attractive alternative. Experimental study of ferric iron reduction by sphalerite and its comparison with pure zinc sulphide leaching will be a subject of a separate communication (Markus et al., 2004).

2. Experimental methods

Ferric iron sulphate ($Fe_2(SO_4)_3 \cdot 5H_2O$) of 97% purity was supplied by Aldrich, reagent grade zinc sulphide (ZnS) of 97% purity was supplied by Riedel–de Haën, and sulphuric acid (H_2SO_4) of 95–96% purity by J.T. Baker. The BET surface area of the zinc sulphide was determined to be 10.8 m^2/g, as measured by nitrogen adsorption. The conditions for the reduction experiments varied from 75–95°C, 0.2–0.4 mol/l initial concentration of ferric iron, 0.5:1–2:1 zinc sulphide-to-ferric iron molar ratio (where 1:1 is stoichiometric ratio and 2:1 is overstoichiometric amount of zinc sulphide) and 0.41–1.02 mol/l (40–100 g/l) sulphuric acid concentration.

In a typical experiment, a solution of sulphuric acid, ferric iron sulphate and de-ionized water was preheated to the reaction temperature in a 1000 ml stirred glass reactor, where 750 ml of the volume was used for the liquid and solid phases. Efficient agitation was obtained with a pitched-blade turbine (eight blades). The reactor was provided with a heating jacket using silicone oil as the heat transfer fluid. Moreover, it was equipped with an oil lock, baffles and a reflux condenser. Zinc sulphide, dispersed in water, and some extra water were preheated on hot-plates to the reaction temperature. The experiment was initiated by pouring the zinc sulphide and water into the reactor. The reaction was carried out under atmospheric pressure and nitrogen flow (99.999%, AGA) in 2 h, with some exceptions. The temperature and redox potential were continuously stored on a computer during the reaction. The redox potential was measured with a platinum electrode (Metrohm), using an Ag/AgCl reference electrode in a

3 mol/l KCl solution. A typical stirring rate was 420 rpm, but the reaction was also conducted with other stirring rates to investigate the influence of mass transfer resistance. Samples (5 ml) were withdrawn at discrete time intervals with a syringe. The solid–liquid ratio was kept constant during the reaction by removing equivalent amount particles and liquid. The separation of the particles from the liquid was performed with a filter attached to the syringe. The concentration of ferric iron was determined by sequential injection analysis (SIA) using the reagent Tiron (0.05 mol/l, 1,2-dihydroxy-3,5-benzenedisulphonic acid disodium salt dissolved in 0.05 mol/l sulphuric acid). Samples of solid particles were prepared for SEM–EDS as follows: samples (5 ml) of equivalent amount of solid particles and liquid were withdrawn with a syringe and injected into a test tube. As the particles had settled, the liquid was removed with a pipette. The particles were washed with distilled water several times. The washed particles were then dried in air at room temperature. Before the analysis by SEM–EDS the particles were homogenized with a spatula. Samples of particles in solution were analysed by laser diffraction technique (Malvern 2600 Particle Sizer), to observe changes of the particle size distribution. The diameter of a particle, obtained by analysis with laser diffraction, can be calculated in two ways: the volume-based method sets the diameter equal to the diameter for a sphere with the same volume as the particle, while the area-based method sets the diameter equal to the diameter of a sphere with the same surface area.

3. Modelling procedure

To model the reaction system based on the batch reactor concept, a rate expression consisting of a temperature depending factor, the concentration of sulphuric acid and ferric iron, as well as a factor representing the solid particles was specified. The temperature-dependent factor originates from the Arrhenius equation. Equations for the dissolution of solid particles are summarized in Table 1. The equations and corresponding notations are taken from Dickinson and Heal (1999) and Órfão and Martins (2002). In Table 1, R3 represents the reaction on a spherical particle, as the surface reaction is the rate-determining step, and it is thus valid for both shrinking particle and product layer models. R4 represents film diffusion in the case of shrinking particle model.

Functions $g(\alpha)$ and $f(c_{\mathrm{ZnS}})$ in Table 1 are explained as follows: the reaction rate of the particles, as a function of the conversion, can be written as

$$r = \frac{\mathrm{d}\alpha}{\mathrm{d}t} = k' f(\alpha). \tag{3}$$

The conversion of the solid component (ZnS), α, is given by

$$\alpha = \frac{c_{0\mathrm{ZnS}} - c_{\mathrm{ZnS}}}{c_{0\mathrm{ZnS}}}, \tag{4}$$

where $c_{0\mathrm{ZnS}}$ and c_{ZnS} represent the total amount of zinc sulphide per liquid volume in the beginning of the reaction and after a certain time of reaction. The reaction rate can consequently be expressed as a function of the concentration (total amount of zinc sulphide per liquid volume),

$$r = k'' f(c_{\mathrm{ZnS}}). \tag{5}$$

In the literature, expression (3) is often given in integrated form,

$$g(\alpha) = \int_0^{\alpha} \frac{\mathrm{d}\alpha}{f(\alpha)} = k' \int_0^{t} \mathrm{d}t. \tag{6}$$

In the overall rate expression, the factor representing the solid particles is presented by the form of Eq. (5), $f(c_{\mathrm{ZnS}})$ in Table 1. Function $g(\alpha)$ in Table 1 was never used in the parameter estimation in the present study, it is only given to facilitate the recognition. Furthermore, it is assumed that

Table 1
Expressions of $g(\alpha)$ and $f(c_{\mathrm{ZnS}})$for the kinetic models used in this work

Notation	$g(\alpha)$	$f(c_{\mathrm{ZnS}})$	Type of model	p_1	p_4
F1	$-\ln(1-\alpha)$	$c_{\mathrm{ZnS}}/c_{0\mathrm{ZnS}}$	First-order kinetics	1	–
F3/2	$(1-\alpha)^{-1/2}-1$	$(c_{\mathrm{ZnS}}/c_{0\mathrm{ZnS}})^{3/2}$	Three-halves-order kinetics	$\frac{3}{2}$	–
F2	$(1-\alpha)^{-1}$	$(c_{\mathrm{ZnS}}/c_{0\mathrm{ZnS}})^{2}$	Second-order kinetics	2	–
R2	$1-(1-\alpha)^{1/2}$	$(c_{\mathrm{ZnS}}/c_{0\mathrm{ZnS}})^{1/2}$	One-half-order kinetics; 2-D advance of the reaction interface	$\frac{1}{2}$	–
R3	$1-(1-\alpha)^{1/3}$	$(c_{\mathrm{ZnS}}/c_{0\mathrm{ZnS}})^{2/3}$	Two-thirds-order kinetics; 3-D advance of the reaction interface	$\frac{2}{3}$	–
R4	$1-(1-\alpha)^{2/3}$	$(c_{\mathrm{ZnS}}/c_{0\mathrm{ZnS}})^{1/3}$	One-thirds-order kinetics; film diffusion	$\frac{1}{3}$	–
D3	$[1-(1-\alpha)^{1/3}]^2$	$(c_{\mathrm{ZnS}}/c_{0\mathrm{ZnS}})^{2/3}/(1-(c_{\mathrm{ZnS}}/c_{0\mathrm{ZnS}})^{1/3})$	Jander; 3-D	$\frac{2}{3}$	$\frac{1}{3}$
D4	$1-2\alpha/3-(1-\alpha)^{2/3}$	$(c_{\mathrm{ZnS}}/c_{0\mathrm{ZnS}})^{1/3}/(1-(c_{\mathrm{ZnS}}/c_{0\mathrm{ZnS}})^{1/3})$	Crank–Ginstling and Brounshtein	$\frac{1}{3}$	$\frac{1}{3}$
D5	$[1/(1-\alpha)^{1/3}-1]^2$	$(c_{\mathrm{ZnS}}/c_{0\mathrm{ZnS}})^{5/3}/(1-(c_{\mathrm{ZnS}}/c_{0\mathrm{ZnS}})^{1/3})$	Zhuravlev, Lesokhin and Tempelman	$\frac{5}{3}$	$\frac{1}{3}$
D8	$[1-(1-\alpha)^{1/2}]^2$	$(c_{\mathrm{ZnS}}/c_{0\mathrm{ZnS}})^{1/2}/(1-(c_{\mathrm{ZnS}}/c_{0\mathrm{ZnS}})^{1/2})$	Jander; cylindrical diffusion	$\frac{1}{2}$	$\frac{1}{2}$
D10	$1/(1-\alpha)^{1/3}-1$	$(c_{\mathrm{ZnS}}/c_{0\mathrm{ZnS}})^{4/3}$	Dickinson and Heal	$\frac{4}{3}$	–

k', which is depending on the concentration of the leaching species around the particle (here: Fe^{3+}), is constant, although the concentration of the ferric iron varies around the particles in this case, k' is an apparent one. However, model D5 takes into account that the concentration around the particle varies with the conversion (Dickinson and Heal, 1999). When fitting the experimental data to models F1, F3/2, F2, R2–R4, and D10, the following rate expression was used,

$$r = k \exp\left(-\frac{E_a}{R}\left(\frac{1}{T} - \frac{1}{T_{\text{mean}}}\right)\right) \times \left(\frac{c_{\text{ZnS}}}{c_{0\text{ZnS}}}\right)^{p_1} c_{\text{H}_2\text{SO}_4}^{p_2} c_{\text{Fe}^{3+}}^{p_3}. \quad (7)$$

and for the models D3–D5, and D8,

$$r = k \exp\left(-\frac{E_a}{R}\left(\frac{1}{T} - \frac{1}{T_{\text{mean}}}\right)\right) \times \frac{\left(\frac{c_{\text{ZnS}}}{c_{0\text{ZnS}}}\right)^{p_1}}{1 - \left(\frac{c_{\text{ZnS}}}{c_{0\text{ZnS}}}\right)^{p_4}} c_{\text{H}_2\text{SO}_4}^{p_2} c_{\text{Fe}^{3+}}^{p_3}. \quad (8)$$

In the expressions above E_a is the activation energy, R is the gas constant, T is the temperature, T_{mean} is the mean temperature of the experiments, c_{ZnS} and $c_{0\text{ZnS}}$ are the concentration and initial concentration of zinc sulphide correspondingly, $c_{\text{Fe}^{3+}}$ and $c_{\text{H}_2\text{SO}_4}$ denote the concentrations of ferric iron and sulphuric acid. Parameters p_2 and p_3 are exponents for the sulphuric acid and ferric iron concentrations. As the rate expression (7) was used, the exponent p_1 was fixed during the screening of different models and when Eq. (8) was used, both p_1 and p_4 were fixed a priori. An estimation, where none of the parameters were fixed, was also made for the rate expression (7).

Since the rates of the compounds, r_i, are related to the reaction rate by the stoichiometric coefficients, v_i, the consumption rates for ferric iron versus zinc sulphide ($v_{\text{Fe}^{3+}} = -2$ and $v_{\text{ZnS}} = -1$) can be written as

$$\frac{\mathrm{d}c_{\text{Fe}^{3+}}}{\mathrm{d}t} = r_{\text{Fe}^{3+}} = -2r, \quad (9)$$

$$\frac{\mathrm{d}c_{\text{ZnS}}}{\mathrm{d}t} = r_{\text{ZnS}} = -r. \quad (10)$$

The amount of zinc sulphide in the liquid, i.e. the total amount per liquid volume, is calculated as

$$c_{\text{ZnS}} = \frac{m_{\text{ZnS}}}{M_{\text{ZnS}} V_L}, \quad (11)$$

where m_{ZnS} is the mass, M_{ZnS} the molar mass and V_L the volume of the ferric sulphate–sulphuric acid solution. The change in V_L, due to the sampling, is not taken into consideration in the modelling, since both particles and liquid are removed in the samples, and therefore the situation is considered to be similar in the beginning and the end of the reaction.

Nonlinear regression analysis was performed using the simulation and parameter estimation software MODEST (Haario, 2001). The system of ordinary differential equations (Eqs. (9) and (10)) was solved with the backward difference method implemented in the software ODESSA. All sets of experimental data, containing the ferric iron concentration and temperature as a function of time, as well as the concentration of sulphuric acid and initial concentration of zinc sulphide, were merged together. The sum of residual squares, Q, was minimized with the hybrid simplex–Levenberg–Marquardt method,

$$Q = \|c_{\text{exp}} - c_{\text{est}}\|^2 = \sum_t \sum_i (c_{\text{exp},it} - c_{\text{est},it})^2, \quad (12)$$

where c_{exp} denotes experimental data and cest the estimated values. An indication of the goodness of the model is the degree of explanation, R^2,

$$R^2 = 100(1 - \|(c_{\text{exp}} - c_{\text{est}}\|^2 / \|c_{\text{exp}} - \bar{c}_{\text{exp}})\|^2), \quad (13)$$

where $\bar{c}_{\text{exp}}$ is the mean value of the experimental data.

4. Qualitative analysis

To study the influence of initial concentration of ferric iron on the reaction kinetics, concentrations within the range of 0.2–0.4 mol/l were used. The experimental and estimated values from three experiments with varying initial concentrations of ferric iron are shown in Fig. 1. The figure demonstrates that higher concentration of ferric iron enhanced the reduction rate. In all of the figures, the solid lines represent the prediction of model F1. When Rath et al. (1981) dissolved chemical grade zinc sulphide powder in aqueous ferric chloride solution (0.2–0.8 mol/l), a logarithmic plot of the initial rate at 5 and 10 min against the ferric iron concentrations was made and the slopes 1.12 and 1.28, respectively were obtained. The temperature range was 30–70°C and no acid was used. In this work the logarithmic plot of the initial rate at 10 min against the ferric iron concentration, in the temperature range 75–95°C,

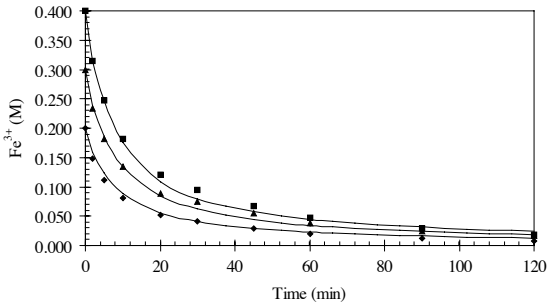

Fig. 1. Influence of initial concentration of ferric iron: ♦ = 0.2 M, ▲ = 0.3 M, and ■ = 0.4 M. Conditions: zinc sulphide-to-ferric iron molar ratio, 1:1; sulphuric acid concentration, 0.41 mol/l; temperature, 85°C.

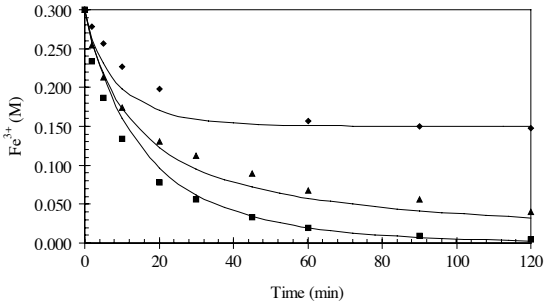

Fig. 2. Influence of zinc sulphide-to-ferric iron molar ratio: ♦ = 0.5 : 1, ▲ = 1 : 1, and ■ = 2 : 1. Conditions: initial concentration of ferric iron, 0.3 M; sulphuric acid concentration, 0.41 mol/l; temperature, 75°C.

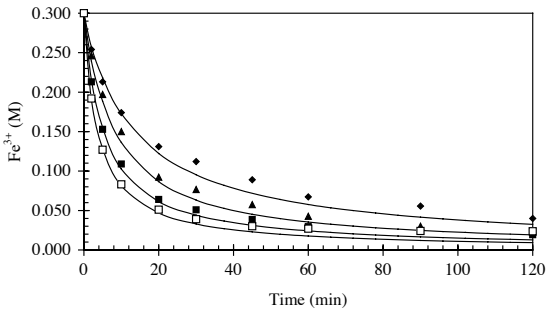

Fig. 3. Influence of sulphuric acid concentration: ♦ = 0.41 mol/l, ▲ = 0.61 mol/l, ■ = 0.82 mol/l, and □ = 1.02 mol/l. Conditions: zinc sulphide-to-ferric iron molar ratio, 1:1; initial concentration of ferric iron, 0.3 M; temperature, 75°C.

were made and the slopes between 0.76 and 0.94 were obtained. The slope 0.76 was obtained when using the lowest temperature and the highest acid concentration and the slope 0.94 was obtained with the lowest temperature and the lowest acid concentration. Slopes between these two values were obtained using the lowest acid concentration at different temperatures. It could be noticed that the steepest descent was achieved at the lowest acid concentration and temperature; when increasing the acid concentration, the descent decreased. Also an increase in temperature decreased the descent, but not as much as the change in sulphuric acid concentration did. Since sulphuric acid was used and the temperatures were higher than the temperatures used by Rath et al. (1981) the lower value of the slope was logical. Moreover, in this work a stoichiometric amount of ferric iron–zinc sulphide was used, while the stoichiometric ratio varied in the work by Rath et al. (1981). This could also affect the value of the slope.

Different zinc sulphide-to-ferric iron molar ratios in the range of 0.5:1–2:1 were used. As demonstrated by Fig. 2, the reduction rate increased with increasing amount of reduction agent in relation to the amount of ferric iron. To investigate whether sulphuric acid had any influence on the reaction kinetics, concentrations in the range of 0.41–1.02 mol/l (40–100 g/l) were applied. The concentration of sulphuric acid had a remarkable effect on the reduction rate, as illustrated by Fig. 3. Several authors have proposed that the hydronium ions contribute to the leaching by forming hydrogen sulphide, which is re-oxidized by ferric iron yielding hydronium ions, ferrous iron and elemental sulphur (Verbaan and Crundwell, 1986; Kammel et al., 1987). It has been suggested that the amount of hydrogen sulphide dramatically decreases as ferric iron is added (Verbaan and Crundwell, 1986). The effect of temperature on the reduction rate was investigated in the range 75–95°C. Fig. 4 shows the results originating from three experiments; it can be concluded that the reaction temperature had a profound influence on the reaction rate. The activation energy of the reaction was calculated by parameter estimation according to Eqs. (7) and (8).

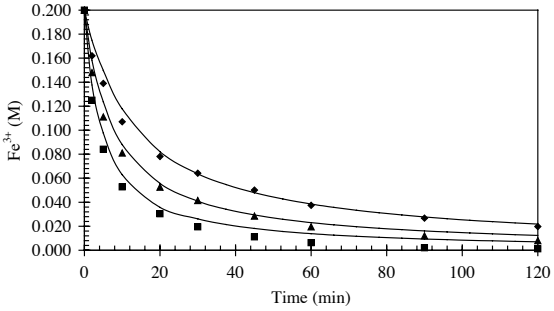

Fig. 4. Influence of temperature: ♦ = 75°C, ▲ = 85°C, and ■ = 95°C.Conditions: zinc sulphide-to-ferric iron molar ratio, 1:1; initial concentration of ferric iron, 0.2 M; sulphuric acid concentration, 0.41 mol/l.

5. Particle size analysis of the solids

The results from SEM–EDS and laser diffraction analyses are visualized in Figs. 5 and 6. Big particles of elemental sulphur are present (large dark areas) along with smaller particles (light areas), which contain more zinc, were found on the surface (Fig. 5). From these results it can be concluded that sulphur particles formed are larger than zinc sulphide particles consumed, and, what is most important, that no sulphur layer is formed around the zinc sulphide particles. Fig. 6 confirms this conclusion. Fig. 6(a) shows an unimodal particle size distribution, the mean diameter obtained by the volume-based method being 5.75 μm and by the area-based method 3.87 μm. The result after leaching in 7 min, with 70% of the starting material left, is given in Fig. 6(b) demonstrating more peaks, among which the larger particles represent the elemental sulphur formed, and the smaller particles zinc sulphide left. The mean particle diameters were 21.75 and 8.02 μm obtained by the volume- and area-based methods, respectively. Fig. 6(c) shows convincingly that the distribution is a bimodal one, where

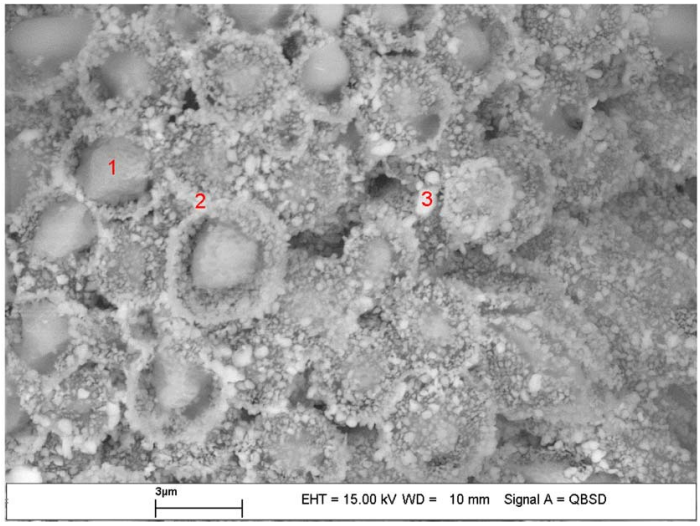

Fig. 5. SEM–EDS micrograph of final leach residue in 2 h (×5000). Darker areas consist of more sulphur, lighter areas of more zinc. Result from point analysis performed by EDS: (1) 96.61% sulphur, 3.36% zinc, (2) 75.39% sulphur, 24.61% zinc, and (3) 69.96% sulphur and 30.05% zinc. Conditions: zinc sulphide-to-ferric iron molar ratio, 1:1; initial concentration of ferric iron, 0.4 M; sulphuric acid concentration, 0.41 mol/l; temperature, 95°C.

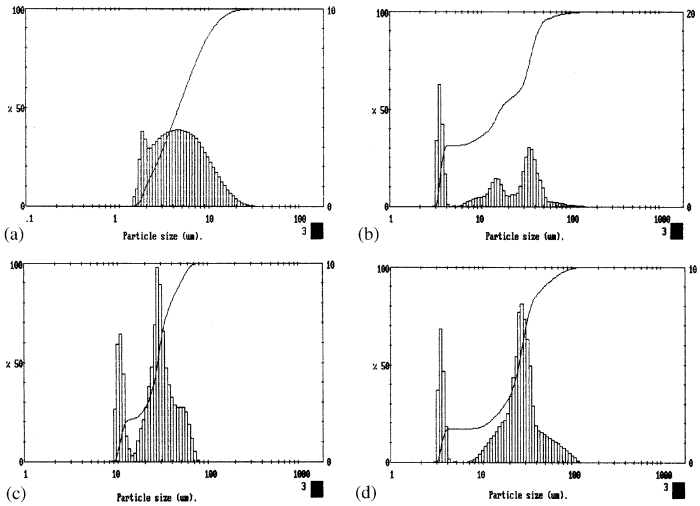

Fig. 6. Particle size distribution determined by laser diffraction technique. (a) unreacted ZnS dispersed in water (63 mm objective), (b) leached in 7 min (100 mm objective), (c) leached in 35 min (300 mm objective), and (d) leach residue in 2 h (100 mm objective). Conditions: zinc sulphide-to-ferric iron molar ratio, 1:1; initial concentration of ferric iron, 0.4 M; sulphuric acid concentration, 0.41 mol/l; temperature, 75°C.

the peak with larger particles, sulphur, grows, while the peak with smaller particles, zinc sulphide, diminishes. The mean diameters calculated were 28.68 μm according to the volume-based and 21.57 μm according to the area-based methods. At this point, 35% of the ferric iron is still to be reduced. In the leaching residue obtained after 2 h, as 14% of the starting material is left, Fig. 6(d) shows that a narrow peak of small zinc sulphide particles is still remaining. The diameter was 26.48 μm (volume-based) and 11.88 μm (area-based).

6. Estimation of kinetic parameters

Concerning the reaction mechanism of the reduction of ferric iron and at the same time the dissolution of zinc sulphide, two reaction paths can be considered. The first path

Table 2
Results from modelling

Model	p_1 (fixed)	p_4 (fixed)	k	E_a (kJ/mol)	p_2 (H_2SO_4)	p_3 (Fe^{3+})	Residual SS Q	Explained R^2 (%)
F1	1	–	0.19 ± 0.01 $l^{1.51}/(mol^{1.51}min)$	67.1 ± 2.6	1.48 ± 0.05	1.03 ± 0.05	0.0231	98.08
F3/2	$\frac{3}{2}$	–	0.16 ± 0.01 $l^{1.26}/(mol^{1.26}min)$	71.7 ± 2.1	1.53 ± 0.04	40.73 ± 0.03	0.0128	98.93
F2	2	–	0.13 ± 0.01 $l^{1.05}/(mol^{1.05}min)$	77.2 ± 2.6	1.60 ± 0.05	0.45 ± 0.04	0.0176	98.54
R2	$\frac{1}{2}$	–	0.26 ± 0.03 $l^{1.83}/(mol^{1.83}min)$	63.9 ± 3.7	1.46 ± 0.07	1.37 ± 0.07	0.0507	95.78
R3	$\frac{2}{3}$	–	0.23 ± 0.02 $l^{1.71}/(mol^{1.71}min)$	64.8 ± 3.3	1.46 ± 0.06	1.25 ± 0.06	0.0394	96.72
R4	$\frac{1}{3}$	–	0.29 ± 0.03 $l^{1.93}/(mol^{1.93}min)$	63.0 ± 4.0	1.45 ± 0.08	1.48 ± 0.04	0.0640	94.67
D3	$\frac{2}{3}$	$\frac{1}{3}$	0.01 ± 0.00 $l^{1.18}/(mol^{1.18}min)$	81.5 ± 3.2	1.70 ± 0.06	0.48 ± 0.05	0.0257	97.86
D4	$\frac{1}{3}$	$\frac{1}{3}$	0.01 ± 0.05 $l^{1.29}/(mol^{1.29}min)$	76.9 ± 2.7	1.63 ± 0.05	0.66 ± 0.02	0.0206	98.29
D5	$\frac{5}{3}$	$\frac{1}{3}$	0.01 ± 0.15 $l^{0.93}/(mol^{0.93}min)$	96.7 ± 6.5	1.93 ± 0.12	0.00 ± 0.01	0.0720	94.00
D8	$\frac{1}{2}$	$\frac{1}{2}$	0.01 ± 0.03 $l^{1.26}/(mol^{1.26}min)$	78.0 ± 2.8	1.65 ± 0.05	0.61 ± 0.05	0.0212	98.23
D10	$\frac{4}{3}$	–	0.17 ± 0.01 $l^{1.35}/(mol^{1.35}min)$	70.0 ± 2.1	1.52 ± 0.04	0.83 ± 0.04	0.0145	98.80

involves sulphuric acid, which has already been mentioned in Section 4,

$$ZnS(s) + H_2SO_4 \rightarrow ZnSO_4 + H_2S(aq), \quad (14)$$

$$Fe_2(SO_4)3 + H_2S(aq) \rightarrow 2FeSO_4 + H_2SO_4 + S(s). \quad (15)$$

The second path is the direct reaction between ferric iron and zinc sulphide, as in Eq. (1), which also is the net result from reactions (14) and (15). From the experimental data we can clearly see that the sulphuric acid takes part in the reaction, which would suggest the first reaction path. Also the formation of separate sulphur particles is a strong evidence for a reaction via liquid phase. Another possibility could be that both reaction paths occur simultaneously. It is difficult to reveal if the reaction goes through both ways. However, the first step in the modelling was to try different models proposed for solid–liquid reactions, and for this 11 different models were fitted to the experimental data according to the procedure discussed in Section 3. Table 2 summarizes the modelling results. The result from the estimation, where none of the parameters were fixed, is not included in Table 2, but it is quite close to the result of model F3/2; the degree of explanation was the highest one 98.95, k was $0.15\ l^{1.23}/(mol^{1.23}min)$, E_a was 72.4 kJ/mol, and p_1, p_2, and p_3 were 1.58, 1.54, and 0.69, respectively. It can be concluded from Table 2 that models F1, F3/2, F2, D4, D8, and D10 all give a degree of explanation (R^2) exceeding 98%. Model D3, with R^2 just below 98%, could also be regarded as acceptable. The difference between these models, considering R^2, is rather minor. Models F3/2, D10, and F2 are relatively simple models, where the reaction rate is proportional to the reduction agent in the power of $\frac{3}{2}$, $\frac{4}{3}$ and 2, and they explain the experimental data best. Model D10 represents the case when the rate controlling step is the mass transfer across the contracting area of a sphere (Dickinson and Heal, 1999). The simplest model of all, F1, with a first-order dependence on the reduction agent, explains the system well and might indicate that the reduction rate depends on the fraction zinc sulphide left and not on diffusion through a film or product layer. This is in accordance with the results obtained from particle size analysis (Section 5). Model D4, an equation originally proposed by Crank–Ginstling and Brounshtein, and frequently used (Rath et al., 1981; Lochmann and Pedlík, 1995; Babu et al., 2002), represents the case where spherical powdered particles react with a fluid creating a nonporous reaction product, which forms a layer around the particle and therefore, the further reaction is retarded by diffusion resistance through this layer. A high value of R^2 was obtained by fitting the data to model D8, which assumes that the reacting species is of cylindrical geometry. Model D5 had a poor degree of explanation, in fact the lowest one of the models tried. Since D5 is the only model that takes into consideration that the concentration around the particle varies with the conversion (Dickinson and Heal, 1999), this poor result was unexpected. Model R3, representing the surface-reaction control for both shrinking particle and product layer models, also gave a lower R^2-value than expected. According to this model, each of the particle sizes would continue to react according to Eq. R3, but the overall reaction rate would be a compound rate, which is

determined by the size distribution (Herbst, 1979). This implies that when using an average k-value for all the particle sizes, and not a separate k-value for each particle size, a broad particle size distribution will not obey this equation at higher conversions, since the smaller particles will be totally leached before the rest is leached. If the experimental data are used in the integrated form of model R3 (see Eq. (2)), this should create a straight line if the model is obeyed. This is often the case in the beginning of the reaction, since particles of all sizes are left, but a parabolic relationship is obtained at higher conversions due to the fact that some of the particles have been totally leached. The parabolic relationship has been explained by several authors to be a result of a product layer formed, but the reason could in fact be the size distribution. In our case, the size distribution of the particles was relatively narrow; 90% of the particles were smaller than 11.06 μm, 50% smaller than 4.55 μm and 10% smaller than 1.98 μm, but still there are smaller particles that will be leached more rapidly. The reaction was fast, so the explanation may also be that the rate is not dependent on the surface area available. In the models D3, D4, and D8 the reduction rate approaches infinity in the beginning of the reaction, since the denominator is close to zero. As the term $c_{\mathrm{ZnS}}/c_{0\mathrm{ZnS}}$ approaches zero, the denominator approaches unity, and the factor representing the solid particles approaches the value of the nominator. For model D8 this is the same as model R2, model D3 equal to R3, and for model D4 similar to R4. Apparently, the high value of R^2 obtained with the diffusion-control models do not give any evidence that the reaction is controlled by diffusion, they only somewhat compensate the experimental discrepancies by changing both the nominator and the denominator.

The estimated parameter p_3, the exponent of the ferric iron concentration, evidently follows the exponents of the reduction agent (Table 2). When a higher value is fixed for p_1, parameter p_3 gets a lower value. In model F1, when p_1 is given the value one, the parameter p_3 also obtains the value one, which is logical. Since a stoichiometric amount of zinc sulphide is used in most of the experiments, the parameter $c_{\mathrm{ZnS}}/c_{0\mathrm{ZnS}}$ in the model F1 could at the same time represent the fraction of iron left. In the beginning, the value of the parameter is one, which means that 100% of the iron is still to be reduced. As 50% of the zinc sulphide is leached, the value of the parameter is 0.5, and 50% of the iron is still to be reduced, when using a stoichiometric amount of reduction agent. If an overstoichiometric amount is used, all the ferric iron is reduced when the parameter takes the value 0.5. This could affect the fitting of model F1 to experiments with nonstoichiometric amount of reduction agent. Model D5 gives zeroorder dependence with respect to the ferric iron concentration, which is logical since this model takes into account the concentration of ferric iron in the factor representing the reduction agent. The value of the parameter p_2, i.e. the exponent of the sulphuric acid concentration, was relatively constant for all models; the mean value was 1.58 and the standard deviation 0.14. The activation energy, E_a, varied between 63 and 97 kJ/mol, depending on the model used. This is quite a high value and indicates against the presence of diffusion limitation. Rath et al. (1981) reported the activation energy to be 90.0 ± 12.5 kJ/mol in the reaction between pure zinc sulphide and ferric chloride in the temperature range 30–70°C. Even though they received such a high value of the activation energy, they suggested the diffusion of ferric ions through a layer of elemental sulphur to be the rate-controlling step. The conclusion was based on the fact that the equation, developed by Crank–Ginstling and Brounshtein (D4), explained the experimental data well. The present study indicates, however, the danger of mechanistic speculations based on kinetic data fitting solely. Moreover, dry samples of solid materials do not give a picture of the actual situation in liquid, for example sulphur sticks to the surface of the metal sulphide when the aqueous solution is removed, while the analysis by laser diffraction technique shows the behaviour in liquid. If a high degree of explanation is obtained with a simple model, when modelling a reaction system, this gives a hint what is the mechanism of the reaction. When adding more parameters, to the model, the degree of explanation often increases, but not necessarily the probability of finding the right mechanism. If we add a term representing the direct reaction between ferric iron and zinc sulphide (Eq. (1)) to the reaction rate in Eq. (7), we get the following expression

$$r = k_1 \exp\left(-\frac{E_{a1}}{R}\left(\frac{1}{T}-\frac{1}{T_{\mathrm{mean}}}\right)\right)\left(\frac{c_{\mathrm{ZnS}}}{c_{0\mathrm{ZnS}}}\right)^{p_1} c_{\mathrm{H_2SO_4}}^{p_2} c_{\mathrm{Fe^{3+}}}^{p_3} + k_2 \exp\left(-\frac{E_{a2}}{R}\left(\frac{1}{T}-\frac{1}{T_{\mathrm{mean}}}\right)\right)\left(\frac{c_{\mathrm{ZnS}}}{c_{0\mathrm{ZnS}}}\right)^{p_4} c_{\mathrm{Fe^{3+}}}^{p_5}. \quad (16)$$

The results from the modelling are visualized in Table 3. The first result is obtained when none of the parameters were fixed, and this gave the highest degree of explanation. The second result, when the exponent of zinc sulphide, p_1 was fixed to one as in model F1 (Tables 1 and 2), gave the second highest degree of explanation. The value of k_2 is small, which means that the second term is of less importance than the first. The exponent p_4 is large, while the exponent p_5 is almost zero. The third column in Table 3 shows the result when both p_1 and p_4 are fixed to one. The major change was that the exponent p_5 (Fe^{3+}, second term) increased, when the exponent p_4 (ZnS, second term) was forced to decrease from six to one, which again shows the correlation between ferric iron and zinc sulphide. In the fourth column (Table 3) the exponent p_1 was put to two thirds ($\frac{2}{3}$) as in model R3 (Tables 1 and 2). The response was similar as when p_1 was fixed to one; the value of k_2 and p_5 were small, while p_4 was large. When the exponent p_4 (ZnS, second term) was fixed to two thirds, the value of k_2 approached zero. This clearly shows that the second term is insignificant. The same observation was noted when p_1 was fixed to one and p_4 to two-thirds, in the last column. From this it can be concluded that there is no relevance of complicating the rate expression (7) by adding an extra term, because the minor

Table 3
Results from the modelling (Eq. (16))

	Not fixed	$p_1 = 1$	$p_1,\ p_4 = 1$	$p_1 = \frac{2}{3}$	$p_4 = \frac{2}{3}$	$p_1 = 1,\ p_4 = \frac{2}{3}$
k_1	0.16 ± 0.01 $l^{1.58}/(mol^{1.58}min)$	0.17 ± 0.01 $l^{1.77}/(mol^{1.77}min)$	0.23 ± 0.05 $l^{2.23}/(mol^{2.23}min)$	0.20 ± 0.02 $l^{2.13}/(mol^{2.13}min)$	0.17 ± 0.02 $l^{1.34}/(mol^{1.34}min)$	0.19 ± 0.02 $l^{1.49}/(mol^{1.49}min)$
E_{a1} (kJ/mol)	81.4 ± 2.8	81.8 ± 2.9	85.7 ± 10.2	84.1 ± 3.4	68.4 ± 3.3	66.8 ± 3.8
p_1	1.22 ± 0.08	1	1	$\frac{2}{3}$	1.72 ± 0.05	1
p_2	1.75 ± 0.05	1.80 ± 0.04	2.08 ± 0.33	1.95 ± 0.06	1.62 ± 0.06	1.46 ± 0.09
p_3	0.83 ± 0.06	0.97 ± 0.06	1.15 ± 0.17	1.18 ± 0.04	0.72 ± 0.05	1.03 ± 0.08
k_2	0.01 ± 0.004 $mol^{0.96}/(l^{0.96}min)$	0.01 ± 0.002 $mol^{0.99}/(l^{0.99}min)$	0.02 ± 0.01 $mol^{0.16}/(l^{0.16}min)$	0.03 ± 0.003 $mol^{0.90}/(l^{0.90}min)$	$5e-4 \pm 6e-4$ $mol^{0.79}/(l^{0.79}min)$	$8e-8 \pm 8e-4$ $mol^{0.95}/(l^{0.95}min)$
E_{a2} (kJ/mol)	13.8 ± 27.2	20.3 ± 18.9	33.6 ± 29.6	40.6 ± 12.5	113.7 ± 32.2	$33.9 \pm 2.1e3$
p_4	6.56 ± 1.26	6.16 ± 0.59	1	4.74 ± 0.32	$\frac{2}{3}$	$\frac{2}{3}$
p_5	0.04 ± 0.24	0.01 ± 0.10	0.84 ± 0.21	0.10 ± 0.13	0.21 ± 0.38	$0.05 \pm 1.8e3$
R^2 (%)	99.30	99.25	98.14	99.07	99.07	98.08

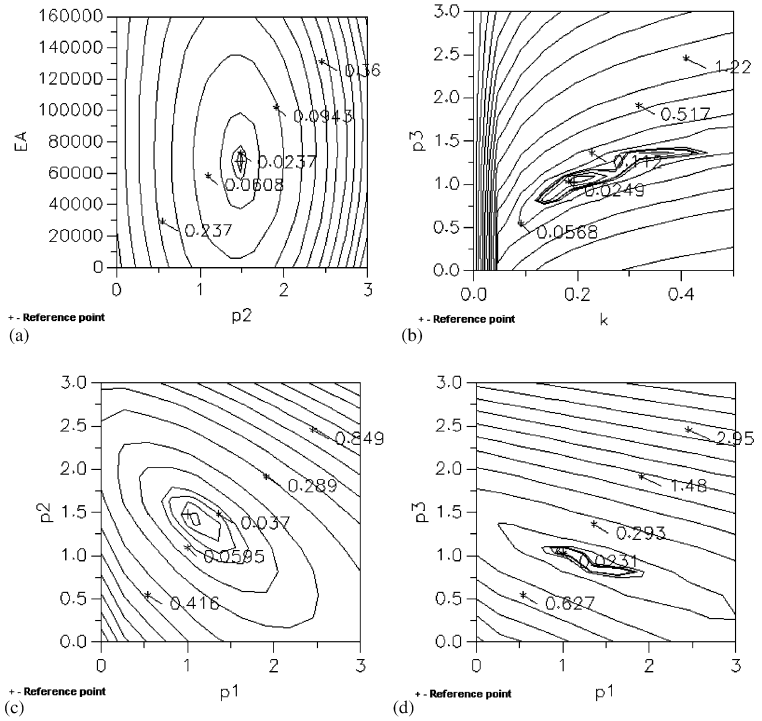

Fig. 7. Contour plots with the residual sum of squares for (a) parameters p_2 and E_a, (b) parameters k and p_3, (c) parameters p_1 and p_2, and (d) parameters p_1 and p_3.

increase in the degree of explanation does not compensate for the loss of handiness that a relatively simple model gives when simulating the system.

For practical purposes, a very simple model, F1, can be selected to describe the reaction kinetics. The reduction rate is proportional to the concentration of ferric iron and reduction agent,

$$r = k \exp\left(-\frac{E_a}{R}\left(\frac{1}{T} - \frac{1}{T_{\text{mean}}}\right)\right)\left(\frac{c_{\text{ZnS}}}{c_{0\text{ZnS}}}\right) c_{\text{H}_2\text{SO}_4}^{1.5} c_{\text{Fe}^{3+}}, \tag{17}$$

where k is 0.2 $l^{1.5}/(mol^{1.5}min)$, E_a is 67 kJ/mol and T_{mean} is 353.15 K (80°C). Figs. 1–4 illustrate the results estimated with this model (solid lines) compared with the experimental data. The estimated values follow the experimental values, although minor discrepancies are visible when using different zinc sulphide-to-ferric iron molar ratios (Fig. 2). The sensitivity analysis of the model parameters (F1) in the form of contour plots is presented in Fig. 7. The figure reveals that model F1 is well-defined and that the correlation between the parameters is relatively low. Fig. 7(a), where

the parameters p_2 and E_a are plotted against each other, represents at the same time the relationship between E_a and the other parameters, i.e. p_3, k, and p_1, whose sensitivity plots are rather similar to Fig. 7(a). No correlation could be found between E_a and the other parameters. Some correlation was visible between the parameters k and p_3 (Fig. 7(b)). Correlation between p_1 and p_3 (Fig. 7(d)) could also be noticed and the same thing can be concluded from Table 2, where the value of the parameter p_3 decreases when the value of p_1 increases.

7. Conclusions

The reduction of ferric iron to ferrous iron with pure zinc sulphide was studied in a stirred batch reactor. The reduction rate increased when the ferric iron concentration and the amount of zinc sulphide in proportion to the amount of ferric iron were increased. The temperature and concentration of sulphuric acid concentration had a great impact on the reaction kinetics; the rate increased when the temperature and acid concentration were increased. Analysis of unreacted and reacted zinc sulphide particles with SEM–EDS and laser diffraction techniques revealed that no product layer was formed during the reaction, instead elemental sulphur was forming separate larger particles. Several competing kinetic models were fitted to the experimental data. The models represented first- and second-order kinetics, surface reaction control, as well as diffusion control through films and product layers. After evaluation of the models, it appears that the reduction rate depends on the amount of the reduction agent in first order. Therefore, a simple model was proposed, according to which the rate is proportional to the zinc sulphide available and the concentration of ferric iron. Moreover, sulphuric acid had a remarkable influence on the reduction rate, which is proportional to the concentration of sulphuric acid in the power of 1.5. In general, the best rate equation (17) and the particle analysis suggest that the reaction takes place in liquid phase via a chemical mechanism between dissolved ZnS and ferric ions and that the reaction goes through a state where sulphuric acid takes part as an intermediate.

Notation

c	concentration
E_a	activation energy
f	rate function
g	integrated rate function
k	rate constant at reference temperature (T_{mean})
k'	rate constant
k''	modified rate constant
m	mass
M	molar mass
p_1, p_2, p_3, p_4, p_5	rate exponents
Q	sum of residual squares
r	rate
R	gas constant
R^2	degree of explanation
t	time
T	temperature
V_L	liquid volume

Greek letters

α	conversion
v	stoichiometric coefficient

Acknowledgements

This work is part of the activities at the Åbo Akademi Process Chemistry Group within the Finnish Centre of Excellence Programme (2000–2005) by the Academy of Finland. The authors are grateful to Mr. Clifford Ekholm (Inorganic chemistry) for the analysis by SEM–EDS, Mr. Krister Steinby (Physical chemistry) for his contribution to the particle size analysis by laser diffraction, Dr. Johan Wärnå (Industrial chemistry) for help in modelling with MODEST software, and Mr. Markus Kass (Analytical chemistry) for help with sequential injection analysis.

References

Babu, M.N., Sahu, K.K., Pandey, B.D., 2002. Zinc recovery from sphalerite concentrate by direct oxidative leaching with ammonium, sodium and potassium persulphates. Hydrometallurgy 64, 119–129.

Cheng, C.Y., Clarkson, C.J., Manlapig, E.V., 1994. The leaching of zinc sulphide concentrate in sulphate–chloride solutions with ferric ions. The AusIMM Proceedings 2, 57–62.

Crundwell, F.K., 1987. Kinetics and mechanism of the oxidative dissolution of a zinc sulphide concentrate in ferric sulphate solutions. Hydrometallurgy 19, 227–242.

Crundwell, F.K., Verbaan, B., 1987. Kinetics and mechanisms of the non-oxidative dissolution of sphalerite (zinc sulphide). Hydrometallurgy 17, 369–384.

Dickinson, C.F., Heal, G.R., 1999. Solid–liquid diffusion controlled rate equations. Thermochimica Acta 340–341, 89–103.

Ekinci, Z., Colak, S., Cakici, A., Sarac, H., 1998. Leaching kinetics of sphalerite with pyrite in chlorine saturated water. Minerals Engineering 11 (3), 279–283.

Haario, H., 2001. MODEST 6.0-User's Guide. Profmath Oy, Helsinki.

Herbst, J.A., 1979. Rate processes in multiparticle metallurgical systems. In: Sohn, H.Y., Wadsworth, M.E. (Eds.), Rate Processes of Extractive Metallurgy. Plenum Press, New York, Chapter 2.

Kammel, R., Pawlek, F., Simon, M., Xi-Ming, L., 1987. Oxidizing leaching of sphalerite under atmospheric pressure. Metall 41, 158–161.

Levenspiel, O., 1972. Chemical Reaction Engineering, 2nd Edition, Wiley, New York.

Lochmann, J., Pedlik, M., 1995. Kinetic anomalies of dissolution of sphalerite in ferric sulfate solution. Hydrometallurgy 37, 89–96.

Markus, H., Fugleberg, S., Valtakari, D., Salmi, T., Murzin, D. Yu., Lahtinen, M., 2004. Reduction of ferric to ferrous with sphalerite concentrate, kinetic modelling. Hydrometallurgy, in press.

Momade, F.W.Y., Momade, Zs.G., 1999. A study of the kinetics of reductive leaching of manganese oxide ore in aqueous methanol–sulphuric acid medium. Hydrometallurgy 54, 25–39.

Órfão, J.J.M., Martins, F.G., 2002. Kinetic analysis of thermogravimetric data obtained under linear temperature programming—a method based on calculations of the temperature integral by interpolation. Thermochimica Acta 390, 195–211.

Palencia Perez, I., Dutrizac, J.E., 1991. The effect of the iron content of sphalerite on its rate of dissolution in ferric sulphate and ferric chloride media. Hydrometallurgy 26, 211–232.

Rath, P.C., Paramguru, R.K., Jena, P.K., 1981. Kinetics of dissolution of zinc sulphide in aqueous ferric chloride solution. Hydrometallurgy 6, 219–225.

Suni, J., Henein, H., Warren, G.W., Reddy, D., 1989. Modelling the leaching kinetics of a sphalerite concentrate size distribution in ferric chloride solution. Hydrometallurgy 22, 25–38.

Verbaan, B., Crundwell, F.K., 1986. An electrochemical model for the leaching of a sphalerite concentrate. Hydrometallurgy 16, 345–359.

ELSEVIER

Available online at www.sciencedirect.com

SCIENCE DIRECT®

Hydrometallurgy 73 (2004) 269–282

hydrometallurgy

www.elsevier.com/locate/hydromet

Reduction of ferric to ferrous with sphalerite concentrate, kinetic modelling

Heidi Markus[a], Sigmund Fugleberg[a], Daniel Valtakari[a], Tapio Salmi[a], Dmitry Yu. Murzin[a,*], Marko Lahtinen[b]

[a] *Laboratory of Industrial Chemistry, Process Chemistry Centre, Åbo Akademi University, Biskopsgatan 8, FIN-20500 Åbo/Turku, Finland*

[b] *Outokumpu Research Oy, P.O. Box 60, FIN-28101 Björneborg/Pori, Finland*

Received 27 October 2003; received in revised form 27 November 2003; accepted 28 November 2003

Abstract

Reduction of dissolved ferric iron (Fe^{3+}) to ferrous iron (Fe^{2+}) with sphalerite (zinc sulphide) concentrate (Red Dog, Alaska) as the reducing agent was studied in an isothermal batch reactor under nitrogen flow. The influence of temperature (75–95 °C), initial concentration of ferric iron (0.1–0.3 mol/L), reducing agent-to-ferric iron molar ratio (0.5:1–2.1:1), as well as sulphuric acid concentration (0.20–1.02 mol/L) on the reduction kinetics was investigated. The sulphuric acid had no influence on the reduction kinetics. Analysis of unreacted and reacted sphalerite particles was performed by SEM-EDS and laser diffraction techniques to study the changes of the solid particles with time and to confirm whether a product layer was present. The result from SEM-EDS gave no evidence of product layer formation. The analysis with laser diffraction technique suggested that sulphur was formed, creating particles distinct from the unreacted material. The reaction kinetics was modelled by comparing the experimental data with several models proposed for solid–liquid reactions, and the parameters were estimated by nonlinear regression analysis. The models represented first- and second-order dependence of the reducing agent, surface reaction on spherical and cylindrical particles, as well as diffusion through a liquid film and a product layer. From the estimation results, it was concluded that a good description is obtained with a simple model, where the reaction rate is proportional to the concentration of reducing agent.

Keywords: Ferric; Ferrous; Sphalerite concentrate; Kinetic modelling

1. Introduction

The direct oxidative leaching of sphalerite concentrates (zinc sulphide concentrates) with ferric iron under atmospheric pressure has been studied in several investigations (Kammel et al., 1987; Crundwell, 1987; Suni et al., 1989; Palencia Perez and Dutrizac, 1991; Cheng et al., 1994; Lochmann and Pedlík, 1995). In the direct leaching of zinc concentrate with ferric iron, the zinc is dissolved, and the ferric iron is simultaneously reduced to ferrous iron in acidic environment by the sulphide sulphur in the concentrate according to the following overall reaction stoichiometry:

$$Fe_2(SO_4)_3(aq) + ZnS(s) \rightarrow 2FeSO_4(aq) + ZnSO_4(aq) + S(s) \quad (1)$$

* Corresponding author. Tel.: +358-2-215-4985; fax: +358-2-215-4479.

E-mail address: dmurzin@abo.fi (D. Yu. Murzin).

0304-386X/$ - see front matter © 2004 Elsevier B.V. All rights reserved.
doi:10.1016/j.hydromet.2003.11.002

In current commercial operations, the produced ferrous iron is reoxidized with oxygen in order to continue the leaching (Svens et al., 2003). However, if the aim is to reduce the ferric iron, the sphalerite concentrate can successfully be used just as a reducing agent and is then leached at the same time. This would be a stage in a new leach process, where jarosite is precipitated without need for neutralisation with calcine, and thus, the problem with losses of zinc is avoided (Fugleberg, 2002). The reduction of ferric to ferrous, and then oxidation and precipitation of ferrous iron as jarosite would solve the problems in the jarosite process; no neutralization is needed, because less acid is produced when jarosite is precipitated from ferrous iron compared with the precipitation from ferric iron, and also other valuable metals can be collected (Ga, Ge, In) since the pH of the solution can be kept at a relatively high level without ferrous iron precipitating as hydroxide. This process would also overcome the problems in the conversion process, where several valuable metals (Au, Ag, Pb) are lost in the precipitation. To accomplish this, the ferric solution first has to go through a reduction step, which at the same time serves as direct leaching of concentrate.

Crundwell (1987) leached sphalerite concentrate (Gamsberg deposit, size range 44–53 μm) in a solution of ferric iron and sulphuric acid. Surface reaction control model was applied to explain the experimental data

$$k't = 1 - (1 - \alpha)^{1/3} \quad (2)$$

but the linear dependence deviated at 30 min of leaching (at about 70% conversion) and became parabolic (k' is the rate constant, t is time, and α is conversion). The deviation was explained by product-layer diffusion, but no analysis of leached particles was performed. The activation energy was estimated to be 46 kJ/mol.

Suni et al. (1989) dissolved sphalerite concentrates in acidic ferric chloride solution. A model was developed, in which the leaching rate was surface limited and the multi-size distribution of the sphalerite particles was taken into consideration by integration over a number of particle size classes instead of using an average rate constant. Two concentrates with different particle size distributions (45–106 and 14.3–250 μm) were used in the experiments. For the first concentrate, the model predicted the leaching rate slightly better than the model using an average rate constant. For the second concentrate, the result deviated remarkably from the surface reaction model (<90% extraction). A nonzero intercept was obtained, when the rate constant vs. the inverse particle radius (linear relationship) was plotted. When the model was changed, taking into consideration the nonzero intercept, a good fit of the experimental results was obtained. The results indicated that the prediction of the leaching was strongly dependent on the form of the rate constant–particle size relationship assumed. The good fit with an average rate constant with the first concentrate was a result of a relatively small particle size range.

Palencia Perez and Dutrizac (1991) leached sphalerite samples (75–104 μm) in both ferric iron sulphate–sulphuric acid and ferric iron chloride–hydrochloric acid solutions. The influence of solid solution iron content on the leaching rate was investigated, and it was demonstrated that the rate increased linearly with increasing iron content. The activation energy decreased as the iron content of the sphalerite increased. In ferric sulphate media, the activation energy was about 70 kJ/mol for sphalerite with an iron content of 0.04 wt.% and approximately 40 kJ/mol for sphalerite with an iron content of 12.5 wt.%. The experimental data were described by the function of surface reaction-controlled leaching (Eq. (2)) at 50–90 °C and for zinc extractions over 85%. The dissolution kinetics was similar in both ferric sulphate and ferric chloride systems.

Cheng et al. (1994) dissolved zinc sulphide concentrate (Mount Isa Mines, Australia) in a solution of ferric sulphate, sulphuric acid, and sodium chloride. The shrinking core model was used to describe the dissolution reaction. The experimental data followed Eq. (2), until the concentrate was leached about 60–70%, after which pore diffusion was stated to control the reaction. To verify this, a comparative experiment was performed, where the leaching residue was washed after a certain time of reaction and then re-leached. It was claimed that the leaching rate was higher for the washed material compared to the other material, suggesting sulphur formation controlling the rate. The activation energy was 49 kJ/mol at 60–90 °C, indicating surface-reaction control. A

straight line with a small intercept (which was assumed to be within the experimental error) was obtained when the apparent rate constant was plotted against the reciprocal of the average particle diameter, and this also indicated that the leaching was controlled by surface reaction. The effect of ferric iron concentration was investigated; the zinc leaching rate increased with increasing concentration, until a ferric iron concentration was 1.00 mol/L, at which the obtained rate was, unexpectedly, even slower than 0.10 mol/L and almost the same as 0.03 mol/L.

Lochmann and Pedlík (1995) leached sphalerite concentrates (Horní Benešov ore deposit, Czech Republic as well as Rosh Pinah and Black Mountain, South Africa) in an acidic ferric sulphate solution. A product layer, which nature was revealed through washing of the passivated concentrate to dissolve anglesite, jarosite or elemental sulphur, limited the extraction. As the washed concentrate was re-leached, an improved extraction was noticed only in the case where elemental sulphur was removed. Thus, it was concluded that a layer of elemental sulphur controlled the dissolution rate.

The dissolution kinetics of a solid compound depends on the processes taking place at the solid–liquid boundary. The processes are complex and involve both chemical reactions and mass transfer. Different steps, such as chemical reaction, charge transfer, and mass transfer, can determine the dissolution rate (Crundwell, 1987; Crundwell and Verbaan, 1987; Momade and Momade, 1999). For solid–fluid reactions the shrinking particle and the shrinking core (product layer) models (Levenspiel, 1972) have been frequently used, and the latter has been suggested by many authors to be valid for sphalerite leaching (Palencia Perez and Dutrizac, 1991; Lochmann and Pedlík, 1995; Cheng et al., 1994; Suni et al., 1989; Ekinci et al., 1998; Babu et al., 2002). On the other hand, the opinion whether the rate is controlled by the chemical reaction or the mass transfer through the product layer differs. However, as kinetic modelling cannot solely provide an indisputable answer on the mechanism; thus, particle characterization methods should also be employed.

In this work, the reduction of ferric iron to ferrous iron with sphalerite concentrate (Red Dog, Alaska) was experimentally investigated. SEM-EDS analysis of dried solid material and analysis by laser diffraction technique of solid material in liquid were utilised to reveal if a product layer was present and to follow the changes in the particles with time. The experimental data was compared with several kinetic models of solid–liquid reactions, which represented first- and second-order dependence of the reducing agent, surface reaction on spherical and cylindrical particles, as well as diffusion through a liquid film and a product layer. Moreover, the results obtained with zinc sulphide concentrate were compared with those obtained with pure zinc sulphide (Markus et al., 2003).

2. Experimental

2.1. Materials

Ferric iron sulphate ($Fe_2(SO_4)_3 \cdot 5H_2O$) of 97% purity was supplied by Aldrich and sulphuric acid (H_2SO_4) of 95–96% purity by J.T. Baker. The reducing agent, the sphalerite concentrate Red Dog, Alaska, contained 54.0 wt.% zinc, 5.1 wt.% iron, 29.2 wt.% sulphur, 3.2 wt.% lead, 0.15 wt.% copper, 0.32 wt.% cadmium, and 1.5 wt.% silicon. Minor amounts of other metals were also present, but less than 0.1 wt.% of each. The reducing agent was defined as the sulphide sulphur, which was available for reduction. The amount of sulphide sulphur was determined by analysis of the leach residue taken from an experiment performed with a substoichiometric amount of reducing agent. The sulphur in pyrite was then excluded, since it was not accessible for reduction. This gave that 26.9 wt.% of the concentrate was available sulphide sulphur. The conditions for the reduction experiments varied from 75–95 °C, 0.1–0.3 mol/L initial concentration of ferric iron, 0.5:1–2.1:1 reducing agent-to-ferric iron molar ratio (where 0.5:1 is substoichiometric ratio and 2.1:1 is superstoichiometric amount of reducing agent) and 0.20–1.02 mol/L (20–100 g/L) sulphuric acid concentration. The amount of concentrate used in the experiments was for 0.1 mol/L ferric iron initial concentration 3.19–12.75 g/L (0.5:1–2.1:1 reducing agent-to-ferric iron molar ratio), for 0.2 mol/L, 6.37–25.48 g/L, and for 0.3 mol/L, 9.55–38.23 g/L.

2.2. Apparatus and procedure

A solution of sulphuric acid, ferric iron sulphate, and deionized water was preheated to the reaction temperature in a 1000-ml stirred glass reactor, where 750 ml of the volume was used for the liquid and solid phases. The reactor was provided with a heating jacket, using silicone oil as the heat-transfer fluid, a pitched-blade turbine, an oil lock, baffles, and a reflux condenser. Sphalerite concentrate, dispersed in water, and some additional water were preheated on hot plates to the reaction temperature. The experiment was initiated by pouring the concentrate and water into the reactor. The reaction was carried out under atmospheric pressure and nitrogen flow (99.999%, AGA) for 4 h (with some exceptions). The temperature and redox potential were continuously stored on a computer during the reaction. The redox potential was measured with a platinum electrode (Metrohm), using an Ag/AgCl reference electrode in a 3 mol/L KCl solution. The stirring rate was 420 rpm, but the reaction was also conducted with other stirring rates to investigate the influence of mass transfer resistance. Samples (5 ml) were withdrawn at discrete time intervals with a syringe. The solid–liquid ratio was kept constant during the reaction by removing equivalent amount of particles and the liquid. The separation of the particles from the liquid was performed with a filter attached to the syringe.

The concentration of ferric iron was determined by sequential injection analysis (SIA) using the reagent Tiron (0.05 mol/L, 1,2-dihydroxy-3,5-benzenedisulfonic acid disodium salt dissolved in 0.05 mol/L sulphuric acid). SIA is a further development of flow-injection analysis (FIA) and is a relatively new and suitable analysing method in process control (Ruzicka and Marshall, 1990; Gübeli et al., 1991). It has robustness, low reagent consumption, and a simplified design, which makes it suitable when analysing solutions on-line in the industrial process. The SIA system is equipped with a single piston pump, single valve, and single channel. The piston pump, the reaction channel (which leads to the detector), the wash solution, the sample, and the reagent are attached to the selector valve. The measurement starts by aspirating a wash solution, which is followed by first sample injection and then reagent injection through backward movement of the piston of the pump. This results in sequential zones of sample and reagent. Then, the direction of the piston is reversed, moving forward through the reaction channel towards the detector. During the transport, the sample and the reagent zones partially mix creating a product. In the new zone, the concentration of the product varies from zero to a maximum value and back to zero. The product is detected; the height, area, and width of the peak are related to the concentration of the detected component. After the detection, the channel is washed, and the detector signal reaches the starting point.

For analysis by SEM-EDS, samples of solid particles were taken with a syringe and injected into a test tube. As the particles had settled, the liquid was removed with a pipette. The particles were washed several times with distilled water, dried in air at room temperature, and homogenized with a spatula before analysis by SEM-EDS. Samples of particles in solution were analysed by laser diffraction technique (Malvern 2600 Particle Sizer), to observe changes of the particle size distribution. The diameter of a particle, obtained by analysis with laser diffraction, can be calculated in two ways: the volume-based method sets the diameter equal to the diameter for a sphere with the same volume as the particle, while the area-based method sets the diameter equal to the diameter of a sphere with the same surface area.

2.3. Modelling procedure

A temperature-dependent factor (originating from the Arrhenius equation), the concentration of sulphuric acid and ferric iron, as well as a factor representing the solid particles, were specified and put into a rate expression used to model the reaction system (batch reactor). Equations for the dissolution of solid particles are summarized in Table 1. The equations and corresponding notations are taken from Dickinson and Heal (1999) and Órfão and Martins (2002).

Functions $g(\alpha)$ and $f(c_S)$ in Table 1 are explained as follows: the reaction rate r of the particles, as a function of the conversion, can be written as

$$r = \frac{d\alpha}{dt} = k' f(\alpha) \tag{3}$$

Table 1
Expressions of $g(\alpha)$ and $f(c_S)$ for the kinetic models used in this work

Notation	$g(\alpha)$	$f(c_S)$	Type of model	p_1	p_4
F1	$-\ln(1-\alpha)$	c_S/c_{0S}	first-order kinetics	1	–
F3/2	$(1-\alpha)^{-1/2}-1$	$(c_S/c_{0S})^{3/2}$	three-halves-order kinetics	3/2	–
F2	$(1-\alpha)^{-1}$	$(c_S/c_{0S})^{2}$	second-order kinetics	2	–
R2	$1-(1-\alpha)^{1/2}$	$(c_S/c_{0S})^{1/2}$	one-half-order kinetics; two-dimensional advance of the reaction interface	1/2	–
R3	$1-(1-\alpha)^{1/3}$	$(c_S/c_{0S})^{2/3}$	two-thirds-order kinetics; three-dimensional advance of the reaction interface	2/3	–
R4	$1-(1-\alpha)^{2/3}$	$(c_S/c_{0S})^{1/3}$	one-thirds-order kinetics; film diffusion	1/3	–
D3	$[1-(1-\alpha)^{1/3}]^2$	$(c_S/c_{0S})^{2/3}/(1-(c_S/c_{0S})^{1/3})$	Jander; three-dimensional	2/3	1/3
D4	$1-2\alpha/3-(1-\alpha)^{2/3}$	$(c_S/c_{0S})^{1/3}/(1-(c_S/c_{0S})^{1/3})$	Crank-Ginstling and Brounshtein, mass transfer across a nonporous product layer	1/3	1/3
D5	$[1/(1-\alpha)^{1/3}-1]^2$	$(c_S/c_{0S})^{5/3}/(1-(c_S/c_{0S})^{1/3})$	Zhuravlev, Lesokhin and Tempelman, diffusion, concentration of penetrating species varies with α	5/3	1/3
D8	$[1-(1-\alpha)^{1/2}]^2$	$(c_S/c_{0S})^{1/2}/(1-(c_S/c_{0S})^{1/2})$	Jander; cylindrical diffusion	1/2	1/2
D10	$1/(1-\alpha)^{1/3}-1$	$(c_S/c_{0S})^{4/3}$	Dickinson and Heal, transfer across the contracting area	4/3	–

or in the integrated form, which is frequently used in the literature,

$$g(\alpha) = \int_0^{\alpha} \frac{d\alpha}{f(\alpha)} = k' \int_0^{t} dt \tag{4}$$

Function $g(\alpha)$ in Table 1 is not used in the estimation in this study, it is only given to facilitate models identification.

Furthermore, since the conversion of the solid component (available sulphur), α, is given by

$$\alpha = \frac{c_{0S} - c_S}{c_{0S}} \tag{5}$$

where c_{0S} and c_S represent the total amount of sulphide sulphur per liquid volume in the beginning of the reaction and after a certain time of reaction. Thus, reaction rate (3) can be expressed as a function of the concentration, $f(c_S)$,

$$r = k'' f(c_S) \tag{6}$$

Function $f(c_S)$ in Table 1 is used in the overall rate expression as the factor representing the solid particles. It is assumed that k', which is dependent on the concentration of the leaching species around the particle (here: Fe^{3+}), is constant. However, in this study, the concentration of the ferric iron varies around the particles, which makes k' an apparent one. At the same time, model D5 in Table 1 takes into account that the concentration around the particle varies with the conversion (Dickinson and Heal, 1999).

The amount of sulphide sulphur in the liquid (concentration), i.e., the total amount sulphur available for reduction per liquid volume, is calculated as

$$c_S = \frac{m_S}{M_S V_L} \tag{7}$$

where m_S is the mass, M_S the molar mass, and V_L the volume of the ferric sulphate–sulphuric acid solution. The change in V_L due to the sampling is not taken into consideration in the modelling, since both particles and liquid are removed in the samples, and therefore, the situation is considered to be similar in the beginning and the end of the reaction.

Two rate expressions were established; the first, Eq. (8), is used when models F1, F3/2, F2, R2−R4, and D10 were fitted to the experimental data, the second, Eq. (9), is used when models D3−D5, and D8, were tried,

$$r = k\exp\left(-\frac{E_a}{R}\left(\frac{1}{T}-\frac{1}{T_{mean}}\right)\right)\left(\frac{c_S}{c_{0S}}\right)^{p_1} c_{H_2SO_4}^{p_2} c_{Fe^{3+}}^{p_3} \quad (8)$$

$$r = k\exp\left(-\frac{E_a}{R}\left(\frac{1}{T}-\frac{1}{T_{mean}}\right)\right)\frac{\left(\frac{c_S}{c_{0S}}\right)^{p_1}}{1-\left(\frac{c_S}{c_{0S}}\right)^{p_4}} \times c_{H_2SO_4}^{p_2} c_{Fe^{3+}}^{p_3} \quad (9)$$

In the rate expressions, E_a is the activation energy, R is the gas constant, T is the temperature, T_{mean} is the mean temperature of the experiments, c_S and c_{0S} are the concentration and initial concentration of sulphur available for reduction, and c_{Fe3+} and H_2SO_4 denote the concentrations of ferric iron and sulphuric acid. Parameters p_2 and p_3 are exponents for the sulphuric acid and ferric iron concentrations. As the rate expression (8) was used, the exponent p_1 was fixed during the screening of different models, and when Eq. (9) was applied, both p_1 and p_4 were fixed a priori. An estimation, where none of the parameters were fixed, was also made for the rate expression (8).

The consumption rates for ferric iron and sulphide sulphur are obtained when relating the stoichiometric coefficients, v_i, to the reaction rates ($v_{Fe3+}=-2$ and $v_S=-1$):

$$\frac{dc_{Fe^{3+}}}{dt} = -2r \quad (10)$$

$$\frac{dc_S}{dt} = -r \quad (11)$$

The estimation was made by nonlinear regression analysis using the simulation and parameter estimation software MODEST (Haario, 2001). The system of ordinary differential equations (Eqs. (10) and (11)) was solved with the backward difference method implemented in the software ODESSA. All sets of experimental data, containing the ferric iron concentration and temperature as a function of time, as well as the concentration of sulphuric acid and initial concentration of available sulphur, were merged together. The sum of residual squares, Q, was minimized with the hybrid simplex–Levenberg–Marquardt method,

$$Q = \| c_{exp} - c_{est} \|^2 = \sum_t \sum_i (c_{exp,it} - c_{est,it})^2 \quad (12)$$

where c_{exp} represents experimental data and c_{est} the estimated values. An indication of the goodness of the model is the degree of explanation, R^2,

$$R^2 = 100\left(1 - \frac{\| c_{exp} - c_{est} \|^2}{\| c_{exp} - \bar{c}_{exp} \|^2}\right) \quad (13)$$

where $\bar{c}_{exp}$ is the mean value of the experimental data.

3. Results and discussion

3.1. Qualitative analysis

The influence of the initial concentration of ferric iron on the reduction kinetics was studied in the range of 0.1–0.3 mol/L. Fig. 1 shows the experimental and estimated values from three experiments with varying initial concentration of ferric iron. The solid lines represent the prediction of model F1, while the dashed lines represent the prediction of model D4. Higher concentration of ferric iron increased the reduction rate; the initial rates, calculated at 10 min of reaction, for 0.3, 0.2, and 0.1 mol/L initial concentration of ferric iron (experiments visualized in Fig. 1) are 0.30 mol/(m^{3}s), 0.20 mol/(m^{3}s) and 0.09 mol/(m^{3}s).

Different reducing agent-to-ferric iron molar ratios in the range of 0.5:1–2.1:1 were used in order to study the influence of the amount of sulphur in the concentrate. The reduction rate increased with increasing amount of sulphur in relation to the amount of ferric iron, as shown in Fig. 2.

The concentration of sulphuric acid was varied in the range of 0.20–1.02 mol/L (20–100 g/L) to investigate whether sulphuric acid had any influence on the reduction kinetics. Fig. 3 illustrates that the concentration of sulphuric acid did not affect the reaction rate. Several authors have proposed that the hydronium ions contribute to the leaching by forming hydrogen sulphide, which is then oxidized by the ferric iron yielding hydronium ions, ferrous iron, and elemental

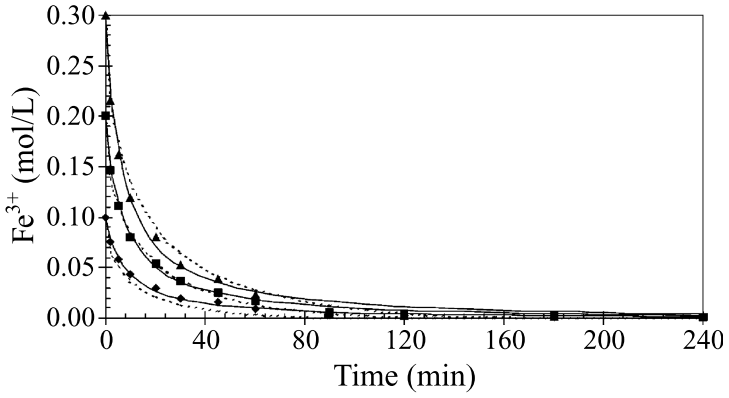

Fig. 1. Influence of initial concentration of ferric iron: ♦=0.1 mol/L, ■=0.2 mol/L, and ▲=0.3 mol/L. Conditions: reducing agent-to-ferric iron molar ratio, 1.1:1; sulphuric acid concentration, 0.41 mol/L; temperature, 95 °C. Solid lines=fit of model F1, dashed lines=fit of model D4.

sulphur (Verbaan and Crundwell, 1986; Kammel et al., 1987). It has been suggested that the amount of hydrogen sulphide dramatically decreases as ferric iron is added (Verbaan and Crundwell, 1986).

The influence of temperature on the reaction kinetics was investigated in the range 75–95 °C, and as shown by Fig. 4, temperature had a profound effect on the reduction rate. The activation energy of the reaction was calculated by parameter estimation according to Eqs. (8) and (9).

3.2. Characterization of solid particles

Analysis of the particle surface was performed by SEM-EDS (Fig. 5). Fig. 5a demonstrates the unleached material, where point analysis by EDS revealed larger amounts of zinc, sulphur, iron, and lead. Minor amounts of other metals were also present. Fig. 5b illustrates the leach residue after 4 h; a great amount (grey, diffuse areas) of sulphur is present, but also smaller (lighter areas) of zinc sulphide and traces of combinations of lead and sulphur (white areas). From this picture, it is difficult to determine if sulphur is forming a layer around the zinc sulphide, but no evidence of product layer formation is given.

Particle size distribution in liquid at different reaction times was determined by laser diffraction technique (Fig. 6). The size distribution of unreacted material, visualized by Fig. 6a, was a multi-size distribution with several maxima. The starting material

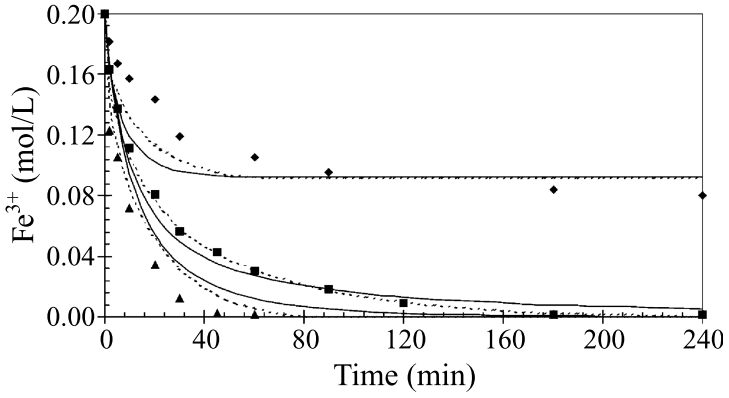

Fig. 2. Influence of reducing agent-to-ferric iron molar ratio: ♦=0.5:1, ■=1.1:1, and ▲=1.6:1. Conditions: initial concentration of ferric iron, 0.2 mol/L; sulphuric acid concentration, 1.02 mol/L; temperature, 85 °C. Solid lines=fit of model F1; dashed lines=fit of model D4.

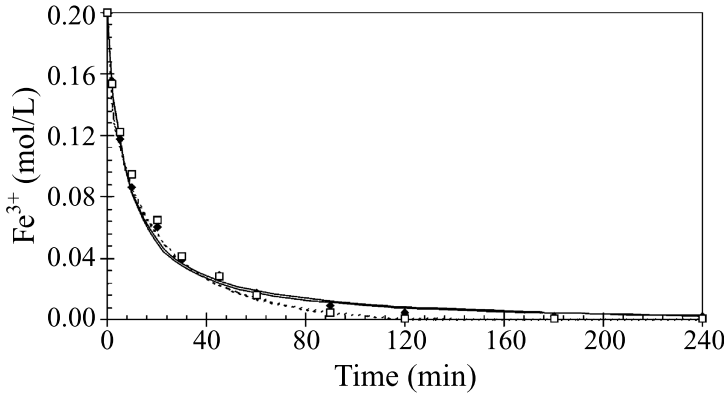

Fig. 3. Influence of sulphuric acid concentration: ♦=0.20 mol/L and □=1.02 mol/L. Conditions: reducing agent-to-ferric iron molar ratio, 1.1:1; initial concentration of ferric iron, 0.2 mol/L; temperature, 95 °C. Solid lines=fit of model F1; dashed lines=fit of model D4.

had a mean diameter of 22.89 μm, obtained with the volume-based method (6.21 μm with the area-based method); 90% of the particles were smaller than 40.32 μm, 50% smaller than 11.71 μm, and 10% smaller than 3.22 μm. After 7 min of reaction, when 60% of the ferric iron was left, the size distribution had not changed much, as illustrated by Fig. 6b. The mean diameter was 22.41 μm with the volume-based method (6.92 μm [area-based method]), 90% of the particles were smaller than 60.18 μm, 50% smaller than 13.11 μm, and 10% smaller than 3.24 μm. In Fig. 6c, some changes in the size distribution can be observed, after 35 min, when 25% of the ferric iron was still present. The mean diameter was 15.44 μm with the volume-based method (7.10 μm [area-based method]), 90% of the particles were smaller than 31.20 μm, 50% smaller than 11.43 μm, and 10% smaller than 3.27 μm. The size distribution of the leach residue (Fig. 6d), when 1% of the ferric iron was left, was different from those in Fig. 6a–c. One larger peak, with two smaller maxima, can be observed in Fig. 6d, and the mean diameter was 16.77 μm with the volume-based method (10.36 μm [area-based method]), 90% of the particles were smaller than 34.05 μm, 50% smaller than 13.74 μm, and 10% smaller than 5.14 μm.

In our previous study (Markus et al., 2003), pure zinc sulphide was used as the reducing agent, and it was concluded from the analysis with SEM-EDS that sulphur formed larger particles than zinc sulphide. When the analysis by laser diffraction technique was

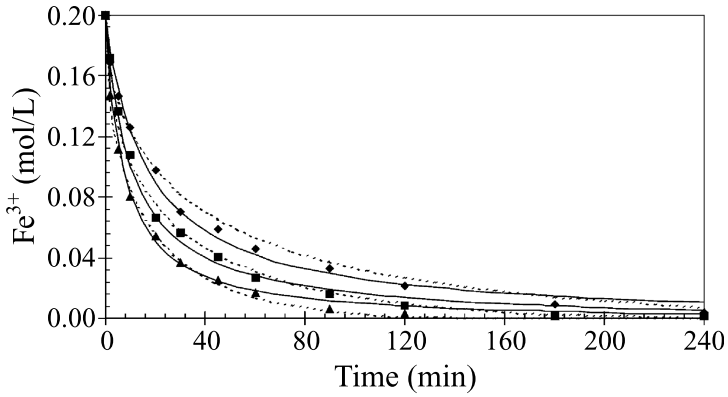

Fig. 4. Influence of temperature: ♦=75 °C, ■=85 °C, and ▲=95 °C. Conditions: reducing agent-to-ferric iron molar ratio, 1.1:1; initial concentration of ferric iron, 0.2 mol/L; sulphuric acid concentration, 0.41 mol/L. Solid lines=fit of model F1; dashed lines=fit of model D4.

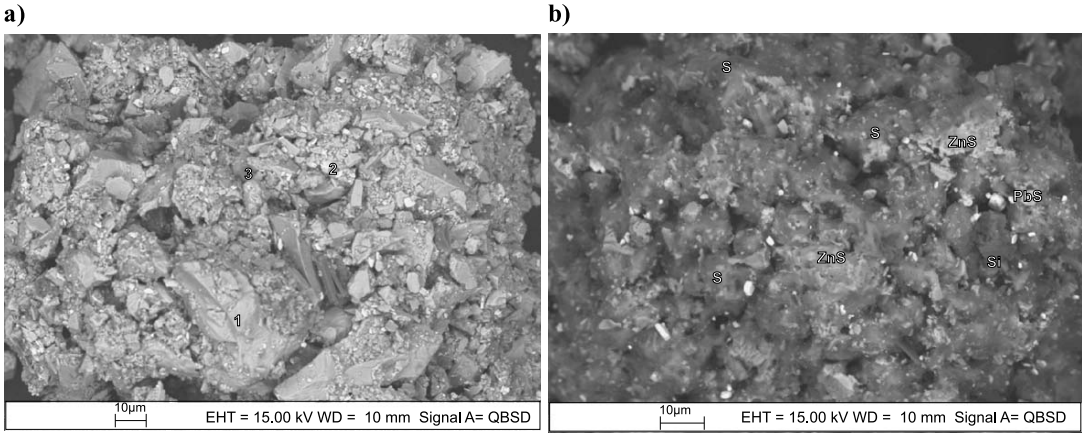

Fig. 5. SEM-EDS microgram of sphalerite concentrate. (a) unleached material, point analysis by EDS: (1) 50.83 at.% sulphur, 47.09 at.% zinc, and 2.08 at.% iron, (2) lead and sulphur, and (3) 57.21 at.% sulphur, 12.75 at.% zinc, and 30.04 at.% iron. (b) leach residue in 4 h, points of zinc sulphide, sulphur, lead and sulphur, as well as silicon are marked in the picture. Conditions: reducing agent-to-ferric iron molar ratio, 1.1:1; initial concentration of ferric iron, 0.2 mol/L; sulphuric acid concentration, 0.41 mol/L; temperature, 95 °C.

performed, it was observed that the particles had a unimodal size distribution in the beginning of the reaction. After some minutes of reaction, this distribution became bimodal, with one peak of sulphur and one of unreacted zinc sulphide. This clearly showed that sulphur formed separate particles. If a product layer would exist, the response from the analysis by laser diffraction would probably be that the size pattern is unchanged and slowly moved to the right, that means towards larger particle sizes. This is not the case in Fig. 6. A peak of small particles is visible in Fig. 6a–c, but not in Fig. 6d, when almost everything has reacted. The distribution moves towards one maximum, where the highest point is at 20.2 μm. When pure zinc sulphide was used, the maximum of the sulphur peak was at 32.0 μm. This could indicate that sulphur is forming separate, larger particles also in the case when sphalerite concentrate is used, but to confirm this, sphalerite particles with a unimodal size distribution should be investigated.

When analysing solid materials, the laser diffraction technique gives a more real picture since the particles are dispersed in the liquid, as in the reaction. Dry samples of solid materials do not give a picture of the actual situation in liquid, for example, sulphur sticks to the surface of the metal sulphide when the aqueous solution is removed, but on the other hand, one can see the structure and the composition of the material.

3.3. Kinetic modelling: parameter estimation

Reduction of ferric iron and at the same time dissolution of zinc sulphide concentrate can take place through two probable reaction paths. The first path involves the acid, or hydronium ions,

$$ZnS(s) + H_2SO_4 \rightarrow ZnSO_4 + H_2S(aq) \quad (14)$$

$$Fe_2(SO_4)_3 + H_2S(aq) \rightarrow 2FeSO_4 + H_2SO_4 + S(s) \quad (15)$$

The second path is a direct reaction between ferric iron and zinc sulphide concentrate, as in Eq. (1), which also is the net result from reactions (14) and (15). Since the sulphuric acid had practically no effect on the reaction rate, the first reaction pathway would not be the choice.

Lotens and Wesker (1987) have presented reaction paths of leaching: in acidic dissolution, hydronium ions oxidize the metal sulphide, forming metal ions and hydrogen sulphide (Eqs. (14) and (15)). In oxidative dissolution, an oxidizer oxidizes the metal sulphide, forming metal ions and oxidation products.

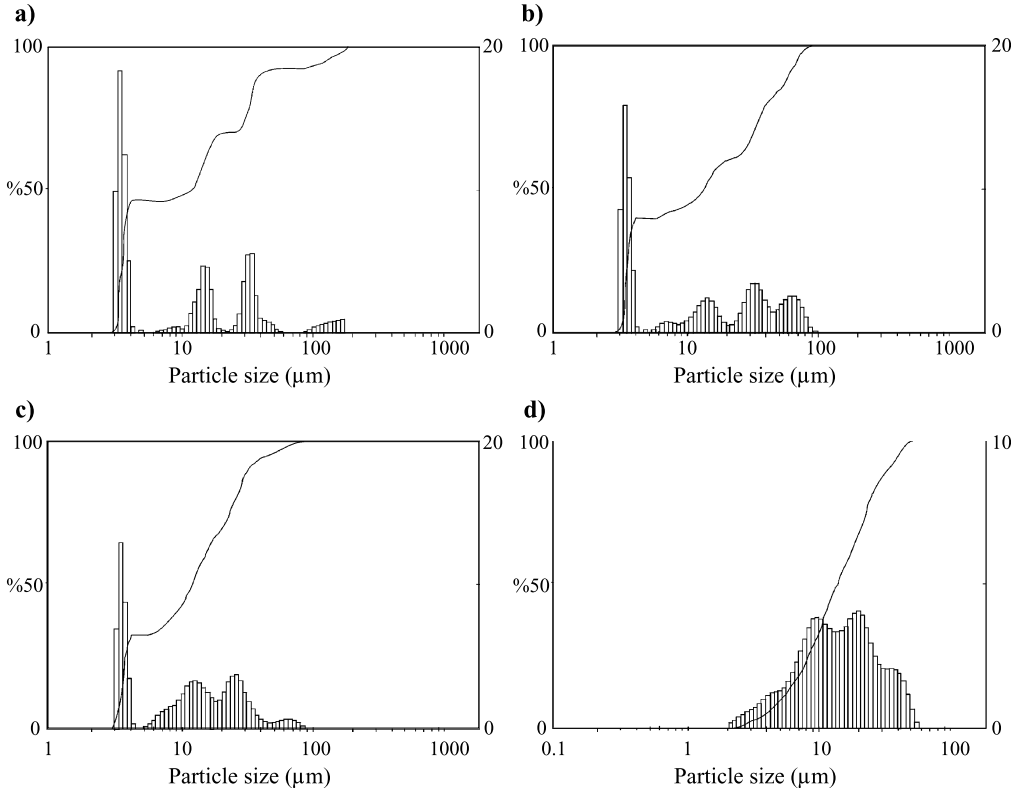

Fig. 6. Particle size distribution determined by laser diffraction technique. (a) Unreacted sphalerite concentrate dispersed in water (100 mm objective), (b) leached in 7 min (100 mm objective), (c) leached in 35 min (100 mm objective), and (d) leach residue in 4 h (63-mm objective). Conditions: reducing agent-to-ferric iron molar ratio, 1.1:1; initial concentration of ferric iron, 0.2 mol/L; sulphuric acid concentration, 0.41 mol/L; temperature, 85 °C.

When a certain material-specific pH value is exceeded, the first reaction (acidic dissolution) does not proceed to a significant extent. Lotens and Wesker (1987) state that for sphalerite, this pH is approximately zero. In the reaction path proposed for oxidative dissolution, the sulphur in the metal sulphide is not only oxidized to elemental sulphur by the oxidizer, but further to S(I) and possibly S(II), depending on the type of oxidizer. This would mean that even more than two ferric ions could be reduced by one metal sulphide.

When pure zinc sulphide (Markus et al., 2003) was used, the sulphuric acid had a profound influence, and therefore, the first reaction path is very probable. With pure zinc sulphide, the process could be more complex with both pathways occurring simultaneously but at different rates. It was concluded based on kinetic modelling that the second pathway with direct reaction was of minor importance. In the present study, the first step in the modelling was to try different models, proposed for solid–liquid reactions in Table 1, through fitting to the experimental data according to the procedure discussed in Section 2.3. From the modelling results summarized in Table 2, it can be concluded that models F1, F3/2, F2, D3–D4, D8, and D10 all give a degree of explanation, R^2, above 95%. The lower values of R^2 obtained with sphalerite concentrate compared to pure zinc sulphide (Markus et al., 2003) are probably a result of the multi-size distribution of sphalerite particles, compared to the unimodal distribution of pure zinc sulphide. The result from the estimation, where none of the parameters were fixed,

Table 2
Results from the modelling

Model	p_1 (fixed)	p_4 (fixed)	k	E_a (kJ/mol)	p_2 (H_2SO_4)	p_3 (Fe^{3+})	Residual SS Q	Explained R^2 (%)
F1	1	–	0.07 ± 0.01 $L^{0.15}/(mol^{0.15}min)$	47.4 ± 4.4	0.04 ± 0.05	1.11 ± 0.09	0.0312	95.06
F3/2	3/2	–	0.05 ± 0.01 $mol^{0.16}/(L^{0.16}min)$	54.3 ± 4.1	0.05 ± 0.05	0.79 ± 0.08	0.0262	95.85
F2	2	–	0.03 ± 0.00 $mol^{0.47}/(L^{0.47}min)$	61.7 ± 4.2	0.06 ± 0.05	0.47 ± 0.08	0.0259	95.91
R2	1/2	–	0.11 ± 0.02 $L^{0.47}/(mol^{0.47}min)$	40.7 ± 5.0	0.03 ± 0.06	1.44 ± 0.10	0.0408	93.54
R3	2/3	–	0.10 ± 0.01 $L^{0.36}/(mol^{0.36}min)$	42.8 ± 4.6	0.03 ± 0.06	1.33 ± 0.06	0.0371	94.13
R4	1/3	–	0.13 ± 0.02 $L^{0.58}/(mol^{0.58}min)$	38.8 ± 4.9	0.03 ± 0.06	1.55 ± 0.07	0.0449	92.89
D3	2/3	1/3	0.002 ± 0.02 $mol^{0.61}/(L^{0.61}min)$	64.3 ± 3.5	0.01 ± 0.04	0.38 ± 0.06	0.0179	97.16
D4	1/3	1/3	0.002 ± 0.01 $mol^{0.41}/(L^{0.41}min)$	59.4 ± 3.3	0.01 ± 0.04	0.58 ± 0.06	0.0169	97.33
D5	5/3	1/3	0.001 ± 0.02 $mol^{0.99}/(L^{0.99}min)$	78.7 ± 5.5	0.01 ± 0.07	0.00 ± 0.10	0.0343	94.57
D8	1/2	1/2	0.003 ± 0.01 $mol^{0.47}/(L^{0.47}min)$	60.9 ± 3.3	0.01 ± 0.04	0.52 ± 0.06	0.0169	97.32
D10	4/3	–	0.05 ± 0.01 $mol^{0.06}/(L^{0.06}min)$	52.0 ± 4.2	0.05 ± 0.05	0.89 ± 0.08	0.0274	95.67

is not included in Table 2. In this estimation, R^2 was 95.97, k was 0.04 $mol^{0.34}/(L^{0.34}min)$, E_a was 58.5 kJ/mol, and p_1, p_2, and p_3 were 1.79, 0.06, and 0.60, respectively. Models F3/2, F2, and D10 are rather simple ones, where the reaction rate is proportional to the amount of reducing agent in the power of 3/2, 2, and 4/3. Model D10 represents the case when mass transfer across the contracting area of a sphere is the rate-controlling step (Dickinson and Heal, 1999). Model F1, where the reaction rate is proportional to the reducing agent, is the simplest model of all tested. This model was chosen for the reduction of ferric iron with pure zinc sulphide (Markus et al., 2003). Model F1 gave a slightly lower value of R^2 in the reduction with concentrate compared to zinc sulphide, but it could still be used for practical purposes.However, one should not rely completely on the degree of explanation when choosing a model; therefore, the estimated values of both model F1 (solid lines), the simplest model and the model chosen for pure zinc sulphide (Markus et al., 2003), as well as the values predicted by model D4 (dashed lines), with the highest R^2, are plotted in Figs. 1–4 as a comparison to the experimental data. Model D4, originally proposed by Crank-Ginstling and Brounshtein, has frequently been used in modelling of leaching (Rath et al., 1981; Lochmann and Pedlík, 1995; Babu et al., 2002). When the modelled values are compared to the experimental data at different initial concentrations of ferric iron (Fig. 1), the estimated values of model F1 comes closer to the experimental data than those of model D4. However, when the influence of the stoichiometric ratio is investigated (Fig. 2), the effect is reverse. Concentration of sulphuric acid has no influence on the reduction kinetics (Fig. 3), and both models fit the experimental data well. The models follow each other to approximately 85% conversion, but in the end, they somewhat differ; model F1 comes closer to the experimental values obtained with 0.20 mol/L sulphuric acid, and model D4 closer to 1.02 mol/L sulphuric acid. When different temperatures are used (Fig. 4), both models come quite close to the experimental data, but not at the same time. Model F1 fits the data well at the lowest temperature, 75 °C, and also to about 90% conversion at 85 and 95 °C. Model D4 follows closer the experimental data obtained at 85 and 95 °C.The lowest degree of explanation was obtained with the model R4, where film diffusion is the rate-determining step. Also, model D5, which is the only model that takes into account that the concentration around the particle varies with the conversion (Dickinson and Heal, 1999), had a rather low explanation degree. Model R3, representing the surface-reaction control for both shrinking particle and product layer models, gave lower R^2-value than expected. According to this model, particles of all sizes would continue to react following the equation R3, but the overall reaction rate would be a compound rate, which is determined by the size distribution (Herbst, 1979). This means that when using an average k-value for particles of all sizes, and not a separate k-value for each size, a broad particle size distribution will not obey this equation at higher conversions, since the smaller particles will be totally leached before the rest is leached. If the experimental data are plotted in the integrated form of model R3 (see Eq. (2)), this should create a straight line if the model is obeyed. This is often the case in the

beginning of the reaction, since particles of all sizes are present, but the parabolic relationship, which is often obtained at higher conversions, is due to the fact that some of the particles have been totally leached, while others are still to be leached. Several authors have explained the parabolic relationship to be a result of a product layer formed, but the reason could in fact be the size distribution, as in the present case, where the particle size distribution is broad.

The estimated parameter p_3, the exponent of the ferric iron concentration, evidently follows the exponents of the reducing agent (Table 2). When a higher value is fixed for p_1, parameters p_3 gets a lower value, which is logical. When p_1 is fixed to one (model F1), the parameter p_3 obtains a value close to one, 1.1. When pure zinc sulphide was used, p_3 got the value one, in the estimation of model F1 (Markus et al., 2003). Model D5 gave zero-order dependence with respect to the ferric iron concentration, which is logical since this model takes into account the concentration of ferric iron in the factor representing the reducing agent. The calculated value of activation energy, E_a, varied between 38.8 and 78.7 kJ/mol, depending on the model used. This is quite a high value and indicates against the presence of diffusion limitation. Palencia Perez and Dutrizac (1991) estimated the activation energy to be 70 kJ/mol for sphalerite with an iron content of 0.04 wt.% and

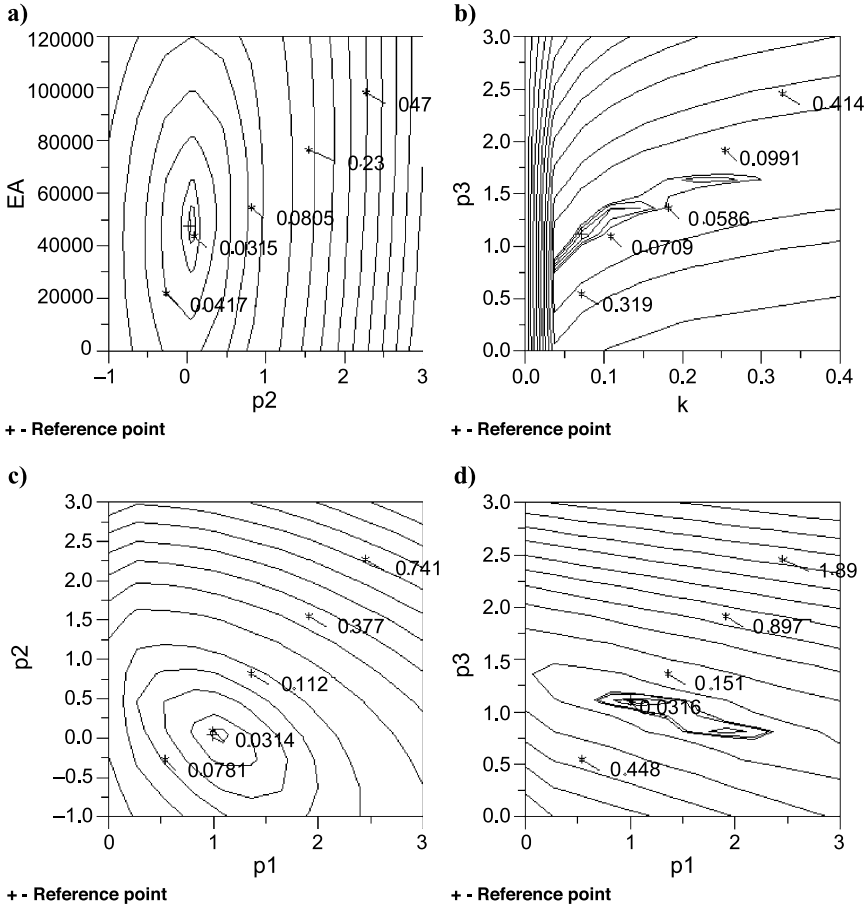

Fig. 7. Contour plots with the residual sum of squares for (a) parameters p_2 and E_a, (b) parameters k and p_3, (c) parameters p_1 and p_2, and (d) parameters p_1 and p_3.

approximately 40 kJ/mol for sphalerite with an iron content of 12.5 wt.%. In the estimation, they used the surface reaction control (integrated form of model R3 or Eq. (2)) at 50–90 °C. Approximately 50 kJ/mol activation energy was obtained for 6.0 wt.% iron content, which is comparable with the activation energy in the present study with the model R3, 42.8 kJ/mol, and 5.1 wt.% iron content. Moreover, Cheng et al. (1994) calculated the activation energy 49 kJ/mol at 60–90 °C with a zinc sulphide concentrate with an iron content above 8 wt.%, which is also in accordance with the present data.

A more general model, where one term represents the reaction path where sulphuric acid participates (Eqs. (14) and (15)) and another term the direct reaction between ferric iron and zinc sulphide (Eq. (1)), leads to the following expression

$$r = k_1 \exp\left(-\frac{E_{a1}}{R}\left(\frac{1}{T}-\frac{1}{T_{mean}}\right)\right)\left(\frac{c_S}{c_{0S}}\right)^{p_1} c_{H_2SO_4}^{p_2} c_{Fe^{3+}}^{p_3} + k_2 \exp\left(-\frac{E_{a2}}{R}\left(\frac{1}{T}-\frac{1}{T_{mean}}\right)\right)\left(\frac{c_S}{c_{0S}}\right)^{p_4} c_{Fe^{3+}}^{p_5} \quad (16)$$

which was previously applied for the reaction between pure zinc sulphide and ferric iron (Markus et al., 2003). The fitting of Eq. (16) to the experimental data from the reduction of ferric iron with concentrate should give similar or only slightly better description, since it has already been stated that the sulphuric acid did not affect the reaction rate.

A very simple model, F1, can be chosen for practical purposes to describe the reduction kinetics. The reduction rate is proportional to the amount of reducing agent,

$$r = k \exp\left(-\frac{E_a}{R}\left(\frac{1}{T}-\frac{1}{T_{mean}}\right)\right)\left(\frac{c_S}{c_{0S}}\right) c_{Fe^{3+}}^{1.1} \quad (17)$$

where k is 0.07 $L^{0.1}/(mol^{0.1}min)$, E_a is 47.4 kJ/mol, and T_{mean} is 362.15 K (89 °C). The sensitivity analysis of the model parameters (F1) in the form of contour plots is presented in Fig. 7. The figure reveals that model F1 is well defined, and that the correlation between the parameters is relatively low. The parameters p_2 and E_a are plotted against each other in Fig. 7a, and no correlation could be found between these two or in any other combination of parameters with E_a. Some correlation was visible between the parameters k and p_3 (Fig. 7b) and also between p_1 and p_3 (Fig. 7d).

4. Conclusion

The reduction of ferric iron to ferrous iron with sphalerite concentrate as the reducing agent was studied in an isothermal, stirred batch reactor. The reaction rate increased when the ferric iron concentration and the amount of reducing agent in proportion to the amount of ferric iron were increased. The concentration of sulphuric acid had no influence on the reduction rate. The temperature had a great impact on the reduction kinetics; the activation energy was calculated to 47.4 kJ/mol at 75–95 °C. The analysis of the leach residue by SEM-EDS did not give any evidence of product layer formation. Investigation of the particle size distribution at different times of reaction suggested that no product layer was formed. Several rival kinetic models, representing first- and second-order kinetics, surface reaction control on a cylindrical and a spherical particle, as well as diffusion control through a film and a product layer, were fitted to the experimental data. For practical purposes, a model where the reaction rate depends on the amount of the reducing agent in first order can be chosen to describe the system adequately.

List of symbols

c	concentration
E_a	activation energy
F	rate function
G	integrated rate function
k	rate constant at reference temperature (T_{mean})
k'	rate constant (in Eqs. (2)–(4))
k''	modified rate constant (in Eq. (6))
M	molar mass
m	mass
p_1, p_2, p_3, p_4, p_5	rate exponents (in (Eqs. (8), (9) and (16))
Q	sum of residual squares
R	gas constant
R^2	degree of explanation
r	rate
T	temperature

t time
V_L liquid volume

Greek letters
α conversion
ν stoichiometric coefficient

Acknowledgements

This work is part of the activities at the Åbo Akademi Process Chemistry Centre within the Finnish Centre of Excellence Programme (2000–2005) by the Academy of Finland. The authors are grateful to Clifford Ekholm for the analysis by SEM-EDS, Krister Steinby for his contribution to the particle size analysis by laser diffraction, Dr. Johan Wärnå for assistance in modelling with MODEST software, and Markus Kass for help with sequential injection analysis.

References

Babu, M.N., Sahu, K.K., Pandey, B.D., 2002. Zinc recovery from sphalerite concentrate by direct oxidative leaching with ammonium, sodium and potassium persulphates. Hydrometallurgy 64, 119–129.

Cheng, C.Y., Clarkson, C.J., Manlapig, E.V., 1994. The leaching of zinc sulphide concentrate in sulphate–chloride solutions with ferric ions. The AusIMM Proceedings 2, 57–62.

Crundwell, F.K., 1987. Kinetics and mechanism of the oxidative dissolution of a zinc sulphide concentrate in ferric sulphate solutions. Hydrometallurgy 19, 227–242.

Crundwell, F.K., Verbaan, B., 1987. Kinetics and mechanisms of the non-oxidative dissolution of sphalerite (zinc sulphide). Hydrometallurgy 17, 369–384.

Dickinson, C.F., Heal, G.R., 1999. Solid–liquid diffusion controlled rate equations. Thermochimica Acta 340–341, 89–103.

Ekinci, Z., Colak, S., Cakici, A., Sarac, H., 1998. Leaching kinetics of sphalerite with pyrite in chlorine saturated water. Minerals Engineering 11, 279–283.

Fugleberg, S., 2002. Method for the hydrolytic precipitation of iron. Patent No. WO0246481.

Gübeli, T., Christian, G.D., Ruzicka, J., 1991. Fundamentals of sinusoidal flow sequential injection spectrophotometry. Analytical Chemistry 63, 2407–2413.

Haario, H., 2001. MODEST 6.0—User's Guide Profmath Oy, Helsinki.

Herbst, J.A., 1979. Rate processes in multiparticle metallurgical systems. In: Sohn, H.Y., Wadsworth, M.E. (Eds.), Rate Processes of Extractive Metallurgy. Plenum, New York. pp. 53–112.

Kammel, R., Pawlek, F., Simon, M., Xi-Ming, L., 1987. Oxidizing leaching of sphalerite under atmospheric pressure. Metallurgy 41, 158–161.

Levenspiel, O., 1972. Chemical Reaction Engineering, 2nd ed. Wiley, New York. Chap. 12.

Lochmann, J., Pedlík, M., 1995. Kinetic anomalies of dissolution of sphalerite in ferric sulfate solution. Hydrometallurgy 37, 89–96.

Lotens, J.P., Wesker, E., 1987. The behaviour of sulphur in the oxidative leaching of sulphidic minerals. Hydrometallurgy 18, 39–54.

Markus, H., Fugleberg, S., Valtakari, D., Salmi, T., Murzin, D.Yu., Lahtinen, M., 2003. Kinetic modelling of a solid–liquid reaction: reduction of ferric iron to ferrous iron with zinc sulphide. Chemical Engineering Science (accepted).

Momade, F.W.Y., Momade, Zs.G., 1999. A study of the kinetics of reductive leaching of manganese oxide ore in aqueous methanol–sulphuric acid medium. Hydrometallurgy 54, 25–39.

Órfão, J.J.M., Martins, F.G., 2002. Kinetic analysis of thermogravimetric data obtained under linear temperature programming—a method based on calculations of the temperature integral by interpolation. Thermochimica Acta 390, 195–211.

Palencia Perez, I., Dutrizac, J.E., 1991. The effect of the iron content of sphalerite on its rate of dissolution in ferric sulphate and ferric chloride media. Hydrometallurgy 26, 211–232.

Rath, P.C., Paramguru, R.K., Jena, P.K., 1981. Kinetics of dissolution of zinc sulphide in aqueous ferric chloride solution. Hydrometallurgy 6, 219–225.

Ruzicka, J., Marshall, G.D., 1990. Sequential injection: a new concept for chemical sensors, process analysis and laboratory assays. Analytica Chimica Acta 237, 329–343.

Suni, J., Henein, H., Warren, G.W., Reddy, D., 1989. Modelling the leaching kinetics of a sphalerite concentrate size distribution in ferric chloride solution. Hydrometallurgy 22, 25–38.

Svens, K., Kerstiens, B., Runkel, M., 2003. Recent experiences with modern zinc processing technology. Erzmetall 56, 94–103.

Verbaan, B., Crundwell, F.K., 1986. An electrochemical model for the leaching of a sphalerite concentrate. Hydrometallurgy 16, 345–359.

III

III. Precipitating indium and gallium with or as basic sulphates of aluminium, gallium and indium

III.1.Background

The precipitation and separation of In and Ga from zinc production process liquors using basic sulphates is a selective recovery method that minimally alters the conditions in the main process. Although the zinc production process liquors are here used as a reference, the idea of the method may be applied also to other similar solutions.

In the current study the precipitation of basic sulphates in a zinc production process conditions were studied, pH below 3.7 and temperature between 85°–90°C. The aim was to recover In and Ga from the process solutions either by directly precipitating them as basic sulphates or by co-precipitation with the basic aluminium sulphate *alunite*. The precipitation and separation of In and Ga had to be carried out considering the main process. This implied that the original process should be altered as little as possible in terms of pH and temperatures. None of the changes in the process should affect the Zn recovery efficiency. Further, any changes to the recovery processes should be financed with profits later generated by using an improved process. Fe contained in native zinc recovery solutions is an obstacle because the chemistry of Fe, In and Ga is so alike.

The presented study has a focus on In and Ga basic sulphates and precipitation, both in native process liquors and synthetic water-based solutions. The effects of interfering metal ions in the process solution have been studied as well as simultaneous In and Ga basic sulphates formation. Optimal precipitation conditions were investigated, too.

III.2. Basic sulphates

Basic sulphates are crystalline and rather beautiful with their symmetrical forms. They are based on, for example, Al, In, Ga or Fe and formed in H_2SO_4-solutions. The formation is faster at elevated temperatures. Chemically the basic sulphates may be described as:

$MX_3(SO_4)_2(OH)_{6(s)}$,

Where X = Al^{3+}, Ga^{3+}, In^{3+}, M = K^+, Na^+, NH_4^+, H_3O^+, s=solid.

The basic sulphates are formed according to the formula:

$$3X_2(SO_4)_{3(aq)} + M_2SO_{4(aq)} + 12H_2O \rightarrow 2MAl_3(SO_4)_2(OH)_{6(s)} + 6H_2SO_{4(l)} \qquad \text{Equation 1}$$

Where X = Al^{3+}, Ga^{3+}, In^{3+}, M = K^+, Na^+, NH_4^+, H_3O^+.

The basic sulphates relevant for the work are given in Table 1.

Table 1.Basic sulphates of Al, Ga, In and Fe.

Basic sulphate	Formula
Alunite	$MAl_3(SO_4)_2(OH)_6$
Galliunite	$MGa_3(SO_4)_2(OH)_6$
Indiunite	$MIn_3(SO_4)_2(OH)_6$
Jarosite	$MFe_3(SO_4)_2(OH)_6$

The jarosites are soluble in sulphuric acid or in liquors with high sulphuric acid content but they are not soluble in water. The solubility is also strongly affected by pH and temperature and increases with increasing temperature and lower pH.

The basic sulphates have a nice regular crystalline structure as displayed in Figure 3, and the X-atoms vary from species to species. In some cases, for example Al and Ga, the atoms are to some extent interchangeable, depending on the size of the ions, Figure 1. This behaviour can be used in co-precipitation of similar elements.

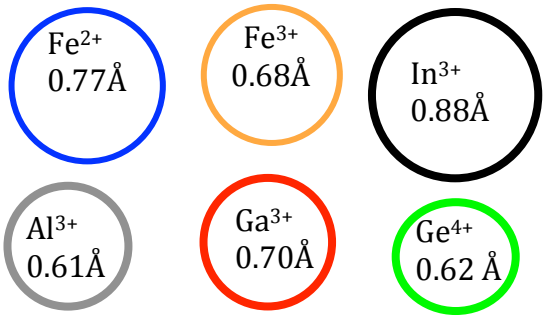

Figure 1. Ion radius for In, Ga, Ge, Al and Fe ions (1 Å = 10^{-10} m), (Lang, 2014).

Ga and Al both have an ion radius of about 0.6-0.7 Å. Based on this it may be assumed that Ga^{3+} can substitute Al^{3+} in the alunite crystal, leading to a co-precipitation of Ga. Interchangebility (substitution) may occur also between alunite and jarosite where Al^{3+} may be exchanged for Fe^{3+}.

According to the study at the given process environment a temperature above 70°C is required for basic sulphates to be formed. For precipitation and co-precipitation of In and Ga a suitable pH is required and it is around 1.5–3.7 depending of the kind of basic sulphate in question. Co-precipitation of In and Ga with alunite is most successful at pH 1.5–2.5 and precipitation of In and Ga as basic sulphates is most successful at pH between 2.7–3.6. The obtained precipitates are washable and do not dissolve in water.

The experiments showed that Ga precipitate is not only formed faster than In but it also sediments more rapidly. In both cases the samples were treated in the same way and the centrifuge was used at the same rpm. A clear explanation for this was not

found. A plausible explanation may be the different particle size of the precipitate where the In precipitate may have a smaller particle size and thus be forming a colloidal solution.

The study did not give a clear answer on whether to precipitate In and Ga directly as a basic sulphate or to co-precipitate with a basic sulphate that may have been prepared in advance or in situ (compare to Willard, 1937).

XRD results obtained from Outokumpu/Pori showed that Ga precipitates as basic Ga-sulphates while In precipitates could not be identified but they seem to be a mixture of different In compounds.

III.2.1. Alunite – a basic aluminium sulphate

Alunite is a crystal, Figures 2. and 3., consisting of oxygen (54.08 %), sulphur (15.48 %), hydrogen (1.46 %) and aluminium (19.54 %) and has a molecular weight of 414.2 g.

Figure 2. An image of an alunite crystal, (http://www.a-m.de/englisch/-lexikon/-mineral/sulfate/alunit.htm, © 2000 Büro für angewandte Mineralogie · Dr. Stephan Rudolph · D-47918 Tönisvorst).

The chemical formula for the basic aluminium sulphate alunite is $MAl_3(SO_4)_2(OH)_6$, and is formed according to

$$3Al_2(SO_4)_{3(aq)} + M_2SO_{4(aq)} + 12H_2O \rightarrow 2MAl_3(SO_4)_2(OH)_{6(s)} + 6H_2SO_{4(l)}$$

Equation 2

$M = K^+, Na^+, NH_4^+, H_3O^+$.

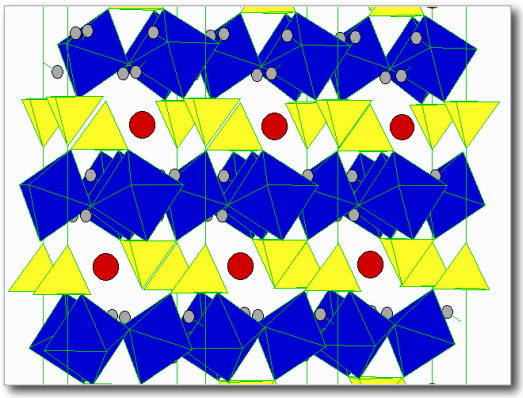

Figure 3. Image of the crystal structure of alunite $(K, Na, NH_4)Al_3(SO_4)_2(OH)_6$. Notation Al in octahedral coordination (blue) and sulphur in tetrahedral coordination (yellow) and potassium in irregular 12-fold coordination (red), (http://www.a-m.de/englisch/-lexikon/mineral/sulfate/alunit.htm , © 2000 Büro für angewandte Mineralogie · Dr. Stephan Rudolph · D-47918 Tönisvorst).

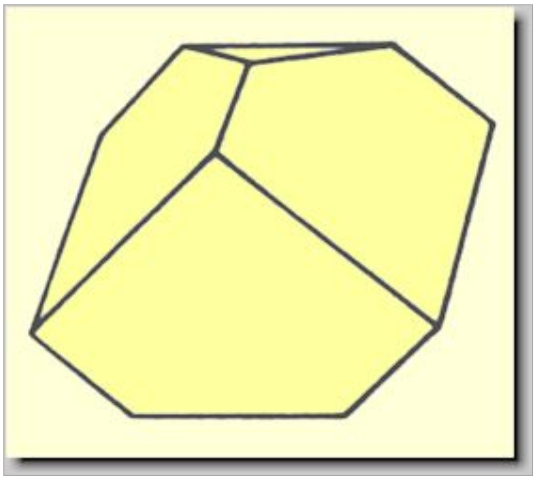

Figure 4. Crystal habit (trigonal) of Alunite, (http://www.a-m.de/englisch/lexikon/mineral/sulfate/alunit-kris1.htm, © 2000 Büro für angewandte Mineralogie · Dr. Stephan Rudolph · D-47918 Tönisvorst).

Table 2. Alunite properties, (http://www.a-m.de/englisch/lexikon/mineral/-sulfate/alunit.htm, © 2000 Büro für angewandte Mineralogie · Dr. Stephan Rudolph · D-47918 Tönisvorst.).

Alunite	
Chemistry	$KAl_3[(OH)_6\|(SO_4)_2]$
Hardness	3.5 – 4
Lustre	vitreous, pearly
Colour	white, grey, yellowish grey, reddish grey or yellowish white
Density [g/cm^3]	2.6 – 2.9
Crystal	habit trigonal, Figure 4
Cleavage, fracture	[0001] good
Other characteristics and occurrences	Rock-forming mineral, formed by alteration of feldspar-rich rocks
Molecular weight [g/mol]	414.21
Oxygen	54.08 %
Sulphur	15.48 %
Hydrogen	1.46 %
Aluminium	19.54 %

In the study alunite is added to the liquor or produced in situ for the purpose of precipitating Ga in a selective manner. Al and Ga have an ion radius close to each other and this is considered to be a contributing factor. The particle size effect was, however, not studied separately and was not part of the study.

Alunite can also be used to precipitate In but the precipitation is not as efficient and as complete as for Ga. It was also interesting to find out that Ge was not precipitated with alunite. In the cases were Ge did precipitate it was as co-precipitation and highly pH dependent.

III.2.2. Galliunite – a basic gallium sulphate

The chemical formula for the basic gallium sulphate galliunite is $MGa_3(SO_4)_2(OH)_6$, and is formed as shown in:

$$3Ga_2(SO_4)_{3(aq)} + M_2SO_{4(aq)} + 12H_2O \rightarrow 2MGa_3(SO_4)_2(OH)_{6(s)} + 6H_2SO_{4(l)}$$

Equation 3

$M = K^+, Na^+, NH_4^+, H_3O^+$.

Gallium can here be precipitated either as basic sulphate (Willard, 1937), galliunite, or by a co-precipitation with alunite. In both cases up to a complete removal of Ga can be obtained. The process is strongly dependant on temperature (above 70°C) and pH (1.5–3.7 depending on precipitation method). In case of co-precipitation it has to be separately evaluated if the basic sulphate is produced in situ or in advance and then added to the process.

The removed Ga precipitate is non-soluble in water and washable (compare with Wurtz, 1880). The method is also rather selective. If the target solution contains In as well, then In will precipitate to some extent and this has to be accounted for.

Galliunite is the most stable of the studied jarosite type compounds and precipitates well. The formation of galliunite is slow. It can be boosted with ferric iron.

III.2.3. Indiunite – a basic indium sulphate

The chemical formula for the basic indium sulphate indiunite is $MIn_3(SO_4)_2(OH)_6$, and is formed as shown:

$$3In_2(SO_4)_{3(aq)} + M_2SO_{4(aq)} + 12H_2O \rightarrow 2MIn_3(SO_4)_2(OH)_{6(s)} + 6H_2SO_{4(l)}$$

Equation 4

$M = K^+, Na^+, NH_4^+, H_3O^+$.

Indium precipitation from the standard process liquor was studied. It can be precipitated and sedimented but slightly less efficiently than Ga. If, in case of precipitation as a basic sulphate, the solution contains Ga then In recovery will fall behind that of Ga and both will suffer if the aim is to have a selective precipitation. If both can be precipitated at the same time or the used solutions do not contain Ga then In can be separated by precipitation as a basic sulphate (compare with Deichman, 1957). When using co-precipitation with alunite then In will not precipitate and Ga can be removed rather selectively.

III.2.4. Jarosite – a basic iron sulphate

Jarosite is a well-known basic sulphate of iron used in the waste treatment of hydrometallurgical Zn plants. It has a very low solubility and is used to remove accumulated iron and other waste elements from the process. Jarosite is very efficient in removing In and Ga as well, (Dutrizac et al., 2000). Removing In and Ga from jarosite

are difficult. This may be due to the very similar chemistry between Fe, In and Ga. Thus recovering In and Ga from jarosite in an economically feasible way is a challenge.

Jarosite is formed according to:

$$3Fe_2(SO_4)_{3(aq)} + M_2SO_{4(aq)} + 12H_2O \rightarrow 2MFe_3(SO_4)_2(OH)_{6(s)} + 6H_2SO_{4(l)}$$

Equation 5

$M = K^+, Na^+, NH_4^+, H_3O^+$.

Experimental and analytical Section

III.3.Equipment

The experiments with basic sulphates were carried out at 90°C under continuous stirring. During the experiment parameters such as time, pH, conductivity and temperature were monitored and recorded.

The centre of the experiments were three Torrey Pines heater and stirrer plates, models HS 30 (2 pieces) and HS 10-2 (1 piece) with Torrey Pines HS 30-600 (glass) and HS 30-603 (steel) thermoelements. The pH and conductivity were recorded with the simultaneous use of a Radiometer Meterlab PHM 210 pH-meter with a pHC2401-8 electrode and a Radiometer Meterlab CDM 210 conductometer with temperature correction during the data acquisition, Figure 5. The data were collected with a computer.

The mini-reactor, 50 ml, experiments were carried out in a closed water bath, shown in Figure 6, specially designed for long term runs up to 72 h at 95 °C. The equipment could be safely run at extended periods of time at constant temperature and mixing. Each reactor tube (50 ml) contained a small magnet propelled by a larger magnet in the bath, placed in a cut decanter glass in the middle of the vessel. All reactors were closed during the reaction and opened only for samples to be withdrawn.

To avoid interference between the units, an optical connector was placed between the pH-meter and the computer.

The analysis of the withdrawn sample solutions was carried out using an ARL Fisons DCP–AES direct current plasma emission spectroscopy instrument, type SS-7 DCP, Figure 7., with a Gibson Minipump 2 peristaltic pump and an IBM 286 computer with an ARL program to run the analysis. The analysis is based on the intensity of the emissions by different compounds that are recorded and analysed spectroscopically. With this instrument one element at the time may be analysed.

Figure 5. Equipment for conductometric, pH and redox and measurements.

Figure 6. A mini-reactor system/water-bath on a Torrey Pines HS30-2 mixer plate. The plate includes electronically controlled mixer and heater. Each reactor tube (50 ml) contains a small magnet propelled by a larger magnet in the bath, placed in a cut decanter glass in the middle of the vessel.

Figure 7. The ARL Fisons direct current plasma emission spectroscopy instrument model SS-7.

DCP-AES analysis is based on plasma, i.e. partially ionised gas, and produced by ionisation of the sample liquid with direct current. The plasma is obtained between a wolfram cathode up and with two graphite anodes below, Figure 7. The plasma is ignited via temporary contact of the anodes with the cathode. The anodes and the cathode are surrounded by an argon gas flow. The sample is injected upwards and vaporized with an inert gas between the cathodes and the anode where the electrons in the sample are excited. Usually the electrons in the atoms are situated on the lowest energy level. A sufficient high-energy input will move the utmost electrons to a higher energy level. When the excited electrons return to the lowest energy level they emit the surplus energy as radiation according to:

$$M + \text{energy} \rightarrow M^* \rightarrow M + h\upsilon$$

Equation 6

The emitted radiation is separated into different wavelengths and is transformed into a two dimensional spectra. Each wavelength has a specific place in this spectrum that reaches from 190–800 nm.

The plasma itself is induced in an inert gas surrounding, Figure 8., and then reflected to a detector in the instrument, Figure 9. It needs only an effect of about 700 W and the induced plasma is sufficiently stable. The temperature in the detection area is about 5 000 Kelvin, Figure 10. The instrument consumes inert argon gas at a rate of 15–20 l/min.

Figure 8. The cathode (up, in the white tube), the anodes (down left and right, in the white tubes) and the sample inlet (down, middle) in the DCP-AES instrument.

Figure 9. The plasma is reflected to the instrument through a window with a prism behind. The spectre is then passed to a detector inside the instrument.

Figure 10. The plasma induced in the ARL Fisons direct current plasma emission spectroscopy instrument model SS-7. The sample is vaporised with an inert gas before entering the plasma zone.

A computer connected to the instrument calculates the concentration of the sample. Prior to the calculation a calibration has been done with low and high standard solutions, i.e. blank, 5 ppm, 10 ppm, 25 ppm, 50 ppm and 100 ppm.

An instrument with a multi-element analysis capability is recommended in further studies due to the long response time between experiments and analysis. The instrument had also an occasional tendency for drifting. This was known and monitored during the analysis by standard solution sampling. If serious drifting was observed then the analysis was repeated.

III.3.1. Chemicals

The main purpose of the research was to determine the behaviour of the NL2-solution (Neutral Leach 2 -solution) under conditions close to those in the Zn-production. The NL2-solution was used when process and production conditions were simulated. To have a reference, also ultra purified water (ELGA) was used.

The NL2-solution was delivered by Outokumpu Zink Oy in Kokkola, Finland, and represented a native NL2-solution directly from the process.

The target metals investigated are in such small concentrations in the native NL2-solution that it was necessary to spike the solutions with predetermined amounts of the target metals needed. For this purpose gallium sulphate, indium sulphate and germanium hydroxide of analytical purity were used.

Table 3. Chemicals used in the basic sulphates research.

Compounds used	Formula	Source
NL2-solution	Mixture	Kokkola Zink Oy
ELGA-water	Purified water	ELGA-purifier, ÅA lab.
Gallium sulphate	$Ga_2(SO_4)_3*18H_2O$	ALFA
Indium sulphate	$In_2(SO_4)_3*6H_2O$	ALFA
Germanium hydroxide	GeO_2	ALFA
Aluminium sulphate	$Al_2(SO_4)_3*18H_2O$	KEBO lab Oy
Ferrous sulphate	$FeSO_4*7H_2O$	ALDRICH
Ferric sulphate	$Fe_2(SO_4)_3*5H_2O$	ALDRICH
Sulphuric acid	H_2SO_4	J. T. Baker Chemicals NV
Nitric acid	HNO_3	J. T. Baker Chemicals NV
Sodium hydroxide	NaOH	J. T. Baker Chemicals NV
Potassium hydroxide	KOH	J. T. Baker Chemicals NV
Magnesium hydroxide	$Mg(OH)_2$	J. T. Baker Chemicals NV
Ammonia	NH_4	Not Available

When synthetic solutions were used, i.e. solutions based on ultra purified ELGA water, it was necessary also to add other vital chemicals that are contained in the native NL2-solution. Thus, also aluminium hydroxide, ferrous- and ferric sulphate were added when required. Also these were of analytical grade, Table 3.

In the cases when the pH of the solution needed to be adjusted the proper acids and bases were used. The acids used were sulphuric acid and nitric acid. Nitric acid was mainly used for keeping the liquid samples precipitation free prior to analysis with the DCP. The bases used were sodium hydroxide, potassium hydroxide and magnesium hydroxide, all analytical purity grades.

III.3.2. Experiments

III.3.2.1. Background for the experiments

The experiments were carried out either in native NL2-solution or in pure aqueous solution, depending on the intensions. An experiment done in NL2-solution simulated production conditions both physically and chemically. An experiment done in aqueous solutions would give a reference to the physical and chemical behaviour of the NL2-solution tests or it would be used for synthesis of pure basic sulphate material as reference for the databases and the basic sulphates obtained in the NL2-solution tests.

III.3.2.2. Carrying out the experiments

The formation and precipitation kinetics of basic sulphates are highly pH-dependent and precipitation increases with decreased pH.

The experiments had to reveal suitable operating conditions for a precipitation based on basic sulphates formation. These conditions had to be within the limits given by the main Zn-production process. Experimental conditions were as close to the real production conditions as possible, with pH below 3.7 and temperatures between 85–90°C. During the experiments parameters such as sampling time, solution temperature and pH were recorded.

The experiments were carried out at different volumes depending on the sampling need. If no or few intermediate samples were required, then the experiments were carried out in closed 50 ml reactors preventing any evaporation. Up to five reactors could be used at the same time and the external conditions were the same for all. A heating and stirring system was designed specially for the experiments with the 50 ml reactors.

In the case of basic sulphates synthesis or kinetic experiments larger reactors for volumes up to 1 000 ml were used to allow for more product or repeated sampling.

To be able to closer simulate the production conditions the NL2-solution or ELGA-water used in the experiments was preheated to the reaction temperatures before any mixing was allowed with the other reagents. Thus all experiments could be considered as started at target temperature, usually 90°C. The mixing of the reagents was done quickly and so the experiment had begun.

The experiments were run between 6–72 hours. A possible loss in the solution by evaporation was accounted for by correcting the volumes.

For the alunite tests alunite was weighed out and added into a 250 ml beaker. The alunite was dissolved and diluted with stirring to 200 ml in H_2SO_4 acidic water (pH~1.67) of ELGA quality. The pH was adjusted at room temperature with NaOH or H_2SO_4 to target pH. A 5 ml sample was taken.

The beaker was covered with foil to prevent evaporation and then heated to target temperature (90°C) with constant stirring. At target temperature the pH was adjusted and a 5 ml sample was taken. The hot solution was allowed to stand for five hours with constant stirring and heat control. A 5 ml sample was taken every 30 minutes for the first two hours and then one every hour. If needed, the pH was adjusted before the sample was taken. Tolerable difference in the pH was +/- 0.5 pH.

To be sure that the evaporation was not affecting the results, the liquid level was marked on the beaker. In this way it was possible to follow if the solution level had decreased between the samples taken.

The samples were centrifuged before the DCP-test on the aluminium concentration.

The process solution experiments were carried out as in the description for the synthetic one, but instead of diluting the alunite in water, the alunite was diluted in native process solution.

The experiments where In and Ga were precipitated with alunite were carried out as in the descriptions above, but in the beginning In, Ga and Ge was weighed out and added to the undissolved alunite in the beaker.

The samples were immediately centrifuged after the experiment. The DCP test was run on the Al, Ga, and Ge and In concentrations.

III.3.2.3. Closing the experiments

After the experimental runs were over a final sample was taken of both liquid and solid phases. In some cases, when there was enough material, some of the suspension would be left aside and analysed later as a reference for the ageing effect. Also any available precipitate was saved for further experiments (stability tests etc.) and analysis (composition etc.).

III.3.3. Analysis

III.3.3.1. Sample preparation

When large experimental volumes, >50 ml, or continuous sampling were used the samples were withdrawn from the reactor with a syringe equipped with a suction filter to avoid basic sulphate crystals uptake. The sample volume was between 3–5 ml depending on the dilution needs. Before dilution 0.05 ml nitric acid (HNO3) was added to avoid further precipitation and a change in the target metal levels in the sample solution.

When small experimental volumes, 50 ml, were used without intermediate sampling then one sample was withdrawn according to the above description and another one was prepared by centrifugation of the rest of the sample when still hot, >80 °C. In this sample the clear liquid phase was separated from the precipitate and nitric acid was added as above. The precipitate was washed three times with sufficient amounts of water.

III.3.3.2. DCP-AES

The analysis of the target metals was carried out by analysing the liquid phase with Direct Current Plasma Emission Spectroscopy (DCP–AES). The target metal content of the liquid phase gave a direct indication of the success of the precipitation in each case, (Sara et al., 1981).

The accuracy of the used method and instrument are considered good and it met the accuracy requirements posed on it. An instrument with simultaneous multi element detection capacity would have been preferred by the team, but was economically out of range in this particular project. However, all samples could be analysed, and in cases of doubt, the samples were re-analysed after a thorough calibration of the instrument.

Strange and non-fitting results were discarded only after repeating the experiment in question since the possibility that new reactions might take place and that formed compounds might transform into other ones had to be accounted for.

During the DCP–AES analysis the instrument was calibrated both prior to the analysis and during the analysis. In some cases a clear instrumental drift would be detected and the instrument had to be calibrated again and the samples had to be reanalysed.

The analysed concentrations varied from 5 mg/l to 3 000 mg/l (as undiluted). The accurate working range of the instrument varies between 3 mg/l to 100 mg/l (Ga) or 3mg/l to 1 000 mg/l (In), depending on the analysed metal in question. Dilutions were made according to that.

III.3.3.3. Titration – Fe(III)–EDTA

During the project Fe contents had to be measured frequently and accurately. This was carried out spectrophotometrically without indicators allowing for a fast and precise analysis with a minimum of effort. The method is developed at the Laboratory of Analytical Chemistry and is one of the basic methods students are required to learn. The method is especially suitable not only for our work since samples need no particular pre-treatment but occasional dilution. The method that is described in detail by L. Harju and S-G. Huldén (Harju et al., 1980(a, b)) allows also for spectrophotometric titration of some other metal ions, depending on pH range and wavelength.

The Fe(III) - EDTA titration without an indicator is based on the formation of a stable 1:1 Fe(III) - EDTA chelate spectroscopically detectable at λ = 370–450 nm. Fe(II) reacting with EDTA will not be detected in the used wavelength and pH range, Figure 12. The titration proceeds through a 2:1 Fe(III) - EDTA chelate (Fe = 2, EDTA = 1) illustrated in figure with lines for the 2:1 titration (L1), 1:1 titration (L2) and achieved equivalence (Eq.). The equivalence volume of the EDTA used may be read from the graph at the crossing point of the lines L2 and Eq. in Figure 12. It may also be calculated from the equations of the lines obtained by linear regression. In an equal manner, the crossing point of the lines L1 and L2 indicate the halfway consumption of the reaction. The starting point of the titration is the same as the starting point of line L1.

During the oxidation some of the Fe(II) may start to oxidize to Fe(III), which in turn will react with the added EDTA. This will then induce an error in the titration and the initial Fe(III)-contents will appear higher than they are. Thus the titration should be carried out rather swiftly.

Although there are several metal ions that react with EDTA (In, Fe(II), Al Ca, Mg Na, K) none of them will interfere with the spectroscopical titration of Fe(III) if pH is kept between 0 and 6 and if a wavelength between 370 and 450 nm is used, Figure 13.

The analysis of the experimental Fe-solutions was carried out with Metrohm Spectrophotometer, Figure 11, with a dip-in light electrode and a range from 400 nm to 700 nm. The addition of EDTA was done through a Titrino 751 GPD titrimeter monitored by a Toshiba Satellite 4080 portable computer with a TiNET titration program.

Figure 11. Metrohm Spectrophotometer with a Titrino 751 GPD titrimeter (front right), dip in light-electrode (400-700 nm) and Stirrer 728 (back left).

Depending on estimated Fe(III) concentrations the samples were analysed as such or as diluted. The titration was almost completely automatical and only the equivalence volume of EDTA had to be calculated to corresponding Fe(III) values.

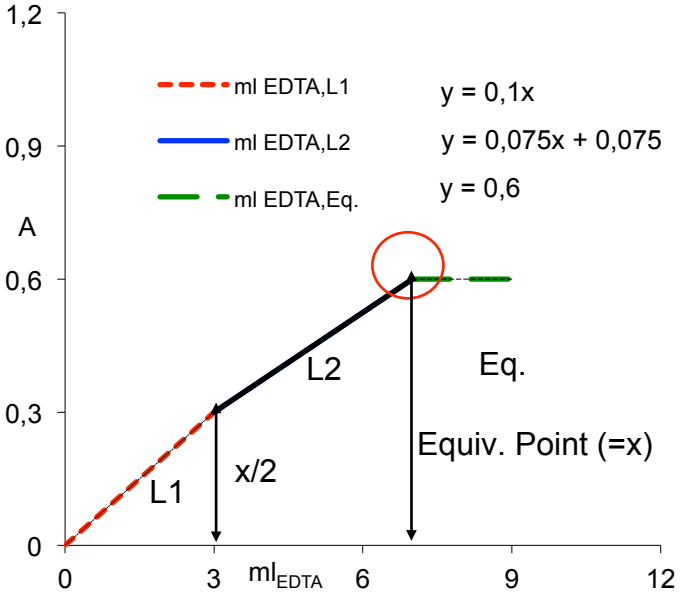

Figure 12. Spectroscopic titration of Fe(III) with EDTA without an indicator: λ = 370 – 450 nm and pH = 0 – 6, illustrated with a schematic graph. The equivalence volume of titrated EDTA is found where the lines for L2 and Eq. cross (encircled).

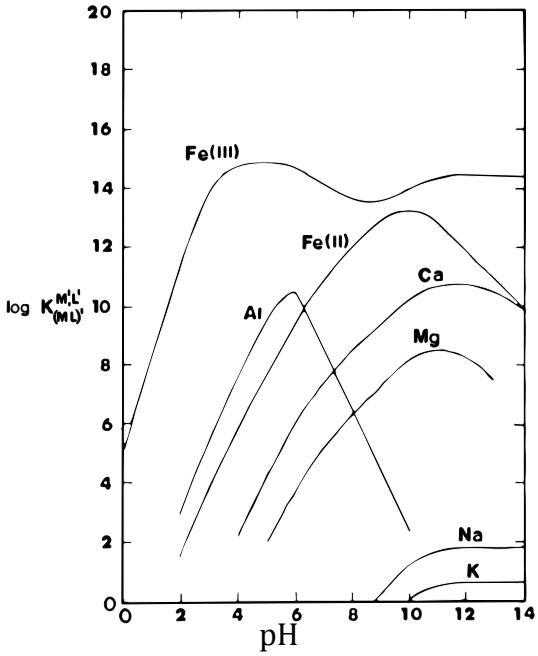

Figure 13. Conditional stability constants of some metal EDTA-complexes as functions of pH, (Harju et al., 1980a).

The pH was kept low in the diluted samples by using pre-acidified water with a pH < 1.6 to dilute the samples. This corresponded to the average pH of our samples. The TiNET program was run on fixed sampling intervals. A 0.05–0.1 M EDTA solution prepared from titrisols was mainly used. The equipment was tested and calibrated with synthetic and spiked process Fe(III)- and Fe(III) - Fe(II) -solutions.

The application of the Spectrophotometric titration of Fe^{3+} with EDTA -procedure in the laboratory is easy and fast. The following procedure has been used

1. a sample is taken and the volume is noted in ml,
2. the sample is diluted with acidic water, pH ~ 1.5 or with a buffer solution of pH ~1.5,
3. the diluted sample volume is noted an indicated as V_0,
4. the sample is placed in the photometer,
5. the sample is titrated with EDTA.

The data is graphically processed to find the equivalence point. The result, ml EDTA consumed, is converted to amount Fe^{3+} (g/l) in the sample solution.

An example is depicted in Figures 14. and 15. (not from the actual test series), an actual test run is depicted in Figures 16. and 17. and the parameters for this test are given in Table 4.

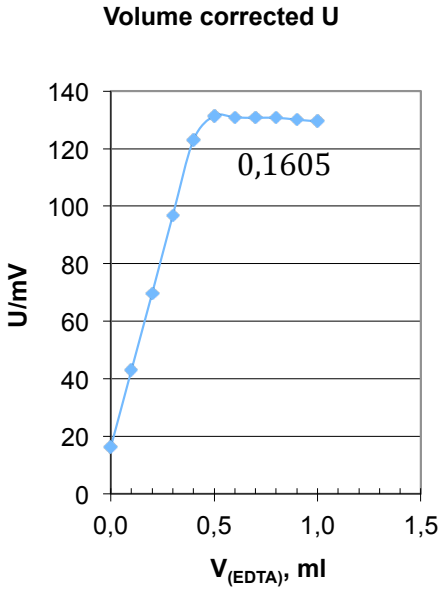

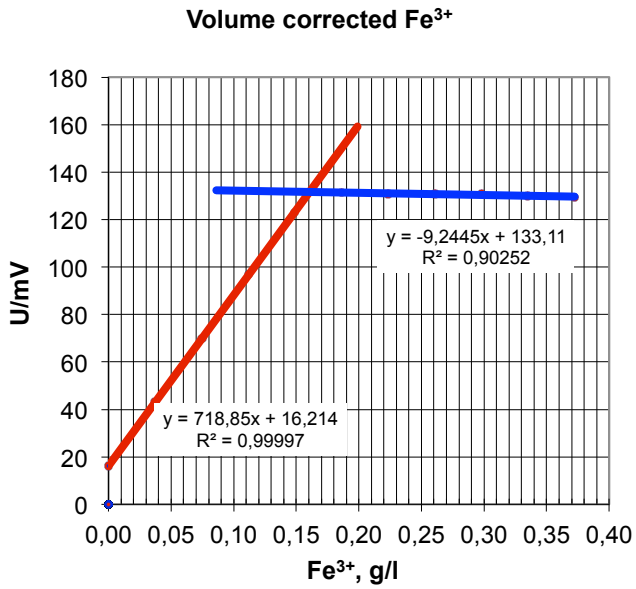

Figure 14. Volume corrected Fe(III)-EDTA titration (left figure).

Figure 15. Volume corrected Fe(III)-EDTA titration on the x-axis with EDTA values converted to giving directly Fe^{3+} concentration g/l (right figure).

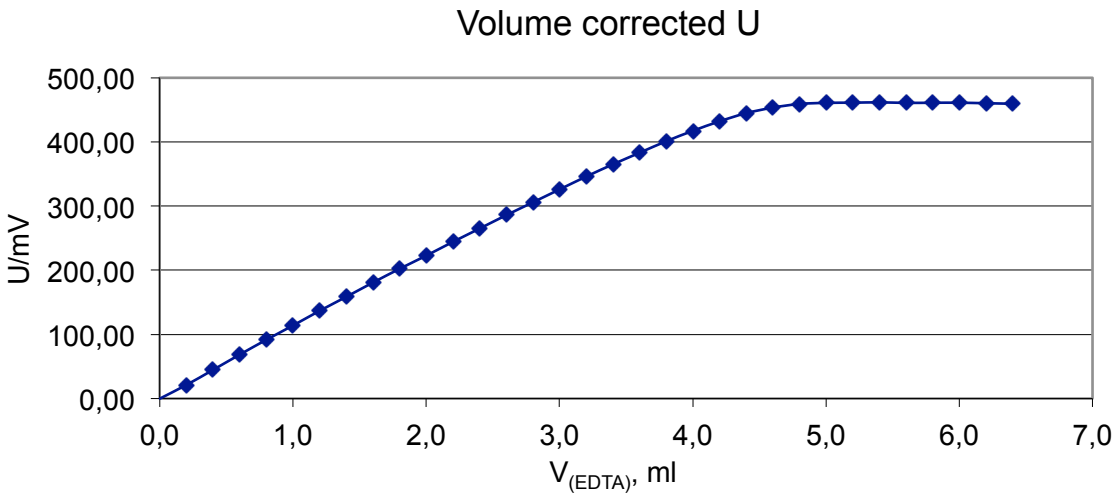

Figure 16. Photometric titration of Fe(III) and Fe(II) with EDTA. Volume corrected U is shown in the figure. Parameters are given in Table 4.

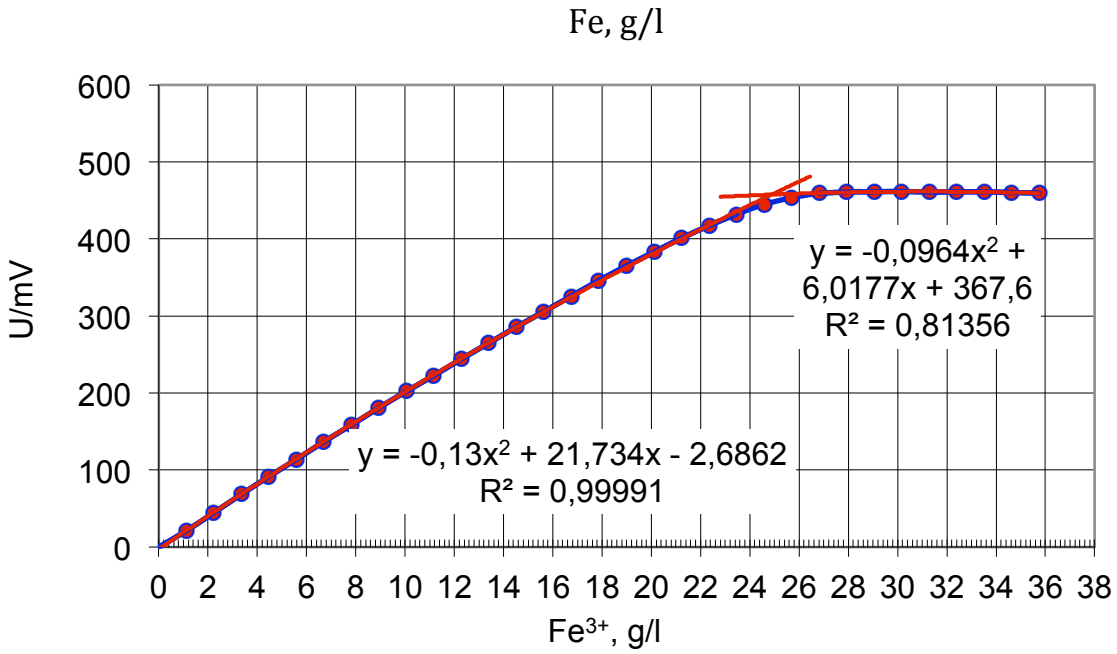

Figure 17. Photometric titration of Fe(III) and Fe(II) with EDTA. Volume corrected U shown in the upper figure. Parameters are given in Table 4.

Table 4. Photometric titration of Fe(III) and Fe(II) with EDTA

Test run ID:	00022402	
Determination of Fe(II) and Fe(III)		
Conc $_{(EDTA)}$:	0,05	M
Added H_2O_2:	1	ml
$V_{(sample)}$:	0,5	ml
$V_{(initial)}$:	28	ml
Conc Fe:	24,3	g/l

III.3.4. Experimental part remarks

The experimental part struggled with some difficulties like achieving sufficient stirring and keeping the target pH levels in some experiments. The overall experimental part was good and reliable. The test runs were evaluated after each series was done or, in case of inconsequent results, during the tests.

Samples were withdrawn for the analysis and the precipitation was sedimented by centrifugation. Some sample liquids and precipitates were also photographed for visual inspection and evaluation.

The objective was to find a selective way of precipitating the target metals and also to determine whether it was possible to recycle the precipitating agent in case of co-precipitation.

Results section

It is possible to precipitate Ga, Figure 24., and In, Figure 25., in a selective process and not affect Ge, Figure 27. The results were as expected. With proper adjustment of the process it is possible to circulate the coprecipitated alunite.

The experiments were done both in synthetic solutions as well as in native Zn liquor solutions. Both behaved as predicted and expected. The precipitation is strongly dependent on both temperature and pH. The pH was adjusted sulphuric acid.

The alunite stability experiments were carried out with solutions containing 5 g/l alunite under stirring, Figures 18. – 23. It was difficult to maintain good stirring conditions throughout the experiments. The temperature was 90°C and pH was varied. Both synthetic and native process solutions were used.

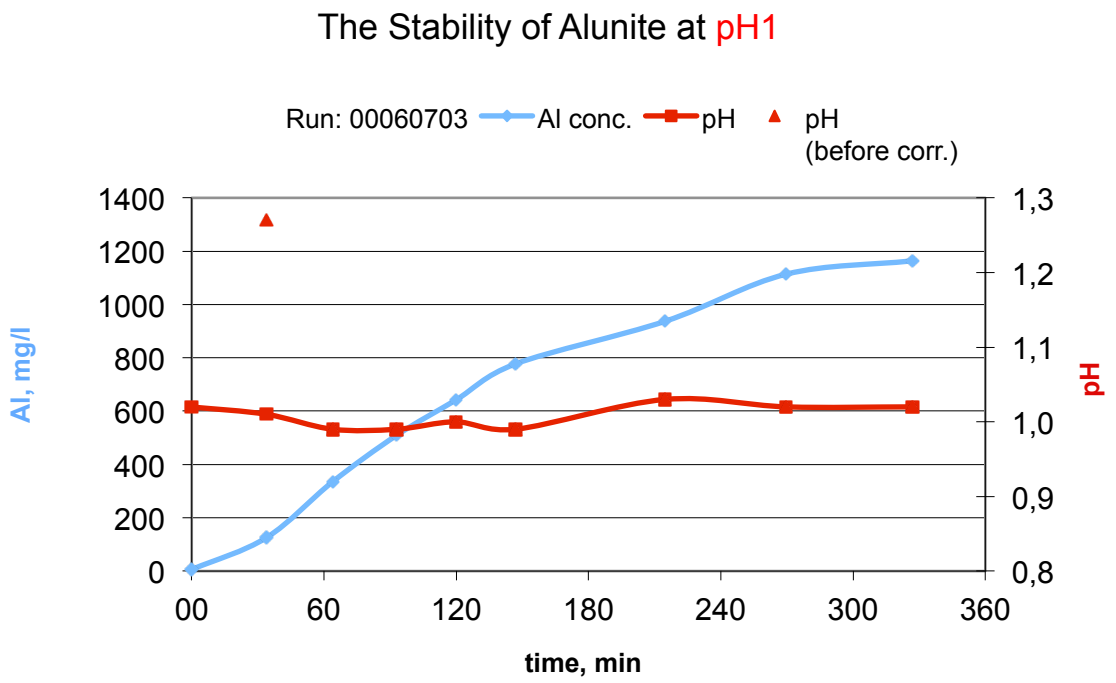

Figure 18. Dissolved Al as function of time at pH1. Initial amount of added Al = 5 g/l (5 000 mg/l). Synthetic solution. DCP-AES-analysis.

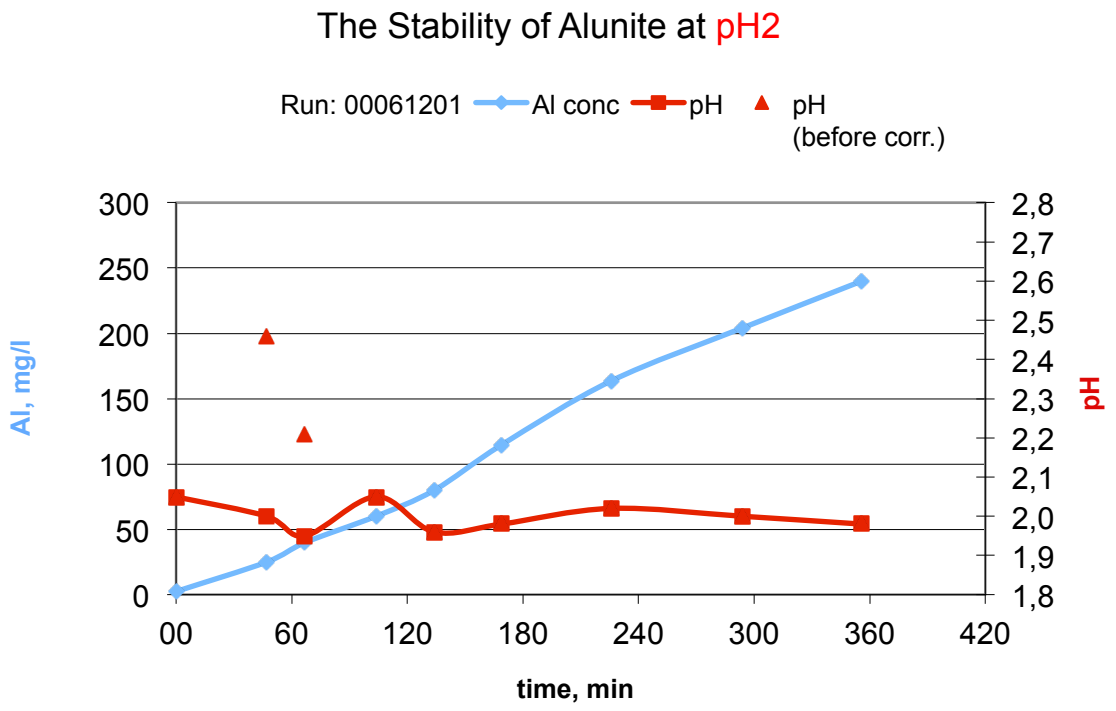

Figure 19. Dissolved Al as function of time at pH2. Initial amount of added Al = 5 g/l (5 000 mg/l). Synthetic solution. DCP-AES-analysis.

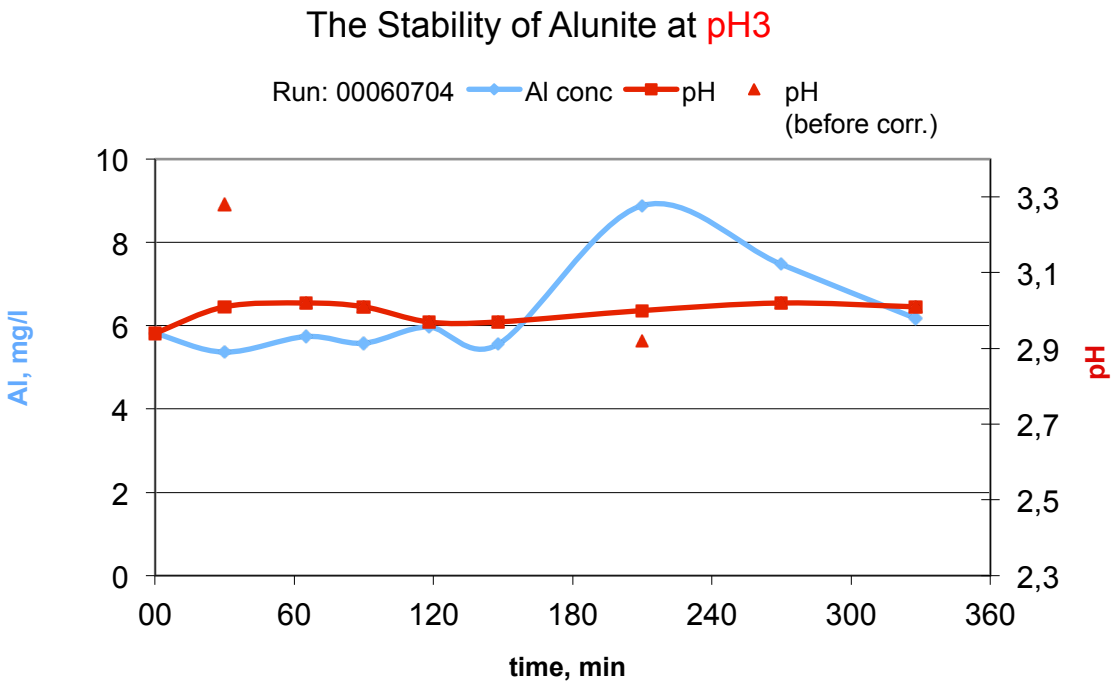

Figure 20. Dissolved Al as function of time at pH3. Initial amount of added Al = 5 g/l (5 000 mg/l). Synthetic solution. DCP-AES-analysis.

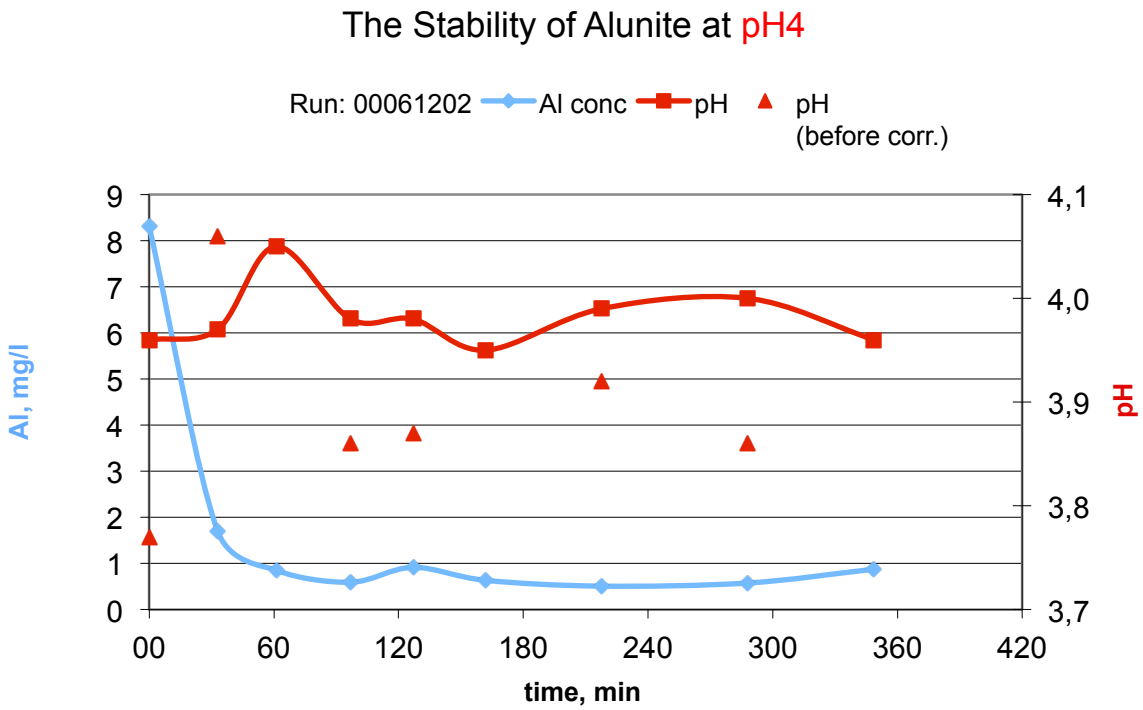

Figure 21. Dissolved Al as function of time at pH4. Initial amount of added Al = 5 g/l (5 000 mg/l). Synthetic solution. DCP-AES-analysis.

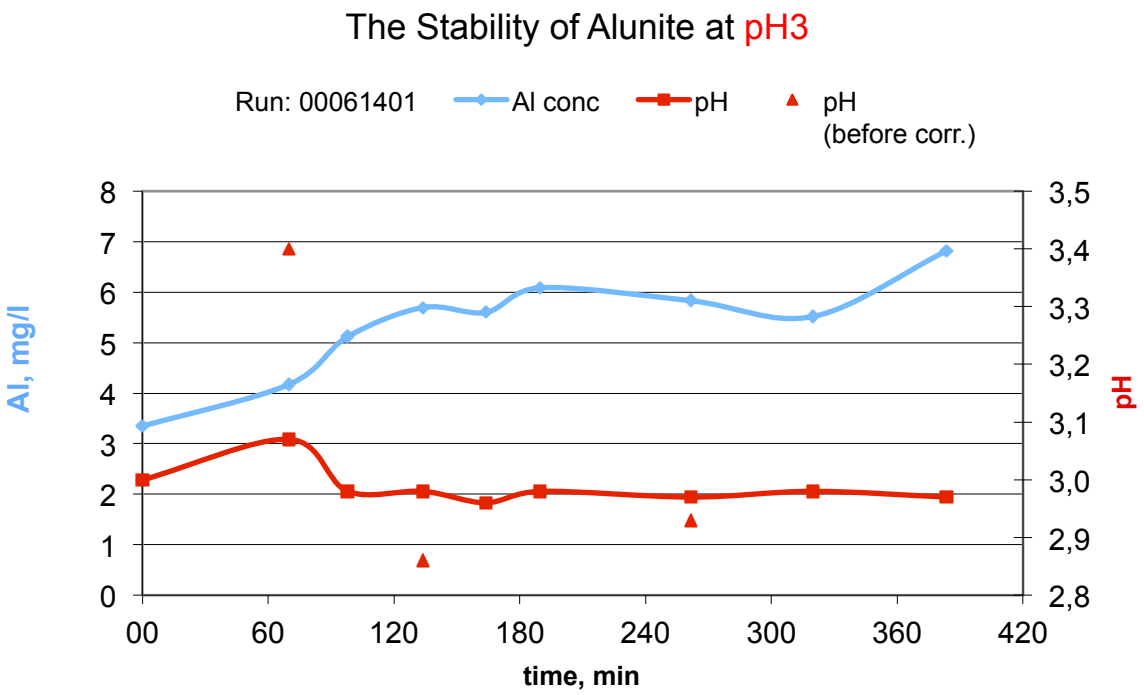

Figure 22. Dissolved Al as function of time at pH3. Initial amount of added Al = 5 g/l (5 000 mg/l). Process solution. DCP-AES-analysis.

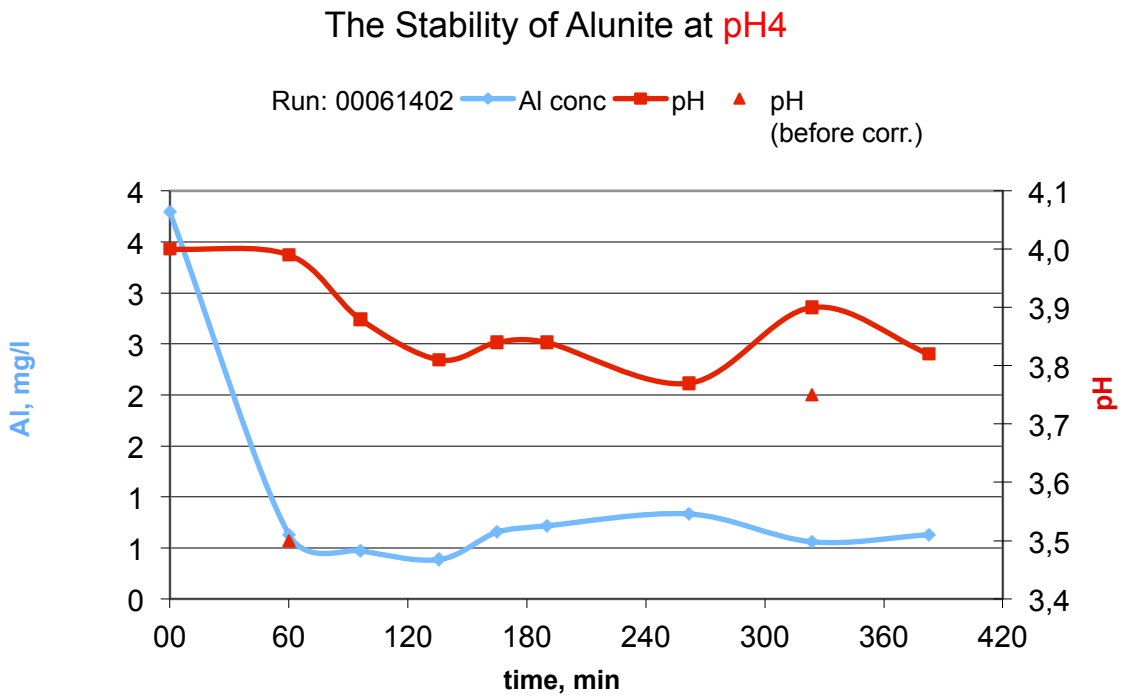

Figure 23. Dissolved Al as function of time at pH4. Initial amount of added Al = 5 g/l (5 000 mg/l). Process solution. DCP-AES-analysis.

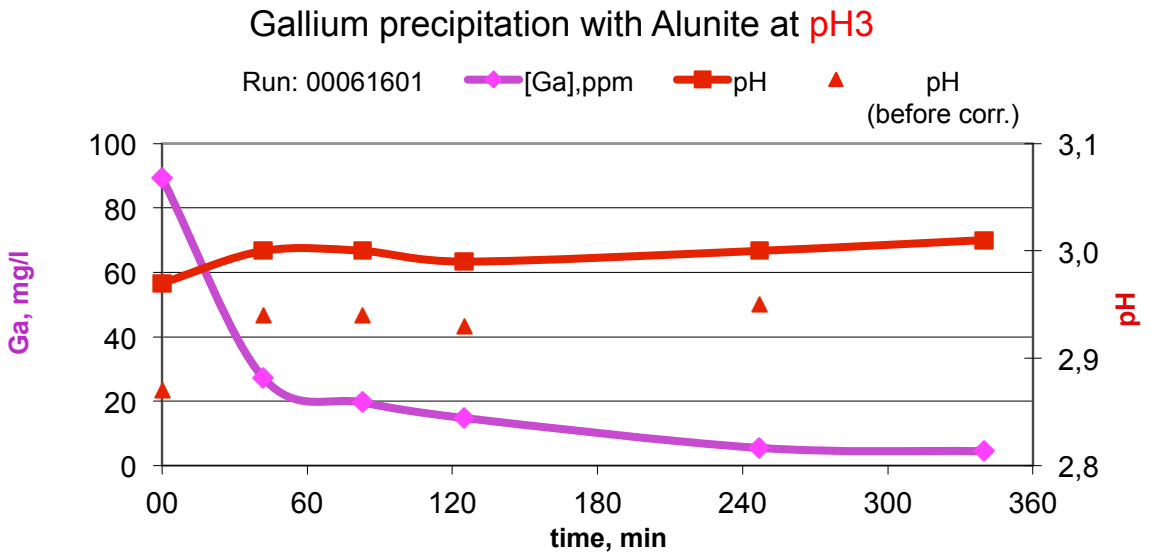

Figure 24. Example of Ga precipitation with alunite pH3. Initial concentrations were 1 g/l alunite, 0.105 g/l Ga, 0.106 g/l Ge and 0.105 g/l In. T = 90°C. pH was adjusted with H_2SO_4 and NaOH. DCP-AES-analysis.

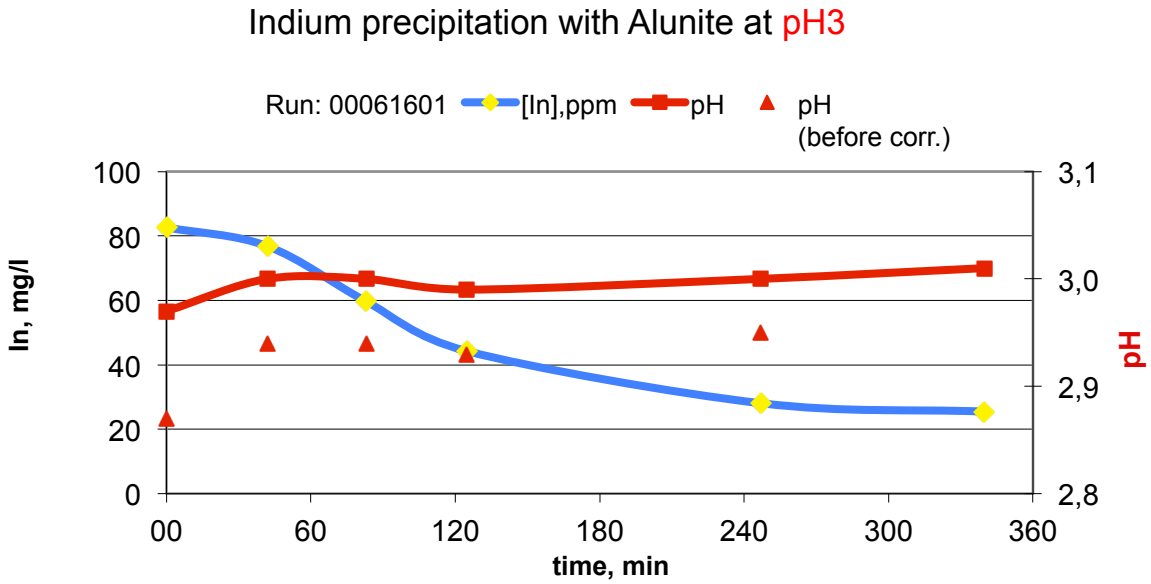

Figure 25. Example of In precipitation with alunite pH3. Initial concentrations were 1 g/l alunite, 0.105 g/l Ga, 0.106 g/l Ge and 0.105 g/l In. T = 90°C. pH was adjusted with H_2SO_4 and NaOH. DCP-AES-analysis.

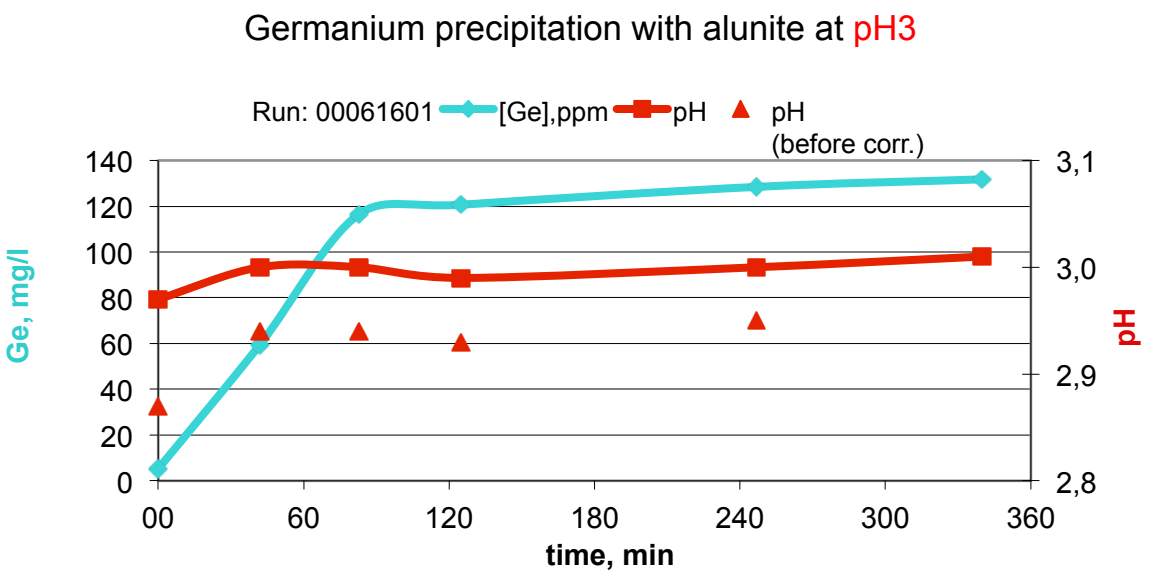

Figure 26. Example of Ge precipitation with alunite pH3. Initial concentrations were 1 g/l alunite, 0.105 g/l Ga, 0.106 g/l Ge and 0.105 g/l In. T = 90°C. pH was adjusted with H_2SO_4 and NaOH. DCP-AES-analysis.

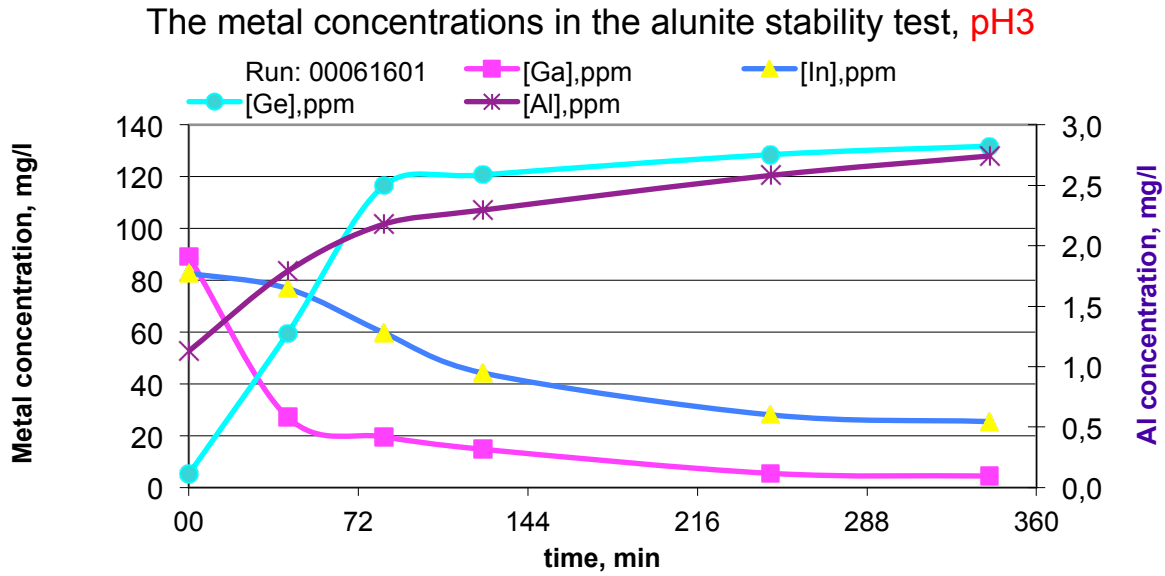

Figure 27. Metal concentrations in alunite stability tests at pH3. Initial concentrations were 1 g/l alunite, 0.105 g/l Ga, 0.106 g/l Ge and 0.105 g/l In. T = 90°C. pH was adjusted with H_2SO_4 and NaOH. DCP-AES-analysis.

III.3.5. Particular results from the study

The tests with authentic Zn-sulphate liquors showed that Ga was removed (precipitated) completely and selectively both in the alunite and in the galliunite methods. Ga was either coprecipitated with alunite or precipitated as a Ga basic sulphate.

In the indiunite method both Ga and In were precipitated. Ga performed better here as well. In was not removed as efficiently as Ga. For as selective precipitation between Ga and In the Ga precipitation and removal has to take place before the In step.

The studied basic sulphate methods did not affect Ge and no Ge was precipitated.

III.3.5.1. Basic sulphate precipitation

The reactions of Ga and In precipitation were rather rapid and selective in all three studied basic sulphate precipitation options:

1. Alunite method
2. Galliunite method
3. Indiunite method

It is important to note, that due to the nature of the project itself and the cooperation around it, most of the experimental series in this part of the study are to some extent limited. The results are accurate as well as the conclusions. However, there is a limitation on the number of data that can be used for further calculations, such as overall precipitation kinetics.
The study also showed that In, Ga and Al all start precipitating at around the same time when pH is below 3 and temperature 90°C. Ge did not produce any significant precipitate. In zinc process solutions the precipitation of Zn is significantly slower than for In, Ga and Al under the studied circumstances. It is possible that increased ion strength in the solution makes the colloid precipitate. This happens directly in process solutions and is also desired in aqueous solutions.

The primary objective of finding out selective precipitation methods and suitable circumstances was achieved. It could also be established that the reactions happen with such speed that they can be applied in an actual process environment.

III.4. Conclusions and future perspectives

According to the study the following conclusions can be made:

Ga precipitates completely with alunite or as a basic sulphate as galliunite and can be separated from the process liquor. This process is selective in favour of Ga. The Ga precipitates and sediment about twice as rapidly than In precipitates and this should be taken advantage of in a recovery process.

In precipitates well but not completely with alunite and at approximately half the rate of Ga. Still, the precipitation rate is high enough to be utilised in a recovery process.

The studied processes are applicable for indium and gallium recovery.

For solutions containing In, Ga and Ge and were precipitation of all three is desired the order of the processes must be chosen correctly depending on the general recovery process environment in order to optimise the recovery results.

The studied recovery processes can be applied in a novel kind of local recovery processes that can act as intermediates when local recycled raw material is pre-treated for further use at larger specialized recovery units.

III.5. References

Deichman, E. N., 1957, Study of the properties of indium hydroxide, and the separation of indium from zinc, N. S. Kumakov Institute of General and Inorganic Chemistry of the Academy of Sciences of the USSR

Dutrizac, J. E., Chen, T. T., 2000, The Behaviour of Gallium During Jarosite Precipitation, Canadian Mineralogist, Vol. 39, Issue 1, pp. 1-14.

Harju, L., Huldén, S-G., 1980a, Determination of Total Iron in Standard Rocks by Spectrophotometric Titration with EDTA, Talanta, Vol. 27, 811-814.

Harju, L., Huldén, S-G., 1980b, Standardization of EDTA by Spectrophotometric Titration, with Metallic Copper as Standard, Talanta, Vol. 27, 815-817.

Lang, H., Fall 2014, Geology 284: Mineralogy, West Virginia University, Dept. of Geology & Geography.

Sara, R., Huldén, S-G, Harju, L., 1981, Kaariplasmaemissio (DCP) analyysitekniikkana, Kemia-Kemi, n:o 12, page 774-778.

Willard, H. H., Fogg, H. C., 1937, The Precipitation of Basic Gallium Sulfate by Means of Urea. 11. The Separation and Determination of Gallium [CONTRIBUTION FROM THE CHEMICAL LABORATOORFYTHE UNIVERSITY OF MICHIGAN]

Wurtz, C. A., 1880, Elements of Modern Chemistry, Reprint, London: Forgotten Books, 2013. 334-5

www.a-m.de/englisch/lexikon/mineral/sulfate/alunit-kris1.htm , © 2000 Büro für angewandte Mineralogie · Dr. Stephan Rudolph · D-47918 Tönisvorst.

www.a-m.de/englisch/lexikon/mineral/sulfate/alunit.htm , © 2000 Büro für angewandte Mineralogie · Dr. Stephan Rudolph · D-47918 Tönisvorst.

IV

IV. Precipitating germanium with tannic acid

IV.1. Background

Tannic acid readily reacts with the Ge in the solution (Kul et al., 2008). In the studied process environment the reaction is selective. One of the tasks was to determine proper reaction conditions for a recovery process and the reaction stoichiometry. Tannin and tannic acid as well as the chemistry are well described by Hagerman (1998).

Precipitating and separating Ge from *zinc production process liquors* using tannic acid is a very selective recovery method that minimally affects the conditions in the main process. Although the zinc production process liquors are here used as a reference, the idea of the method might be applied also to other solutions of similar consistency.

Tannin has largely been studied, and the patents date back to the 1940's. Tannin, usually containing up to 50-80% of tannic acid (Kul et al., 2008), is widely used in different metal recovery processes and tannin and tannic acid as recovery agents are continuously studied, (Nakamura et al., 1998 (a, b); Liang et al., 2008 (a, b); Kul et al., 2008; Zischkau et al., 1941 (a,b); Pu et al., 2013; Zhou, 2009). The use of tannic acid is safe, but proper safety measures should be undertaken to avoid direct skin and eye contact and not to inhale it (EFSA, 2014).

In the current work the precipitation of Ge using tannic acid in the zinc production process conditions have been investigated. The aim has been to recover Ge from the process solutions by directly precipitating it. The precipitation and separation of Ge had to be done considering the main process. This implied that the original process should be altered as little as possible in terms of pH and temperatures. No significant amounts of tannic acid could be permitted to remain in circulation as the tannic acid may disturb the electrolysis in the Zn recovery efficiency. Further, any changes to the recovery processes should be financed with profits later generated from the improvement.

The presented work had the focus on precipitation in native process liquors and synthetic water based solutions. Further the effects of interfering metal ions in the process solution have been studied. Optimal precipitation conditions will also be proposed.

Tannic acid reacts with germanium as shown in Equation 1, (Kul et al., 2008) and forms a precipitate.

$$Ge^{4+} + O_2 + H_6T \rightarrow 2GeO*H_6T$$

Equation 1

H_6T = tannic acid

IV.2. What is tannic acid

Tannic acid, also known as gallotannic acid, is a type of tannin. Tannin itself is a common molecule in nature. Most plants contain tannin and it is widely found in the nature, Figure 1.

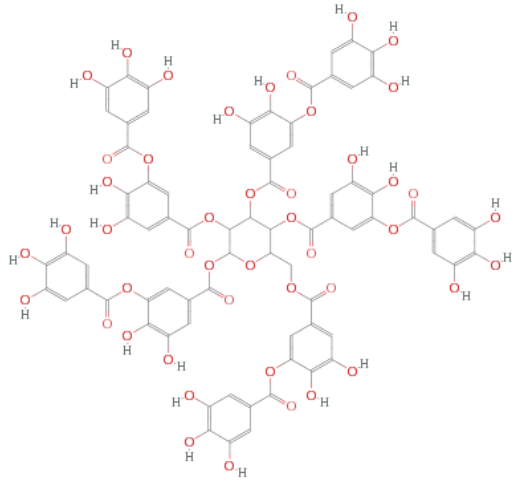

Figure 1. The tannic acid molecule, (Wolfram|Alpha Knowledgebase, 2015)

Table 1. Properties of tannic acid, (Wolfram|Alpha Knowledgebase, 2015).

Tannic acid	
Formula*	$C_{76}H_{52}O_{46}$
Molecular weight*, g/mol	1701.2
Melting point*	218 °C (slight decomposition)
Solubility in water**	Soluble
Solubility in alcohol**	Very soluble
Source*: Wolfram|Alpha Knowledgebase, 2015	
Source**: experimentally tested during the study	

Experimental and analytical section

IV.3. Equipment – Conductometry, pH and redox potentials

The tannic acid experiments have been carried out with the simultaneous use of a conductometer (Radiometer, Meterlab CDM 210) and pH-meter (Radiometer, Meterlab PHM 210) with temperature correction during the data acquisition. The data were collected with a computer, Figure 2.

To avoid interference between the units, an optical connector was placed between the pH-meter and the computer.

The sampling intervals (5s–3min) could easily be adjusted to the needs of the individual experiments. The recorded data has after the experimental runs been transferred to EXCEL for further analysis of the data.

Figure 2. Equipment for pH, redox and conductometric measurements.

The mini-reactor, 50 ml, experiments were done in a closed water bath, Figure 3, specially designed for long term runs up to 72h at 95°C. The equipment could be safely run at extended periods of time at constant temperature and mixing. Each reactor tube (50 ml) contained a small magnet propelled by a larger magnet in the bath, placed in a cut decanter glass in the middle of the vessel. All reactors were closed during the reaction and opened only for samples to be withdrawn.

Figure 3. A mini-reactor system/water-bath on a Torrey Pines HS30-2 mixer plate. The plate includes electronically controlled mixer and heater. Each reactor tube (50 ml) contains a small magnet propelled by a larger magnet in the bath, placed in a cut decanter glass in the middle of the vessel.

The analysis of the withdrawn sample solutions was carried out using an ARL Fisons DCP–AES direct current plasma emission spectroscopy instrument, type SS-7 DCP, Figure 4, with a Gibson Minipump 2 peristaltic pump and an IBM 286 computer with an ARL program to run the analysis. The analysis is based on the intensity of the emissions by different compounds that are recorded and analysed spectroscopically. With this instrument one element at the time may be analysed.

Figure 4. The ARL Fisons direct current plasma emission spectroscopy instrument model SS-7.

DCP-AES analysis is based on plasma, i.e. partially ionised gas, and produced by ionisation of the sample liquid with direct current (Sara et al., 1981). The plasma is obtained between a wolfram cathode up and with two graphite anodes below, Figure 4. The plasma is ignited via temporary contact of the anodes with the cathode. The anodes and the cathode are surrounded by an argon gas flow. The sample is injected upwards and vaporized with an inert gas between the cathodes and the anode where the electrons in the sample are excited. Usually the electrons in the atoms are situated on the lowest energy level. A sufficient high-energy input will move the utmost electrons to a higher energy level. When the excited electrons return to the lowest energy level they emit the surplus energy as radiation according to:

$$M + \text{energy} \rightarrow M^* \rightarrow M + h\upsilon, \qquad \text{Equation 1}$$

The emitted radiation is separated into different wavelengths and is transformed into a two dimensional spectra. Each wavelength has a specific place in this spectrum that reaches from 190–800 nm.

The plasma itself is induced in an inert gas surrounding, Figure 5, and then reflected to a detector in the instrument, Figure 6. It needs only an effect of about 700 W and the induced plasma is sufficiently stable. The temperature in the detection area is about 5 000 K, Figure 7. The instrument consumes inert argon gas at a rate of 15 – 20 l/min.

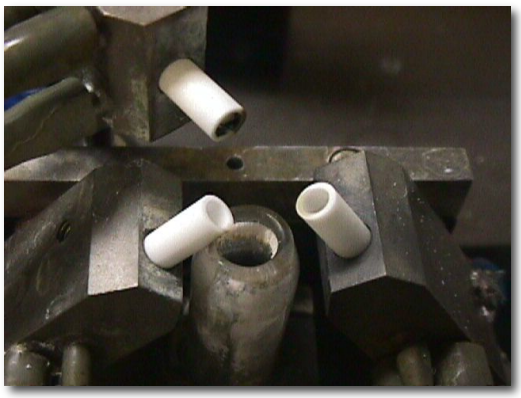

Figure 5. The cathode (up, in the white tube), the anodes (down left and right, in the white tubes) and the sample inlet (down, middle) in the DCP-AES instrument.

Figure 6. The plasma is reflected to the instrument through a window with a prism behind. The spectre is then passed to a detector inside the instrument.

Figure 7. The plasma induced in the ARL Fisons direct current plasma emission spectroscopy instrument model SS-7. The sample is vaporised with an inert gas before entering the plasma zone.

A computer connected to the instrument calculates the concentration of the sample. Prior to the calculation a calibration has been done with low and high standard solutions, i.e. blank, 5 ppm, 10 ppm, 25 ppm, 50 ppm and 100 ppm.

An instrument with a multi-element analysis capability is recommended in further studies due to the long response time between experiments and analysis. The instrument had also an occasional tendency for drifting. This was known and monitored during the analysis by standard solution sampling. If serious drifting was observed then the analysis was repeated.

IV.3.1. Chemicals

As the purpose of the research was to determine the precipitation behaviour of Ge-tannic acid complexes in the NL2-solution (Neutral Leach 2 -solution) under conditions close to those in the Zn-production NL2-solution was used when process and production conditions were simulated. To have a reference, also ultra purified water (ELGA) was used.

The NL2-solution was delivered by Outokumpu Zink Oy in Kokkola, Finland, and represented a native NL2-solution directly from the production process, Table 2.

The target metal originally comes in such small concentrations from the raw material to the NL2-solution that it was necessary to spike the solution with predetermined amounts of Ge. For this purpose germanium hydroxide of analytical purity was used. In case synthetic solution was used, i.e. a solution based on ultra purified water, it

was necessary also to add other metals that are found in the native NL2-solution, Table 2. Thus, also aluminium hydroxide, ferrous- and ferric sulphate as well as In- and Ga sulphate were added when required. Also these were of analytical grade.

In the cases when the pH of the solution needed to be adjusted the proper acids and bases were used. The acids used were sulphuric acid and nitric acid. Nitric acid was mainly used for keeping the liquid samples precipitation free prior to analysis with the DCP. The bases used were sodium hydroxide, potassium hydroxide and magnesium hydroxide, all analytical purity grades.

Table 2. Chemicals used in the Ge-tannic acid precipitation research (the most important).

Compounds used	**Formula**	**Source**
NL2-solution	Mixture	Kokkola Zink Oy
ELGA-water	Purified water	ELGA-purifier, ÅA lab.
Tannic acid	$C_{76}H_{52}O_{46}$	Not Available
Gallium sulphate	$Ga_2(SO_4)_3*18H_2O$	ALFA
Indium sulphate	$In_2(SO_4)_3*6H_2O$	ALFA
Germanium hydroxide	GeO_2	ALFA
Aluminium sulphate	$Al_2(SO_4)_3*18H_2O$	KEBO lab Oy
Ferrous sulphate	$Fe_2(SO_4)_3*5H_2O$	ALDRICH
Ferric sulphate	FeO_4S*7H_2O	ALDRICH
Sulphuric acid	H_2SO_4	J. T. Baker Chemicals NV
Nitric acid	HNO_3	J. T. Baker Chemicals NV
Sodium hydroxide	NaOH	J. T. Baker Chemicals NV
Potassium hydroxide	KOH	J. T. Baker Chemicals NV
Magnesium hydroxide	$Mg(OH)_2$	J. T. Baker Chemicals NV
Ammonia	NH_4	Not Available

IV.3.2. Experiments

IV.3.2.1. Background the experiments

The experiments were carried out either in native NL2-solution or in pure aqueous solution, depending on the intensions. An experiment carried out in NL2-solution simulated production conditions both physically and chemically. An experiment carried out in aqueous solutions gives a reference to the physical and chemical behaviour of the NL2-solution.

IV.3.2.2. Carrying out the experiments

The formation and precipitation kinetics of Ge-tannic acid complexes depend on the ionic strength of the solution. The ionic strength of the NL2-solution in the Zn-production process is obviously high because of the high amounts of different dissolved metals. Experimental conditions were as close to the real production conditions as possible.

The experiments had to reveal suitable operating conditions for a precipitation based on Ge-tannic acid complex formation. These conditions had to be within the limits given by the main Zn-production process. During the experiments parameters such as sampling time, solution temperature and pH were recorded.

The experiments were carried out at different volumes depending on the sampling need. If no or few intermediate samples were required, then the experiments were carried out in closed 50 ml reactors preventing any evaporation, Figure 3. Up to five reactors could be used at the same time and the external conditions were the same for all. A heating and stirring system was designed specially for the experiments with the 50 ml reactors. The equipment could be safely run at extended periods of time at constant temperature and mixing. Each reactor tube (50 ml) contained a small magnet propelled by a larger magnet in the bath, placed in a cut decanter glass in the middle of the vessel. All reactors were closed during the reaction and opened only for samples to be withdrawn.

A larger reactor for volumes up to 1 000 ml was used to allow for repeated sampling when kinetic experiments were carried out.

To be able to closer simulate the production conditions the NL2-solution or ELGA-water used in the experiments was preheated to the reaction temperatures before any mixing was allowed with the other reagents. Thus all experiments could be considered as started at target temperature, usually 90°C. The mixing of the reagents was done quickly and so the experiment had begun.

The experiments were run between 0.5–72 hours. A possible loss in the solution by evaporation was accounted for.

Indium and gallium were weighed out and added into a 250 ml beaker and dissolved in some ELGA quality water. Germanium was weighed out and separately dissolved in a few drops of 0.5M NaOH with stirring. The Ge was added to the In, Ga and the solution was diluted to 200ml with ELGA water and pH was adjusted with NaOH or H_2SO_4 to target pH. A 10 ml sample was taken.

The beaker was covered with foil to prevent evaporation and then heated to target temperature (90°C) with constant stirring. At target temperature the pH was adjusted and a 10 ml sample was taken. Dissolved tannic acid was added to the solution. The solution was allowed to stand for one hour with constant stirring and heat regulation (target temperature was still 90°C). A 10 ml sample was taken every 15 minutes starting immediately after the tannin addition.

If needed, the pH was adjusted before the sample was taken. Tolerable difference in the pH was +/- 0.5 pH.

To make sure that the evaporation was not affecting the results, the liquid level was marked at the beaker. This way it was possible to follow if the solution level has decreased between the samples taken.

The samples were centrifuged before the DCP-test on the In, Ga and Ge concentrations.

The experiments with native process solutions were carried out as described for the synthetic solution experiments, but instead of diluting the dissolved In, Ga and Ge in water, they were diluted in process solution.

IV.3.2.3. Closing the experiments

After the experimental runs were over a final sample was taken of both liquid and solid phases. In some cases, when there was enough material, some of the suspension would be left aside and analysed later as a reference for the ageing effect. Also any available precipitate was saved for further experiments (stability tests etc.) and analysis (composition etc.).

IV.3.3. Analysis

IV.3.3.1. Sample preparation

When large experimental volumes, >50 ml, or continuous sampling were used the samples were withdrawn from the reactor with a syringe equipped with a suction filter to avoid basic sulphate crystals uptake. The sample volume was between 3–5 ml depending on the dilution needs. Before dilution 0.05 ml nitric acid (HNO_3) was added to avoid further precipitation and a change in the target metal levels in the sample solution.

When small experimental volumes, 50 ml, were used without intermediate sampling then one sample was withdrawn according to the above description and another one was prepared by centrifugation of the rest of the sample when still hot, >80°C. In this sample the clear liquid phase was separated from the precipitate and nitric acid was added as above. The precipitate was washed three times with sufficient amounts of water.

IV.3.3.2. DCP-AES

The analysis of Ge was carried out by analysing the liquid phase with *Direct Current Plasma Emission Spectroscopy* (DCP–AES), (Sara et al, 1981). The target metal content of the liquid phase gave a direct indication of the success of the precipitation in each case.

The accuracy of the used method and instrument is considered good and it met the accuracy requirements posed on it, (Sara et al, 1981). An instrument with simultaneous multi element detection capacity would have been far more practical, but was economically out of range in this particular project. However, all samples could be analysed, and in cases of doubt, the samples were re-analysed after a thorough calibration of the instrument. Strange and non-fitting results were discarded only after repeating the experiment in question since the possibility that new reactions might take place and that formed compounds might transform into other ones had to be accounted for.

During the DCP–AES analysis the instrument was calibrated both prior to the analysis and during the analysis. In some cases a clear instrumental drift would be detected and the instrument had to be calibrated again and the samples had to be reanalysed.

The analysed concentrations varied from 5 mg/l to 3 000 mg/l (as undiluted). The accurate working range of the instrument varies between 3 mg/l to 100 mg/l (Ga) or 3 mg/l to 1 000 mg/l (In), depending on the analysed metal in question. Dilutions were made according to that.

IV.3.3.3. Titration – Fe(III)–EDTA

During the project Fe contents had to be measured when required. This was done spectrophotometrically without indicators allowing for a fast and precise analysis with a minimum of effort. The method is developed at the Laboratory of Analytical Chemistry and is one of the basic methods students are required to learn. The method is especially suitable not only for our work since samples need no particular pretreatment apart from occasional dilution. L. Harju and S-G. Huldén describe the method in detail (Harju et al., 1980 (a, b)) and it allows also for spectrophotometric titration of some other metal ions, depending on pH range and wavelength.

The Fe(III)–EDTA titration without an indicator is based on the formation of a stable 1:1 Fe(III)–EDTA chelate spectroscopically detectable at λ = 370 – 450 nm. Fe(II) reacting with EDTA will not be detected in the used wavelength and pH range, as depicted in Figure 8. The titration proceeds through a 2:1 Fe(III) - EDTA chelate (Fe = 2, EDTA = 1). The titration is illustrated in, with lines for the 2:1 titration (L1), 1:1 titration (L2) and achieved equivalence (Eq.). The equivalence volume of the EDTA used may be read from the graph at the crossing point of the lines L2 and Eq. in Figure 8. It may also be calculated from the equations of the lines obtained by linear regression (a direct feature in MS Excel). In an equal manner, the crossing point of the lines L1 and L2 indicate the halfway consumption of the reaction. The starting point of the titration is the same as the starting point of line L1.

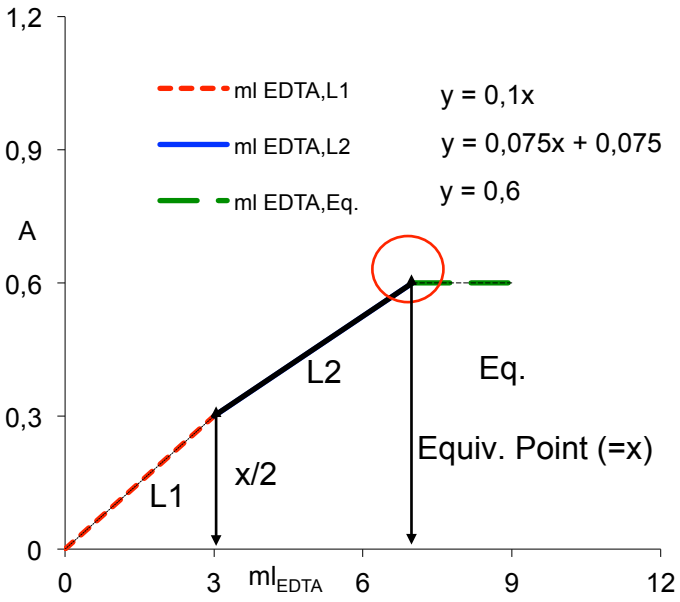

Figure 8. Spectroscopic titration of Fe(III) with EDTA without an indicator: λ = 370 – 450 nm and pH = 0 – 6, illustrated with a schematic graph. The equivalence volume of titrated EDTA is found where the lines for L2 and Eq. cross (encircled).

During the oxidation some of the Fe(II) may start to oxidize to Fe(III), which in turn will react with the added EDTA. This will then induce an error in the titration and the initial Fe(III)-contents will appear higher than they are. Thus the titration should be carried out rather swiftly.

Although there are several metal ions that react with EDTA (In, Fe(II), Al, Ca, Mg, Na, K) none of them will interfere with the spectroscopical titration of Fe(III). Spectroscopical titration is successful if pH is kept between 0 and 6 and if a wavelength between 370 and 450 nm is used, as the conditional stability constants of some metal-EDTA complexes as functions of pH in Figure 9. indicate.

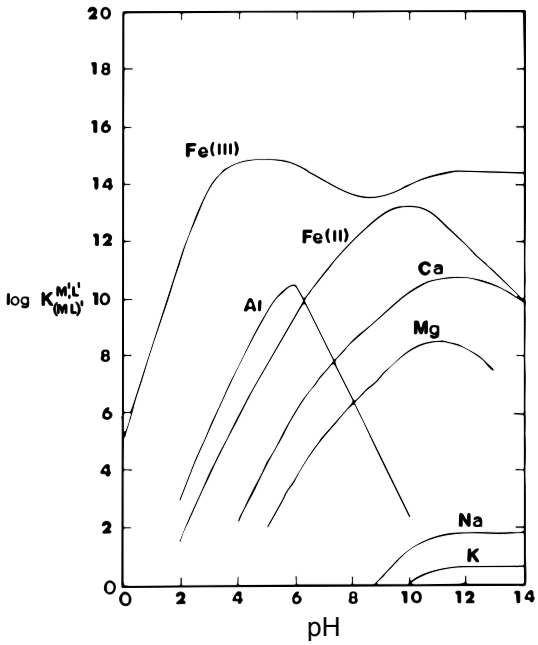

Figure 9. Conditional stability constants of some metal EDTA-complexes as functions of pH, (Harju et al., 1980a).

The analysis of the experimental Fe-solutions was done with Metrohm Spectrophotometer, Figure 10., with a dip-in light electrode and a range from 400 nm to 700 nm. The addition of EDTA was done through a Titrino 751 GPD titrimeter monitored by a Toshiba Satellite 4080 portable computer with a TiNET titration program. Depending on estimated Fe(III) concentrations the samples were analysed as such or as diluted. The titration was almost completely automatical and only the equivalence volume of EDTA had to be calculated to corresponding Fe(III) values.

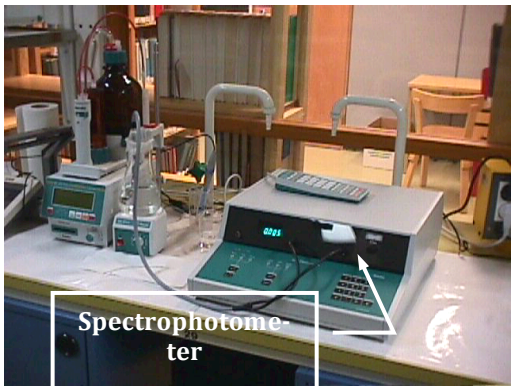

Figure 10. Metrohm Spectrophotometer with a Titrino 751 GPD titrimeter (front right), dip in light-electrode (400-700 nm) and Stirrer 728 (back left).

The pH was kept low in the diluted samples by using pre-acidified water with a pH < 1.6 to dilute the samples. This corresponded to the average pH of our samples. The TiNET program was run on fixed sampling intervals. A 0.05 – 0.1 M EDTA solution prepared from titrisols was mainly used. The equipment was tested and calibrated with synthetic and spiked process Fe(III)- and {Fe(III) - Fe(II)}-solutions.

The application of the Spectrophotometric titration of Fe^{3+} with EDTA -procedure in the laboratory is easy and fast. The following procedure has been used:

1. A sample is taken. The volume is noted in ml.
2. The sample is diluted with acidic water, pH ~ 1.5 or with a buffer solution of pH ~1.5.
3. The diluted sample volume is noted an indicated as V_0.
4. The sample is placed in photometer.
5. The sample is titrated with EDTA.

The data is graphically processed to find the equivalence point. The result, ml EDTA consumed, is converted to amount Fe^{3+} (g/l) in the sample solution.

The graphs in Figures 11. and 12. depict an example (not from the actual test series). An actual test run is depicted in Figures 13. and 14. and the parameters for this test are given in Table 3.

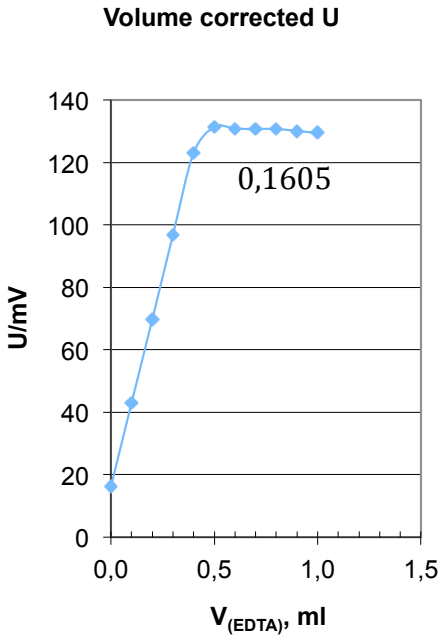

Figure 11. Volume corrected Fe(III)-EDTA titration.

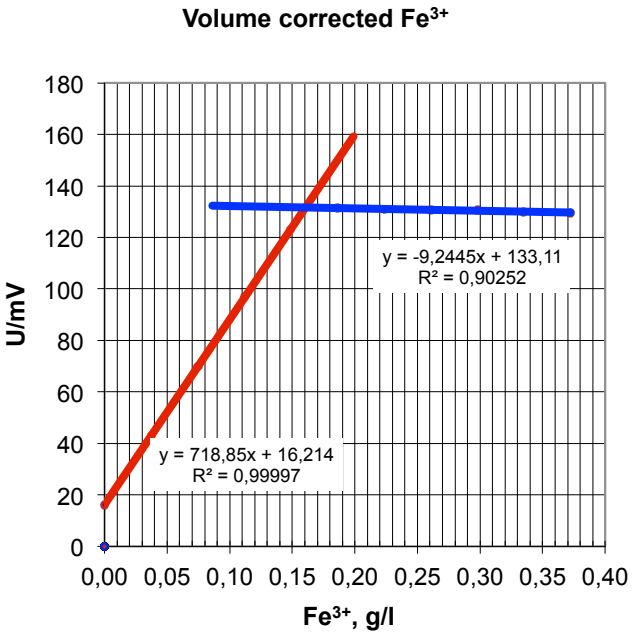

Figure 12. Volume corrected Fe(III)-EDTA titration on the x-axis with EDTA values converted to giving directly Fe^{3+} concentration g/l.

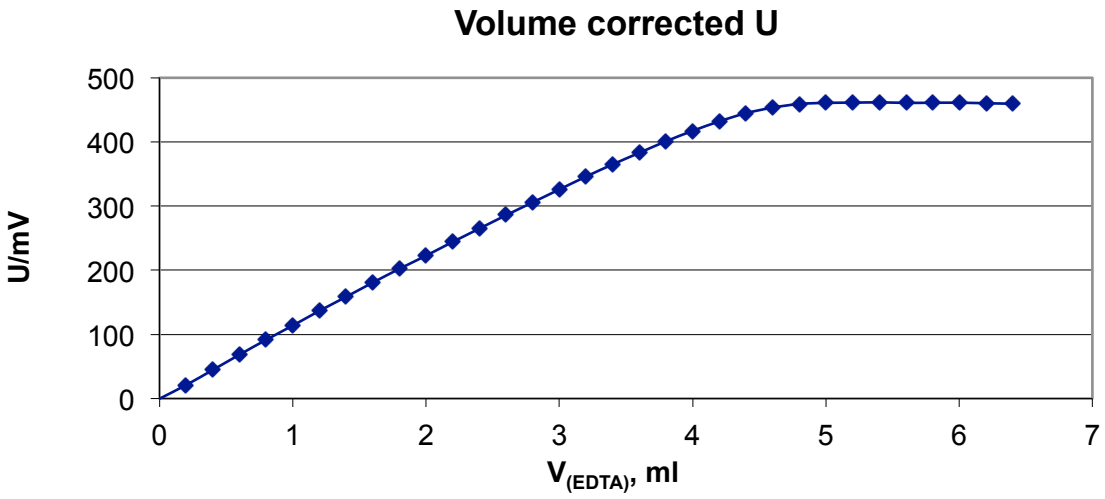

Figure 13. Photometric titration of Fe(III) and Fe(II) with EDTA. Volume corrected U is shown in the figure. Parameters are given in Table 3.

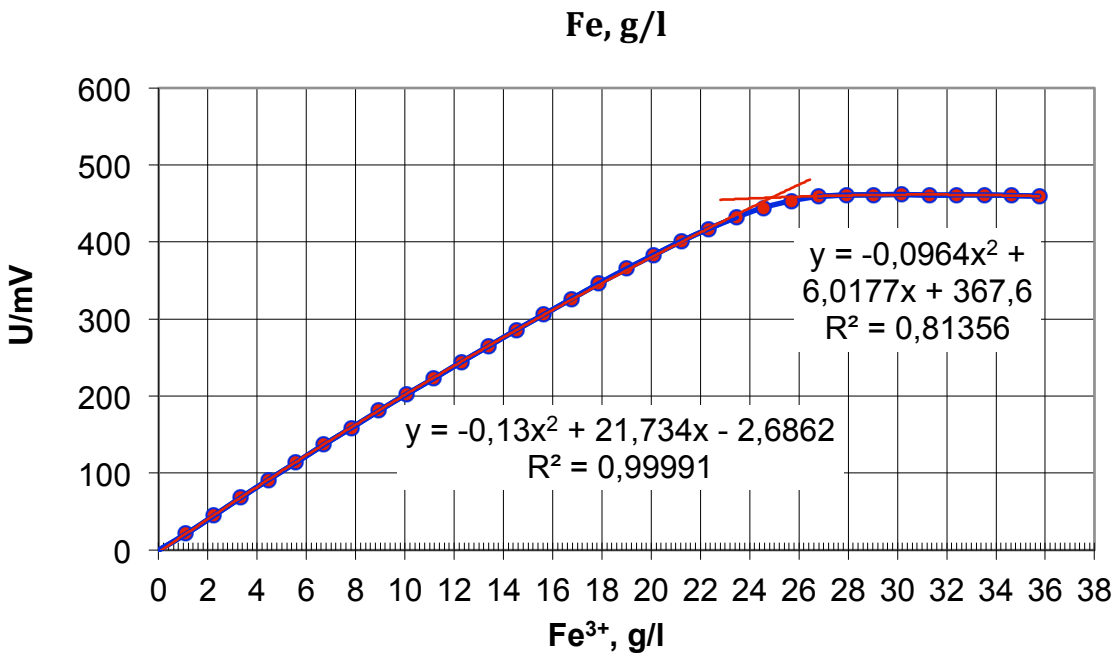

Figure 14. Photometric titration of Fe(III) and Fe(II) with EDTA. Volume corrected U shown in the upper figure. Parameters are given in Table 3.

Table 3. Photometric titration of Fe(III) and Fe(II) with EDTA

Determination of Fe(II) and Fe(III)		
Test run ID:	00022402	
Conc $_{(EDTA)}$:	0.05	M
Added H_2O_2:	1	ml
$V_{(sample)}$:	0.5	ml
$V_{(initial)}$:	28	ml
$Conc_{Fe}$:	24.3	g/l

IV.3.4. Experimental - remarks

The results from the tannic acid experiments are summarised with respect to the different pH environments that they were carried out in.

Precipitation tests with tannic acid and In, Ga and Ge were carried out under vigorous stirring at 90°C in synthetic and process solutions. A solution with approx. 100 mg/l of In, Ga and Ge each was added to ELGA water or process solution and precipitated with tannic acid.

Results section

The pH clearly affects the precipitation of Ge. Some In and Ga is also precipitated, but with tannic acid. In the highly acidic sulphuric acid environment also other reactions may take place. The reaction rates are thus important.

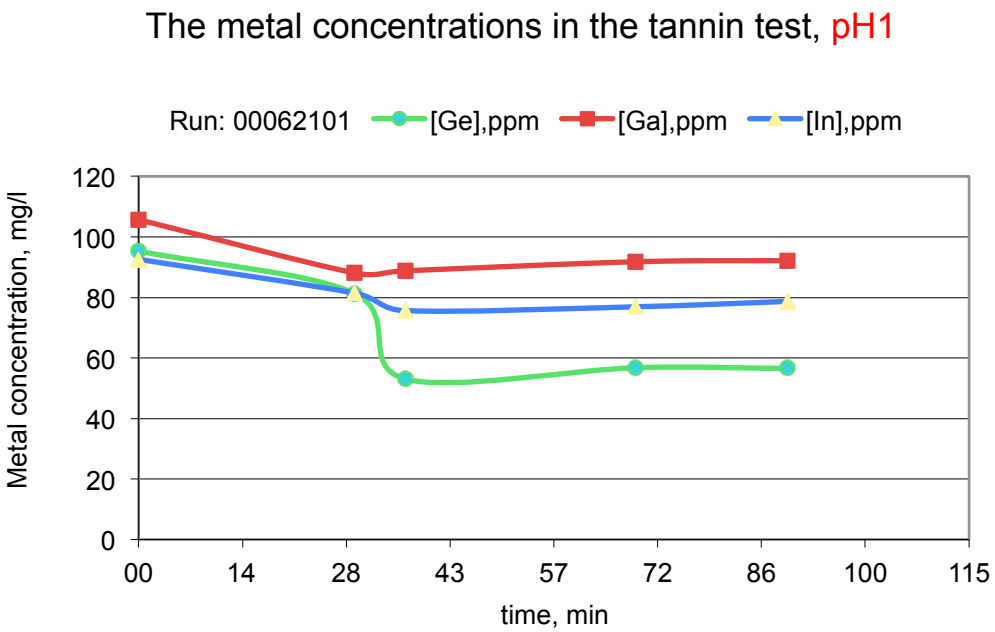

Figure 15. Example of tannic acid precipitation, test at pH 1. In, Ga and Ge each 100 mg/l, T = 90°C, synthetic solution, tannic acid 850 mg/l. DCP-AES-analysis.

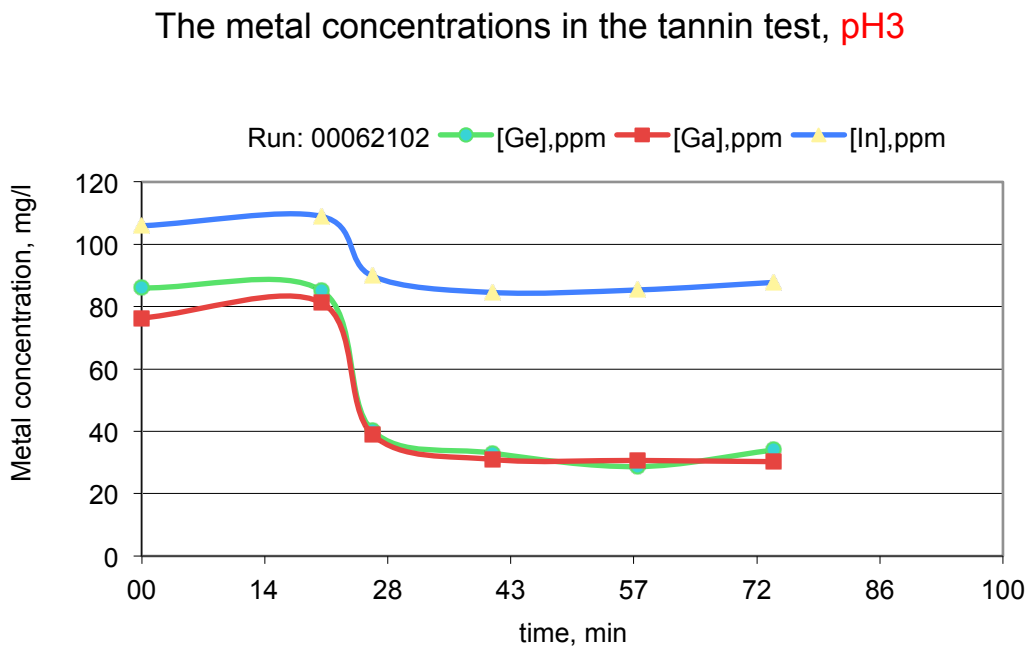

Figure 16. Example of tannic acid precipitation, test at pH 3. In (100 mg/l), Ga (80 mg/l) and Ge (80 mg/l), T = 90°C, synthetic solution, tannic acid 980 mg/l. DCP-AES-analysis.

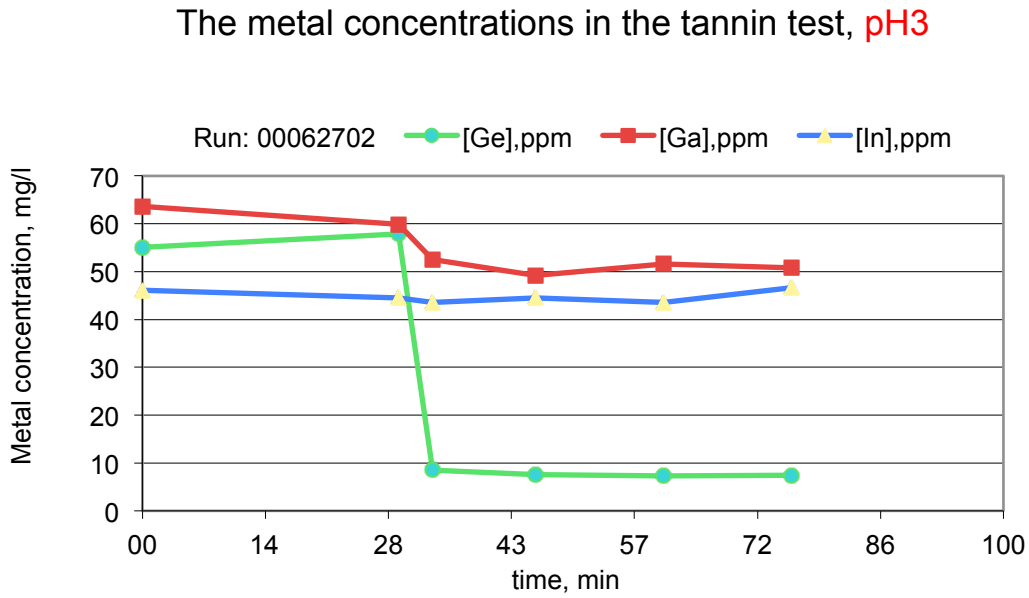

Figure 17. Example of tannic acid precipitation, test at pH 3. In (50 mg/l), Ga (60 mg/l) and Ge (55 mg/l), T = 90°C, process solution, tannic acid 980 mg/l. DCP-AES-analysis.

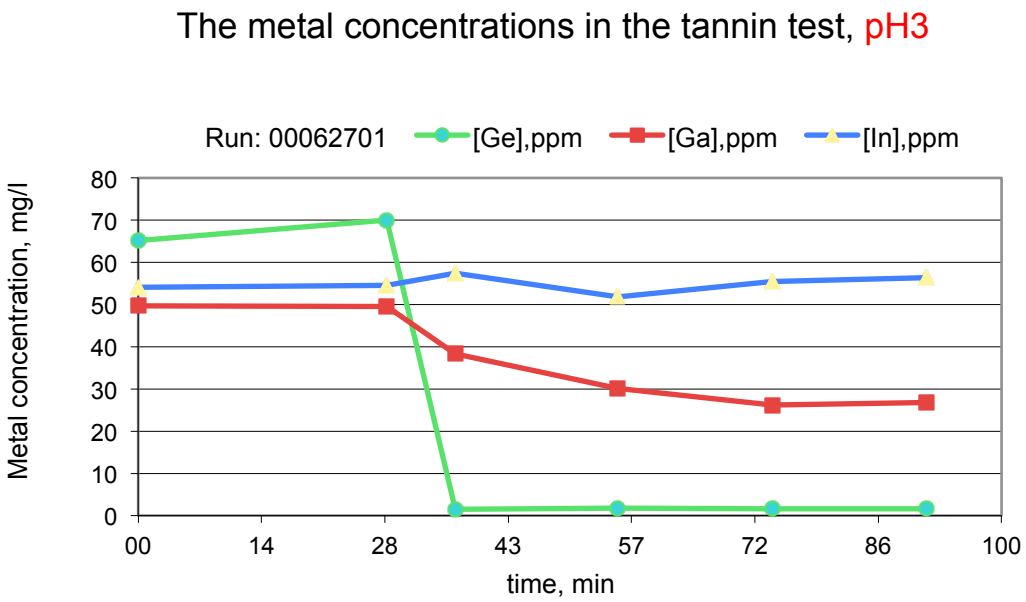

Figure 18. Example of tannic acid precipitation, test at pH 3. In (50 mg/l), Ga (50 mg/l) and Ge (65 mg/l), T = 90°C, process solution, tannic acid 2 400 mg/l. Tannic acid : Ge ratio corresponds to 1:1 molar ratio of tannic acid and Ge. DCP-AES-analysis.

IV.3.5. Reaction tannic acid – indium

In is not precipitated with tannic acid. To form basic indium sulphate the overall reaction time is not long enough.

IV.3.6. Reaction tannic acid – gallium

Ga precipitates during the tannic acid precipitation process of Ge, but not with tannic acid itself but as a basic sulphate. Ga reacts faster than In and succeeds in producing some basic sulphate precipitate while Ge is precipitated with tannic acid.

IV.3.7. Reaction tannic acid – germanium

In the studied process environment and process conditions the reaction is very selective. Tannic acid readily reacts with Ge (Kul et al., 2008) producing a good precipitation with tannic acid without any significant disturbance by other elements in the zinc production process solution, Table 4. In 40 minutes and at 90°C almost all of the Ge precipitated. The best results were obtained at pH 3 and with a molar ratio 1:1 of Ge:tannic acid. At this pH Al and Fe co-precipitation can be kept at a minimum level.

It must be noted, however, that under the same environmental conditions other precipitation reactions may take place. For an overall selective Ge precipitation all the parameters need to be fine tuned for a as rapid as possible Ge precipitation before significant other precipitation will take place, Figures 16. – 18.

The obtained results are to some extent contradictory to some other results described in the literature, (Liang et al., 2008b; Zhou et al., 2013).

IV.3.8. Reaction with iron

Fe reacts but does not precipitate with tannic acid and does not interfere with the Ge-tannic acid precipitation. Fe may also be used to improve the Ge recovery in certain kind of processes, (Liang et al., 2008a).

IV.3.9. Reaction with aluminium

Al does not precipitate with tannic acid in the tested environment, Table 4, and does not in interfere with the Ge-tannic acid precipitation according to this study.

IV.3.10. Tannic acid reactions with different ions

Tannic acid reactions with different ions in synthetic water solution were studied and have been collected in Table 4. Of the tested ions only Ge precipitated when KCl was added to help precipitate the reacted Ge-tannic acid. The results are in line with studies on behaviour of tannins in germanium recovery by tannin processes, (Liang et al., 2008b).

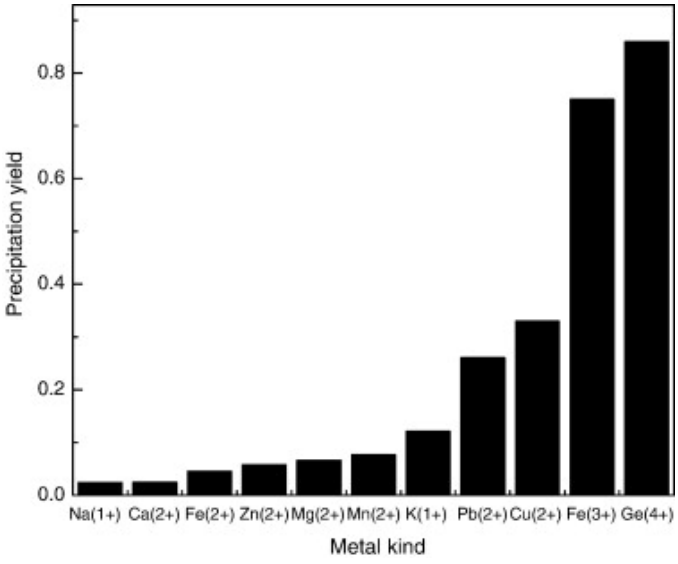

Figure 19. Binding ability of metal in single-metal solution and by tannin process. Complexation condition: stirring rate, 10 rps; complexation temperature, 373 K; complexation duration, 500 s, (Liang et al., 2008b).

Table 4. Tannic acid reactions with different ions in a synthetics water solution. The ions have been added to the solution in corresponding order. KCl was added to precipitate the reacted Ge-tannic acid.

Element	Volume, ml	Concentration, mg/ml	Colour	Type	Solubility
$Al^{(III)}$	0.25	1000	Clear		Ok
$Ga^{(III)}$	0.25	1000	Clear		Ok
$In^{(III)}$	0.25	1000	Clear		Ok
$Pb^{(II)}$	0.25	1000	Clear		Ok
$Cu^{(II)}$	0.25	1000	Clear		Ok
$Zn^{(II)}$	0.25	1000	Clear		Ok
$Co^{(II)}$	0.25	1000	Clear		Ok
$Ni^{(II)}$	0.25	1000	Clear		Ok
$Bi^{(III)}$	0.25	1000	Clear		Ok
$Ag^{(I)}$	0.25	1000	Clear		Ok
$Fe^{(II)}$	0.25	1000	Blue	Disapp.	Ok
$Fe^{(III)}$	0.25	1000	Blue	Disapp.	Ok
$Ti^{(IV)}$	0.25	1000	Yellow	Stable	Ok
$Sn^{(IV)}$	0.25	1000	Clear		Ok
$Si^{(IV)}$	0.25	1000	Clear		Ok
$Ce^{(IV)}$	0.25	1000	Clear		Ok
$Ge^{(IV)}$	*0.25*	*1000*	*Brownish*	*Stable*	*Precipitates*
KCl*	0.25	Saturated	Clear		

IV.3.11. Conductivity and pH in the tannic acid experiments

Together with the Ge precipitation tests the pH and conductivity of the solutions were measured, Figure 20, while titrating Ge in the solution with tannic acid.

The purpose of the conductivity measurement is to gain additional information about the reaction and enables to have an on-line monitoring of the process.

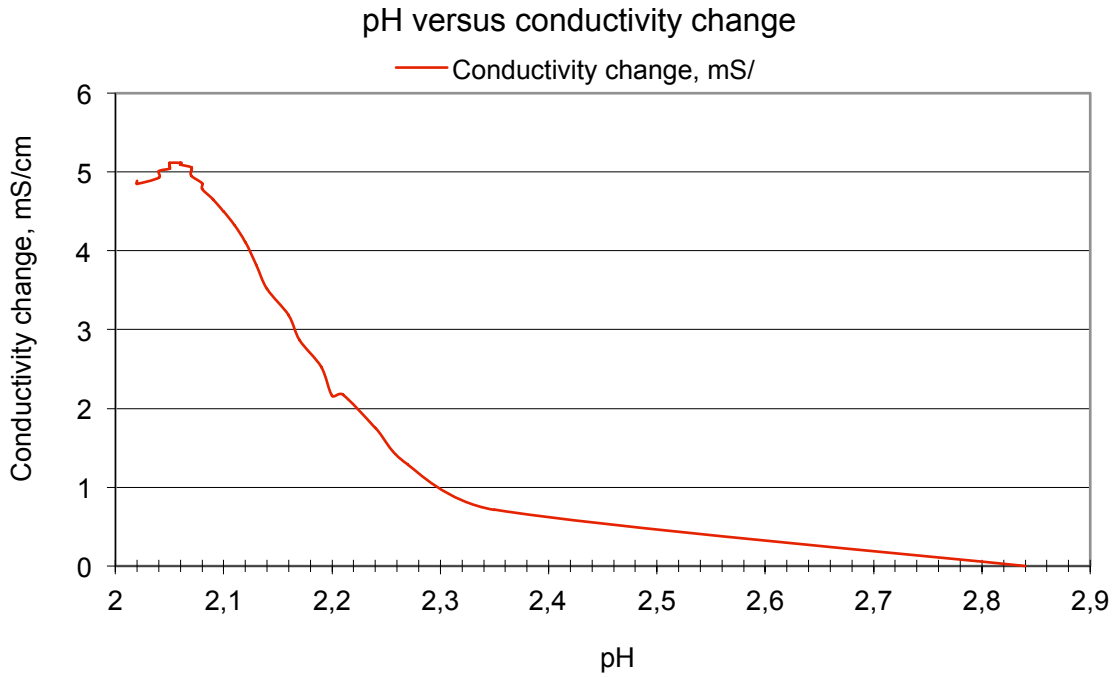

Figure 20. Example of conductivity versus pH, Ge 1 000 ppm 50 ml titrated with tannic acid 0.01 M. The tannic acid has been added in portions of 0.5 ml. Conductivity and pH has been recorded with 3-second intervals.

IV.3.12. Tannic acid precipitation

As explained previously, due to the nature of the project, the experimental setup was focused on finding suitable mechanisms for selectively separating In, Ga and Ge from zinc process liquors. To some extent this limited the number of experiments carried out and proper kinetic models cannot be presented.

The precipitation of Ge is selective and rapid, which allows the method to be used for selective separation of Ge from highly acidic sulphuric acid solutions.

Under different circumstances and in different solutions tannic acid can be used to separate also such metals as uranium and plutonium as well as other heavy metals. That separation requires special technology and those reactions do not affect the studied precipitation of Ge, (Nakamura et al., 1998 (a, b)).

IV.3.13. Indium precipitation

In did not precipitate with tannic acid and the time was not long enough to allow for indium basic sulphates to form.

IV.3.14. Gallium precipitation

Ga did not precipitate with tannic acid and gallium basic sulphate was not formed during the precipitation of Ge with tannic acid.

IV.3.15. Germanium precipitation kinetics

Ge precipitates rapidly with tannic acid and this takes mostly place before other elements have formed compounds that can precipitate and sediment. Due to the nature of the project and its nature the number of experimental runs was to some extent limited and proper kinetic models cannot be presented.

IV.4. Conclusions and future perspectives

The obtained results clearly show that in the studied environment tannic acid can successfully be used to precipitate Ge in a selective manner. The Ge precipitation is rapid enough to take place before In and Ga have had the time to form compounds which are able to precipitate.

The selectivity of the process is good and is not disturbed by other elements in the studied solutions. Thus the *tannic acid – Ge* precipitation can be used as a selective process step for precipitating Ge. The obtained results are to some extent contradictory to some other results described in the literature, (Liang, 2008 (a, b); Zhou, 2013).

Ge precipitated almost completely with tannic acid. As Ge was precipitated from the zinc process solution approximately 40% of Ga was co-precipitated and no In was co-precipitated. The reaction is rapid with almost complete removal of Ge within 40 minutes. The presence of Al and Fe or other elements did not affect the reaction.

Considering the overall process tannic acid can be used to precipitate Ge and this could well be done as the last step of the process. For solutions containing Ga, In and Ge and were precipitation of all three is desired the order of the process steps must be optimised for the overall recovery process in question.

The studied recovery processes can be applied in a novel kind of local recovery processes that can act as intermediates when local recycled raw material is pre-treated for further use at larger specialized recovery units.

IV.5. References

EFSA, 2014, Scientific Opinion on the safety and efficacy of tannic acid when used as feed flavouring for all animal species, EFSA Panel on Additives and Products or Substances used in Animal Feed (FEEDAP)2,3 European Food Safety Authority (EFSA), Parma, Italy

Hagerman, A. E., 1998 (2002 update), Tannin Chemistry, Department of Chemistry and Biochemistry, Miami University

Harju, L., Huldén, S-G., 1980a, Determination of Total Iron in Standard Rocks by Spectrophotometric Titration with EDTA, Talanta, Vol. 27, 811-814.

Harju, L., Huldén, S-G., 1980b, Standardization of EDTA by Spectrophotometric Titration, with Metallic Copper as Standard, Talanta, Vol. 27, 815-817.

Kul, M., Topkaya, Y., June 2008, Recovery of germanium and other valuable metals from zinc plant residues, Hydrometallurgy, Volume 92, Issue 3-4, Pages 87–94.

Liang, D., Wang, J. and Wang, Y., November 2008a, Germanium recovery by co-precipitation of germanium and iron in conventional zinc metallurgy, The Journal of The Southern African Institute of Mining and Metallurgy, VOLUME 108, 715-718.

Liang, D., Wang, J., Wang, F., Jibo Jiang, August 2008b, Behaviour of tannins in germanium recovery by tannin process, Hydrometallurgy, Volume 93, Issue 3-4, Pages 140–142.

Nakamura, Y., Shirato, W., Nakamura, Y., 1998b New Liquid Waste Control with Tannin Adsorbent, Proceedings of the 11th Pacific Basin Nuclear Conference

Nakamura, Y., Shirato, W., Yamakawa, H., Tominaga, Y., Nakamura Y., 1998a, Liquid Waste Treatment System with Insoluble Tannin, 62th Annual Meeting of The Society of Chemical Engineers

Pu, S., Lan, Y., Li. Y., 2013, Recovery Ge from Pulverized Fuel Ash Through the Method of H2SO4-NH4F-NaClO3 - leaching-tannin Precipitation, Physical and Numerical Simulation of Geotechnical Engineering 12th Issue, Sep. 2013

Sara, R., Huldén, S-G, Harju, L., 1981, Kaariplasmaemissio (DCP) analyysitekniikkana, Kemia-Kemi, n:o 12, page 774-778.

Wolfram|Alpha Knowledgebase, 2015.

Zischkau, C., Woodbridge, N. J., 1941, Separation of germanium, US 2249341 A, Patented July 15, 1941 Application June 12, 1940, Serial No. 340,089

Zischkau, C., Woodbridge, N. J., 1941, US Patent 2,249,341, Separation of germanium

Zhou J., Wang J. K., Li Y., 2009, Study on extracting and recovering germanium from leaching solution of Ge-rich Zinc Sulphide Concentrates, J. Nonferrous Metals (Extractive Metallurgy), 2009, 5: 25-27.

Zhou, Z., Chu, G., Gan, H., Yang, T., Chen, L., 2013, Ge and Cu recovery from precipitating vitriol supernatant in zinc plant.

ISBN 978-952-12-3270-1